Author:
Yates, Emma

Title:
Development of instrumentation and measurements of non-methane hydrocarbons at a remote background site

Development of instrumentation and measurements of non-methane hydrocarbons at a remote background site.

Emma Yates, M.Chem.

A dissertation submitted to the University of Bristol in accordance with the requirements of the degree of Doctor of Philosophy in the Faculty of Science.

School of Chemistry
University of Bristol
October, 2007

Text: 40,951 words

Abstract

Non-methane hydrocarbons (NMHCs) play an important role in tropospheric ozone chemistry, an important constituent in photochemical smog. Long-term in-situ measurements of NMHCs at a remote research site, such as Mace Head, Ireland provide useful information on NMHC trends and seasonal cycles. The prevailing westerly wind brings clean, Atlantic air to Mace Head, allowing analysis of NMHCs in northern hemisphere background air which can be compared with Pollution events, when easterly winds bring air from Europe to the site. This gives vital information to assess European NMHC emissions. Given the predominant removal mechanism for NMHCs is by reaction with the hydroxyl (OH) radical, the trends in NMHC ratios infer photochemical loss rates and can be used to determine the photochemical processing and age of an air mass. Any variation in NMHC seasonal cycles can be used to asses deviations in emission sources. In-depth analysis of two years of NMHC data measured by the Medusa-GCMS has been performed, along with the use of trajectory analysis and transport modelling.

Given that NMHCs in a remote environment are in the pptv concentration range, measurements of NMHCs require a pre-concentration step to 'concentrate' an air sample making detection possible. Development of an automated pre-concentration system for long-term in-situ measurements of NMHCs in a remote environment has been conducted. A number of analytical and technical challenges have been addressed. Pre-concentration requires sub-ambient temperatures and the use of adsorbent-filled traps, a range of adsorbents have been assessed for their retentive properties of the most volatile NMHCs. A range of chromatography columns have been investigated for the separation, resolution and identification of NMHCs for use in the new NMHC system. Sub-ambient temperatures bring the added challenge of water removal from air samples prior to pre-concentration and two different methods of water management have been assessed.

Acknowledgments

I owe a sincere thank you to my supervisors Dudley Shallcross and Simon O'Doherty for all their support and guidance over the last three years. Thank you to Graham Nickless and Peter Simmonds for helpful advice during this research. I would also like to thank Brian Greally, Damien Martin and Dickon Young for technical guidance and patience.

Many thanks to Alan Knights and everyone at the mechanical and electronic workshops.

Thanks to all my co-workers at the Atmospheric Chemistry Research Group – Steve, Iain, Roisin, Fred, Anwar, Laura, Paul, Alex and project student Kirsty.

Special thanks to my parents, Jennie, Hannah (and Jasper) and finally to Stephen, *Go raibh míle maith agat.*

Funding for this research was received from a University Scholarship from the Department of Chemistry, University of Bristol and through AEA Technology.

Authors' declaration

I declare that the work in this dissertation was carried out in accordance with the Regulations of the University of Bristol. The work is original, except where indicated by special reference in the text, and no part of the dissertation has been submitted for any other academic award. Any views expressed in the dissertation are those of the author.

SIGNED: ..... DATE: 10/12/07 .....

Contents

List of Figures

Chapter 1: Introduction

Chapter 2: Retention of analytes on selected adsorbents

Chapter 3: Chromatographic separation of NMHCs

Chapter 4 NMHC instrument design

Chapter 5: Observations at Mace Head

Chapter 6: Trajectory analysis and transport modelling

Chapter 7: Conclusions and recommendations

List of tables

Chapter 1: Introduction

Chapter 2: Retention of analytes on selected adsorbents

Chapter 3: Chromatographic separation of NMHCs

Chapter 4: NMHC instrument design

Chapter 5: Observations at Mace Head

Chapter 6: Trajectory analysis and transport modelling

Abbreviations

ADS	adsorption desorption system
AGAGE	advanced global atmospheric gas experiment
BADC	British atmospheric data centre
BTV	breakthrough volume
CFC	chloroflurocarbon
CI	chemical ionisation
CMS	carbon molecular sieve
DC	direct current
ECD	electron capture detector
ECNC	effective carbon number contribution
EI	electron impact ionisation
EPA	environmental protection agency
FID	flame ionisation detector
GC	gas chromatograph
GLC	gas liquid chromatography

GSC	gas solid chromatography
HCFC	hydrochloroflurocarbon
HFC	hydroflurocarbon
HID	helium ionisation detector
HOx	hydrogen containing free radicals (OH, HO_2)
LOD	limit of detection
LPG	liquid petroleum gas
MS	mass spectrometer
NAME	numerical atmospheric dispersion modelling environment
NAQS	national air quality strategy
NILU	Norwegian institute for air research
NIST	national institutes for standards and technology
NMHC	non-methane hydrocarbon
NOx	$NO + NO_2$
NUI	national university of Ireland
OVOC	oxygenated volatile organic compound
PAN	peroxyacetyl nitrate

PID	photoionisation detector
PLOT	porous layer open tubular
PORG	photochemical oxidants review group
ppbv	parts per 10^9 by volume
ppmv	parts per 10^6 by volume
pptv	parts per 10^{12} by volume
PTM	photochemical transport model
SIM	selective ion monitoring
SOGE	system for the observation of greenhouse gases in Europe
TCD	thermal conductivity detector
TIC	total ion chromatogram
TOC	total organic carbon
UM	united model
VOC	volatile organic compound
WCOT	wall coated open tubular

1. Introduction

1.1. The Role of NMHCs in Tropospheric Ozone Production

It was the work of Haagen-Smit and Fox (1956) that first identified the importance of non-methane hydrocarbons (NMHCs) as precursors in the formation of high levels of tropospheric ozone (referred to as smog). NMHCs include: alkanes, alkenes, alkynes and aromatics. Methane is considered separately due to its long atmospheric lifetime and high concentration compared with NMHCs (Wayne et al., 1991).

The mechanism by which NMHCs react to form ozone is well defined. Sunlight provides near-UV radiation which dissociates certain molecules that lead to the formation of hydrogen-containing free radicals (HOx).

HOx are generated by the photolysis of certain atmospheric gases. HOx includes OH, HO_2 and in some definitions also includes organic radicals since they are readily converted to OH and HO_2 under atmospheric conditions (Jenkin and Clemitshaw, 2000). The major source of OH is the photochemical degradation of ozone:

1.1. $O_3 + h\nu \rightarrow O(^1D) + O_2$

1.2. $O(^1D) + H_2O \rightarrow 2OH$

Only the $O(^1D)$ electronically excited state of the oxygen atom can react with H_2O to form the hydroxyl radical. The ground state of the oxygen atom is the $O(^3P)$, its reaction with H_2O is endothermic and therefore it adds to O_2 to reform O_3.

Incident sunlight penetrates lower layers of the atmosphere at wavelengths longer than approximately 290 nm; species that absorb light at this wavelength may be photolysed. Photolysis occurs so long as the energy of absorbed radiation is sufficient to break the weakest bond. The O_3 absorption cross-section is wavelength dependent,

decreasing as wavelength increases. Hence, photolysis rate varies with altitude, latitude and season (Jacobson, 2005).

In the presence of nitrogen oxides, NO_X (NO and NO_2) and HOx, volatile organic compounds, VOCs are oxidised to CO_2 and H_2O via a series of mechanisms.

NO_X are released into the troposphere from biogenic (natural) and anthropogenic (man's activities) sources, mainly in the form of NO. The dominant pathway for the conversion of NO to NO_2 under most tropospheric conditions is by reaction with O_3.

1.3. $NO + O_3 \rightarrow NO_2 + O_2$

During the daytime NO_2 is converted back to NO by photolysis:

1.4. $NO_2 + h\nu\ (\lambda < 420\,nm) \rightarrow NO + O(^3P)$

1.5. $O(^3P) + O_2\ (+M) \rightarrow O_3\ (+M)$

(M commonly N_2).

Oxidation of NMHCs is inhibited by reaction with the OH radical leading to a rapid sequence of reactions.

1.6. $OH + RH \rightarrow R + H_2O$

1.7. $R + O_2\ (+M) \rightarrow RO_2\ (+M)$

1.8. $RO_2 + NO \rightarrow RO + NO_2$

1.9. $RO \rightarrow\rightarrow\rightarrow$ carbonyl product(s) $+ HO_2$

1.10. $HO_2 + NO \rightarrow OH + NO_2$

Equation 1.9 is an abbreviated reaction, the mechanism of how RO radical is converted to HO_2 depends on the structure of RO (and hence the structure of RH). Small alkoxy radicals react with O_2 to directly form an aldehyde or ketone and HO_2

(equation 1.11). Mechanisms for the reaction of larger alkoxy radicals are frequently multi-step. Larger alkoxy radicals either decompose or (≥ C4) isomerise, general reactions are shown in equations 1.12 and 1.13 respectively.

1.11 $CH_3O + O_2 \rightarrow HO_2 + HCHO$

1.12

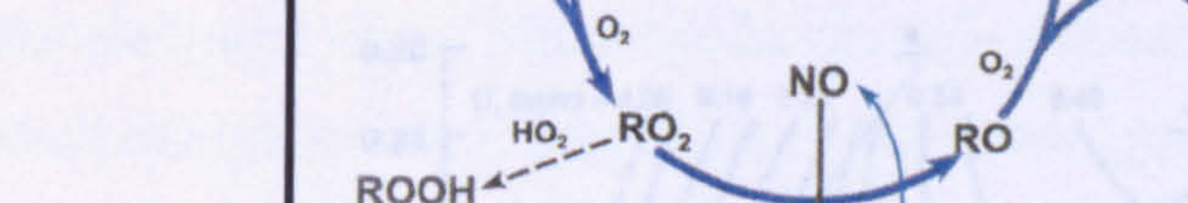

1.13

Figure 1.1 Schematic for the oxidation of a generic hydrocarbon, RH (PORG, 1997).

The key points to note about this cycle are:

- OH is regenerated hence it is a catalytic cycle.
- The key role in O_3 formation is the conversion of NO → NO_2.
- NO_2 is photodissociated by near-UV and visible radiation to form O_3.

1.14. $NO_2 + h\nu\,(< 420\,nm) \rightarrow NO + O(^3P)$

1.15. $O(^3P) + O_2\,(+M) \rightarrow O_3\,(+M)$

- The reaction depends on the structure of RO, hence the structure of RH. See explanation for equations 1.11, 1.12 and 1.13.

- Since O_3 photolysis is a major source of HOx. O_3 may be regarded as an autocatalyst since it stimulates its own production.

The overall reaction is:

1.16. $RH + 4O_2 \rightarrow RO + H_2O + 2O_3$

1.2. The sensitivity of ozone production to changes in VOCs and NOx concentrations.

Ozone formation is strongly dependent upon the relative concentrations on NOx and VOCs of which NMHCs are a sub-set. This dependency can be described by the isopleth shown in Figure 1.2.

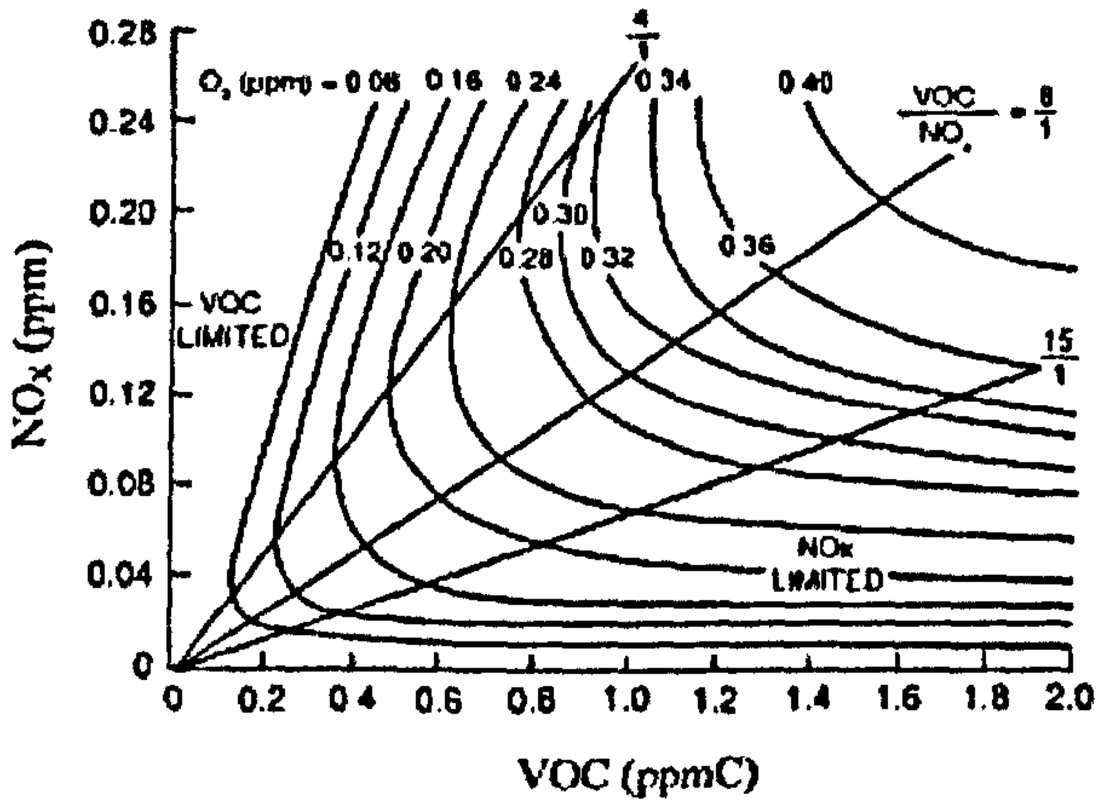

Figure 1.2 Ozone production isopleth (Jenkin and Clemitshaw, 2000).

When the relative concentration of [NOx]/[VOC] is high the situation is said to be VOC-limited. Ozone formation correlates positively with NOx and the ozone isopleth lines tend towards running parallel with VOC concentration. In NOx-limited conditions, when the [NOx]/[VOC] is low the ozone formation correlates positively with VOC concentration and the ozone isopleth runs parallel with NOx concentrations. The non-linear relationship between ozone, NOx and VOC is an important basis for environmental policy, as ozone concentrations can be decreased

only by decreasing emissions of NOx and VOC. Decreasing just VOC concentrations will only be effective in reducing ozone concentrations in VOC limited conditions. Typically, a freshly emitted plume of polluted air is characterised by VOC limited conditions as the air mass ages, the [NOx]/[VOC] ratio decreases as it evolves towards NOx limited chemistry (Silman, 1999).

1.3. The effects of ozone

Ozone is widely known to have adverse effects on human health, materials and vegetation. In humans, ozone causes inflammation of the respiratory tract, leading to problems such as asthma. Materials such as rubber, surface coatings and metal and stone are all affected by ozone. Ozone exposure can cause cracks to appear in natural and some synthetic rubbers. Degradation of surface coatings, including paints, varnishes, lacquers. Ozone in combination with S- and N- pollutants has corrosive effects on metals and stone, which can have major economic consequences. Exposure of vegetation to high levels of ozone effects crop yield, growth and the composition of natural communities (PORG, 1997).

1.4. The effects of benzene

Benzene emissions are predominately from evaporation and combustion of petroleum products. Emissions also arise from industry; benzene is a chemical intermediate in the formation of many foams, solvents and pesticides. Benzene emissions have been decreasing since the 1990s, due to the use of catalytic converters and the fact that benzene content in petrol has decreased. Benzene is carcinogenic; exposure to benzene gives rise to an increased risk of developing leukaemia. Government air quality objectives limit the concentration of benzene to 5.00 ppbv (rolling annual mean) (Dore, et al., 2006).

1.5. The effects of 1,3-butadiene

Emissions of 1,3-butadiene arise from the combustion of petroleum products, 1,3-butadiene is not a constituent of petrol but is formed as a by-product of combustion. Emissions of 1,3-butadiene have been decreasing since the 1990s due to the use of catalytic converters. 1,3-Butadiene is also produced by the chemical industry, used in the production of synthetic rubbers. 1,3-Butadiene is a carcinogen, Government air quality objectives limit the concentration of 1,3-butadiene to 2.25 ppbv (rolling annual mean) (Dore et al, 2006).

1.6. Health effects of other VOCs

Currently in the U.K. benzene and 1,3-butadiene are the only VOCs classified as particularly harmful by the National Air Quality Strategy (NAQS). However, other hydrocarbons including toluene, ethylbenzene, xylene isomers and hexane in the parts per million (ppmv) concentration range can cause damage to the nervous system, dizziness and nausea.

The health effects of other VOCs are compound specific, varying from those that are highly toxic to those with no known health effects. The nature and extent of the health effect depends upon the exposure time and levels. Possible health effects from exposure to VOCs include: Eye, nose and throat irritation, headaches, loss of coordination, nausea, damage to liver, kidney and central nervous system (EPA, 2007).

1.7. Further reaction pathways for hydrocarbons

1.7.1. Ozone

Unsaturated VOCs such as alkenes and dienes may also be oxidised by reaction with O_3. Addition of O_3 to the double bond forms an energy rich ozonide which decomposes via two possible pathways to produce carbonyl compounds and a Criegee biradical (denoted #), which processes excess energy.

1.17 $$CH_3CH=C(CH_3)_2 + O_3 \rightarrow CH_3CHO + [(CH_3)_2COO]^{\#}$$

$$\rightarrow CH_3C(O)CH_3 + [CH_3CHOO]^{\#}$$

The Criegee biradical can either be stabilised by collisions or decompose by a series of reactions to produce radical and molecular products.

1.7.2. Chlorine chemistry

Hydrocarbons can react with Cl atoms, generated by the photolysis of Cl_2, or other precursors, or from the reaction of OH with HCl (Singh and Kasting, 1988). The reaction rates for many NMHCs with Cl are 1-2 orders of magnitude faster than the reaction rates with respect to OH. Thus Cl can compete effectively with OH for photochemical degradation of hydrocarbons at much lower atmospheric concentrations. The ratios of various hydrocarbons have been used as an indirect method to infer Cl levels in the atmosphere.

1.7.3. Night time Chemistry

Although the major oxidation processes in the troposphere are initiated by sunlight there are significant processes that occur during the night. Nighttime processes do not lead to the formation of ozone, but nighttime chemistry results in the oxidation of VOCs and NO_X to form secondary pollutants.

The significance of NO_3 during daylight is suppressed since NO_3 is rapidly photolysed via two possible channels to form NO and O_2 or forming NO_2 and O. Hence the significance of NO_3 during daylight is suppressed.

1.18. $NO_3 + h\nu \rightarrow NO + O_2$

1.19. $NO_3 + h\nu \rightarrow NO_2 + O$

At nighttime NO_2 is slowly converted to NO_3 as follows:

1.20. $NO_2 + O_3 \rightarrow NO_3 + O_2$

Although reaction with OH is the major pathway for NMHCs, during the night NO_3 is the important oxidising species in the troposphere, reacting with NMHCs by either hydrogen abstraction to form HNO_3 or addition to unsaturated bonds.

1.21. $RH + NO_3 \rightarrow HNO_3 + R$

1.22. $C(CH_3)_2 = C(CH_3)_2 + NO_3\ (+M) \rightarrow C(CH_3)_2\ (ONO_2)C(CH_3)_2\ (+M)$

Wayne, et al. (1991) found branched alkenes tend to be more reactive towards NO_3 than un-branched.

1.8. Sources of atmospheric hydrocarbons

1.8.1. Anthropogenic sources

The UK inventory of the most significant NMHCs (in terms of mass) is summarised in Table 1.1.

	Stationary combustion	Production Processes	Extraction and distribution of fossil fuels	Solvent use	Road transport	Other transport	Waste treatment and disposal	Total
ethane	4.42	1.28	34.26	0.00	2.19	0.42	4.82	47.40
propane	2.17	2.26	19.26	3.72	0.80	0.25	4.51	33.02
i-butane	0.76	0.23	11.13	0.96	4.08	0.23	0.01	17.40
n-butane	2.48	4.54	39.06	19.07	9.23	0.48	0.04	74.90
i-pentane	1.98	1.01	9.52	0.05	12.13	0.74	0.02	25.46
n-pentane	1.51	1.90	11.75	0.44	5.91	0.29	0.03	21.83
hexane	0.33	4.08	6.69	2.55	5.44	0.20	0.17	19.45
ethene	5.13	5.71	0.03	0.00	9.50	4.32	1.02	25.71
propene	1.46	6.15	0.02	0.00	4.35	1.45	0.06	13.48
1-butene	0.10	0.65	0.22		3.17	1.37	0.01	5.52
2-butene *(cis and trans)*	0.41	0.14	0.69		1.77	0.20	0.03	3.25
2-pentene *(cis and trans)*	0.26	0.01	1.22		1.09	0.04	0.00	2.62
acetylene	0.07	0.59	0.01	0.00	3.93	1.48		6.09
1,3-butadiene	0.00	0.32	0.01		1.88	1.17	0.01	3.39
benzene	5.86	1.59	0.65	0.00	3.44	1.95	0.96	14.46
toluene	1.31	2.87	0.20	12.24	10.52	2.69	0.25	30.08
m-xylene	0.66	1.08	0.08	12.87	3.14	0.79	0.12	18.73
o-xylene	0.21	0.50	0.04	3.21	2.93	0.83	0.07	7.78
p-xylene	0.16	0.60	0.02	3.56	2.43	0.61	0.09	7.36
ethylbenzene	0.21	1.29	0.02	4.92	2.77	0.74	0.19	10.15
Total	29.49	36.80	134.88	63 59	90 70	20 25	12.41	388 08

Table 1.1UK emissions of the most significant NMHCs in terms of mass emissions (tonnes) (Dore et al, 2006).

Extraction and distribution of fossil fuels is the largest source of NMHCs and includes; mining and production of coal, crude oil and natural gas and processing crude oil into a variety of products. Products from crude oil include, liquid fuels, by-product fuels, such as lubricants and primary petrochemicals: ethene, benzene, toluene. Distribution of fossil fuels includes, storage of fossil fuels, loading of tanker-ships and trucks to re-fuelling vehicles at service stations.

Road transport emissions depend on various parameters such as the vehicle, fuel, the type of driving and ambient air temperature. Emissions are higher when the vehicle starts before the engine and catalytic converter are warm and during winter when the ambient air temperature is cooler. Above average emissions result from driving in urban areas, compared to on motorways at moderate, constant speed, VOC emissions

are exceptionally high within traffic jams. Latella, et al., (2005) studied vehicle emissions and found C_2-C_4 hydrocarbons were the most dominant emissions from vehicles fuelled by liquid petroleum gas (LPG), two-stroke engines emit large quantities of C_2-C_7 compounds, the exhausts containing the highest levels of toxic NMHCs such as 1,3-butadiene. Four-stroke engine emissions were similar to two-stoke but with a higher proportion of non-combusted aromatics. The diesel engines tested produced simpler chromatograms, containing mainly low molecular weight NMHCs.

Solvent use is another major source of NMHCs and includes both industrial and domestic solvent use. There are a large number and variety of solvent emissions, including paints, printing inks, adhesives and consumer goods for private use, such as soaps and personal hygiene products.

Production processes include emissions from the chemical industry, petroleum, food and drink manufacture and iron and steel production. Stationary combustion is categorised as non-transport combustion of fossil fuels including; energy production, commercial and residential sources and industrial sources. Sources from waste disposal arise from incomplete combustion in waste incinerators and from waste dumping sites.

1.8.2. Biogenic sources

The distinction between anthropogenic and biogenic sources is not as straightforward as it seems. Many NMHCs are emitted from both sources, for example alkanes and alkenes are emitted from anthropogenic sources listed in Table 1.1 but also emitted from soils, oceans and wetlands. To further complicate matters, biomass burning could be viewed as a natural process but has been enhanced by agricultural practises.

Natural biogenic emissions from forests and land emit large quantities of isoprene, monoterpenes and OVOCs. Plants emit a range of VOCs due to: stress response, to attract pollinators, tissue damage, defence compounds and to signal alarm to neighbouring plants (Tholl, et al., 2006). Isoprene emissions are both light and temperature dependent. Light provides the energy for biosynthesis of isoprene and temperature effects the emission rate by altering the vapour pressure of isoprene within the leaf (Anastasi, et al., 1991). Seawater has also been proposed as a source of isoprene due to photoplankton activity (Lewis, et al., 2001).

Oceanic emissions of NMHCs are small compared with terrestrial biogenic emissions. Current estimates of oceanic NMHC emissions account for 5 Tg C yr^{-1} (Reimann, et al., 2000). NMHC emissions originate from the photochemical degradation of dissolved organic carbon (Lewis, et al., 2001). Alkenes, including isoprene and alkanes have been found in surface ocean waters at supersaturated levels compared with the atmosphere. The concentrations of NMHCs decrease with increasing carbon number present in the compound.

1.8.3. Atmospheric distribution of VOCs

The atmospheric distribution of VOCs, including NMHCs depends on their sources, reactivity and regional and global transport phenomena. The seasonal cycle of anthropogenic VOCs shows higher concentrations during winter months and lower concentrations in summer months. This cycle is caused by lower concentrations of oxidising agents, particularly the hydroxyl radical during winter resulting in lower chemical reactivity of the atmosphere, combined with higher anthropogenic emissions during winter.

1.8.3.1. Transport to rural areas

Rural areas and global background regions exhibit the same annual cycle discussed previously with their lowest concentrations observed in late summer due to the higher concentrations of oxidising agents. The amplitude of the seasonal cycle is affected by the chemical lifetime of a species; the amplitude is greatest for shorter lived species. Substances which have a lifetime within the range of the transport time from the source to receptor are partly oxidised. Fast reacting species (alkenes) with lifetimes shorter than the transport time are almost totally removed by oxidising agents during transport resulting in extremely low and difficult to measure concentrations. For long lived VOCs (including ethane) intercontinental transport can occur, and this is especially true for the long lived hydrofluorocarbons (HFCs) were intercontinental transport from the USA to Europe has been detected (Greally, et al., 2007).

1.8.3.2. Photochemical degradation of hydrocarbons

Measurements of hydrocarbons can be used to determine the degree of photochemical processing that occurred between their source and the receptor; this is known as the "photochemical age" of hydrocarbons in a sampled air mass. The rate of degradation of hydrocarbon, X is:

$$\frac{d[X]}{dt} = -k_x[OH]t \qquad \textbf{1.23.}$$

Hence,

$$[X] = [X]_0 e^{-k_x[OH]t} \qquad \textbf{1.24}$$

were k_x is the rate constant for the removal of compound X by the reaction with OH radicals and t is the time from emission to sampling, assuming chemical loss is driven by OH only.

The ratios of two hydrocarbons (X and Y) can provide an estimate of photochemical ageing if both hydrocarbons were emitted into the troposphere simultaneously, if their removal is by reaction with OH alone and if dilution effects of an air mass are negligible (Parrish, et al., 1992). The oxidation of X and Y according to equation 1.25 yields:

$$\frac{[X]}{[Y]} = \frac{[X]_0}{[Y]_0} . e^{-(k_x - k_y)[OH]t} \qquad \textbf{1.25.}$$

Where $[X]_0$ and $[Y]_0$ are the initial concentrations of X and Y upon emission into the troposphere. This can also be expressed as:

$$\ln([X]/[Y]) = \ln([X_0]/[Y_0]) - (k_x - k_y)[OH]t \qquad \textbf{1.26.}$$

Rearranging equation 1.26 and solving for t yields the photochemical age with respect to OH oxidation.

$$\textbf{1.27.} \quad t_{OH} = \frac{\ln\left(X_o/Y_0\right) - \ln\left(X/Y\right)}{\left(k_x - k_y\right)[OH]}$$

An analogous equation can also be derived to determine the photochemical age with respect to other oxidants, such as Cl atoms, t_{Cl} or NO_3. Then the age with respect to two oxidants can be calculated.

$$\textbf{1.28.} \quad 1/\tau = 1/t_{OH} + 1/t_{Cl}$$

Simultaneous measurements of three hydrocarbons provide an opportunity to check if two independent measures of photochemical age yield the same result (Parrish, et al., 1992). The following relationship between the ratio of (X/Z) and (Y/Z) exists:

$$\textbf{1.29.} \quad \ln(X/Z) = M\{\ln(Y/Z)\} + D$$

The slope, M, is

$$\textbf{1.30.} \quad M = (k_X - k_Z)/(k_Y - k_Z)$$

And intercept, D, is

$$\textbf{1.31.} \quad \ln([X_o]/[Z_0]) - M\ln([Y_0]/[Z_0])$$

Variation from the linear correlation in equation 1.31 can be caused by the effects of dilution in long range transport (McKeen and Liu, 1993), as well as inaccuracies in kinetic data and detection limits of the instrumentation. It has also been suggested to be an indication of chlorine (Cl) chemistry (Bottenheim and Shepherd, 1995).

	k(OH) (cm^3 s^{-1})	Reference	k(NO_3) (cm^3 s^{-1})	Reference	k(Cl) (cm^3 s^{-1})	Reference	k(O_3) (cm^3 s^{-1})	Reference
Ethane	2.40x10-13	Atkinson et al, 2005	<1.00x10-17	Atkinson et al, 2005	5.90x10-11	Atkinson et al, 2005	-	-
Propane	1.10x10-12	Atkinson et al, 2005	<7.00x10-17	Atkinson et al, 2005	1.40x10-10	Atkinson et al, 2005	-	-
i-Butane	2.12x10-12	Atkinson, 2003	9.8x10-17	Atkinson, 1991	1.43x10-10	Atkinson, 1997	-	-
n-Butane	2.36 x 10-12	Atkinson, 2003	4.60x10-17	Atkinson, 2006	2.18x10-10	Atkinson, 1997	-	-
i-Pentane	3.60 x 10-12	Atkinson, 2003	1.56x10-16	Atkinson et al, 1994	2.20x10-10	Atkinson, 1997	-	-
n-Pentane	3.80 x 10-12	Atkinson, 2003	8.1x10-17	Atkinson, 1991	2.80x10-10	Atkinson, 1997	-	-
n-hexane	5.20 x 10-12	Atkinson, 2003	1.05x10-16	Atkinson, 1991	3.40x10-10	Atkinson, 1997	-	-
Ethene	9.00x10-12	Atkinson et al, 2005	2.10x10-16	Atkinson et al, 2005	1.10x10-10	Atkinson et al, 2005	1.6x10-18	Atkinson et al, 2005
Propene	3.00x10-11	Atkinson et al, 2005	9.50x10-15	Atkinson et al, 2005	2.8x10-10	Atkinson et al, 2005	1.0x10-17	Atkinson et al, 2005
1-Butene	3.14x10-11	Atkinson, 1997	1.25x10-14	Atkinson, 1991	3.38x10-10	Ezell et al, 2002	9.64x10-18	Atkinson et al, 1994
i-Butene	51.4x10-12	PORG, 1997	3.32x10-13	Atkinson, 1991	3.4x10-10	Ezell et al, 2003	1.1x10-17	Atkinson et al, 2005
Trans-2-butene	6.40x10-11	Atkinson, 1997	3.90x10-13	Atkinson, 1991	3.31x10-10	Ezell et al, 2002	1.9x10-16	Atkinson et al, 2005
Cis-2-butene	5.64x10-11	Atkinson, 1997	3.50x10-13	Atkinson, 1991	3.76x10-10	Ezell et al, 2002	1.3x10-16	Atkinson et al, 2005
i-Pentene	8.69x10-11	Atkinson, 1997	9.37x10-12	Atkinson, 1991	3.95x10-10	Ezell et al, 2002	4.1x10-16	Atkinson et al, 2005
1-Pentene	3.14x10-11	Atkinson, 1997			3.97x10-10	Ezell et al, 2002	1.0x10-19	Atkinson et al, 1994
1,3-butadiene	66.6x10-12	PORG, 1997	1.0x10-13	Atkinson, 1991	3.48x10-10	Notario et al, 1997	6.31x10-18	Atkinson et al, 1994
Isoprene	1.00x10-10	Atkinson, 2003	7.00x10-13	Atkinson et al, 2005	5.10x10-10	Finlayson-Pitts et al, 1999	1.27x10-17	Atkinson et al, 2005
Acetylene	9.00x10-13	Atkinson, 1991	5x10-17	Atkinson, 1991	5.20x10-11	Atkinson et al, 2005	1.00x10-20	Atkinson et al, 2005
Benzene	1.23x10-12	Atkinson, 1991	<3x10-17	Atkinson, 1991	4.00x10-11	Wallington et al, 1988	-	-
Toluene	5.96x10-12	Atkinson, 1991	6.8x10-17	Atkinson, 1991	5.90x10-10	Shi and Bernhard, 1997	-	-
Ethylbenzene	7.1x10-12	PORG, 1997	<5.7x10-16	Atkinson, 1991			-	-
m-Xylene	-	-	2.33x10-16	Atkinson, 1991	1.4x10-10	Shi and Bernhard, 1997	-	-
p-Xylene	-	-	3.77x10-16	Atkinson, 1991	1.5x10-10	Shi and Bernhard, 1997	-	-
m+p-Xylene	19x10-12	PORG, 1997	-	-	-	-	-	-
o-Xylene	13.7x10-12	PORG, 1997	4.53x10-16	Atkinson, 1991	1.5x10-10	Shi and Bernhard, 1997	-	-

Table 1.2 Rate coefficients for NMHCs with OH, NO_3, Cl and O_3

1.9. Gas Chromatography

The most common technique for analysis of VOCs is the use of gas chromatography (GC) which when combined with a detector, has been found to be appropriate for separating and quantifying VOCs at low atmospheric concentrations. Gas chromatography is a separation technique. The principle behind gas chromatography is the separation of components (solutes, analytes) in a sample mixture which are transported by a mobile phase (carrier gas, usually helium) over a stationary phase (chromatography column). A suitable sample for analysis by GC consists of stable components that interact with the column material. Attraction of the solute to the stationary phase slows its movement through the column; thus solutes travel through the column at different rates depending on their ability to partition, or transfer between the stationary and mobile phase (Braithwaite and Smith, 1996).

There are three types of gas chromatography, which are:

- Packed column GC:
    - Gas-liquid chromatography (GLC) uses a packed column with a liquid stationary phase.
    - Gas-solid chromatography (GSC) uses packed columns with solid adsorbents where the surfaces of the particles form the stationary phase.
- Capillary column GC uses porous layer open tubular (PLOT) columns with either a solid of liquid stationary phase (used here).

1.9.1. Factors influencing partition

Factors influencing the partition between the stationary and mobile phase include: the properties of the carrier gas, properties of the chromatography column, intermolecular forces between the solutes and temperature, where retention is inversely proportional to temperature. This partition can be based on polarity, boiling point and occasionally chirality of the compounds. The analysis is performed with the column contained in an oven so that the temperature can be controlled. Varying the temperature of the oven allows the best possible separation of compounds to be achieved for a wide range of volatilities. Chromatographic separations can be evaluated by the shape of the peaks. Peak shapes depend on the isotherms that describe the relationship between concentration of the solute in the stationary phase and concentration of the solute in the carrier gas (Grob and Barry, 2004).

1.9.2. Gas chromatography detectors

A GC detector provides a response signal for compounds different from the carrier gas as they elute from the column. The chromatogram is a plot of detector signal against time which forms a concentration profile of solutes present in the carrier gas. Selection of the type of detector depends on the target compound, concentration range and whether qualitative or quantitative analysis is preferred (Braithwaite and Smith, 1996).

1.9.2.1. Flame Ionisation Detector

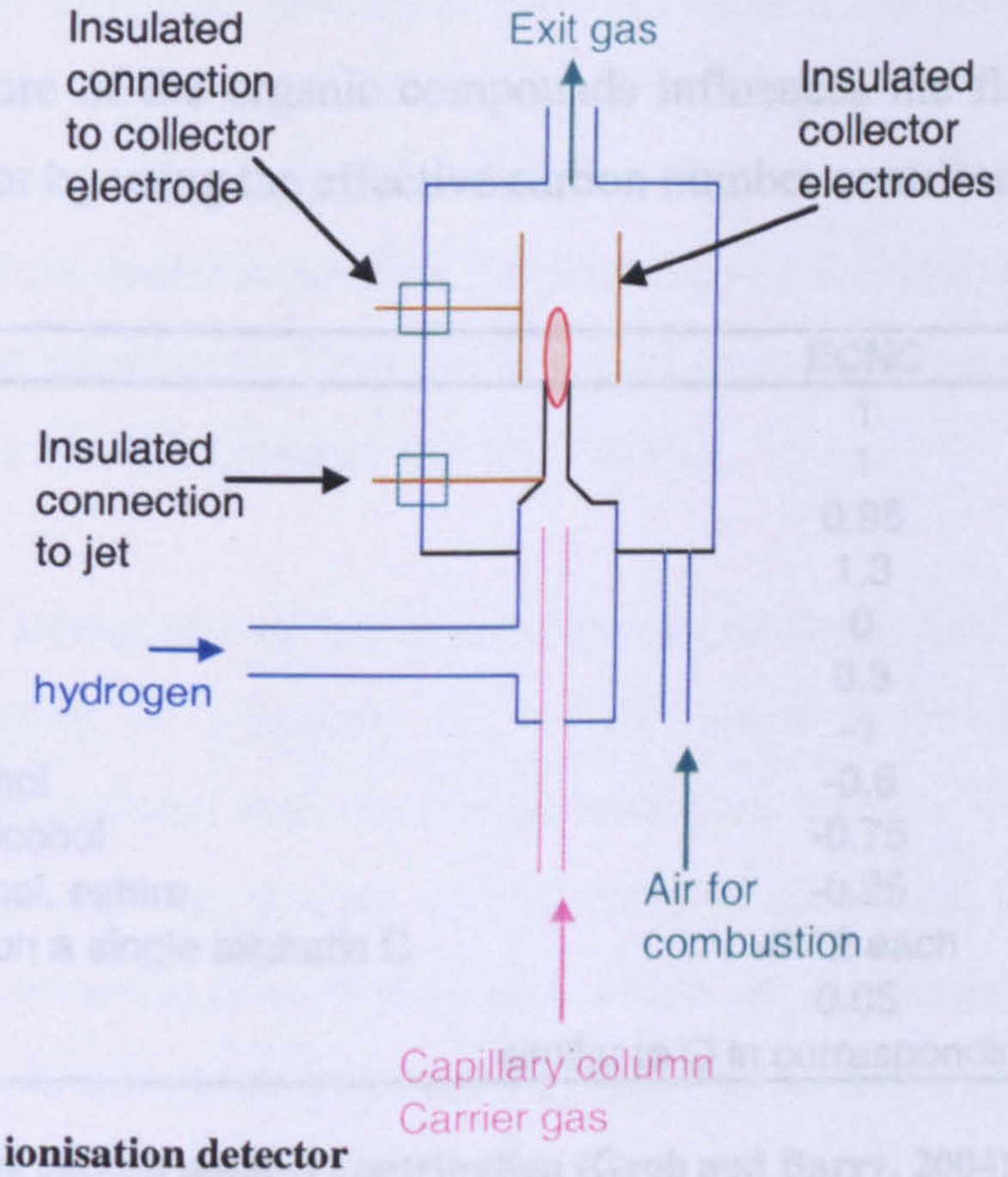

Figure 1.3 The flame ionisation detector

The FID is the predominant method for analysis of light hydrocarbons. Its popularity is due to a number of factors (Braithwaite and Smith, 1996);

- Good response to virtually all organic compounds with sensitivity down to the nanogram level.
- The FID is not affected by modest changes in temperature, pressure or flow rate, producing a stable baseline.
- Under normal operation it does not respond to common carrier gas impurities, for example CO_2 and water.
- Good linearity over a wide sample concentration range, 10^7 orders of magnitude.

The FID consists of a hydrogen-air flame to which eluted compounds from the column are directed. An electrode is positioned above the flame to collect the charge-species produced by igniting the organic compounds present in the carrier gas eluting from the GC column. Changes in current proportional to the carbon within the flame are measured and amplified by an electrometer. These signals are then sent to the

computer to be seen as peaks on the chromatogram. The FID response is such that it is effectively a quantitative counter of the carbon atoms being burned.

The chemical nature of the organic compounds influences the flame response. This can be corrected for by using the effective carbon number contribution (ECNC).

Atom	Type	ECNC
C	Aliphatic	1
C	Aromatic	1
C	Olefinic	0.95
C	Acetylenic	1.3
C	Carbonyl	0
C	Nitrile	0.3
O	Ether	-1
O	Primary alcohol	-0.6
O	Secondary alcohol	-0.75
O	Tertiary alcohol, esters	-0.25
Cl	two or more on a single aliphatic C	-0.12 each
Cl	On olefinic C	0.05
N	Amines	similar to O in corresponding alcohols

Table 1.3 The effective carbon number contribution (Grob and Barry, 2004).

1.9.2.2. Mass spectrometry

A mass spectrometer system consists of 3 major parts: an ion source, a mass analyser and detector and is used to measure the mass-to-charge ratio of ions.

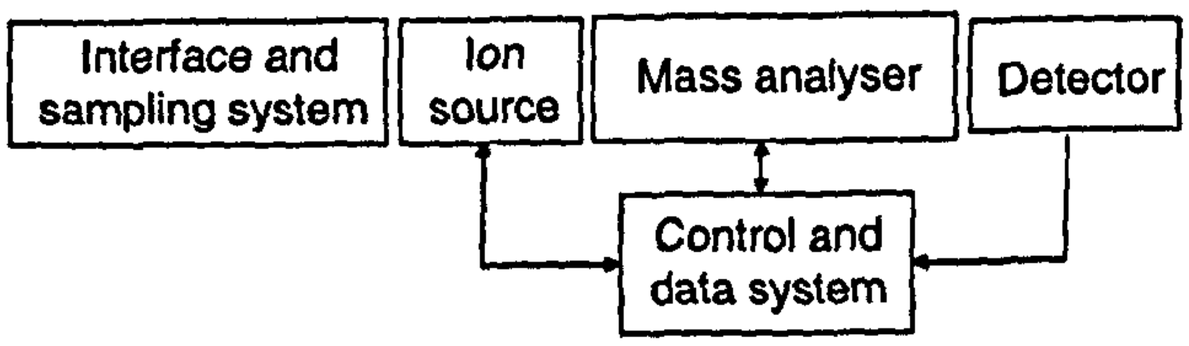

Figure 1.4 Schematic of a mass spectrometer system.

1.9.2.2.1. Ion source

The MS ion source ionises the analytes and is maintained at a pressure of $<10^{-3}$ torr (to avoid unwanted ion-molecule collisions). For GCMS the techniques for ionisation are either: electron impact ionisation (EI) or chemical ionisation (CI).

In an EI source, electrons are produced by heating a wire filament which has a current running through it. Electrons emitted at the hot filament are accelerated towards an anode as they do so, they interact with analytes eluting from the GC. Analytes are ionisied to form an unstable molecular ion which fragments to form smaller ions. The fragmentation ions produced depend on the chemistry of the analyte and the energy of the bombarding electron beam. Thus a specific fragmentation pattern is produced for each molecule (at a specific pressure and ion current).

CI is achieved by interaction of analytes with reagent ions. Analytes and a reactant gas (usually methane or i-butane) up to 10^6 times in excess of the analyte concentration are introduced into the ionisation region and are ionised by electrons. Reactions occur between the analyte, in low concentrations and the reagent ions, in high concentration resulting in secondary ions which are accelerated towards the mass analyser. CI results in a lower energy transfer, resulting in less fragmentation and thus provides extra molecular weight information.

1.9.2.2.2. Mass analyser

The mass analyser separates ions emerging from the ion source by their mass (m/z ratio). In GCMS the most common type of mass analyser is the quadrupole mass analyser.

Quadrupole mass analysers consist of four, parallel circular rods. Opposite rods are connected together electrically, a voltage is applied which consists of direct current (d.c) and radio frequency (r.f), creating an oscillating field between the rods. Ions moving into the quadrupole field begin to oscillate and only when the oscillations of the ion are stable will the ion move through the quadrupole field to the detector. Scanning is achieved by varying the d.c and r.f voltages.

1.9.2.2.3. Detector

The detector usually includes an electron multiplier. An electron multiplier is necessary since the number of ions leaving the mass analyser is small and a significant amplification is needed to produce a signal. The detector then records the current produced when an ion hits a surface. The use of a quadrupole mass analyser to scan over different ions will produce a mass spectrum, recording ions as a function of the m/z ratio.

1.9.3. Other detectors for gas chromatography

I have focussed in detail on the FID and MS detectors, as these are the two detectors used in this study. Other detectors commonly used in atmospheric measurements include:

- The electron capture detector (ECD) uses a β-emitter source to produce electrons on collision with the carrier gas. The ECD was initially designed for measurements of halogen-containing species; it provides high sensitivity to electrophilic compounds with no response to hydrocarbons (Braithwaite and Smith, 1996).
- Thermal conductivity detector (TCD) response is due to a difference in the thermal conductivity of a carrier gas due to the presence of eluted compounds. It is very widely used for detection of CS_2, COS, H_2S, SO_2, CO, CO_2, NO and NO_2 although its use for VOCs is limited due to the development in ionisation detectors which provide improved detectability (Grob and Barry, 2004).
- The photoionisation detector (PID) uses UV radiation to ionise analytes exiting the column whose ionisation potential is below the energy provided by the lamp. PIDs are highly selective, non-destructive detectors used for alkene and aromatic measurements; although its use is limited as it regularly needs calibrating due to decreasing bulb/ionisation intensity (Braithwaite and Smith, 1996).

- In helium ionisation detectors (HID), β-emitters are used to ionise helium gas leading to highly energetic helium species which ionise compounds eluting from the column. HIDs are sensitive to a broad range of compounds and are non-destructive detectors; the drawback is they contain a radioactive source (Braithwaite and Smith, 1996).

1.10. Typical NMHC concentrations

Typical Northern hemispheric NMHC concentrations are reported in Table 1.4. Birmingham and Milan show urban concentrations in the ppbv concentration range. Concentrations from remote sites taken from a North Atlantic cruise and a marine background research site on the west coast of France are in the pptv concentration range.

NMHC	Birmingham[a]	Milan[b]	MBL 80 °N[c]	Porsporder[d]
Ethane	6.7	4.8	442	800
Propane	3.7	2.2	56	300
n-Butane	3.7	3.2	10	180
i-Butane	1.7	2.9	5	120
n-Pentane	0.6	3.8	12	55
i-Pentane	0.2	4.0	6	NM
n-Hexane	0.2	0.4	6	24
Ethene	3.2	8.5	33	170
Propene	2.1	1.5	7	110
i-Butene	NM	1.2	13	NM
1-Butene	0.2	0.2	4	NM
Trans-2-butene	0.3	0.6	2	NM
Cis-2-butene	0.2	0.1	1	NM
1-Pentene	NM	NM	NM	10
Acetylene	5.7	1.4	29	160
1,3-Butadiene	0.2	0.5	1	40
Isoprene	0.1	0.1	2	110
Benzene	1.0	0.8	50	120
Toluene	2.0	3.9	31	170
Ethylbenzene	0.5	1.2	NM	34
m,p-Xylene	1.5	2.4	NM	96
o-Xylene	0.5	1.2	NM	23

Table 1.4 Typical European NMHC concentrations (a) UK, annual mean (ppbv) Derwent, 2000 (b) Italy, September mean (ppbv) Latella, et al., 2005 (c)MBL=Marine boundary layer, 80 °N summer mean (pptv) Hopkins, et al., 2002 (d) French coastal site, July mean (pptv) Boudries, et al., 1994.

1.11 Reasons for measuring NMHCs

Measurements of NMHCs are important in understanding, the direct role of NMHCs, especially for toxic NMHCs such as benzene and 1,3-butadiene. NMHC measurements are also used to assess tropospheric ozone formation and NMHC ratios are used to estimate OH radical concentrations. OH is the main oxidising agent in the troposphere, reacting with most atmospheric trace species including: CO and CH_4 which undergo oxidation by OH to eventually produce CO_2. The key to the understanding of the role of these important greenhouse gases is knowledge of the reactions and role of the OH. Since NMHC seasonal cycles are governed by reaction with OH and given the inherent difficulty in measuring OH, a common method used to estimate OH concentrations is the use of NMHC ratios (Blake, et al., 1993, Wingenter, et al., 1996, Bartenbach, et al., 2007).

1.12. Pre-concentration

Given tropospheric NMHC concentrations are in the parts per billion, ppbv and parts per trillion, pptv concentration range, pre-concentration of an ambient air sample is required to accurately detect these compounds. Pre-concentration is a method of concentrating an air sample prior to detection. Pre-concentration is usually carried out by the use of an adsorbent filled trap, held at sub-ambient temperatures, which traps compounds of interest and is rapidly heated to desorb compounds for detection by gas chromatography (a means of separating compounds) and a detector (usually FID is used for NMHC analysis).

Accurate measurements of NMHCs need to overcome a number of analytical constraints, including:

- Accurate and reliable pre-concentration of target species followed by complete desorption, with no losses of target species or desorption artefacts (see chapters 2 and 4).
- Good resolution on the chromatography column (see chapter 3).

- Use of a detector with a large linearity range and low limits of detection (see section 1.9.2).
- Development of a reliable calibration method to determine accurate concentrations in air samples (unknown) by comparison with a known, standard (see calibration details for the Medusa-GCMS in chapter 5).

In-situ, automated NMHC measurements in a remote environment must overcome these analytical issues as well as added technical constraints. The largest difference between urban measurements and those in a remote environment is the added difficulty of quantifying very low levels of NMHCs in the remote environment. This requires; excellent peak integration, lower limits of detection and higher precision than urban measurements. The pre-concentration system for a remote environment must also be very low maintenance.

Table 1.5 shows a wide variation in pre-concentration methods used in NMHC analysis. The most widely used chromatography columns for NMHC analysis are KCl and Na_2SO_4 deactivated Alumina columns. Although these columns are the most widely used for NMHC analysis, providing good resolution for all C_2-C_8 NMHCs, poor (asymmetric) peak shape of ethane and ethene has been reported on Alumina PLOT columns which can cause problems with the integration and hence, reported concentrations of ethane and ethene (Martin, 2002, Badol, et al., 2004). To try to overcome this problem, some studies have utilised dual chromatography columns (Sive, et al., 2005), where, one column analyses low boiling point hydrocarbons and the other analyses higher boiling point hydrocarbons. A two-step analysis approach has also been used, utilising dual-traps and dual-columns (Wang, et al., 2004) to try and achieve better separation, resolution and detection. Other factors then have to be addressed; ensuring reproducible and reliable methods for splitting an air sample to two columns and addressing time constraints when using a two-step analysis approach.

Most pre-concentration methods use multi-bed adsorbent traps to pre-concentrate an air sample, using thermoelectric devises to maintain a sub-ambient trapping temperature (Badol, et al., 2004, Lewis, et al., 1997, Slemr, et al., 2004). Glass bead traps have also been used at very low, -180 °C temperatures, mainly achieved by the

use of liquid N_2 (Boudries, et al., 1994, Swanson, et al., 2003). Sub-ambient temperatures are used to increase the sample volume (this is discussed in more detail in chapters 2 and 4) and decreasing the limit of detection (chapter 5). When pre-concentrating a sample, a larger sample volume can be achieved by either reducing the pre-concentration trapping temperature or increasing the trap size (amount of adsorbent). This explains why in most cases where thermoelectric devices have been used to maintain trap temperature the sample volume is smaller than at lower temperatures (Table 1.5).

Since pre-concentration of an air sample relies upon sub-ambient temperatures, water must be removed from ambient air to prevent ice forming in the adsorbent trap and blocking the sample flow. Water management has been addressed in a number of ways, the most common methods being; a magnesium perchlorate trap or Nafion drier. Both methods have limitations; the magnesium perchlorate trap requires regular maintenance, Martin, 2002 found this trap to be unsuitable for long-term measurements of NMHCs at Mace Head. The Nafion drier is known to cause alkene artefacts, particularly for propene and butene isomers (Martin, 2002, Boudries, et al., 1994).

Column(s)	Pre-concentration	Water removal	Reference
CP Sil 5CB (50 m, 0.25 mm) Al_2O_3/Na_2SO_4 (50 m, 0.32 mm)	Carbopack B + Carbosieve SIII, -30 °C, 600 ml	Nafion	Badol, et al., 2004
Al_2O_3/KCl (25 m, 0.53 mm)	Carbotrap C + Carbotrap + Carbosieve SIII, -180°C, 1200 ml	Nafion	Boudries, et al., 1994
Al_2O_3/KCl (30 m, 0.53 mm)	Stainless steel tubing at -180 °C, 400 ml	Nafion	Lee, et al., 2006
Al_2O_3/Na_2SO_4 (50 m, 0.53 mm)	Activated charcoal, -25 °C, 1200 ml	Dreschel flask at -8 °C + $[Mg(ClO_4)_2]$ trap	Lewis, et al., 1997 Hopkins, et al., 2002
Al_2O_3/KCl (50 m, 0.32 mm)	Carbosieve SIII + Carboxen 1003 + Carbotrap, -45 °C, 500 ml	Nafion	Martin, 2002
Al_2O_3/KCl (50 m, 0.32 mm)	Carboxen 1000 + Carbopack B, -10 °C, 500 ml	$[Mg(ClO_4)_2]$	Saito, et al., 2000
Al_2O_3/Na_2SO_4 (50 m, 0.53 mm) VF-5ms (60 m, 0.32 mm)	Glass bead trap, -175 °C, 500 – 2000 ml	-20 °C water trap	Sive, et al., 2005
Al_2O_3/Na_2SO_4, (50 m, 0.53mm)	Carbotrap, –25 °C, 400 ml	$[Mg(ClO_4)_2]$+ NaOH	Slemr, et al., 2004
Al_2O_3/KCl, (50m, 0.32 mm)	Carbosieve SIII + Carbotrap + Carbotap C, –30 °C, 500 ml	NaOH	Slemr, et al., 2004
Al_2O_3/KCl, (25 m 0.32 mm)	Carbosieve SIII + Carbotrap + Carbotap C, –21 °C, 1800 ml	Nafion	Slemr, et al., 2004
Al_2O_3/Na_2SO_4, (50 m, 0.53 mm)	Carbosieve SIII + Carbotrap + Carbotrap C, –25 °C, 800 ml	Cold trap + K_2CO_3	Slemr, et al., 2004
Al_2O_3/Na_2SO_4, (50 m, 0.53mm)	Carbosieve SIII, –40 °C, 500 ml	Cold trap + K_2CO_3	Slemr, et al., 2004
CP Sil 5 CB, (50 m, 0.32mm)	Carbotrap + Carbosieve SIII, –10 °C, 2000 ml	None	Slemr, et al., 2004
Silica PLOT (30 m, 0.53 mm)	Glass bead trap, -180 °C, 1519 ml	Whatman air drier	Swanson, et al., 2003
Al_2O_3/KCl (30 m, 0.32 mm) DB-1 (60 m, 0.32 mm)	a) Carbosieve SIII + Carboxen 1000, -30 °C b) Carboxen 1000, Carboxen 1003, 30°C + Carbotrap 200 ml on both traps	None used (limited sample volume to prevent water blocking traps)	Wang, et al., 2004

Table 1.5 Common methods used for pre-concentration.

1.13. Aims

The aim of this thesis is to analyse NMHC data from Mace Head research station, Ireland obtained from the Medusa-GCMS pre-concentration system and to design and develop an improved pre-concentration system for the analysis of NMHCs which will be located at Mace Head for routine NMHC analysis.

The University of Bristol Atmospheric Research Group has measured NMHCs at Mace Head Research station since 2001. From 2001-2004 a specially designed NMHC adsorption-desorption system (ADS) coupled with GC and FID (ADS-GCFID) measured the full range of C_2-C_8 hydrocarbons at Mace Head (Martin, 2002). Also situated at Mace Head was an ADS coupled with GCMS (ADS-GCMS) designed to measure halocarbons and a select number of NMHCs: n-butane, i-butane n-pentane, 1,3-butadiene, isoprene, benzene and toluene. A comparison was made between the two instruments to validate NMHC results (Martin, 2002). The ADS-GCMS was decommissioned in 2004 and replaced by the Medusa-GCMS, an improved pre-concentration system for the analysis of halocarbons. The Medusa-GCMS also measured ethane, benzene and toluene. The NMHC compounds measured by the Medusa-GCMS was extended in January 2005 to include; ethane, propane, n-butane, i-butane, n-pentane, i-pentane, isoprene, benzene, toluene, m,p-xylene, o-xylene and ethylbenzene. Based on the experience and lessons learnt measuring NMHCs at Mace Head, a new pre-concentration system was developed to specifically target C_2-C_8 NMHCs.

Problems associated with the previous ADS-GCFID NMHC instrument (Martin, 2002):

- Trapping issues; 500 ml sample volume is too small a volume to detect the low levels of NMHCs, such as butene isomers in clean, background air samples. The adsorbent filled trap also produced benzene artefacts caused by heating the trap during desorption to the chromatography column.
- chromatography issues; poor peak shape of ethane and ethene, co-elution of m-xylene and p-xylene, co-elution of i-butane and acetylene, high affinity for water on the Alumina PLOT column and long analysis time.

- Water management issues; a Nafion drier was used to remove water from ambient air. Martin, 2002 reported propene and butene isomer artefacts from the Nafion drier.

NMHC measurements on the Medusa-GCMS are limited by number as the Medusa-GCMS is part of the Advanced Global Atmospheric Gas Experiment, AGAGE international network measuring HFCs, HCFCs and SF_6. Additional NMHC measurements could not interfere with the measurements of the core AGAGE target species, hence only a select number of NMHCs can be measured. The Medusa-GCMS uses 2 Nafion driers to remove water from ambient air samples so accurate measurements of alkenes were not possible, except isoprene which is not affected by the presence of the Nafion driers.

The main aim of the new NMHC system is to remove the reliance of the Nafion membrane drier to remove water from ambient air samples. Nafion is a co-polymer of perfluoro-3,6-dioxa-4-methyl-7-octene-sulfonic acid and tetrafluoroethylene (Teflon) that selectively removes water from an air sample. Water moves through the membrane wall and evaporates into the counter-flow of dry air, a process called perevaporation. This process is driven by the humidity gradient between the inside and the outside of the tubing (Permapure, 2007). The Nafion is known to cause alkene artefacts, particularly for the butanes (Martin, 2002). Another common method for water removal is the magnesium perchlorate trap. Doskey (1991) reported an accuracy of C_2-C_8 hydrocarbon analysis of 90 % when using magnesium perchlorate as the water removal stage. However, magnesium perchlorate traps require increased maintenance and were found unsuitable for measurements in remote research stations (Martin, 2002). Novel methods for water management have been investigated in this study, including; the use of a bulk-trap to fractionate between C_2 hydrocarbons, water and C_3 hydrocarbons, a dual-trap dual-column method, requiring a two-step analysis approach and a water trap held at -20 °C to remove water from ambient air samples.

A number of adsorbents have been tested for their efficiency in the adsorption of the most volatile hydrocarbons (C_2 and C_3 hydrocarbons) for use in the adsorbent filled traps used to pre-concentrate samples. A range of chromatography columns have also

been tested for their separation and resolution of NMHCs. A new instrument has been designed and developed and thoroughly tested for its ability to analyse NMHCs.

Analysis of two years NMHC data from the Medusa-GCMS in Mace Head has been performed. To my knowledge, this is the first reported long-term measurements of NMHCs using GCMS. Long term in-situ measurements of NMHCs allow trends and seasonal cycles to be determined. Given the predominant removal mechanism for hydrocarbons is by reaction with the OH radical a lot of information can be determined from these. From the amplitude of the seasonal cycle relative lifetimes can be determined and any deviation in sources. Trends such as alkane isomer ratios suggest tropospheric loss rates and can be used to assess the photochemical aging of an air sample, from anthropogenic source to receptor, the remote Mace Head research site. Mace Head is on the edge of Europe and dominated by westerly winds, hence emissions from the USA of long-lived pollutants (ethane and propane) can be monitored. Mace Head is a coastal location and surrounded by peat bog and forest, hence biogenic emissions from the ocean and land can be measured. Trajectory analysis has been performed on the data, sorting data into four sectors; Ultra clean (S-SW), Westerly (W), High latitude (N) and European (E). A photochemical trajectory model (PTM) and the Met Office's NAME model have been utilised to further examine Mace Head NMHC in detail.

2. Retention of analytes on selected adsorbents

2.1. Introduction

NMHCs in the ambient remote atmosphere are present in the parts per trillion, pptv concentration range (1 in 10^{12} v/v). The trace levels of NMHCs can not be detected by direct sampling to a gas chromatograph and detector (flame ionisation detector). Analysis of NMHCs requires a pre-concentration step to "concentrate" an air sample prior to detection. For long-term in-situ measurements pre-concentration is achieved by sample enrichment on solid adsorbents under sub-ambient conditions (Simmonds, et al., 1997; Lewis, et al., 1997; Slemr, et al., 2004). An ideal adsorbent for pre-concentration of NMHCs should meet the following criteria:

- Complete enrichment for the compounds of interest. The adsorption strength of an adsorbent is given by the breakthrough volume (BTV) of the compounds.
- Complete and fast desorption of the target compounds.
- No generation of artefacts.
- Low affinity to water and inorganic components, such as nitrogen oxide or carbon dioxide.
- High mechanical and thermal stability.

The specific breakthrough volume is defined as the volume of gas that causes a compound to migrate through an adsorbent bed of one gram at a specific temperature (Dettmer and Engewald, 2002). Applications of the BTV include being able to calculate the maximum volume of sample that can be concentrated onto the adsorbent before breakthrough losses occur. The convention for practical purposes is to use two thirds of the reference BTV in sampling an analyte, in order to ensure a safe sampling volume (Kroupa, et al., 2004).

There are two direct experimental methods to determine BTVs, the elution technique and the frontal technique. The two techniques have good correlation for more volatile

compounds, with greater variation between the methods for higher boiling compounds (Dettmer and Engewald, 2002).

2.1.1. The Elution Technique

The elution technique requires a single injection of analyte directed onto the adsorbent which is then purged with a carrier gas onto a chromatography column and detector. The gas chromatography (GC) detector records a Gaussian shaped peak as the analyte elutes from the adsorbent bed. The breakthrough of the sample is due to the migration of the analyte through the adsorbent bed. For this model to work it assumes infinite dilution of the analyte. The reduced breakthrough time is defined as the intersection between the base line and the starting gradient of the elution peak.

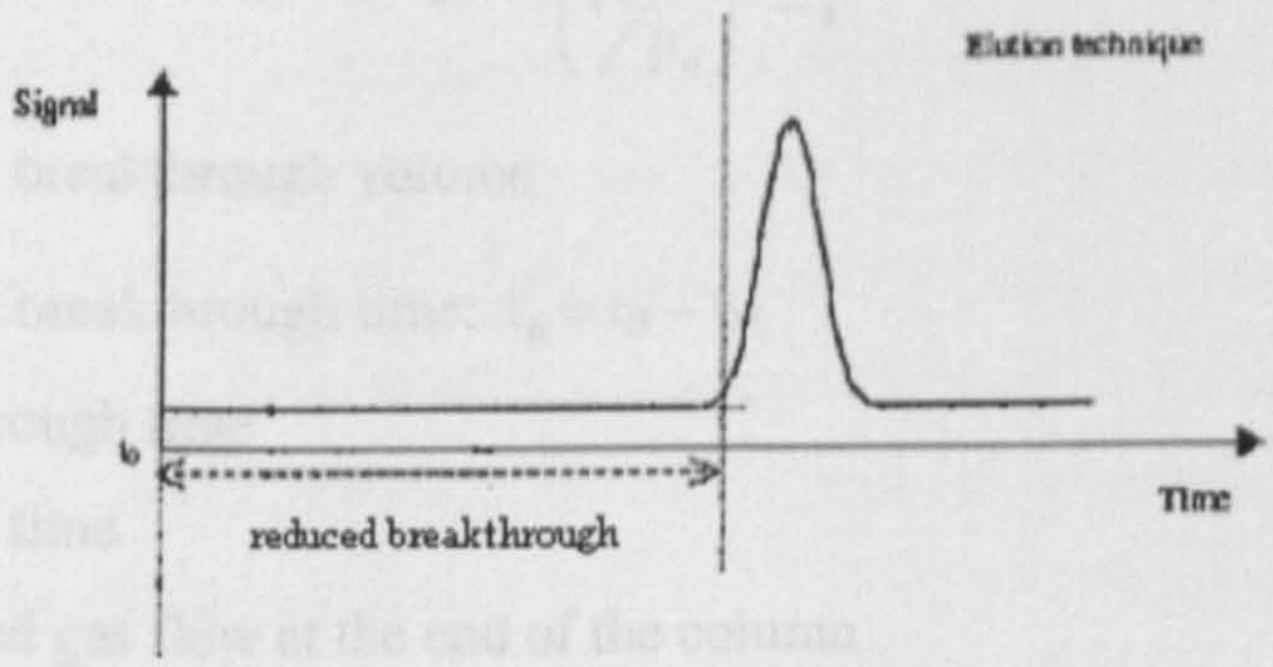

Figure 2.1 Chromatogram for the elution technique (Dettmer and Engewald, 2002).

2.1.2. The Frontal Technique

A continuous flow of gaseous sample is transported through the system. Molecules occupy adsorbent sites on the adsorbent material as the analyte flows through. Breakthrough occurs when all the available adsorption sites are occupied. This chromatogram is called a frontal chromatogram, see Figure 2.2. On this chromatogram, the reduced breakthrough time is defined as the point where there is an increase from the baseline noise.

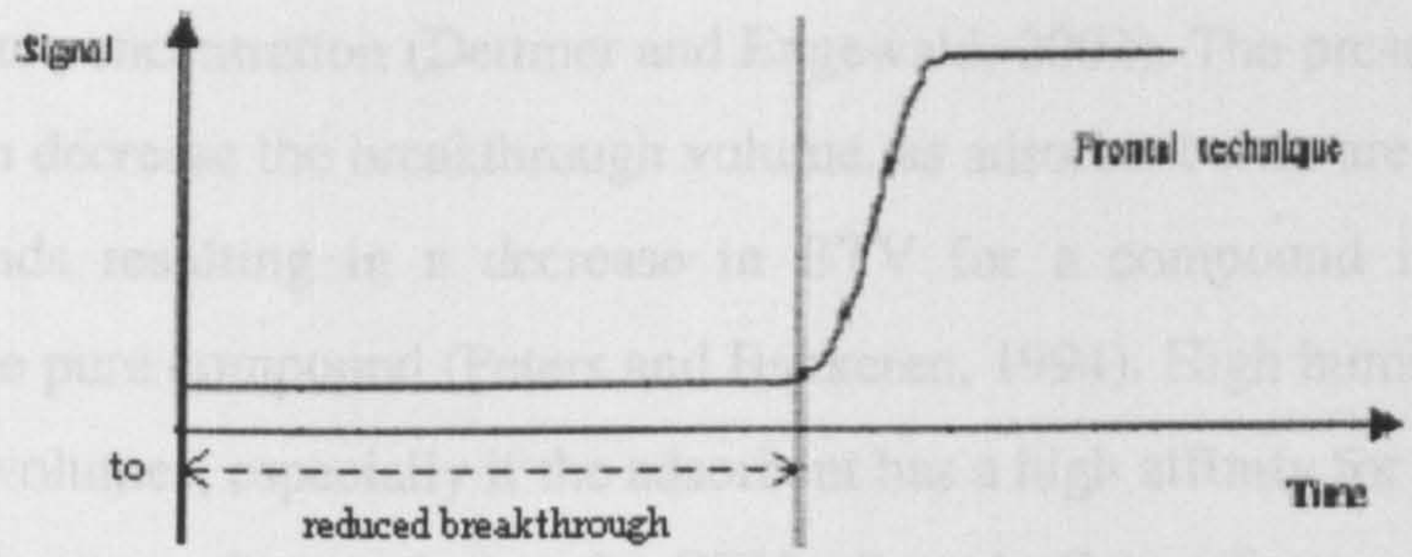

Figure 2.2 Chromatogram for the frontal technique (Dettmer and Engewald, 2002).

From the reduced breakthrough times determined via either method, the specific BTV can then be calculated using the following equation (Dettmer and Engewald, 2002):

2.1.
$$V_{g(B)}^{\theta} = \frac{t_B^{'}}{m_A} * F_a \frac{T_c}{T_a} * \frac{3}{2} \frac{\left(p_i / p_o\right)^2 - 1}{\left(p_i / p_o\right)^3 - 1}$$

$V_{g(B)}^{\theta}$ specific breakthrough volume

$t_B^{'}$ reduced breakthrough time: $t_B^{'} = t_B - t_M$

t_B breakthrough time

t_M hold-up time

F_a measured gas flow at the end of the column

T_a temperature at the end of the column

T_c column temperature

p_i column head pressure

p_o pressure at the end of the column

m_A adsorbent mass

In experimentation, the overall difference between the reduced breakthrough volume and the specific breakthrough volume is generally negligible, so this equation does not have to be used. However, it is useful in order to understand the parameters that can affect the BTV.

The breakthrough behaviour of a compound is affected by a number of different properties. Breakthrough volume decreases with increasing analyte concentrations, although at low concentrations (3-20 $\mu g\ L^{-1}$) breakthrough volume is independent

from the analyte concentration (Dettmer and Engewald, 2002). The presence of other compounds can decrease the breakthrough volume, as adsorbent sites are occupied by other compounds resulting in a decrease in BTV for a compound in a mixture compared to the pure compound (Peters and Bakkeren, 1994). High humidity reduces break-through volumes, especially if the adsorbent has a high affinity for water, water will occupy adsorbent sites, reducing the BTV. Sample flow effects a compound's residence time over the adsorbent, sufficient time must be given for interactions between analyte and adsorbent to occur. Increasing trapping temperature results in a decrease in BTV (Dettmer and Engewald, 2002).

2.1.3. Thermal Desorption

Thermal desorption occurs after the sampling stage, the adsorbent-filled trap is rapidly heated (and held at the desorption temperature for 30-60 seconds) to desorb trapped analytes. A carrier gas, usually helium, purges the trap during desorption and transfers analytes as a fast "plug" to a chromatography column (Harper, 2000). The volume of carrier gas required to fully remove the trapped analyte is known as the thermal desorption volume. Thermal desorption allows complete transfer of all analytes into the gas chromatographic system.

2.2. Adsorbent Types

2.2.1. Active carbon, graphitized carbon and carbon molecular sieve

Active carbon is made out of carbon-containing biological materials, such as wood and coconut shells (Dettmer and Engewald, 2002). Active carbons are micro-porous with a high specific surface area (800-1500 $m^2 g^{-1}$) resulting in active carbons being very strong adsorbents. Active carbons are especially suited to sampling low-molecular weight VOCs. However, these strong adsorbent properties can also be a disadvantage, making it difficult to desorb some compounds after they have been collected. Because of this it is rarely used in the monitoring of NMHCs in ambient air.

Carbon molecular sieves (CMS) are micro-porous with high specific surface areas (1000-1500 m^2 g^{-1}) and sharp pore size distribution. Adsorption is by non-specific interaction (dispersion, induction) and occurs for molecules small enough to pass through the pores, although adsorption can occur on the surface of CMS due to the presence of trace metals, salts of functional groups present (Dettmer and Engewald, 2002).

Graphitized carbons are non-polar adsorbents with a homogenous surface and a lower specific area (5-260 m^2 g^{-1}). Adsorption is by non-specific interactions (as with CMS). Molecule size, shape and also degree of polarity determine adsorption strength. For example, n-butane has a higher BTV than i-butane due to the increased number of contacts with the graphitized carbon surface (Dettmer and Engewald, 2002).

Graphitized carbon and CMS are widely used for sampling VOCs in ambient air. They are less hydrophilic and easier to desorb than activated carbon. Examples of graphitized carbon blacks include Carbotrap and Carbograph ranges. CMS include Carboxen, Carbosieve, Anasorb and Spherocarb.

2.2.2. Porous organic polymers

Porous organic polymers are a large group of adsorbents with different surface areas and polarities. This group of material includes Hayesep and Tenax TA. Porous carbon adsorbents have a homogeneous hydrophobic surface. These adsorbents are stable over a wide pH range; however, some have limited temperature stability, which confines the use of thermal desorption (Dettmer and Engewald, 2002). C_2-C_8 NMHCs vary widely in terms of their volatility (boiling points: ethene -104 °C to o-xylene 144 °C). To fully desorbe the less volatile NMHCs, high desorption temperatures are needed (at least 200 °C). Heating porous organic polymers to high temperatures can produce desorption artefacts; when using a non-selective detector, such as the flame ionisation detector, the response to the artefacts can swamp the whole chromatogram.

2.2.3. Inorganic adsorbents

Inorganic adsorbents cover a wide range of adsorbent types including silica gel, alumina, zeolites and conventional molecular sieves (e.g. 5A, 4A). Silica gel is a porous, amorphous form of silica (SiO_2). Its structure is an extensive network of interconnected microscopic pores, with a wide range of possible diameters; silica gel interacts with analytes by physisorption. Zeolites are minerals with a micro-porous structure; HiSiv, is a type of zeolite, with a crystalline, inorganic silica-alumina structure. Aluminium oxide (Al_2O_3) is a highly polar material and requires deactivation to block some of its excessive active sites. Inorganic salts such as potassium chloride (KCl) and sodium sulphate (Na_2SO_4) are often used as deactivation agents, producing stable deactivation up to 200°C. Molecular sieves consist of an aluminium silicate skeleton with regular sized and shaped pores, which adsorb molecules small enough to pass through the pores. For example, molecular sieve 4A adsorbed ethane (0.4 mm diameter) but not n-butane (0.5 mm diameter).

2.3. Aims

The main concept for the new NMHC instrument is to remove the dependence on the Nafion drier to remove water from ambient air samples prior to pre-concentration using sub-ambient trapping conditions (see Section 1.12). A novel idea of water management was devised, consisting of a bulk-trap maintained at ambient temperature and two separate micro-traps, held at sub-ambient temperatures using Peltier coolers. Only C_2 hydrocarbons are directed through the Nafion drier, since these are not affected by the presence of the Nafion drier. $\geq C_3$ hydrocarbons do not flow through the Nafion drier, removing the possibility for alkene reactions and losses to the Nafion drier.

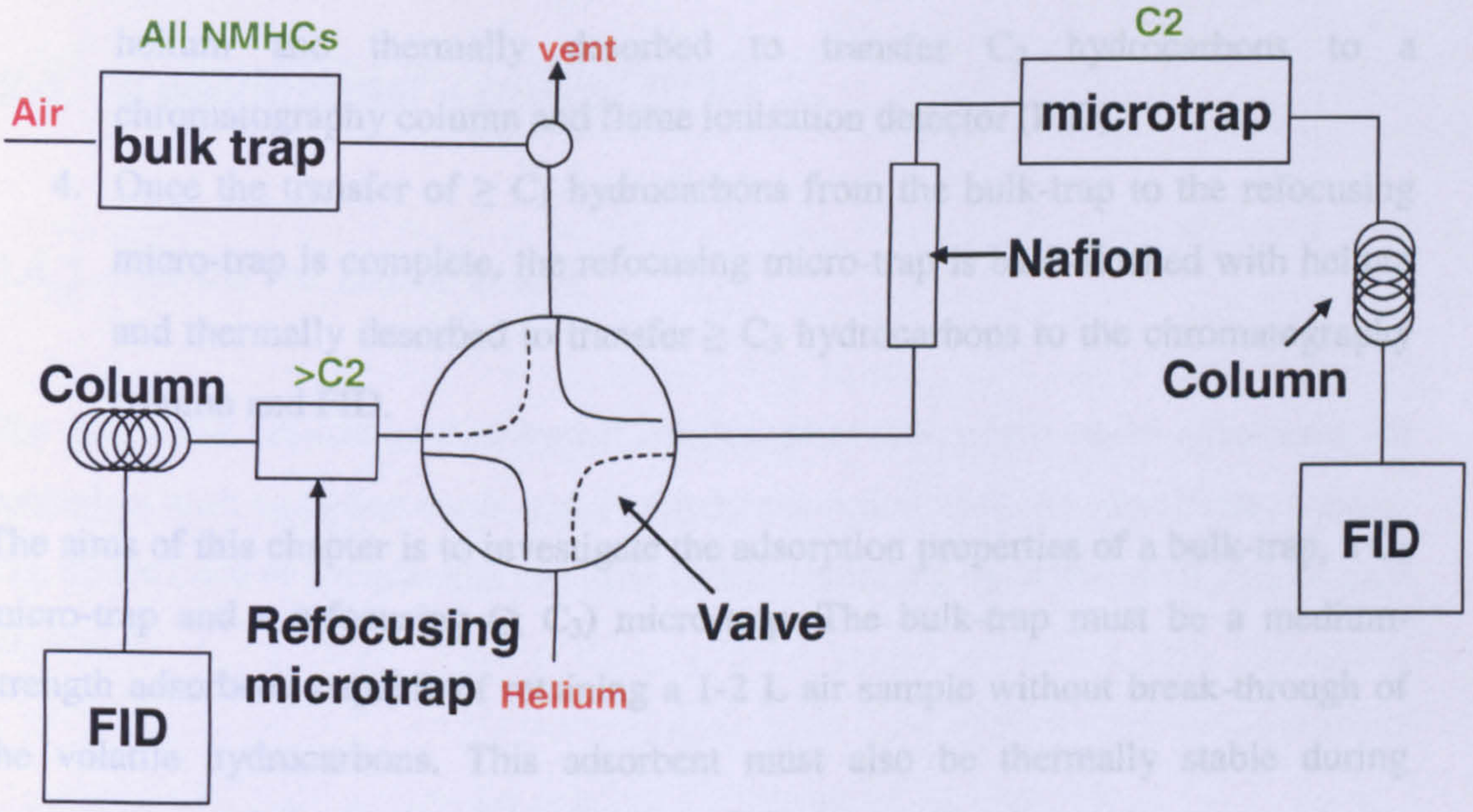

Figure 2.3 Block diagram illustrating the design of the NMHC instrument.

The pre-concentration of NMHCs on the new instrument can be separated into a number of steps:

1. An air sample is pre-concentrated, firstly on an adsorbent-filled bulk-trap, held at room temperature. The use of a bulk-trap enables a large sample volume to be taken (1-2 L) before break-through of volatile hydrocarbons can occur.
2. Once the sampling stage is complete, the bulk-trap is to be purged with the carrier gas (helium) to transfer volatile (C_2) hydrocarbons and water from the bulk-trap, through a Nafion drier to a specially selected C_2 micro-trap. C_2 hydrocarbons are unaffected by the Nafion drier (see Section 1.12). The C_2 micro-trap requires a strong adsorbent capable of retaining C_2 hydrocarbons during the bulk-trap helium purge stage.
3. Once the C_2 hydrocarbons have been transferred to the C_2 micro-trap the bulk-trap is thermally heated and back-flushed with helium to transfer the less volatile ($\geq C_3$) hydrocarbons from the bulk-trap to a specially selected refocusing micro-trap. The re-focusing micro-trap is required as direct thermal desorption from the bulk-trap to a GC chromatography would over-load the column and result in broad, un-resolved peaks. Whilst the bulk-trap is being back-flushed to the refocusing trap, the C_2 micro-trap is back-flushed with

helium and thermally desorbed to transfer C_2 hydrocarbons to a chromatography column and flame ionisation detector (FID).

4. Once the transfer of $\geq C_3$ hydrocarbons from the bulk-trap to the refocusing micro-trap is complete, the refocusing micro-trap is back-flushed with helium and thermally desorbed to transfer $\geq C_3$ hydrocarbons to the chromatography column and FID.

The aims of this chapter is to investigate the adsorption properties of a bulk-trap, a C_2 micro-trap and a refocusing ($\geq C_3$) micro-trap. The bulk-trap must be a medium-strength adsorbent, capable of retaining a 1-2 L air sample without break-through of the volatile hydrocarbons. This adsorbent must also be thermally stable during desorption and fully desorbe less volatile hydrocarbons. The C_2 micro-trap requires a strong adsorbent, capable of retaining C_2 hydrocarbons for the transfer volume from the bulk-trap. The refocusing micro-trap requires a medium-strength adsorbent with similar properties to the bulk-trap.

2.4. Experimental – frontal BTVs

2.4.1. Set-up for Micro-traps

The micro-trap consists of thin-walled stainless steel tubing into which adsorbents are packed; at each end glass beads and a hypodermic rod secures the adsorbents in place. The dimensions of hypodermic rod used varied depending upon the mesh size of each adsorbent.

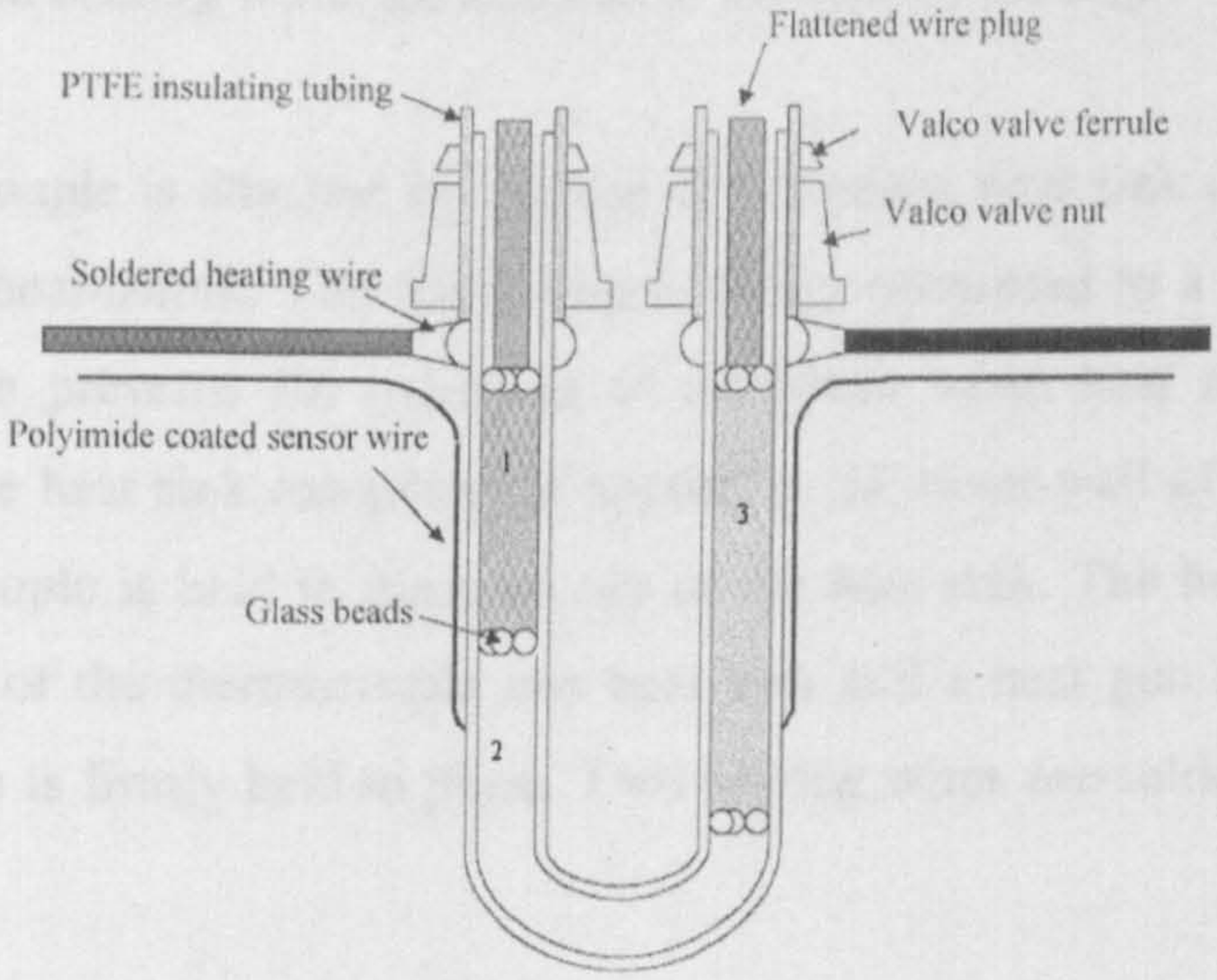

Figure 2.4 Schematic of a micro-trap (Martin, 2002). 1, 2 and 3 indicate possible different adsorbents which can be added to produce a multi-bed adsorbent trap; here only single-bed adsorbents were tested.

Trap length	Outer diameter	Inner diameter
180 mm	1.07 mm	0.81 mm

Table 2.1 Typical dimensions of micro-traps used in the frontal BTV experiments.

2.4.1.1. Construction of the micro-trap

Stainless steel tubing was cut to the correct length. This was then cleaned by sucking acetone and methanol through the trap using a syringe, and placed in an oven set to 70 °C to dry. Once dry, the hypodermic rod was placed in one end of the micro-trap. The micro-trap was connected to a pump and glass beads were sucked into the trap. Adsorbent was sucked into the trap followed by glass beads and the 2nd hypodermic rod. Throughout this process a Dremel was used to apply a vibration to the micro-trap and so prevent adsorbent material sticking to the inner walls of the trap. The trap is bent into positions and a k-type thermocouple is attached to the bottom of the u-shape micro-trap and heating wires are attached to the ends of the trap.

The thermocouple is attached by the use of a silicone heat sink compound and high temperature heat-shrink. The micro-trap is firstly connected to a continuous flow of helium which prevents the oxidation of adsorbent when heat is applied. A small amount of the heat sink compound is applied to the outer-wall of the micro-trap and the thermocouple is held in place on top of the heat sink. The heat-shrink is placed over the top of the thermocouple and heat sink and a heat gun is applied until the thermocouple is firmly held in place. Two heating wires are soldered to each end of the trap.

2.4.1.2. Trap conditioning

Each micro-trap must be conditioned prior to use to remove any potential contamination from the adsorbent. In order to condition a micro-trap it must be connected to a supply of ultra clean helium and directed to vent to prevent contamination of the system. An electrical current is passed through the heating wires and trap walls leading to rapid trap heating. The trap temperature is continually monitored by the k-type thermocouple which relays the trap temperature to a display.

The heating parameters of a micro-trap are checked by heating the trap to lower temperatures and working up to its maximum operating temperature. For example, heating the trap three times to 50 °C hold 1 minute, repeat to 100° C, 150 °C and so on until the maximum temperature is reached. Then the trap is held at its maximum temperature for a period of time (1 hour). The micro-trap was also pulse-heated prior to use. The micro-traps were heated to their maximum operating temperature, remaining at this temperature for 1 minute then allowed to cool for 3 minutes; this was repeated at least ten times for each micro-trap.

The micro-trap is housed in a Peltier cooling system which allows the micro-trap to be tested at sub-ambient temperatures (set to -50 °C) see section 2.4.2. Sub-ambient trapping temperatures are required given the capacity of micro-traps is not large enough to prevent break-through of the volatile, C_2 hydrocarbons at room temperature. Reducing the trapping temperature increases the sample volume which can be taken prior to break-through of the volatile hydrocarbons.

2.4.2. Peltier Coolers

Peltier coolers have been used in many previous instruments designed by the University of Bristol with continuing success; they allow a trapping temperature of approximately -50 °C without the use of expensive liquid cryogens.

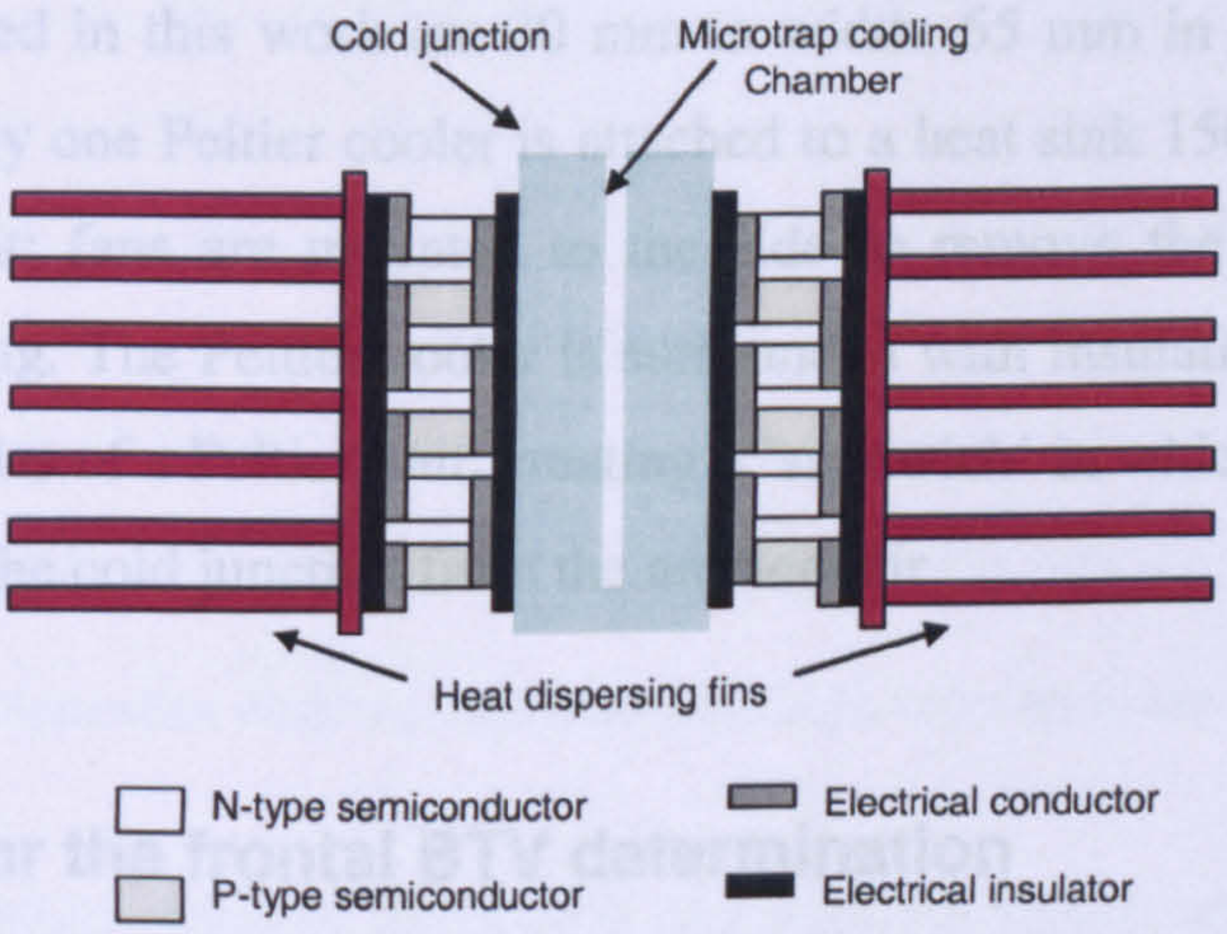

Figure 2.5 Cross section of a Peltier cell

When a DC current is passed through two semiconductors (n-type and p-type) connected to each other at two junctions, heat will be produced at one junction and adsorbed at the other, depending on the direction of current flow.

The Peltier cooler consists of alternating n-type (high energy levels) and p-type (low energy levels) bismuth telluride semiconductors connected by a copper junction. The n-type and p-type couples are connected in series to form a circuit which keeps the heat moving in the same direction. Passing current through the circuit results in heat being adsorbed at the cold junction as electrons move from the p-type semiconductor to the n-type semiconductor. At the hot junction, energy is released as the electrons move from the low energy levels in the p-type to the high energy levels of the n-type and vice versa at the top junction (Figure 2.6).

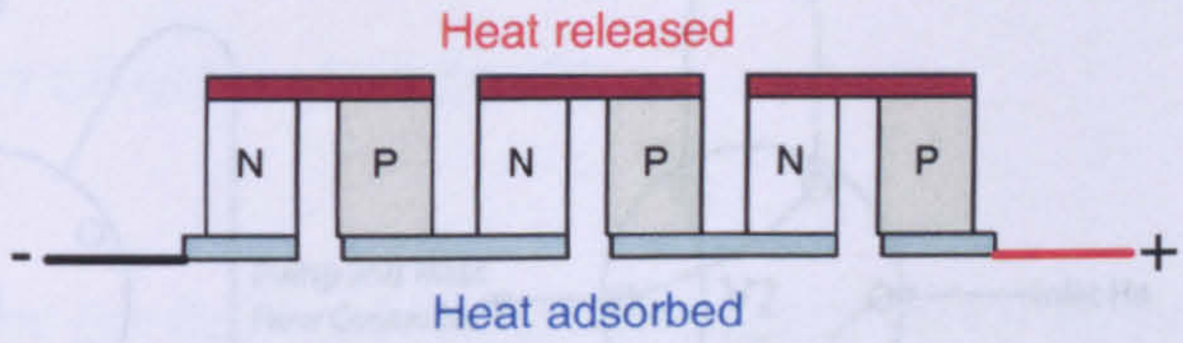

Figure 2.6 Diagram describing the Peltier junction.

Peltier coolers used in this work are 30 mm in width, 65 mm in height and 20 mm thick. Traditionally one Peltier cooler is attached to a heat sink 150 mm in width and 100 mm in height; fans are mounted to the side to remove the released heat and prevent overheating. The Peltier cooler is surrounded with insulating foam, the same is done to both sides of a Peltier unit, creating a `sandwich' in which the micro-trap is housed, isolating the cold junction from the ambient air.

2.4.3. Set-up for the frontal BTV determination

An adsorption desorption system (ADS) attached to a gas chromatography-flame ionisation detector (GC-FID) was used to determine the BTV of C_2 and C_3 hydrocarbons using various adsorbent traps. The ADS was developed at Bristol University to carry out routine sampling of CFCs, HFCs and HCFCs in air samples. The ADS operates as a fully automated sampling, calibration and analysis system controlled by a computerised system, which is operated using a programming language unique to the ADS (Simmonds, et al., 1997).

A HP-5 (29.5 m, 0.32 mm, 0.25 μm) stationary phase GC column was used. The GC oven was operated isothermally at 100°C.The ADS is a three valve (Valco) system as shown in Figure 2.7.

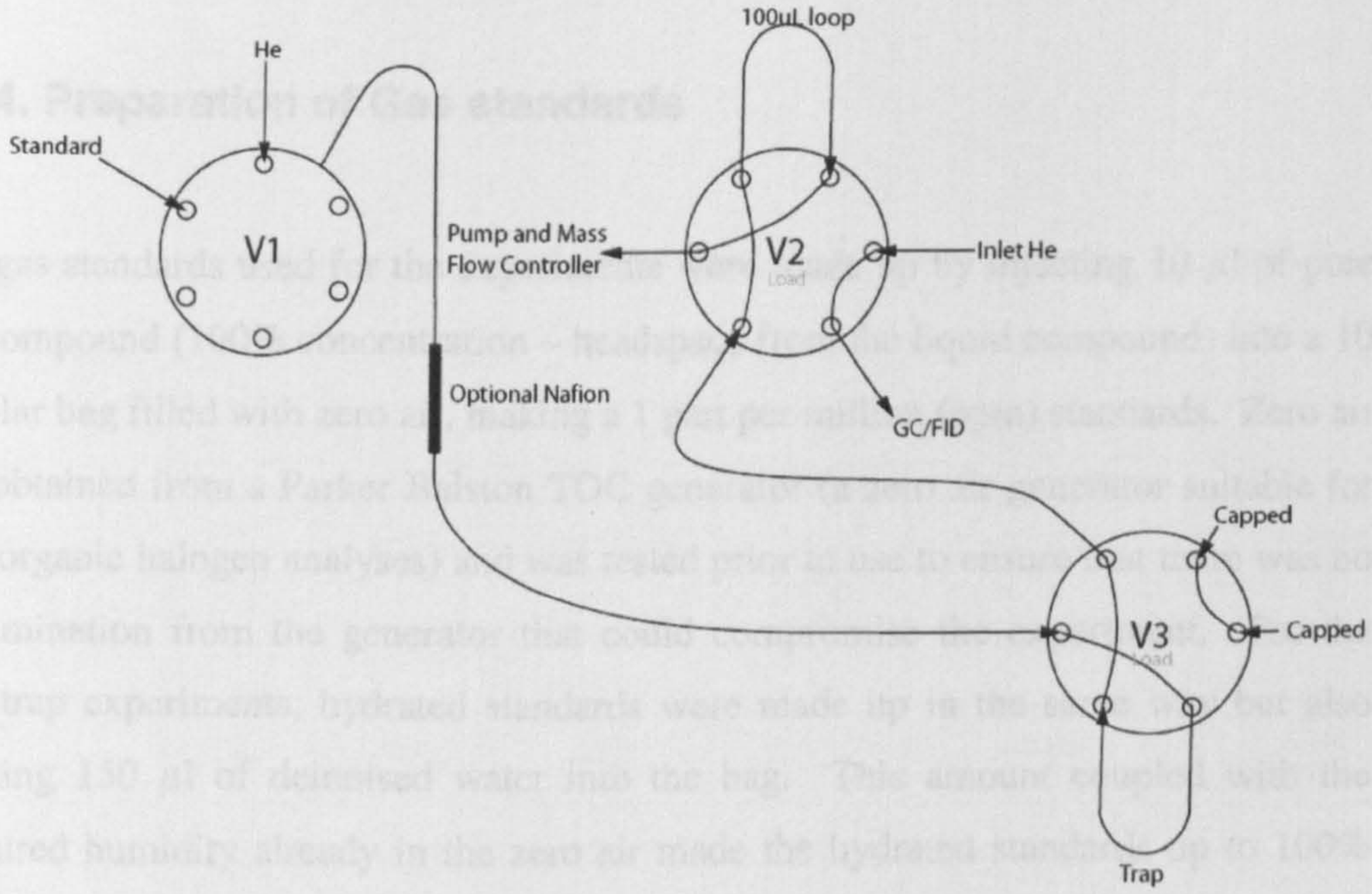

Figure 2.7 Valve configuration diagram with each 2 position valve set in the load position

Valve 1 (V1): A 6-port selector valve with two possible inputs, although it was only used in two positions. In position one the input is the carrier gas, helium. Position 2 samples the standard.

Valve 3 (V3): A two-position valve, that can be set in the load or inject position. In the load position, shown in Figure 2.7, the gas flows through the trap and onto valve 2. In the inject position the gas flows directly to valve 2.

Valve 2 (V2): A two-position valve, that can be set in the load or inject position. In the load position, shown in Figure 2.7, the gas sample coming from valve 3 flows through the 100 μl loop and continues on to the pump and mass flow controller. When in the inject position the 100 μl of gas sample that has been collected in the loop is injected onto the GC-FID.

2.4.4. Preparation of Gas standards

The gas standards used for the experiments were made up by injecting 10 μl of pure gas compound (100% concentration – headspace from the liquid compound) into a 10 l Tedlar bag filled with zero air, making a 1 part per million (ppm) standards. Zero air was obtained from a Parker Balston TOC generator (a zero air generator suitable for total organic halogen analyses) and was tested prior to use to ensure that there was no contamination from the generator that could compromise the experiment. For the bulk trap experiments, hydrated standards were made up in the same way but also injecting 150 μl of deionised water into the bag. This amount coupled with the measured humidity already in the zero air made the hydrated standards up to 100% relative humidity at room temperature.

2.4.5. Procedure

For each standard that was investigated on each different adsorbent material, the following sequence was carried out:

- A 100 μl loop injection of zero air from the Tedlar bag was analysed on the GC-FID, to check the purity.
- A 100 μl loop injection of gas (zero air and standard) was analysed on the GC-FID, to check for a response of the compound of interest.
- The standard sample was adsorbed onto the adsorbent material at a range of temperatures until breakthrough occurred (frontal technique). This was repeated at least three times for every compound on each adsorbent.
- The adsorbent trap was cleaned by flowing helium across the trap and heating the trap to a specified temperature, dependent on the adsorbent degradation limit.

2.4.6. Adsorbent materials

The properties of the different adsorbent materials that were investigated are shown in Table 2.2.

Adsorbent Name	Class	Mesh size	Thermal Stability °C	Surface Area m^2/g	Conditioning Temp °C	Desorption Temp °C
Carbosieve SIII	CMS	60-70	400	975	350	320
Carboxen 1016	CMS	60-80	225	75	200	190
Carboxen 1018	CMS	60-70	400	675	350	320
Hayesep D	Porous polymer	40-60	280	795	190	180
Silica gel	Porous silica	30-60	350	750	190	180
HiSiv 3000	Silica-alumina	50-60	800	1000	260	250

Table 2.2 Properties of the adsorbent materials

2.5. BTV results

The breakthrough time and time taken for full desorption of the analyte were deduced from the frontal chromatogram produced by the GC-FID from these, the breakthrough volumes and desorption volumes per mg of adsorbent were calculated using equation 2.2. Desorption volumes are calculated in a similar way.

$$\text{BTV (per mg)} = \left(\frac{\text{BT time} \times \text{flow rate}}{\text{amount of adsorbent}} \right) \qquad 2.2$$

BT time – breakthrough time in minutes

Flow rate – flow rate in ml/min

Amount of adsorbent – mg

2.5.1. Micro-trap results

Breakthrough volumes ml/mg					
Adsorbent Trap	**Temperature (°C)**	**Ethyne**	**Ethene**	**Ethane**	**Propene**
Hayesep D (28 mg)	-40	0.0 ± 0.0	0.0 ± 0.0	0.0 ± 0.0	5.2 ± 1.6
Silica Gel (25 mg)	-30	0.0 ± 0.0	0.0 ± 0.0	0.0 ± 0.0	30.8 ± 1.1
Carboxen 1016 (30 mg)	-40	0.0 ± 0.0	0.0 ± 0.0	0.0 ± 0.0	6.7 ± 0.3
Carboxen 1018 (25 mg)	-40	7.0 ± 0.2	23.5 ± 1.3	37.3 ± 2.8	-
Cabosieve SIII (50 mg)	-40	26.3 ± 1.5	33.6 ± 0.3	71.9 ± 0.7	-

Table 2.3 BTVs for the micro-trap adsorbents in ml/mg.

Five adsorbents were tested for their retention capabilities of C_2 and C_3 hydrocarbons. The C_2 micro-trap requires high breakthrough volumes (> 500 ml) for C_2 hydrocarbons. A sample volume of > 500 ml is required in order to improve upon the sample volume of the previous Mace Head NMHC ADS-GCFID instrument (see Section 1.12). The ($\geq C_3$) refocusing micro-trap requires a weaker adsorbent, acting to re-focus a potentially large volume obtained from thermal desorption of the bulk trap. Hence the refocusing micro-trap should not retain the C_2 and C_3 hydrocarbons, as using too strong an adsorbent would not allow full recovery of the less volatile hydrocarbons during thermal desorption. Table 2.3 shows the BTV results per mg of adsorbent for the compounds tested at 1 ppm concentration.

2.5.1.1. C_2 micro-trap

Carbosieve SIII is the strongest adsorbent tested as demonstrated by the highest breakthrough volumes for the C_2 hydrocarbons. Since a known flow rate of 40 ml/min was used on the 50 mg Carbosieve SIII micro-trap, the sampling capacity is:

Ethyne: 26.28 ml/mg x 50 mg = 1314 ml sampling volume at -40 °C

This sampling volume was proposed to be large enough to account for the transfer volume of carrier gas to purge the C_2 hydrocarbons from the bulk-trap to the C_2 micro-trap.

Carboxen 1018 was found to be the second strongest adsorbent tested, with a sample capacity for ethyne of 175 ml at -40 °C. This is below the 500 ml sample threshold and hence too low a sample volume to be used as the C_2 micro-trap. For a 500 ml sample to be taken 71 mg of Carboxen 1018 would be required. The fact that Carboxen 1018 is a weaker adsorbent is due to its lower surface area compared to Carbosieve SIII.

Increasing the sample capacity can be done by two methods: decreasing the trapping temperature and increasing the amount of adsorbent in the trap. However, there are limitations as to how large a micro-trap can be. Both in terms of fitting the micro-trap inside the Peltier coolers and increasing the trap size broadens the peak shape of adsorbed compounds and risks overloading the chromatography column.

Hayesep D, Silica gel and Carboxen 1016 are all unsuitable for use as a C_2 micro-trap given their poor retention properties of volatile hydrocarbons.

2.5.1.2. Refocusing micro-trap

Hayesep D, Silica gel and Carboxen 1016 all proved to be medium-strength adsorbents displayed by the fact they do not retain C_2 hydrocarbons in Table 2.3.

Silica gel was found unsuitable for use as a micro-trap since it is extremely hydrophilic. Any residual water from the transfer from the bulk-trap to the refocusing micro-trap would be mopped up by silica gel, with water occupying adsorbent pore spaces preferentially to the relatively non-polar NMHCs. This was investigated using a humidity sensor to measure the dew point comparing the dew points with the Nafion drier and silica gel micro-trap in-line, just the Nafion drier in-line and with neither the Nafion nor micro-trap in-line, see Table 2.4.

In-line with system	Dew point reading (°C)
Nafion drier and micro-trap	-34.6
Nafion drier	-21.0
Neither	-12.2

Table 2.4 Dew point readings.

Table 2.4 shows how the silica gel micro-trap mops up extra water from a humid zero air Tedlar bag sample. This could cause problems in long-term measuring of NMHCs in a remote, marine research site, such as Mace Head. Any residual water from the back-flush of $\geq C_3$ hydrocarbons from the bulk-trap to the refocusing micro-trap would be preferentially adsorbed and form ice within the micro-trap (held at – 40 °C) blocking sample flow rates.

This leaves Carboxen 1016 and Hayesep D as possible adsorbents for the refocusing micro-trap. Both adsorbents do not retain C_2 hydrocarbons and only weakly retain propene; they are good medium strength adsorbents suitable for use as a refocusing micro-trap.

2.5.2. Bulk trap results

Breakthrough volumes ml/mg						
Adsorbent trap	**Ethyne**	**Ethene**	**Ethane**	**Propyne**	**Propene**	**Propane**
Hayesep D (3 g)	0.04 ± 0.0003	0.04 ± 0.0004	0.06 ± 0.001	0.60 ± 0.01	0.41 ± 0.03	0.51 ± 0.05
Hayesep D (2.5g)	0.03 ± 0.0003	0.03 ± 0.0003	0.05 ± 0.0004	0.52 ± 0.01	0.39 ± 0.01	0.49 ± 0.01
HiSiv 3000 (15 mg)	-	2.00 ± 0.003	0.00 ± 0.003	-	4.00 ± 0.001	6.70 ± 1.3
HiSiv 3000 (150 mg)	-	-	-	-	3.10 ± 0.1	-

Table 2.5 BTVs for the bulk-trap adsorbents in ml/mg.

The proposed use of a bulk-trap is to fractionate the C_3 and higher hydrocarbons from the C_2 hydrocarbons to enable C_2 hydrocarbons and water to flow through a Nafion drier to a C_2 micro-trap and avoid sending the $\geq C_3$ hydrocarbons through the Nafion drier. A suitable bulk-trap needs a good retention time for C_3 hydrocarbons and a short desorption time for the C_2 hydrocarbons. This can be observed by looking for a large difference in BTVs between the C_2 and C_3 compounds.

The 3 g Hayesep D bulk-trap provides a good distinction between the BTVs for the C_2 and C_3 compounds. BTV results for the C_2 hydrocarbons are of the order of 1×10^{-2}, whilst BTV results for the C_3 hydrocarbons are of the order of 1×10^{-1}, a ten-fold increase in the BTV, suggesting Hayesep D possesses the fractionating capabilities that are required for the bulk trap.

HiSiv 3000 does not show the same fractionating ability and as such is not suitable for use as an adsorbent in the bulk-trap.

Hayesep D also has the added advantage in that water elutes from Hayesep D between the C_2 and C_3 hydrocarbons. This enables a neat fractionation step to be determined, splitting C_2 hydrocarbons along with most of the water from the $\geq C_3$ hydrocarbons. Other adsorbents with similar retentive properties (with respect to C_2-C_3 hydrocarbons) such as Carboxen 1016 do not exhibit this feature (Scanview, 8.0).

2.5.3. Desorption volume results

The desorption volumes at room temperature of the C_2 hydrocarbons are particularly important to know since they are purged from the bulk trap, which is kept at room temperature, using a carrier gas to be re-focused onto the C_2 micro-trap.

Adsorbent trap	Temperature °C	Ethene	Ethane	Propane	Propene
Hayesep D (3 g)	100	0.02 ± 0.002	0.03 ± 0.01	0.07 ± 0.005	0.07 ± 0.01
Hayesep D (3 g)	Ambient	0.02 ± 0.003	0.06 ± 0.01	-	-

Table 2.6 Desorption volume results for the Hayesep D bulk trap at 100 °C and ambient temperature in ml/mg.

The desorption results suggest ethane (least volatile C_2 hydrocarbon) should be desorbed from the bulk-trap after 180 ml of helium purge at ambient (25 °C) temperatures. This purge volume will not overpower the BTVs of the C_2 micro-trap. The desorption volumes at 100 °C are useful for the consideration of desorption $\geq C_3$ hydrocarbons from the bulk-trap. At 100 °C it should be possible to desorbe C_3 hydrocarbons from the bulk-trap with 210 ml of helium. However, the C_4 hydrocarbons and higher may require a higher desorption temperature to fully desorbe them within 1 L purge (to prevent over-loading the refocusing trap).

2.6. Conclusions from elution technique

The purpose of these frontal BTV experiments was to determine which micro-traps and bulk-traps would be suitable for the purposes:

- A bulk-trap used to fractionate between C_2 hydrocarbons, water and C_3 and higher hydrocarbons. The bulk-trap requires a large difference in BTVs of C_2 and C_3 hydrocarbons.
- A strong adsorbent micro-trap for trapping volatile, C_2 hydrocarbons. This trap requires large BTVs for C_2 hydrocarbons.
- A weaker adsorbent micro-trap targeting C_3 to C_8 hydrocarbons, allowing the full desorption of $\geq C_3$ hydrocarbons. This trap acts as a re-focusing trap, compounds are back-flushed with helium from the bulk-trap which is heated and transfers hydrocarbons to the micro-trap. The micro-trap re-traps the hydrocarbons at sub-ambient temperatures enabling a smaller helium back-flush volume to be used to transfer compounds to the chromatography column and thus preventing over-loading the capillary chromatography column.

2.6.1. Bulk-trap

Two adsorbent materials were tested for the bulk-traps; HiSiv 3000 and Hayesep D. These adsorbent materials were selected for testing based on their physical properties researched from supplier's websites (including www.sigmaaldrich.com, www.vici.com). The Hayesep D (3 g) bulk-trap was found to be the most suitable for use as a bulk-trap in the proposed NMHC instrument. The HiSiv 3000 bulk-trap was unsuitable because the C_2 and C_3 hydrocarbons exhibited similar BTVs and desorption volumes, preventing efficient fractionation between the two. The results for the Hayesep D bulk-trap show a significant distinction between the BTVs and desorption volumes for the C_2 and C_3 hydrocarbons. Hayesep D also has the additional feature in that water elutes from the adsorbent between C_2 and C_3 hydrocarbons. A 1 L sample can be sampled onto the bulk-trap before breakthrough of C_3 and higher hydrocarbons, whilst allowing the C_2 hydrocarbons and water to be

fractionated off onto the C_2 micro-trap. Desorption experiments were carried out on the 3 g Hayesep D to investigate the volume of helium necessary to purge the C_2 hydrocarbons from the bulk-trap (to be re-trapped by the C_2 micro-trap). For ethane, the least volatile C_2 hydrocarbon, 0.06 ml/mg was required at room temperature to desorbe from the bulk-trap, this is equivalent to 180 ml on a 3 g bulk-trap.

2.6.2. C_2 micro-trap

Five adsorbent materials were tested to trap the volatile C_2 hydrocarbons. Two out of the five adsorbents were found suitable to trap C_2 hydrocarbons; Carbosieve SIII and Carboxen 1018. Although Carboxen 1018 showed potential for efficiently adsorbing C_2 hydrocarbons, (the suitability of the Carboxen 1018 is thought to be due to the similarity between the pore size of the CMS-type adsorbent material and the C_2 hydrocarbons, see Figure 2.8), Carbosieve SIII proved to be the strongest adsorbent exhibiting the largest BTVs and thus the largest sampling capacity for C_2 hydrocarbons.

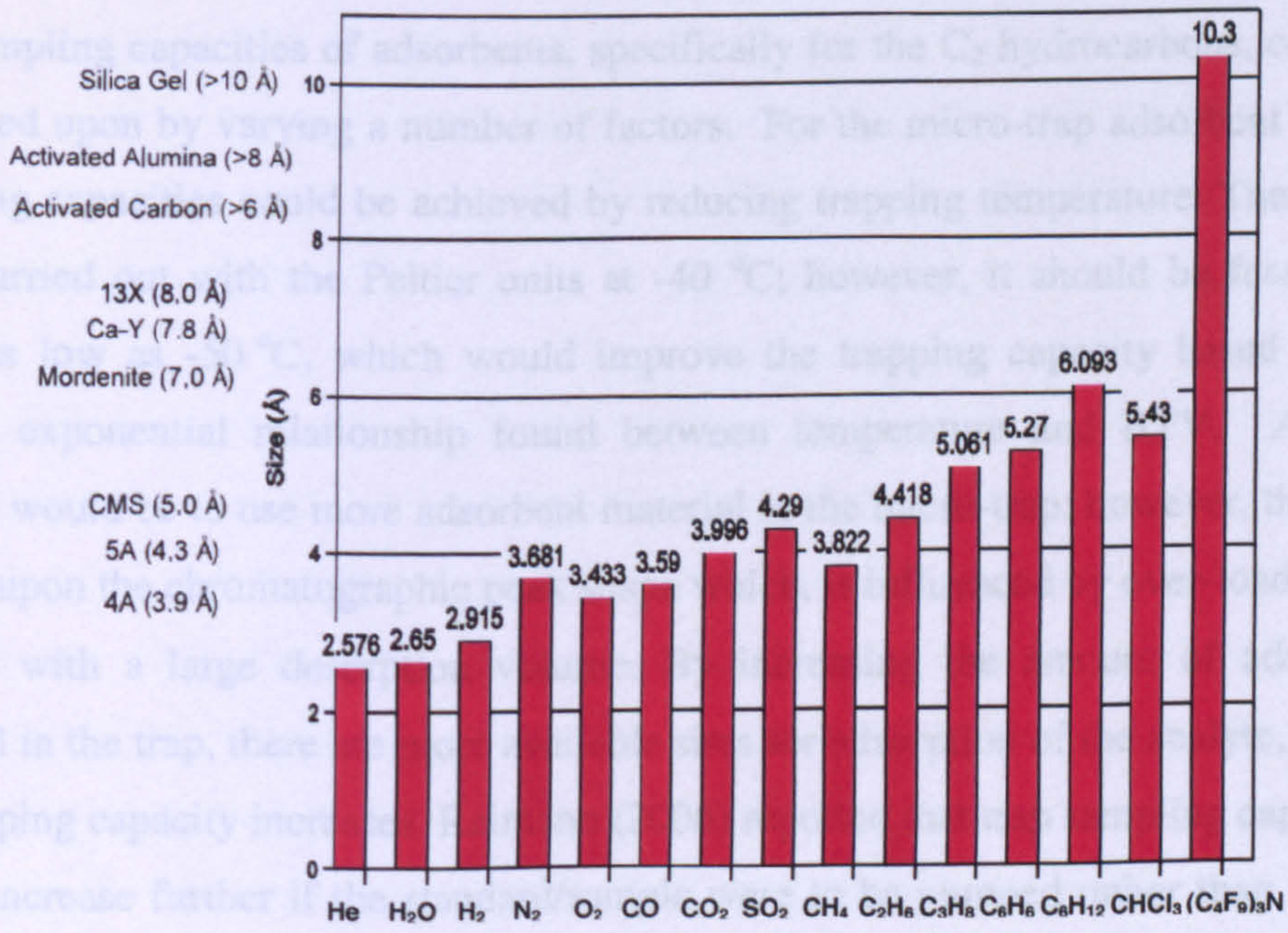

Figure 2.8 Common atmospheric species size compared with adsorbent pore sizes (Kent, 2005).

2.6.3. Refocusing micro-trap

Carboxen 1018 and Carbosieve SIII are too strong an adsorbent to use to trap high molecular weight hydrocarbons ($\geq C_3$ hydrocarbons) to be used in the re-focusing mirco-trap downstream of the bulk-trap. Hayesep D, Carboxen 1016 and Silica gel are medium/weak strength adsorbents, as demonstrated by the immediate break-through of C_2 hydrocarbons. Thus, they could be used as the re-focusing trap, Silica gel is highly hydrophilic, with a very high affinity for water. Thus, any residual water in an air sample which was not removed along with the C_2 hydrocarbons by purging the bulk-trap would occupy pore spaces in the Silica gel adsorbent preferentially to the relatively non-polar hydrocarbons. Carboxen 1016 and Hayesep D proved to be useful adsorbents for the use in the refocusing micro-trap. Hayesep D was the chosen adsorbent to act as the re-focusing micro-trap as it was also hoped that the use of Hayesep D as both the bulk-trap and the re-focusing micro-trap will reduce the number of possible trap artefacts obtained during thermal desorption, as only one adsorbent type is being used.

The sampling capacities of adsorbents, specifically for the C_2 hydrocarbons, could be improved upon by varying a number of factors. For the micro-trap adsorbent greater sampling capacities could be achieved by reducing trapping temperature. These tests were carried out with the Peltier units at -40 °C; however, it should be feasible to reach as low as -50 °C, which would improve the trapping capacity based on the inverse exponential relationship found between temperature and BTV. Another method would be to use more adsorbent material in the micro-trap; however, this may impact upon the chromatographic peak shape which, is influenced by over-loading the column with a large desorption volume. By increasing the amount of adsorbent material in the trap, there are more available sites for adsorption of the analyte, and so the trapping capacity increases. Reimann (2006) reported that trap sampling capacities would increase further if the standard/sample were to be pumped rather than sucked through the trap. The increase in sampling volume is caused by the change in vapour pressure across the trap. When sucking the sample through, a vacuum is produced across the trap causing a lower vapour pressure that encourages molecules to be

pulled off the adsorbent. If the sample were to be pumped through the system, a higher vapour pressure would arise across the trap, which in turn would encourage the molecules to hit the adsorbent more frequently and be adsorbed to the surface. Unfortunately there was not enough time to examine this theory. However, the design of the new NMHC instrument relies on pumping a sample through (rather than sucking as in these experiments) which should increase BTVs from those reported in this chapter. (BTVs are further discussed in chapter 4).

3. Chromatographic separation of NMHCs

3.1. Introduction

The gas chromatography column separates analytes in a sample and thus plays a central role in gas chromatography, especially when a non-selective detector, such as an FID is used. Capillary columns are the preferred GC column type and this chapter focuses on the analytical testing of a variety of capillary columns. Capillary columns have many advantages over packed columns due to their longer length and unrestricted flow paths; unlike packed columns, capillary columns have a film of adsorbent material (liquid or solid) coated to the inside walls of the column.

Development of capillary columns led to Porous layer open tubular (PLOT) capillary columns which specifically target the analysis of low molecular weight atmospheric gases. PLOT columns exhibit strong retention of volatile gases and in doing so allow analysis of VOCs without the need for sub-ambient GC oven temperature programming (Helmig, 1999). PLOT columns are silica capillary columns which have a thin coating of solid adsorbent on the inner capillary column walls, called the stationary phase (Grob and Barry, 2004). Gas chromatography using PLOT capillary columns is more accurately described as gas-solid chromatography (GSC) (Braithwaite and Smith, 1996).

PLOT (GSC) column chromatographic separation is achieved by an interaction between analytes and the stationary phase of the column, thus the choice of column needs to be carefully selected for its application. The volatility and polarity of analytes, the stationary phase, and oven temperature programme all need to be considered before a chromatography column is chosen. The chosen column needs to be tested using a representative sample mixture to identify peak retention times and resolution. An ideal chromatogram separates all analytes in a sample with baseline resolution in the minimum analysis time (Braithwaite and Smith, 1996).

The Al_2O_3/KCl PLOT column (50 m, 0.32 mm) used in the previous NMHC Mace Head instrument had associated with it a number of operational problems. Given the reported problems (Martin, 2002), listed below and the development of new columns, it was decided to test a number of other PLOT columns for suitability as the separating column to be used in analysis of NMHCs in the new instrument.

- Non-symmetric peak shape of ethane and ethene.
- Co-elution of m-xylene and p-xylene, which are reported as the sum of m-xylene and p-xylene.
- Co-elution of i-butane and acetylene.
- Long analysis run time, 87 minutes to obtain the best resolution of C_2 – C_8 NMHCs.
- Alumina PLOT columns have a high affinity for water which it strongly adsorbs resulting in shifts in the hydrocarbon peak retention times.

Various PLOT columns were analysed with the aim to find a suitable replacement for NMHC analysis using the Al_2O_3/KCl PLOT column (50 m, 0.32 mm), see Table 3.1. The columns chosen for analysis were based on example chromatograms downloaded from Scanview 8.0 and based upon what columns were readily available in the laboratory stock. Scanview 8.0 shows example chromatograms along with details on flow rates, temperature programmes and column conditions. Al_2O_3/KCl (50 m, 0.53 mm) and Al_2O_3/Na_2SO_4, Carbograph 1 and Gaspro columns were analysed as potential replacements of the Al_2O_3/KCl (50 m, 0.32 mm) for separation of the full-suite of C_2 – C_8 hydrocarbons. CarboBOND and Carboxen 1006 were chosen for analysis with the view of splitting an air sample to analyse C_2 (and possibly C_3) hydrocarbons on a separate column to the $>C_3$ hydrocarbons. Porabond Q and CP Sil 5CB were analysed with reference to other University of Bristol VOC instruments, to determine the elution order of NMHCs on each column. This was achieved utilising the same oven temperature programs and carrier gas flow rates as the VOC instrument:

- The Mace Head Medusa-GCMS analyses perflurocarbons, SF_6, halocarbons and a select number of NMHCs utilises a Porabond Q column (25 m, 0.32 mm). Carrier gas, helium flow rate 2.2 ml/min.
- The ADS-GCMS (the predecessor to the Medusa) used a CP Sil 5CB column (100 m, 0.32 mm). Carrier gas, helium flow rate 2.2 ml/min. This instrument analysed hydrorflurocarbons, halocarbons and a select number of hydrocarbons.

Column	Stationary phase	Max temp (°C)	Dimensions (length, I.D, d.f)	Supplier
Al_2O_3/KCl	Aluminium oxide deactivated with KCl	200	50 m, 0.32 mm, 5 µm	Varian
Al_2O_3/KCl	Aluminium oxide deactivated with KCl	200	50 m, 0.53 mm, 10 µm	Varian
Al_2O_3/Na_2SO_4	Aluminium oxide deactivated with Na_2SO_4	200	50 m, 0.32 mm, 10 µm	Varian
CarboBOND	Carbon molecular sieve	300	25 m, 0.53 mm, 10 µm	Varian
Carbograph 1	Carbon graphitised	240	30 m, 0.32 mm, 0.25 µm	Alltech
Carboxen 1006	Carbon molecular sieve	250	30 m, 0.53 mm, 3 µm	Agilent
CP Sil 5CB	Porous silica	325	100 m, 0.32 mm, 5 µm	Varian
Gaspro	Proprietary, bonded silica-based	300	60 m, 0.32 mm, #	BAS technical
Porabond Q	Divinylbenzene base porous copolymer	320	25 m, 0.32 mm, 5 µm	Varian

Table 3.1 Chromatography columns analysed. # Film thickness not included as GasPro is a proprietary film thickness.

Analysis of chromatography columns was conducted by carrying out loop injections of ppm-concentration range hydrocarbon standards directly onto each chromatography column. This allowed analysis of retention times and peak shapes. An FID was used as the detector; since this is a non-selective detector, separate hydrocarbon standards were utilised to allow accurate identification of retention times and elution orders of hydrocarbons on each column. The hydrocarbon standards used for analysis are listed in Table 3.2.

Standard	Supplier	Contents	Concentration (ppm)
Alkane	Supelco	Methane Ethane Propane n-Butane n-Pentane n-Hexane	1002 989 974 976 1025 979
Alkene	Scientific & Technical Gases	Ethene Propene 1-Butene 1-Pentene 1-Hexene	1000 998 1009 994 1020
C_4	Scientific & Technical Gases	n-Butane i-Butane Cis-2-butene Trans-2-butene 1-Butene i-Butene 1,3-Butadiene Ethylacetylene	1032 1018 1028 1018 1018 1018 1028 1028
BTEX	Scientific & Technical Gases	Benzene Toluene Ethylbenzene Meta-xylene Ortho-xylene Para-xylene	99 100 99 99 99 99

Table 3.2 Standards used in column analysis accurate to ± 2%

3.1.1. Gas solid chromatography (GSC) stationary phases

Separation of analytes is based on the interaction between the analytes and the column stationary phase. The interaction between analytes and stationary phase are as a result of the following physical adsorption processes:

- Van der Waal's forces arising from either temporary or permanent dipole moments within molecules
- London forces (induced-dipole-induced-dipole) caused by fluctuations in the electron clouds in molecules.
- Hydrogen bonding is an attractive interaction between two species, A and B. species A contains a hydrogen atom covalently bonded to an electronegative atom, such as N, O or F, the molecular orbital is pulled towards the

electronegative atom. Species B contains a lone pair of electrons, which can interact with the electropositive hydrogen of species A (Atkins, 1998).

The interaction can be described in terms of distribution ratio, K (Braithwaite and Smith, 1996):

3.1. $$K = \frac{C_S}{C_M}$$

C_S is the amount of analyte adsorbed on the stationary phase.

C_M is the partial pressure in the mobile (gas) phase.

Too strong an interaction between the analytes and the stationary phase (C_S is large) will result in some molecules "lagging" behind the main peak causing peak tailing. Too weak an interaction (C_M is large) and some molecules will move ahead of the main peak causing peak fronting. Thus a suitable adsorbent must be selected for successful GSC. (Braithwaite and Smith, 1996).

Alumina PLOT columns are the most common capillary columns used in analysis of $C_2 - C_{10}$ hydrocarbons (Ji, et al., 1999), they are composed of Al_2O_3 layer on a silica capillary column. The polar Al-O-Al matrix provides an active surface; however, this needs to be deactivated by inorganic salts, either KCl or Na_2SO_4, without which the Al-O-Al sites would adsorb too strongly causing poor peak shape. Incorporation of inorganic salts into the Al-O-Al matrix blocks excessive active sites, reducing the column's activity, improving the peak shape and giving better separation of $C_2 - C_5$ alkenes and alkanes and separation of cis- and trans- isomers. Retention on Alumina PLOT columns occurs via hydrogen bonding between the alumina surface and analytes. Polar molecules, such as alcohols and water, are highly retained on the alumina surface resulting in poor resolution.

Carbograph 1 is a type of carbon graphitised adsorbent. Graphitisation reduces the polarity and microporosity of carbon surfaces resulting in a non-polar, non-porous,

inert material. Graphitised carbon blacks are suitable for analysis of atmospheric and permanent gases (Braithwaite and Smith, 1996).

CarboBOND and Carboxen 1006 are examples of carbon molecular sieve adsorbents. Carbon molecular sieves are a type of adsorbent containing pores of a very specific size, which act as a filter only allowing adsorption of molecules which are small enough to fit through the pores (Braithwaite and Smith, 1996). CarboBOND is suited for the analysis of CO, CO_2 and $C_2 - C_3$ hydrocarbons. Carboxen 1006 is ideal for the separation of permanent gases and $C_1 - C_3$ hydrocarbons.

The CP-Sil line consists of a range of stationary phases based on the polysiloxane backbone. Polysiloxanes are inorganic-organic polymers with the chemical formula $[R_2SiO]_n$, were R is the organic group. CPSil 5-CB consists of dimethylpolysiloxane. Since analyte separation is based on boiling points, the column is suitable for analysis of VOCs over a large temperature range (Varian, 2007).

Gaspro columns are based on β-cyclodextrins which is a type of oligosaccharide formed by the degradation of starch; it is essentially a seven-sugar-ring-molecule. Cyclodextrin based PLOT columns retain both polar and non-polar analytes. Non-polar analytes are retained in the cyclodextrin cavity and polar analytes form hydrogen bonds with hydroxyl groups in the outer-rim of the cavity (Reid, et al., 1993).

Porabond Q is a type of porous polymer PLOT column, based on a divinylbenzene backbone. Retention on porous polymer PLOT columns is based on a combination of molecular weight, boiling point, polarity of the solid phase. An important feature of porous polymers is that they are not sensitive to water. Water elutes from the Porabond Q PLOT column as a well defined peak and does not result in shifts in retention times, a common problem with most other PLOT columns (Varian, 2007).

3.2. Procedure

Each column was installed inside the GC oven and connected to an external 6-port Valco valve which was used to make 50 µl loop injections of ppm concentration standards onto the GC column, (Figure 3.1). The column is firstly conditioned by slowly heating the oven temperature to the maximum operating temperature of the column, allowing adsorbed contaminants to elute from the column. Column conditioning is carried out without connecting the other end of the column to the detector. A typical conditioning sequence for a column with a maximum operating temperature of 200°C is:

- Heat to 50 °C at a rate of 1°C/minute, hold for 1 hour.
- Heat to 100°C at a rate of 1°C/minute, hold for 1 hour.
- Heat to 150°C at a rate of 1°C/minute, hold for 1 hour.
- Heat to 200°C at a rate of 1°C/minute, hold for 5 hours.

Once a column has been chosen, two parameters can be modified to optimise the resolution of analytes: the oven temperature programme and the carrier gas flow rate. These parameters were modified for each analysed chromatography column to provide the best resolution of the analytes in each standard sample. The column operating conditions reported in this chapter are the conditions which provide the best resolution.

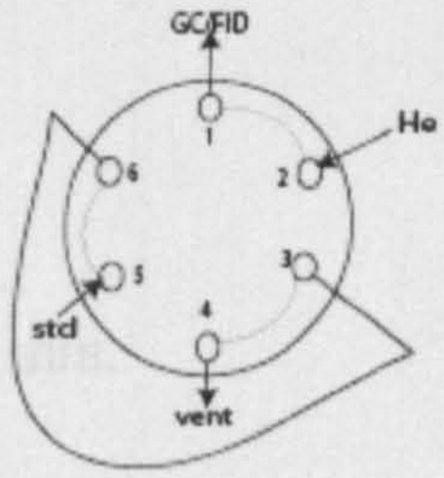

Figure 3.1 External valve set-up for standard loop injections onto various columns.

3.3. Al_2O_3/KCl PLOT column

Two alumina PLOT KCl columns have been analysed;

- 30 m length, 0.32 mm I.D, 5 μm film thickness.
- 50 m length, 0.53 mm I.D, 10 μm film thickness.

Effects of changing column length, internal diameter and film thickness include:

- Increasing column length increases the sample capacity and the resolution but will also increase the analysis time (Grob and Barry, 2004).
- Sample capacity increases with column diameter. Capillary columns of 0.18 – 0.32 mm I.D should be used for GCMS so as not to overload the vacuum system. Larger I.D 0.32 – 0.53 mm columns are generally used for samples whose components differ widely in concentration (Helmig, 1999).
- Increasing film thickness increases the retention and sample capacity. Thin film columns provide higher resolution of high-boiling analytes and lower resolution of low-boiling analytes (Helmig, 1999).

3.3.1. Al_2O_3/KCl column (50 m, 0.32 mm, 5 μm)

A 50 μl aliquot of each hydrocarbon standard were independently injected directly onto the 50 m, 0.32 mm Al_2O_3/KCl PLOT column using the following temperature program and carrier gas flow rate:

Oven temperature program:
35 °C initial
Heat to 61 °C at 6 °C/min, hold 6 min.
Heat to 73 °C at 6 °C/min.
Heat to 130 °C at 3 °C/min hold 8 min.
Heat to 190 °C at 8 °C/min and hold for 40 min.
Carrier gas (He) flow rate: 2.3 ml/min

The temperature program utilised replicates the heating rates used in the previous Mace Head ADS-GC-FID NMHC instrument. These conditions are the optimum temperature profile for this column (Martin, 2002) ensuring the C_4 isomers are fully resolved from one another.

The average retention times and peak widths over three separate loop injections are shown in Table 3.3. Figure 3.2 shows the separation of the C_4 hydrocarbon isomers on this column; all C_4 isomers are well resolved using this temperature program.

Compound	Retention time (min)	Peak width (min)	Compound	Retention time (min)	Peak width (min)
Methane	3.15 ± 0.01	0.03 ± 0.0001	n-Pentane	24.38 ± 0.1	0.12 ± 0.001
Ethane	3.67 ± 0.01	0.03 ± 0.0001	Ethyl acetylene	26.69 ± 0.3	0.10 ± 0.05
Ethene	4.68 ± 0.03	0.02 ± 0.0001	1-Pentene	30.82 ± 0.2	0.08 ± 0.01
Propane	5.83 ± 0.03	0.03 ± 0.0001	1,3-Butadiene	34.77 ± 0.3	0.12 ± 0.04
Propene	10.34 ± 0.2	0.06 ± 0.005	n-Hexane	36.04 ± 0.2	0.18 ± 0.01
i-Butane	12.98 ± 0.2	0.07 ± 0.01	1-Hexene	44.02 ± 0.1	0.12 ± 0.03
n-Butane	13.44 ± 0.2	0.09 ± 0.01	Benzene	51.94 ± 0.04	0.09 ± 0.003
Trans-2-butene	19.42 ± 0.2	0.07 ± 0.02	Toluene	62.65 ± 0.09	0.16 ± 0.001
1-Butene	19.81 ± 0.2	0.07 ± 0.01	Ethyl benzene	82.04 ± 0.2	0.33 ± 0.01
i-Butene	20.80 ± 0.2	0.08 ± 0.02	m,p-Xylene	84.01 ± 0.2	0.63 ± 0.01
Cis-2-butene	21.68 ± 0.2	0.09 ± 0.02	o-Xylene	92.02 ± 0.2	0.46 ± 0.001

Table 3.3 Retention times and elution order on the Al_2O_3/KCl column (30 m, 0.32 mm, 5 μm).

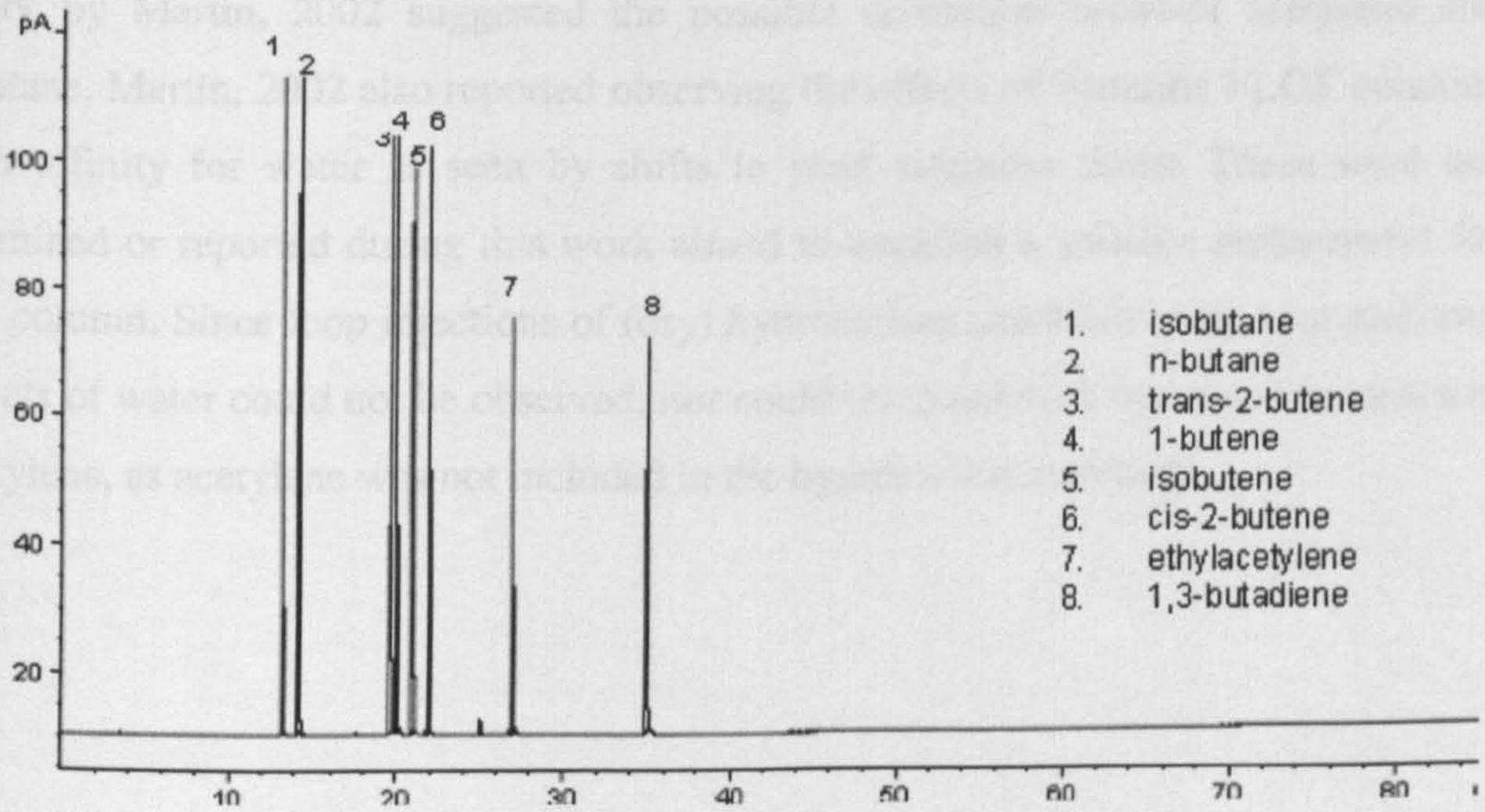

Figure 3.2 Chromatogram of the C_4 standard on the Al_2O_3/KCl column (30 m, 0.32 mm, 5 μm).

3.3.1.1. Discussion - Al_2O_3/KCl (50 m, 0.32 mm, 5 μm) column

The Al_2O_3/KCl column (30 m, 0.32 mm, 5 μm) column was used in the previous University of Bristol NMHC instrument (Martin, 2002). The temperature program and carrier gas flow rate were replicated in this work. The column gave very good separation for all of the hydrocarbons tested. Co-elution existed between m-xylene and p-xylene, which are rarely separated due to their very similar boiling points (139.3 °C + 138.4 °C respectively) and structures. Co-elution of m-xylene and p-xylene occurred on all the columns analysed. Ethylbenzene, m,p-xylene and o-xylene eluted as broader and smaller peaks compared to other hydrocarbon peaks.

The oven temperature program used to achieve the best overall separation of C_2 to C_8 hydrocarbons took 87 minutes to complete. Using this temperature program along with the time taken for air sampling by pre-concentration on an adsorbent-filled trap (sampling 500 ml at 50 ml/min, is equivalent to 10 minutes sample time) limits the analysis time of NMHCs to every two hours.

Work by Martin, 2002 suggested the possible co-elution between acetylene and i-butane. Martin, 2002 also reported observing the effects of Alumina PLOT columns high affinity for water as seen by shifts in peak retention times. These were not examined or reported during this work aimed to establish a suitable replacement for this column. Since loop injections of (dry) hydrocarbon standards were analysed, any effects of water could not be observed, nor could the co-elution between i-butane and acetylene, as acetylene was not included in the hydrocarbon standards.

3.3.2. Al_2O_3/KCl column (50 m, 0.53 mm, 10 µm)

50 µl loop injections of four hydrocarbon standards were injected directly onto the Al_2O_3/KCl (50 m, 0.53 mm, 10 µm) column. The temperature program used was that reported by Blake et al, (1993). They heated the column to 220 °C, in order to resolve ethylbenzene and the xylene isomers. Since this is 20 °C above the recommended operating temperature of the column, it was decided to only heat to 200 °C. The following temperature and carrier gas conditions were utilised:

Oven temperature program:
40 °C, hold for 6 mins.
Heat to 200 °C at 5 °C/min, hold for 2 min.
Carrier gas (He) flow rate: 7.2 ml/min

A much higher flow rate is used compared with the Al_2O_3/KCl (50 m, 0.32 mm) column, since the 0.53 mm column is a mega-bore capillary column. The increased internal diameter increases the sample capacity of the column, resulting in higher carrier gas flow rates and shorter analysis times. Table 3.4 gives the retention times and peak width of NMHCs on this column.

compound	Retention time (min)	Peak width (min)	compound	Retention time (min)	Peak width (min)
Methane	3.44 ± 0.04	0.03 ± 0.001	n-Pentane	24.53 ± 0.001	0.06 ± 0.01
Ethane	4.10 ± 0.04	0.03 ± 0.001	Ethylacetylene	25.03 ± 0.001	0.06 ± 0.01
Ethene	5.13 ± 0.01	0.04 ± 0.01	1-Pentene	27.88 ± 0.002	0.07 ± 0.01
n-Propane	7.89 ± 0.03	0.05 ± 0.01	1,3-Butadiene	30.00 ± 0.007	0.06 ± 0.03
1-Propene	12.81 ± 0.01	0.06 ± 0.01	Benzene	31.46 ± 0.02	0.07 ± 0.01
i-Butane	15.53 ± 0.001	0.06 ± 0.01	n-Hexane	21.71 ± 0.01	0.07 ± 0.02
n-Butane	16.38 ± 0.01	0.06 ± 0.01	1-Hexene	24.59 ± 0.003	0.07 ± 0.04
Trans-2-butene	20.34 ± 0.001	0.06 ± 0.01	Toluene	35.97 ± 0.02	0.06 ± 0.01
1-Butene	20.66 ± 0.01	0.06 ± 0.01	Ethylbenzene	42.74 ± 0.03	0.10 ± 0.03
i-Butene	21.29 ± 0.01	0.06 ± 0.02	m,p-Xylene	53.68 ± 0.08	0.20 ± 0.05
Cis-2-butene	21.88 ± 0.01	0.06 ± 0.01	o-Xylene	54.57 ± 0.09	0.23 ± 0.09

Table 3.4 Retention times and elution order on the Al_2O_3/KCl column (50 m, 0.53 mm, 10 µm).

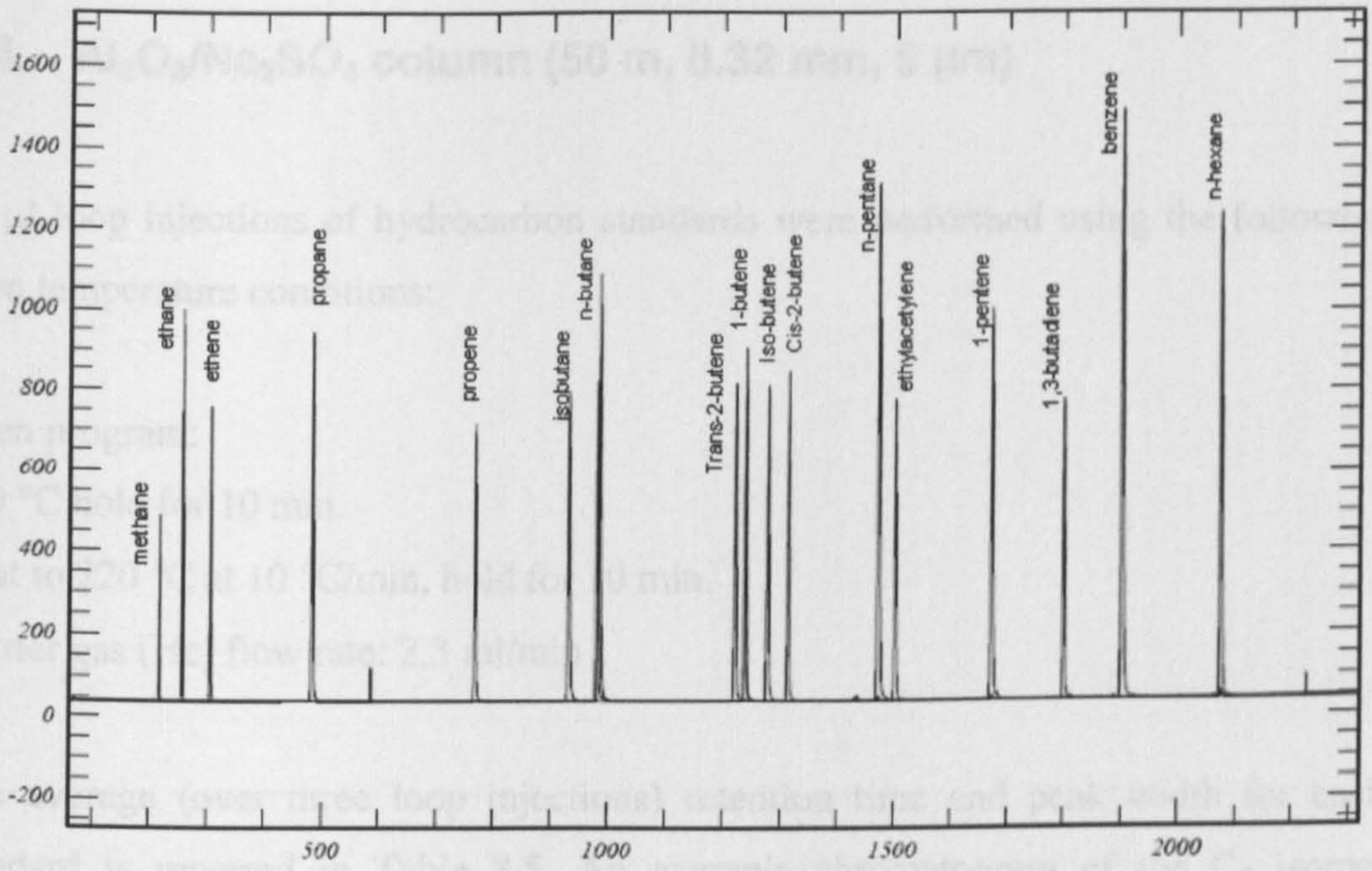

Figure 3.3 Over-laid chromatograms showing $C_2 - C_6$ hydrocarbons on the Al_2O_3/KCl column (50 m, 0.53 mm, 10 µm).

3.3.2.1. Discussion - Al_2O_3/KCl (50 m, 0.53 mm, 10 µm) column

This column gave good separation of all hydrocarbons. The larger internal diameter compared to the Al_2O_3/KCl (50 m, 0.32 mm) column increases flow rates and sample capacity, hence a larger sample can be introduced into the column and increased flow rates result in a significant reduction in run time. The sample analysis time took 55 minutes to complete.

As with the 0.32mm Al_2O_3/KCl column poor peak shapes for the ethane and ethene were observed. Poor peak shapes for ethylbenzene, m,p-xylene and o-xylene are also observed, indicated by the increased peak width in Table 3.4. This has been well reported in literature and can be resolved by heating the column to 220 °C (Blake, et al., 1993).

3.4. Al_2O_3/Na_2SO_4 column (50 m, 0.32 mm, 5 µm)

50 µl loop injections of hydrocarbon standards were performed using the following oven temperature conditions:

Oven program:
110 °C hold for 10 min.
Heat to 220 °C at 10 °C/min, hold for 10 min.
Carrier gas (He) flow rate: 2.3 ml/min

The average (over three loop injections) retention time and peak width for each standard is reported in Table 3.5. An example chromatogram of the C_4 isomer hydrocarbon standard is shown in Figure 3.4 (for comparison with Figure 3.2).

Compound	Retention time (min)	Peak width (min)	compound	Retention time (min)	Peak width (min)
Methane	3.07 ± 0.002	0.05 ± 0.001	n-Pentane	11.65 ± 0.09	0.11 ± 0.002
Ethane	3.22 ± 0.002	0.04 ± 0.001	Ethylacetylene	12.73 ± 0.04	0.13 ± 0.0005
Ethene	3.36 ± 0.003	0.06 ± 0.003	1-Pentene	15.06 ± 0.05	0.12 ± 0.02
Propane	3.73 ± 0.01	0.04 ± 0.001	n-Hexane	17.42 ± 0.07	0.10 ± 0.003
Propene	4.48 ± 0.01	0.06 ± 0.004	1,3-Butadiene	17.48 ± 0.07	0.10 ± 0.007
i-Butane	5.30 ± 0.01	0.05 ± 0.001	1-Hexene	19.51 ± 0.04	0.10 ± 0.01
n-Butane	5.56 ± 0.01	0.05 ± 0.002	Benzene	13.36 ± 0.03	0.03 ± 0.001
Trans-2-butene	7.60 ± 0.02	0.08 ± 0.001	Toluene	15.48 ± 0.04	0.03 ± 0.0003
1-Butene	8.10 ± 0.04	0.10 ± 0.005	Ethylbenzene	17.96 ± 0.05	0.03 ± 0.0007
i-Butene	8.60 ± 0.03	0.10 ± 0.0004	m,p-Xylene	19.60 ± 0.02	0.04 ± 0.02
Cis-2-butene	9.20 ± 0.04	0.12 ± 0.001	o-Xylene	21.67 ± 0.02	0.04 ± 0.01

Table 3.5 Retention times and elution order on the Al_2O_3/Na_2SO_4 column (50 m, 0.32 mm, 5 µm).

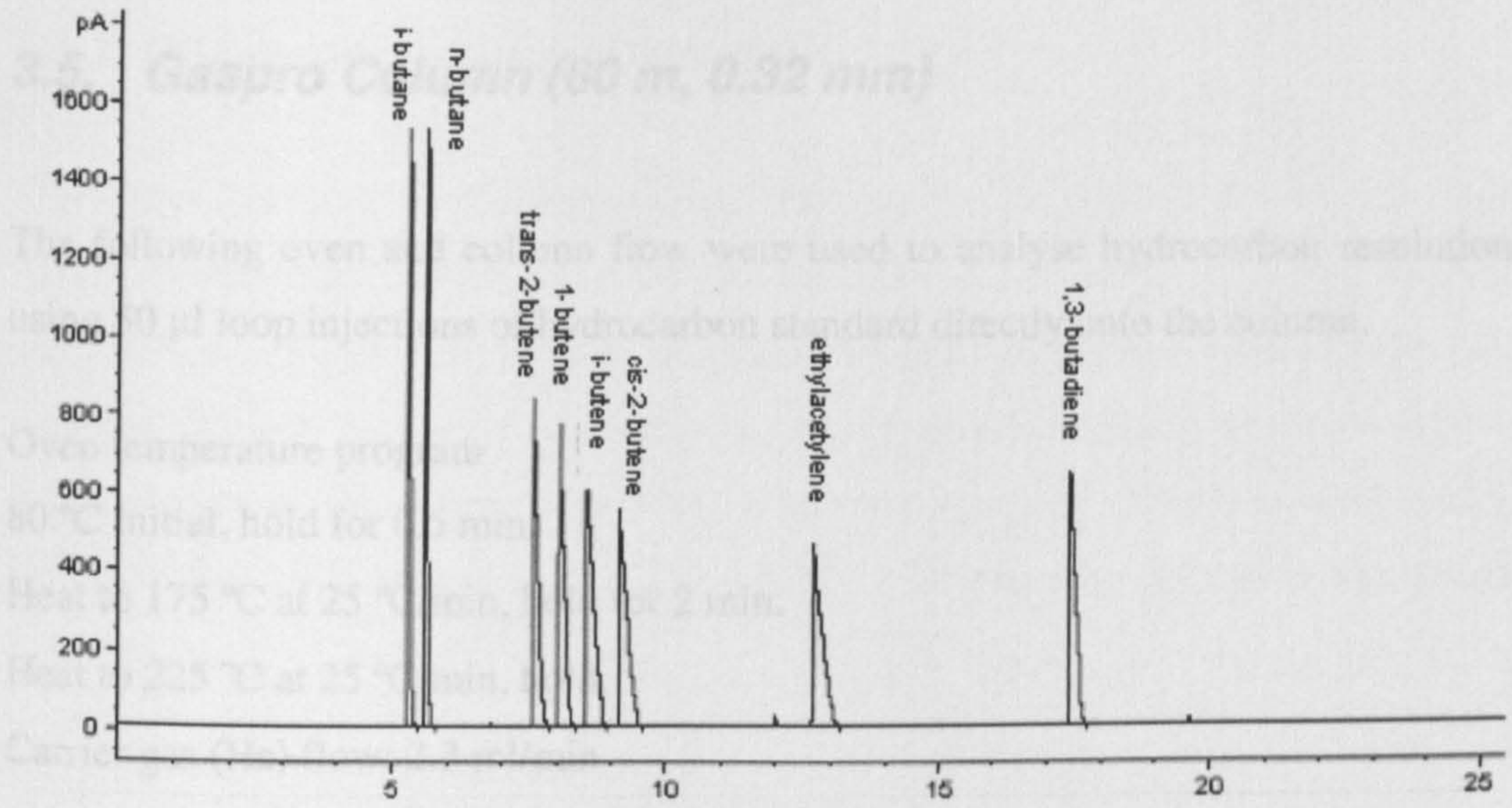

Figure 3.4 Chromatogram of C_4 standard on the Al_2O_3/Na_2SO_4 column (50 m, 0.32 mm, 5 µm).

3.4.1. Discussion - Al_2O_3/Na_2SO_4 column (50 m, 0.32 mm, 5 µm)

The Al_2O_3/Na_2SO_4 column (50 m, 0.32 mm, 5 µm) column gave good separation of hydrocarbons. However, in general peak widths were broader compared to peak shape when using the Al_2O_3/KCl PLOT columns. Poor C_4 hydrocarbon peak shapes were observed, characterised by considerable peak tailing, see Figure 3.4.

Peak width is a measure of peak broadness. Broadening can be a result of non-column and column effects. Examples of non-column effects include poor connections before the column and between the column and the active part of the detector. Peak broadening resulting from column effects can be explained by the Van Deemter model of band broadening (Grob and Barry, 2004). Van Deemter explains the column band broadening effects in terms of random movement through the stationary phase, diffusion in the mobile phase and interaction with the stationary phase.

Non-Gaussian peak shapes and peak tailing can lead to discrepancies in integration and thus discrepancies in peak area and reported concentration.

3.5. Gaspro Column (60 m, 0.32 mm)

The following oven and column flow were used to analyse hydrocarbon resolutions using 50 µl loop injections of hydrocarbon standard directly onto the column.

Oven temperature program

80 °C initial, hold for 0.5 min.

Heat to 175 °C at 25 °C/min, hold for 2 min.

Heat to 225 °C at 25 °C/min, hold.

Carrier gas (He) flow: 2.3 ml/min

Compound	Retention time (min)	Peak width (min)	Compound	Retention time (min)	Peak width (min)
Methane	3.481± 0.2	0.02 ± 0.007	1,3-butadiene	co-elute	-
ethane	3.65 ± 0.4	0.02 ± 0.005	ethyl acetylene	co-elute	-
ethene	3.70 ± 0.1	0.02 ± 0.004	n-pentane	6.18 ± 0.8	0.14 ± 0.05
Propane	4.05 ± 0.5	0.02 ± 0.003	1-pentene	7.55 ± 0.2	0.26 ± 0.04
Propene	4.40 ± 0.1	0.04 ± 0.002	n-hexane	7.99 ± 0.2	0.14 ± 0.04
i-butane	4.69 ± 0.2	0.04 ± 0.004	Benzene	4.73 ± 0.2	0.03 ± 0.01
n-butane	4.84 ± 0.1	0.04 ± 0.001	Toluene	4.88 ± 0.1	0.03 ± 0.01
Trans-2-butene	5.47 ± 0.4	0.05 ± 0.04	ethylbenzene	5.78 ± 0.7	0.04 ± 0.02
1-butene	5.61 ± 0.4	0.04 ± 0.02	m+p-xylene	6.27 ± 0.1	0.07 ± 0.03
Cis-2-butene	co-elute	-	o-xylene	11.95 ± 0.2	0.30 ± 0.03

Table 3.6 Retention times and elution order on the Gaspro column (60 m, 0.32 m).

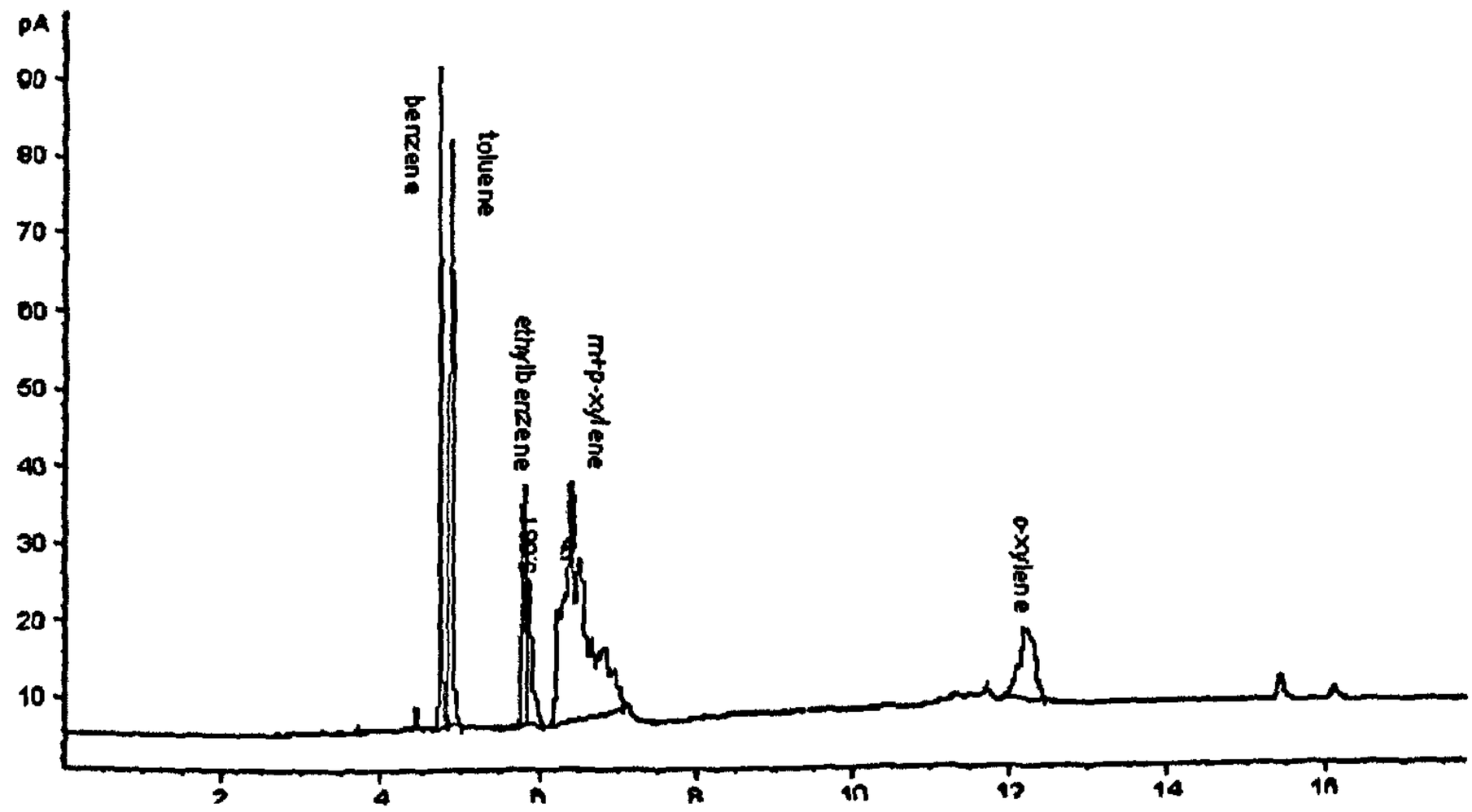

Figure 3.5 Chromatogram of BTEX compounds on Gaspro column (60 m, 0.32 mm).

3.5.1. Discussion – Gaspro column

The Gaspro column is not a good substitute for the Al_2O_3/KCl (50 m, 0.32 mm) PLOT column. The column separated low molecular weight, C_1 - C_3 hydrocarbons very well, see Figure 3.6. Higher molecular weight hydrocarbons were not as well resolved (Figure 3.5) with considerable peak broadening being observed. Poorly resolved compounds include; n-pentane, n-hexane, 1-pentene, 1-hexane, cis-2-butene, ethylacetylene, 1-butene (in the C_4 standard) 1,3-butadiene, m- and p-xylene and o-xylene.

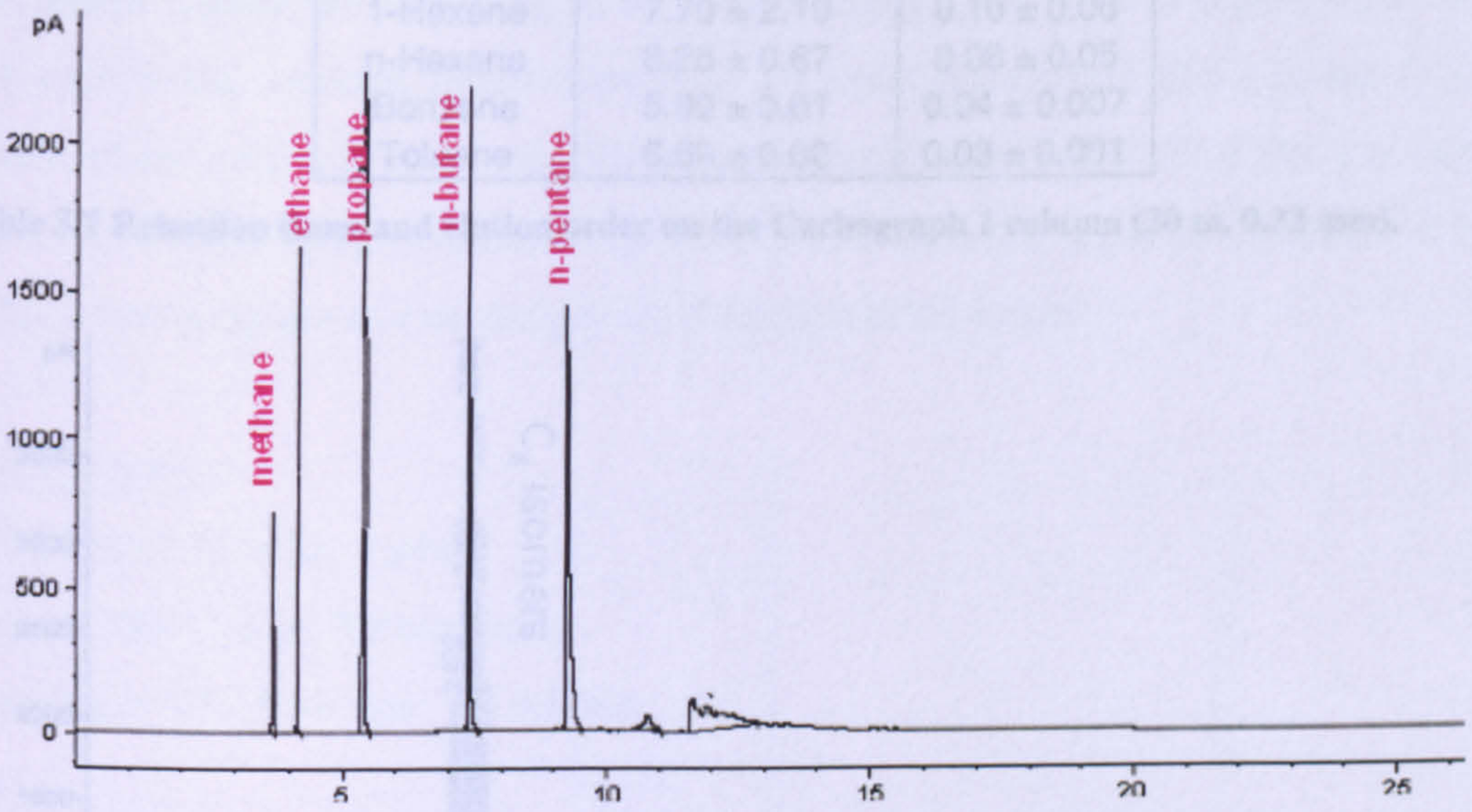

Figure 3.6 Chromatogram of alkane compounds on Gaspro column (60 m, 0.32 mm).

Due to the good separation capabilities of the Gaspro column for C_1 - C_3 hydrocarbons, this column could potentially be used to target the chromatographic analysis of low molecular weight hydrocarbons.

3.6. Carbograph 1 column (30 m, 0.32 mm, 0.25 µm)

The Carbograph 1 column was analysed using the following conditions:

Oven temperature program

30 °C initial, hold for 2 min.

Heat to 150 °C at 10 °C/min, hold.

Carrier gas (He) flow: 2.3 ml/min

Compound	Retention time (min)	Peak width (min)
Methane	co-elute	-
Ethene	co-elute	-
Ethane	co-elute	-
Propene	co-elute	-
Propane	co-elute	-
1-Butene	2.59 ± 0.44	0.04 ± 0.01
n-Butane	2.69 ± 0.50	0.05 ± 0.01
1-Pentene	3.82 ± 0.56	0.05 ± 0.01
n-Pentane	4.52 ± 0.96	0.05 ± 0.008
1-Hexene	7.70 ± 2.10	0.10 ± 0.06
n-Hexane	8.28 ± 0.67	0.08 ± 0.05
Benzene	5.99 ± 0.01	0.04 ± 0.007
Toluene	6.69 ± 0.02	0.03 ± 0.001

Table 3.7 Retention times and elution order on the Carbograph 1 column (30 m, 0.32 mm).

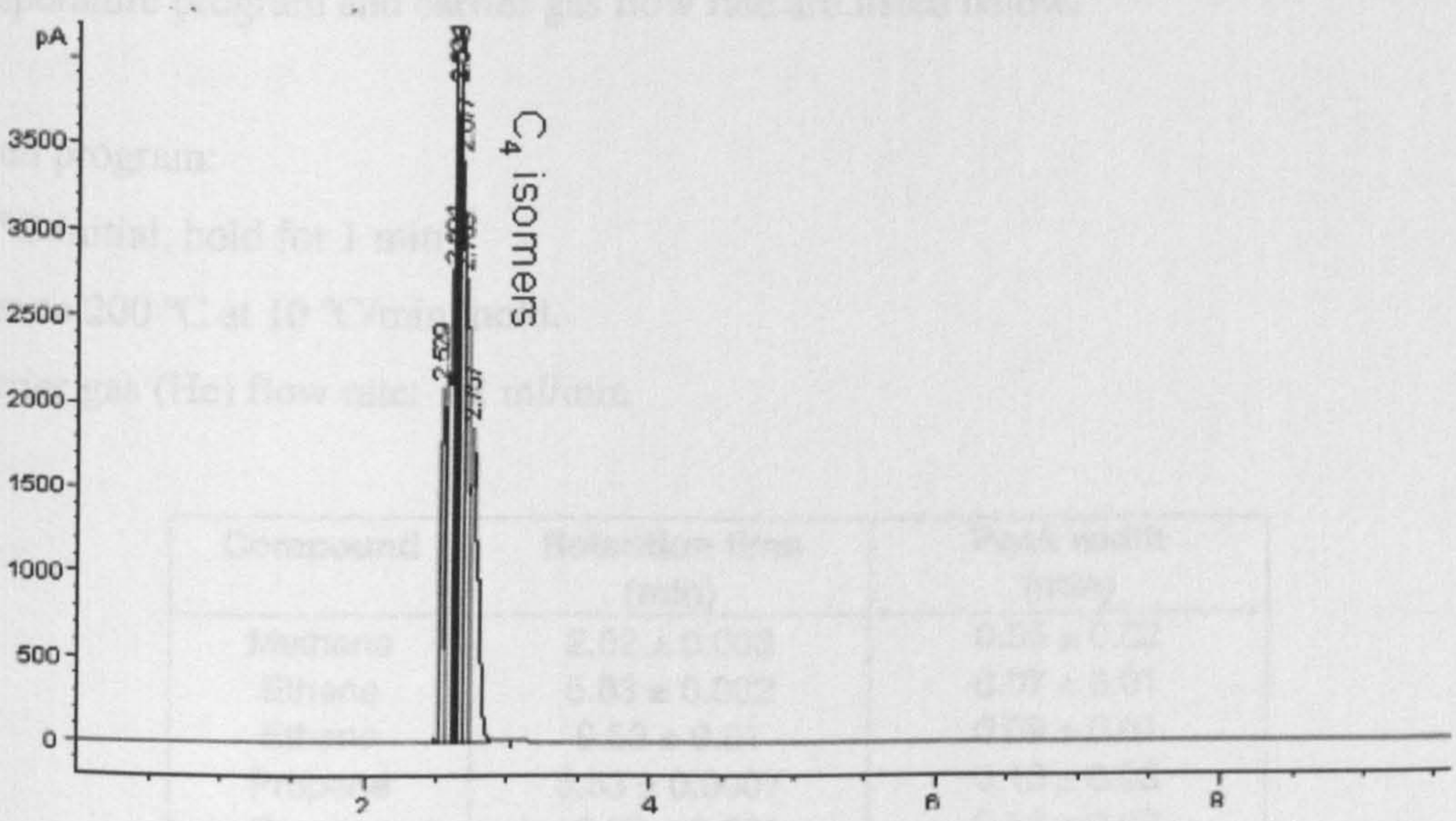

Figure 3.7 C_4 isomer standard run on the Carbograph 1 column (30 m, 0.32 mm).

3.6.1. Discussion – Carbograph column

Methane and ethane co-elute as do ethene and propene; these compounds could not be fully resolved by keeping the column isothermal at 30 °C or changing the carrier gas flow rates. All C_4 compounds also co-elute, and ethylbenzene and xylene isomers do not elute using these conditions; hence, only a select number of hydrocarbons (those

that don't co-elute) are listed in Table 3.7. This column is not a suitable replacement to the Al_2O_3/KCl (50 m, 0.32 mm) column.

3.7. Carboxen 1006 Column (30 m, 0.53 mm, 3 µm)

Carboxen 1006 was investigated for its separating ability of C_2 and C_3 hydrocarbons, to specifically target C_2 (and possibly C_3) hydrocarbons only, since poor peak shapes of C_2 NMHCs were observed by Martin, 2000. The idea of developing an NMHC instrument capable of separating an air sample using a bulk-trap in combination with two specifically selected micro-traps (one for pre-concentration of C_2 (possibly C_3) hydrocarbons and one micro-trap for $>C_3$ hydrocarbons) would allow for a possible separate chromatography columns to be utilised to better separate NMHCs. Oven temperature program and carrier gas flow rate are listed below:

Oven program:

40 °C initial, hold for 1 min

Heat to 200 °C at 10 °C/min, hold.

Carrier gas (He) flow rate: 7.2 ml/min

Compound	Retention time (min)	Peak width (min)
Methane	2.02 ± 0.003	0.05 ± 0.02
Ethene	5.83 ± 0.002	0.07 ± 0.01
Ethane	9.53 ± 0.01	0.09 ± 0.01
Propene	8.53 ± 0.0007	0.10 ± 0.03
Propane	13.08 ± 0.001	0.14 ± 0.02
1-Butene	12.81 ± 0.0007	0.40 ± 0.08
n-Butane	21.69 ± 0.03	0.80 ± 0.02

Table 3.8 Retention times and elution order on the Carboxen 1006 column

3.7.1. Discussion – Carboxen 1006

The baseline increased sharply with temperature after 107 °C. This could potentially be caused by a leak in the column as this column is old and it is unknown when it was previously used. Aside from this, the column achieved very good separation of the C_2

and C_3 hydrocarbons. Higher molecular weight hydrocarbons were retained too long in the column and gave broad peak in the chromatogram or did not elute at all.

An HP-5 transfer (30 m, 0.32 mm, 0.25 μm) line was installed, connecting from the external valve into the oven; using a Valco butt-connector it was connected to the Carboxen 1006 column. It was decided to use a transfer line to investigate whether compounds were being trapped in the stainless steel tubing which attaches the external Valco valve into the GC oven and connects with the chromatography column. The transfer line has little retention capabilities for hydrocarbons so they should quickly flow through the transfer line onto the Carboxen 1006 column. Using this transfer line resulted in improved peak shape for the eluted compounds. The only compounds to elute from the alkane standard were methane, ethane, propane (sharp, resolved peaks) and butane (broad peak). Without the use of the HP-5 transfer line methane and ethane result in sharp peaks and propane produces a broad peak. See Figures 3.8 and 3.9.

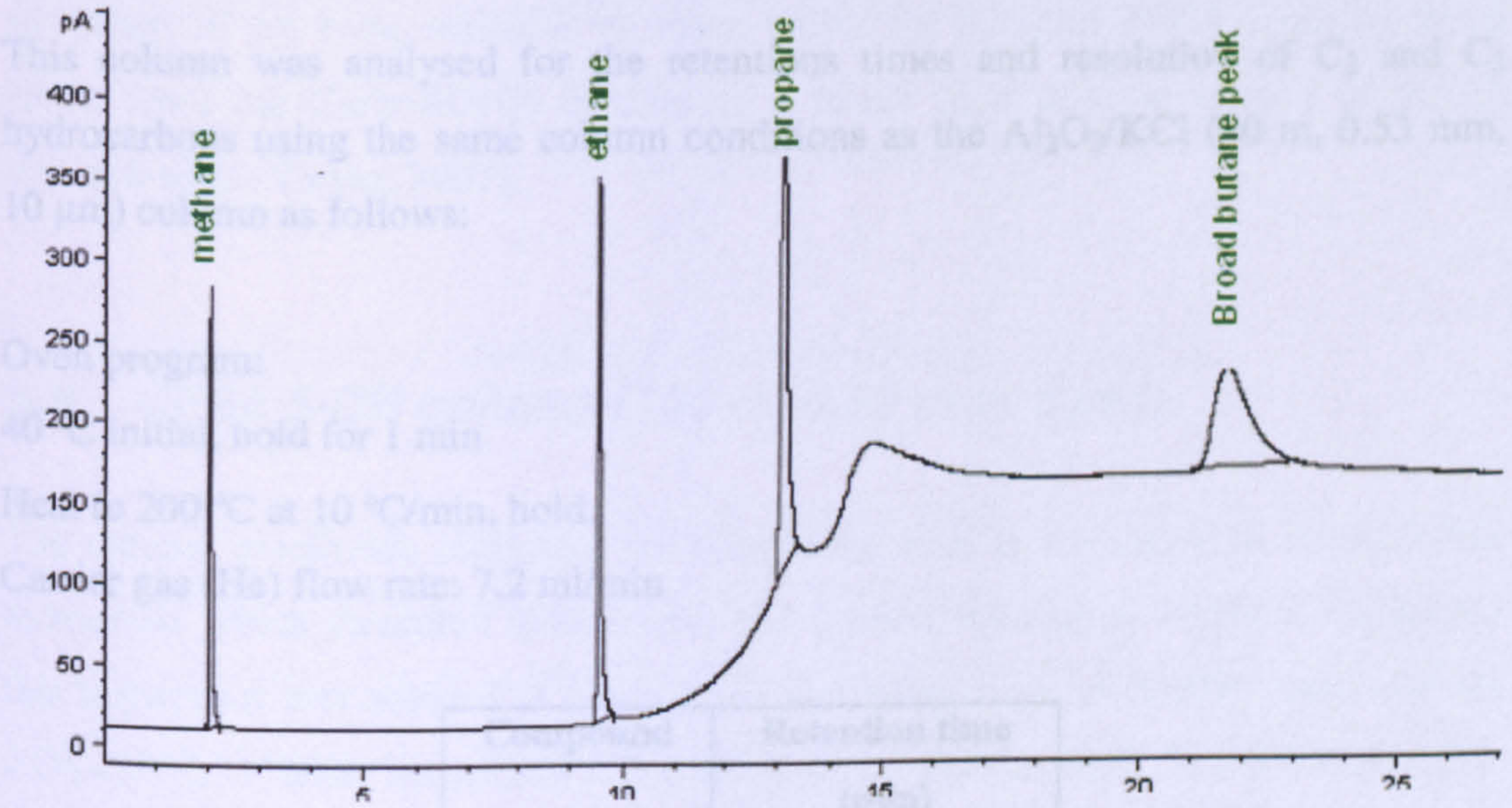

Figure 3.8 Alkane standard on the Carboxen 1006 column (with the transfer line).

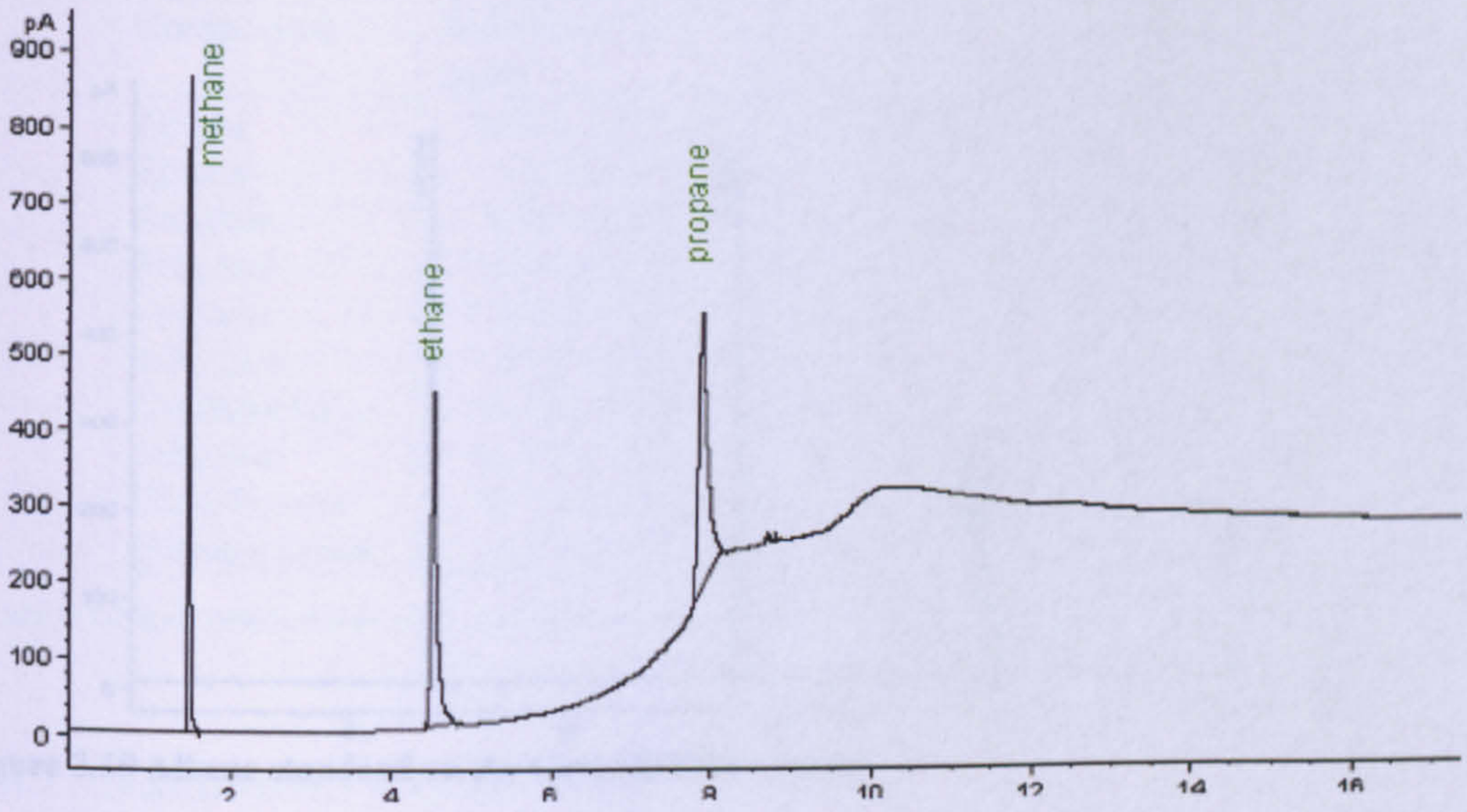

Figure 3.9 Alkane standard on the Carboxen 10006 column (without the transfer line).

3.8. CarboBOND column (25 m, 0.53 mm, 10 µm)

This column was analysed for the retentions times and resolution of C_2 and C_3 hydrocarbons using the same column conditions as the Al_2O_3/KCl (50 m, 0.53 mm, 10 µm) column as follows:

Oven program:

40 ºC initial, hold for 1 min

Heat to 200 ºC at 10 ºC/min, hold.

Carrier gas (He) flow rate: 7.2 ml/min

Compound	Retention time (min)
Methane	1.98 ± 0.01
Ethene	5.42 ± 0.01
Ethane	6.71 ± 0.01
Propene	12.22 ± 0.004
Propane	13.07 ± 0.01
1-Butene	17.90 ± 0.003
n-Butane	19.26 ± 0.02

Table 3.9 Retention times and elution order on the CarboBOND column.

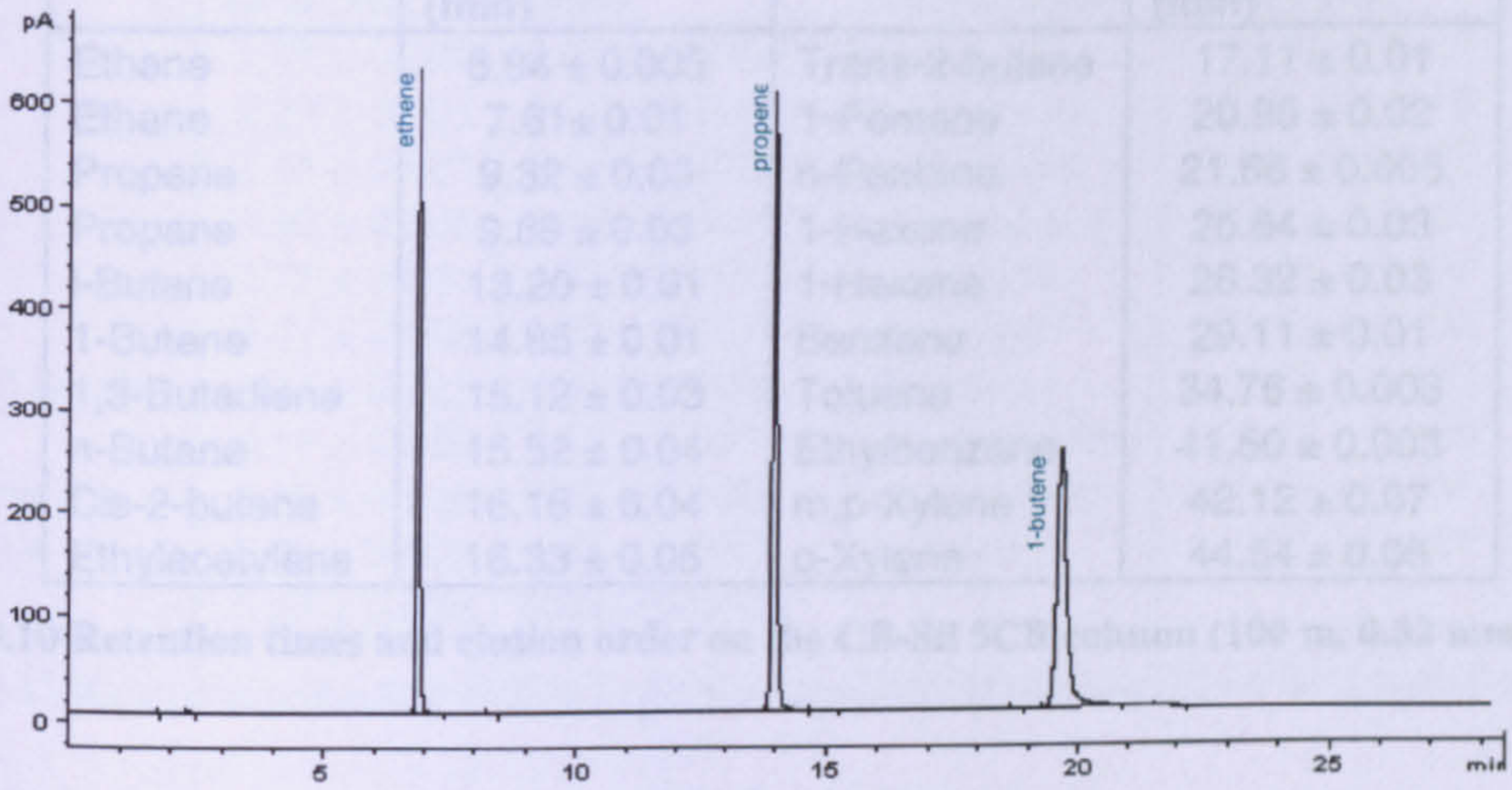

Figure 3.10 Alkene standard on the CarboBOND column.

3.8.1. Discussion – CarboBOND

CarboBOND gives good separation of C_2 and C_3 hydrocarbons, it also has the added advantage of not being sensitive to water, unlike the Alumina PLOT columns, water elutes from the CarboBOND column as a broad peak prior to elution of the C_2 hydrocarbons (Varian, 2007).

3.9. CPSil 5-CB column (100 m, 0.32 mm, 5 µm)

The column conditions replicated the conditions used in the AGAGE ADS-GCMS instrument which measured halocarbons and a select number of NMHCs. Originally this instrument was situated in Mace Head and comparison of NMHC data with the ADS-GCFID NMHC instrument was carried out by Martin, 2002. The AGAGE ADS-GCMS is now located in Carnsore Point, on the East coast of Ireland.

Oven program:

30°C initial, hold for 12 min.

Heat to 150°C at 10 °C/min, hold for 26 min.

Carrier gas (He) flow rate: 2.3 ml/min

Compound	Retention time (min)	Compound	Retention time (min)
Ethene	6.94 ± 0.005	Trans-2-butene	17.11 ± 0.01
Ethane	7.61± 0.01	1-Pentene	20.95 ± 0.02
Propene	9.32 ± 0.03	n-Pentane	21.66 ± 0.005
Propane	9.89 ± 0.03	1-Hexene	25.84 ± 0.03
i-Butane	13.20 ± 0.01	1-Hexane	26.32 ± 0.03
1-Butene	14.85 ± 0.01	Benzene	29.11 ± 0.01
1,3-Butadiene	15.12 ± 0.03	Toluene	34.76 ± 0.003
n-Butane	15.52 ± 0.04	Ethylbenzene	41.50 ± 0.003
Cis-2-butene	16.16 ± 0.04	*m,p*-Xylene	42.12 ± 0.07
Ethylacetylene	16.33 ± 0.05	o-Xylene	44.54 ± 0.05

Table 3.10 Retention times and elution order on the CB-Sil 5CB column (100 m, 0.32 mm, 5 µm).

3.9.1. Discussion – CPSil 5-CB

The column conditions used here replicate the temperature program and flow rates used in the old ADS-GCMS. This column gave poor resolution of the C_4 alkenes and so could not be used as a column to measure the full-suite of C_2 to C_8 hydrocarbons. The main aim of testing this column was to identify hydrocarbon peaks relative to the HFCs so as to confirm the hydrocarbon identification by the old Mace Head ADS-GCMS data from which was reported by Martin, 2000.

3.10. Porabond Q Column (25 m, 0.32mm, 5 µm)

The Porabond Q (25 m, 0.32mm, 5 µm) column is used in the AGAGE Medusa-GCMS, located at Mace Head. The Medusa makes routine measurements of HFCs, HCFCs and SF_6 and a select number of hydrocarbons, (see chapter 5 and 6 for detailed analysis of NMHC measurements taken by the Medusa-GCMS at Mace Head). The temperature program and flow rates replicate the conditions of the Medusa-GCMS.

Oven program:

40 °C initial,

Heat to 200 °C (hold) at 23 °C/min.

Carrier gas (He) flow rate: 2.2 ml/min

Compound	Retention time (min)	Peak width (min)	Compound	Retention time (min)	Peak width (min)
Methane	1.91 ± 0.002	0.05 ± 0.0002	n-Butane	5.32 ± 0.001	0.04 ± 0.0002
Ethene	2.23 ± 0.001	0.03 ± 0.0003	1-Pentene	6.55 ± 0.0005	0.04 ± 0.0001
Ethane	2.41 ± 0.001	0.03 ± 0.0003	n-Pentane	6.71 ± 0.0005	0.04 ± 0.0004
Propene	3.52 ± 0.005	0.02 ± 0.0003	1-Hexene	7.81 ± 0.0005	0.04 ± 0.0007
Propane	3.71 ± 0.001	0.03 ± 0.001	n-Hexane	7.94 ± 0.001	0.04 ± 0.0008
Ethylacetylene	5.01 ± 0.003	0.03 ± 0.0005	Benzene	8.95 ± 0.002	0.02 ±0.0004
1,3-Butadiene/i-butene	5.05 ± 0.003	0.06 ± 0.0008	Toluene	9.49 ± 0.003	0.03 ± 0.0005
1-Butene	5.11 ± 0.005	0.03 ± 0.0001	Ethylbenzene	11.92 ± 0.008	0.06 ± 0.002
Trans/cis butene	5.18 ± 0.002	0.02 ± 0.0002	m,p-Xylene	12.04 ± 0.001	0.06 ± 0.001
Trans/cis butene	5.22 ± 0.003	0.03 ± 0.0003	o-Xylene	12.57 ± 0.01	0.06 ± 0.005
i-Butane	5.29 ± 0.002	0.03 ± 0.0005			

Table 3.11 Retention times and elution order on Porabond Q column (25 m, 0.32 mm, 5 µm).

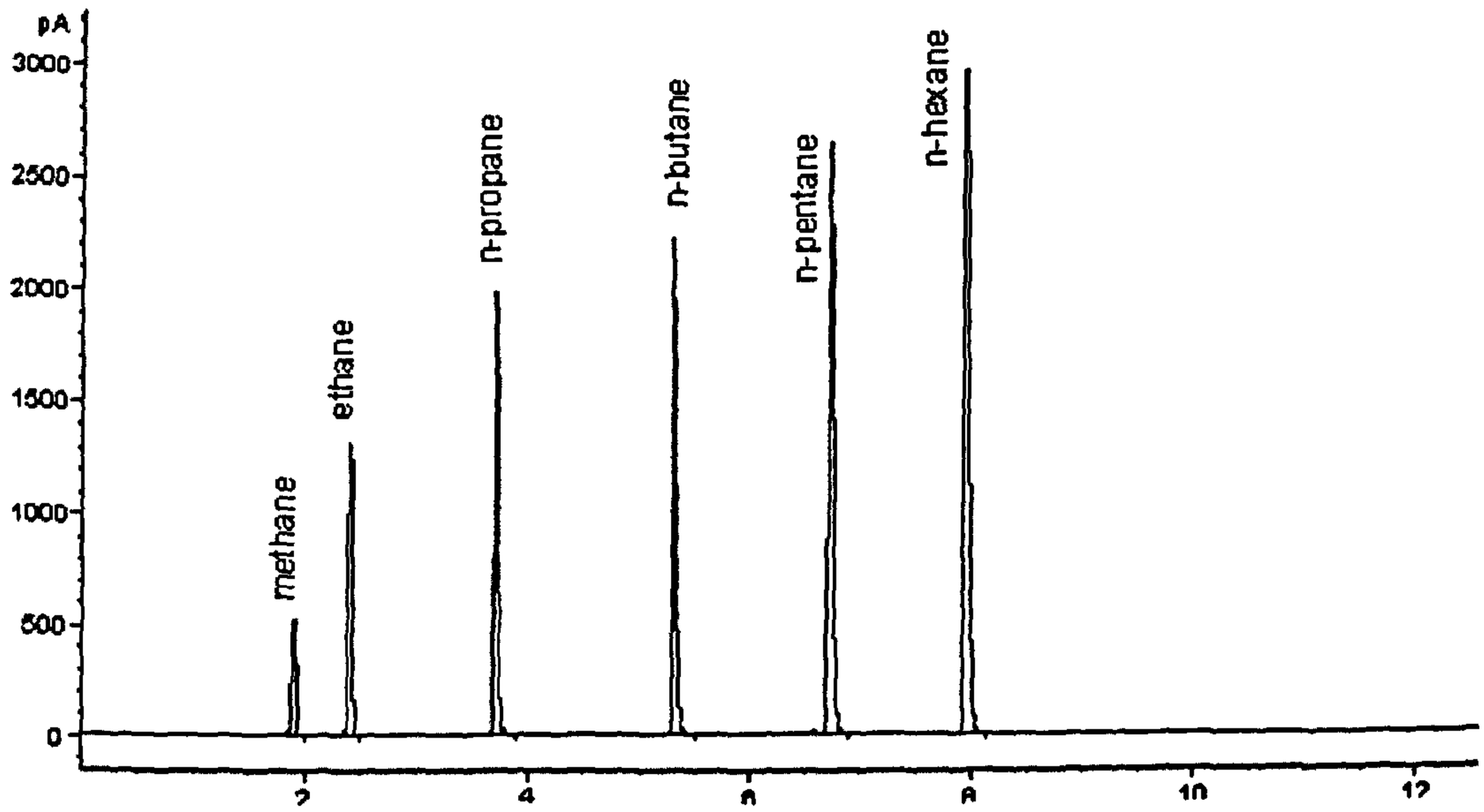

Figure 3.11 Alkane standard on the Porabond Q column (25 m, 0.32 mm, 5 µm).

3.10.1. Discussion – Porabond Q

The Porabond Q chromatography column gives poor resolution of the C_4 isomers as shown in Figure 3.11. Varying the temperature program and flow rates did not help to resolve these compounds.

The main aim for evaluating this column was to identify where hydrocarbons elute on the Porabond Q column with respect to the HFCs so as to enable hydrocarbons to be accurately identified with respect to HFCs on the Porabond Q column used in the Medusa GCMS. The retention times obtained from this experiment were compared

with the NMHC elution times from the Medusa-GCMS to confirm correct identification. Co-elution of 1,3-butadiene and 1-butene occurs on the Porabond Q column; this is a major problem when using a non-selective detector, such as the FID. However, the use of a selective detector such as a mass spectrometer can effectively resolve co-eluting compounds. The Medusa GCMS works in selective ion mode (SIM), rather than scanning (SCAN) over all ions, this means retention times and mass spectral target ions are used to identify a compound of interest. Hence, two co-eluting compounds, X and Y can be resolved if a (major) mass spectral ion in compound X is identified and not found in compound Y (and vice versa). This is discussed in more detail in section 5.5.

3.11. Conclusions

A range of capillary PLOT columns were analysed using direct loop injections of hydrocarbon standards onto the columns to determine the elution order, resolution and column suitability for separating NMHCs.

Al_2O_3/KCl (50 m, 0.53 m), Al_2O_3/Na_2SO_4 (50 m, 0.32 mm), Carbograph 1 (30 m, 0.32 mm) and Gaspro (60 m, 0.32 mm) columns were analysed for their separating ability of C_2 – C_8 hydrocarbons and capacity to act as a suitable substitute to the previously used Al_2O_3/KCl (50 m, 0.32 mm) NMHC chromatography column. The only columns which separate the full range of C_2 – C_8 hydrocarbons are the Alumina PLOT columns. Al_2O_3/KCl (50 m, 0.53 m) and Al_2O_3/Na_2SO_4 (50 m, 0.32 mm) could both be an effective substitute for the Al_2O_3/KCl (50 m, 0.32 mm) column. However, they all show the same disadvantages: poor peak shape of C_2 hydrocarbons, high sensitivity to water and co-elution of m-xylene and p-xylene isomers.

The only advantage of the Al_2O_3/Na_2SO_4 (50 m, 0.32 mm) column over the Al_2O_3/KCl (50 m, 0.32 mm) column is the considerably shorter analysis time, 22 minutes and 87 minutes respectively. However, the Al_2O_3/Na_2SO_4 (50 m, 0.32 mm) column exhibits poorer peak shape of the C_4 isomers. Adsorption on Alumina PLOT columns and therefore peak shape is due to the interaction with the deactivating agents, KCl and Na_2SO_4. Na_2SO_4 is more polar than KCl, hence a stronger interaction between the stationary phase and analytes.

The advantage of Al_2O_3/KCl (50 m, 0.53 mm) over Al_2O_3/KCl (50 m, 0.32 mm) is the shorter analysis time, 55 minutes and 87 minutes respectively. Acetylene and i-butane are well resolved peaks on the Al_2O_3/KCl (50 m, 0.32 mm) column as shown in Scanview, 8.0. The 0.53 mm column combines the attributes of a fused-silica capillary column with the high sample capacity of a packed column (Grob and Barry, 2004). It was decided that although the Alumina PLOT columns have inherent problems with water management and can not separate m,p-xylene, still the best overall column to separate the full range of C_2 – C_8 hydrocarbons is the Al_2O_3/KCl (50 m, 0.53 mm).

Two columns were tested in view of analysing the C_2 (possibly C_3) hydrocarbons, the CarboBOND and Carboxen 1006 columns. This is to overcome the poor peak shapes of C_2 hydrocarbons on the Alumina PLOT column; an air sample could be split allowing separate analysis of light and heavy molecular weight hydrocarbons on two separate columns (housed in the same GC oven). CarboBOND and Carboxen 1006 columns both sufficiently separated C_2 and C_3 hydrocarbons, producing improved peak shapes compared to Alumina PLOT columns. Both columns are 0.53 mm internal diameter, so that when used to analyse C_2 hydrocarbons along with the Al_2O_3/KCl (50 m, 0.53 mm) to measure > C_3 hydrocarbons there would be no issue with variation in flows which would be caused by using a 0.32 mm column with a 0.53 mm column. The CarboBOND column has the advantage of a steady baseline at higher temperatures, compared to the Carboxen 1006 which exhibited an increasing baseline with temperature due to column bleed. Hence the CarboBOND column is a well suited column to be used for analysis of C_2 and C_3 hydrocarbons.

CPSil 5-CB and Porabond Q columns were analysed to determine the elution order of NMHCs; the information obtained from these results were used to help accurately identify the NMHC retention times compared to the halocarbons on the AGAGE ADS-GCMS and Medusa-GCMS instruments, both of which measure a select number of NMHCs in Irish research sites.

4. NMHC instrument design

4.1. Introduction

Based on the initial BTV work described in chapter 2 and the research into column types discussed in chapter 3, a pre-concentration system was built to specifically measure NMHCs in a remote environment. The design features and instrument development are discussed in this chapter an illustrative diagram showing the concept of the instrument is shown in Figure 2.3.

The instrument frame was based on a modified version of the Medusa-GCMS frame. The NMHC instrument frame sits to the left of the GC-FID (Agilent 6890N GC). This is unlike the Medusa frame which sits above the GCMS, because the FID would be obstructed by the frame.

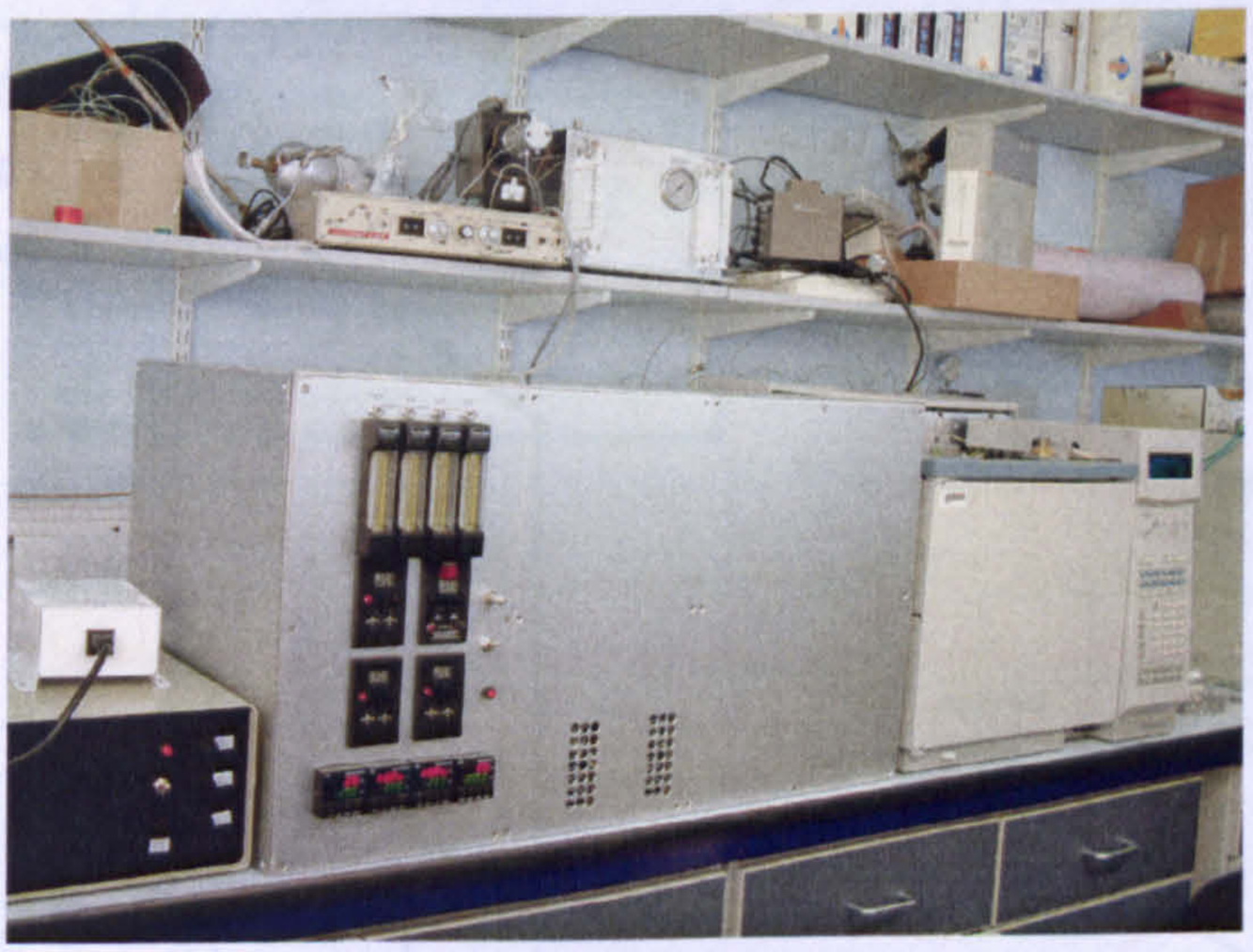

Figure 4.1 NMHC pre-concentration system situated to the left of the GC-FID.

The NMHC instrument is remote controlled using Linux operating software designed by Scripps institute of Oceanography, San Diego, USA.

Conclusions from initial BTV experiments (chapter 2) suggested the 3 g Hayesep D bulk-trap can fractionate, at room temperature C_2 hydrocarbons (and most of the

water) from C_3 and higher hydrocarbons. Two micro-traps were chosen based on their BTV properties; the first trap, the Carbosieve SIII micro-trap specifically adsorbs C_2 hydrocarbons. The second micro-trap, which specifically targets $\geq C_3$ hydrocarbons, is a Hayesep D adsorbent filled micro-trap. The principle is that the more volatile C_2 hydrocarbons (being unaffected by the Nafion drier) are purged from the 3 g Hayesep D bulk-trap at ambient temperature with helium, travel through the Nafion drier (along with water) to the C_2 (Carbosieve SIII) micro-trap, held at –40 °C by Peltier units. The C_3 and higher molecular weight hydrocarbons are back-flushed with helium and heated to desorb from the 3 g Hayesep D bulk-trap and are re-focused using a small transfer volume of helium onto the second micro-trap; a Hayesep D micro-trap, held at –40 °C. The transfer of the $\geq C_3$ hydrocarbons from the bulk-trap to the refocusing micro-trap occurs whilst the C_2 hydrocarbons are analysed by GC-FID. Once this is complete the C_3 and higher hydrocarbons are injected onto the GC column for detection. A valve diagram can be seen in Figure 4.2.

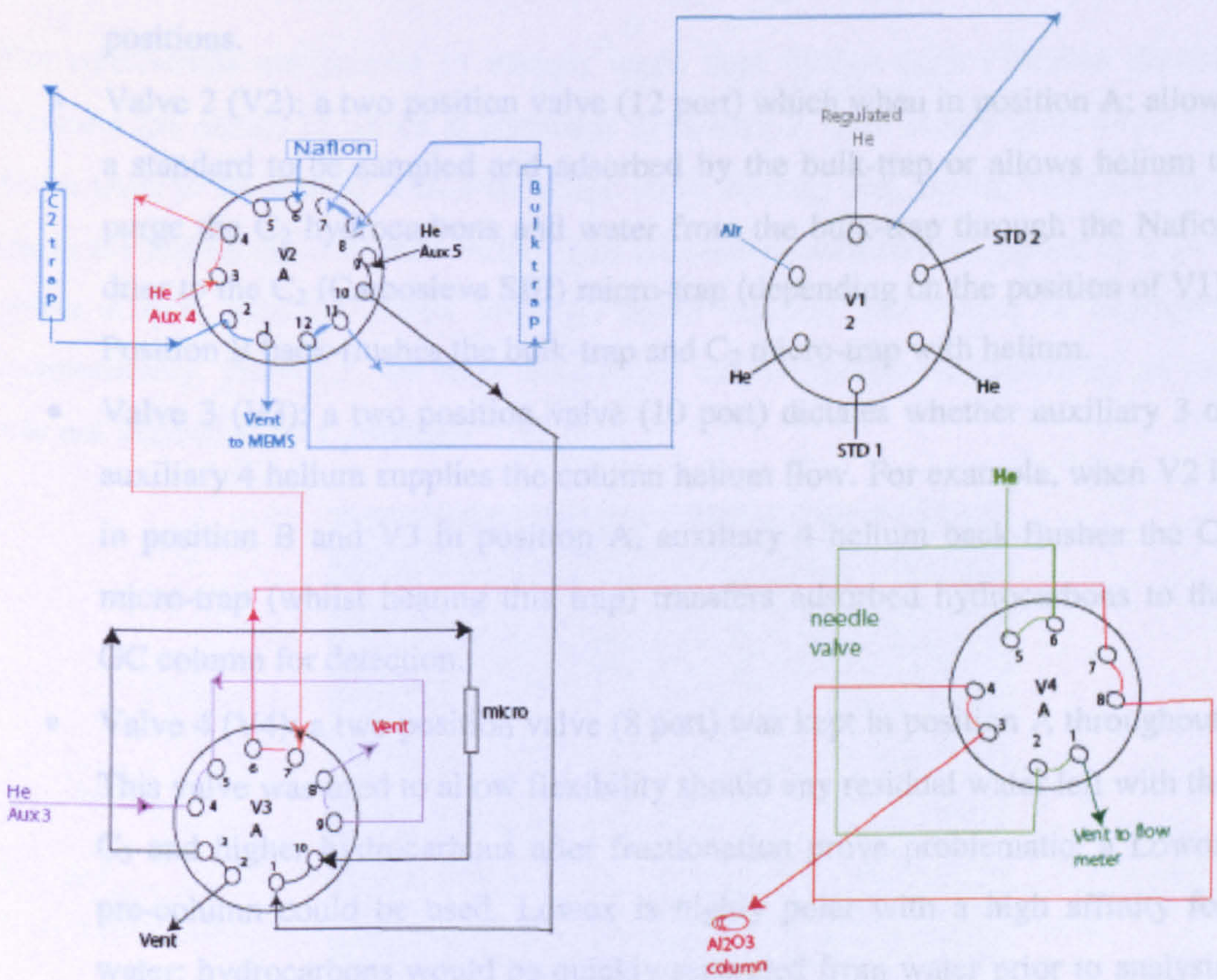

Figure 4.2 Valve diagram of the NMHC instrument

The system utilises four Valco valves situated within a heated zone see Figure 4.3. The valve enclosure is maintained at 40 °C using a heater controlled with the use of a thermal auxiliary channel from the Agilent GC. The 40 V DC from the auxiliary channel is directed through resistance wire, and the heat generated is circulated through the valve enclosure by a small fan. The temperature is fed back to the auxiliary channel using a PT 100 temperature sensor. The valve enclosure is heated to prevent loss of hydrocarbons to the inner wall of the tubing.

Each valve has a purged housing which is swept with helium to keep the valves free of contamination from ambient air or standards.

- Valve 1 (V1): 6 port multi-position valve allowing various gases to be sampled. Helium is plumbed to position 1, lab air to position 2, zero air to position 3, Apel-Reimer standard to position 4 and position 5 and 6 are spare positions.
- Valve 2 (V2): a two position valve (12 port) which when in position A; allows a standard to be sampled and adsorbed by the bulk-trap or allows helium to purge the C_2 hydrocarbons and water from the bulk-trap through the Nafion drier to the C_2 (Carbosieve SIII) micro-trap (depending on the position of V1). Position B back-flushes the bulk-trap and C_2 micro-trap with helium.
- Valve 3 (V3): a two position valve (10 port) dictates whether auxiliary 3 or auxiliary 4 helium supplies the column helium flow. For example, when V2 is in position B and V3 in position A, auxiliary 4 helium back-flushes the C_2 micro-trap (whilst heating this trap) transfers adsorbed hydrocarbons to the GC column for detection.
- Valve 4 (V4): a two position valve (8 port) was kept in position A throughout. This valve was used to allow flexibility should any residual water left with the C_3 and higher hydrocarbons after fractionation prove problematic, a Lowox pre-column could be used. Lowox is highly polar with a high affinity for water; hydrocarbons would be quickly separated from water prior to analysis by GC-FID.

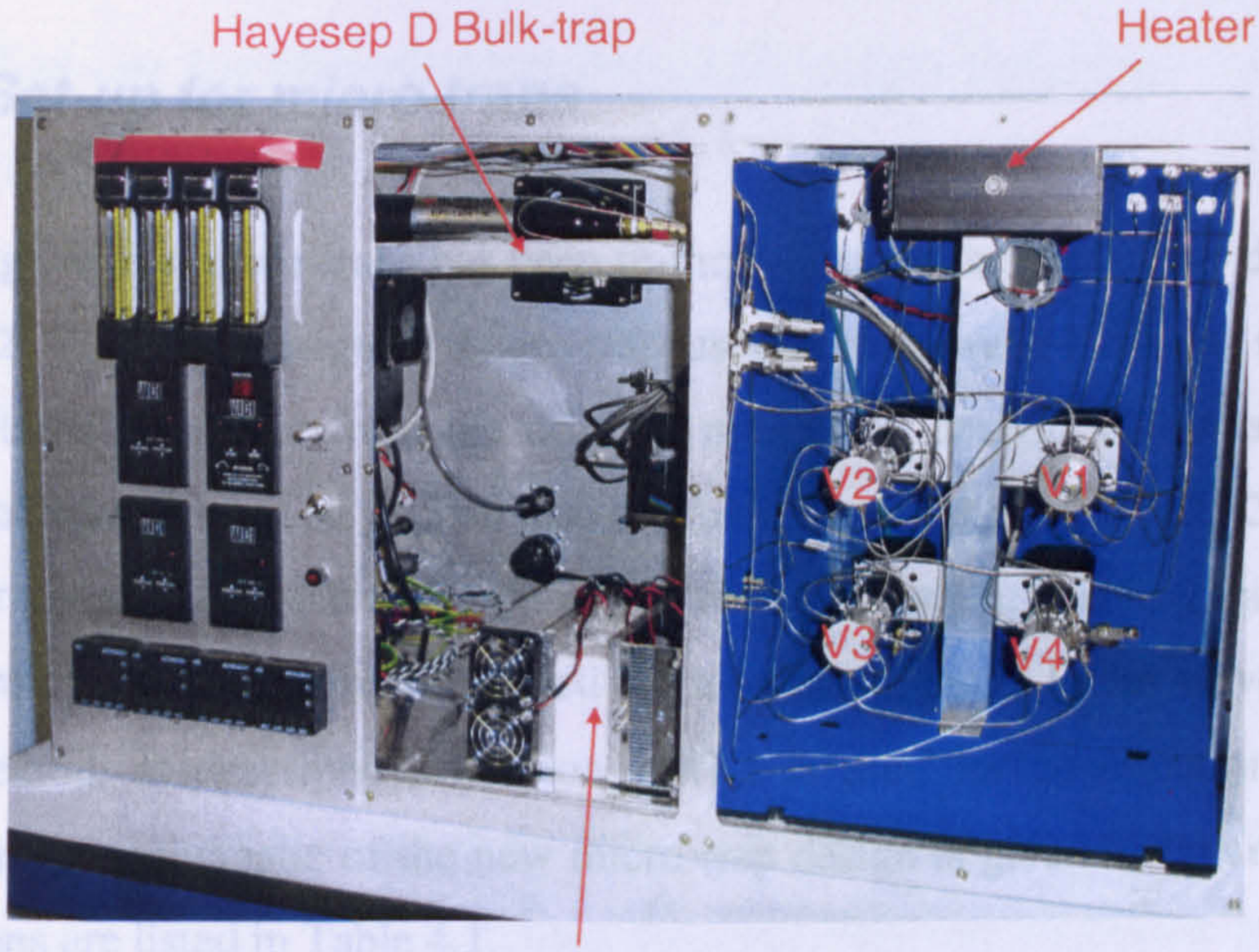

Figure 4.3 View of the inside of the NMHC instrument

The micro-traps are housed in custom made dual Peltier units (Thermo Electric Devices) the details of which is discussed in chapter 2. Dual Peltier units allow two micro-traps to be housed within the same sized cooling fins, saving valuable space inside the instrument. The dual Peltier units are connected in series supplied by a 24 V power supply, thus the Peltier units go on/off together and cannot be controlled independently. However, the traps themselves can be heated independently so this was not deemed to be a problem.

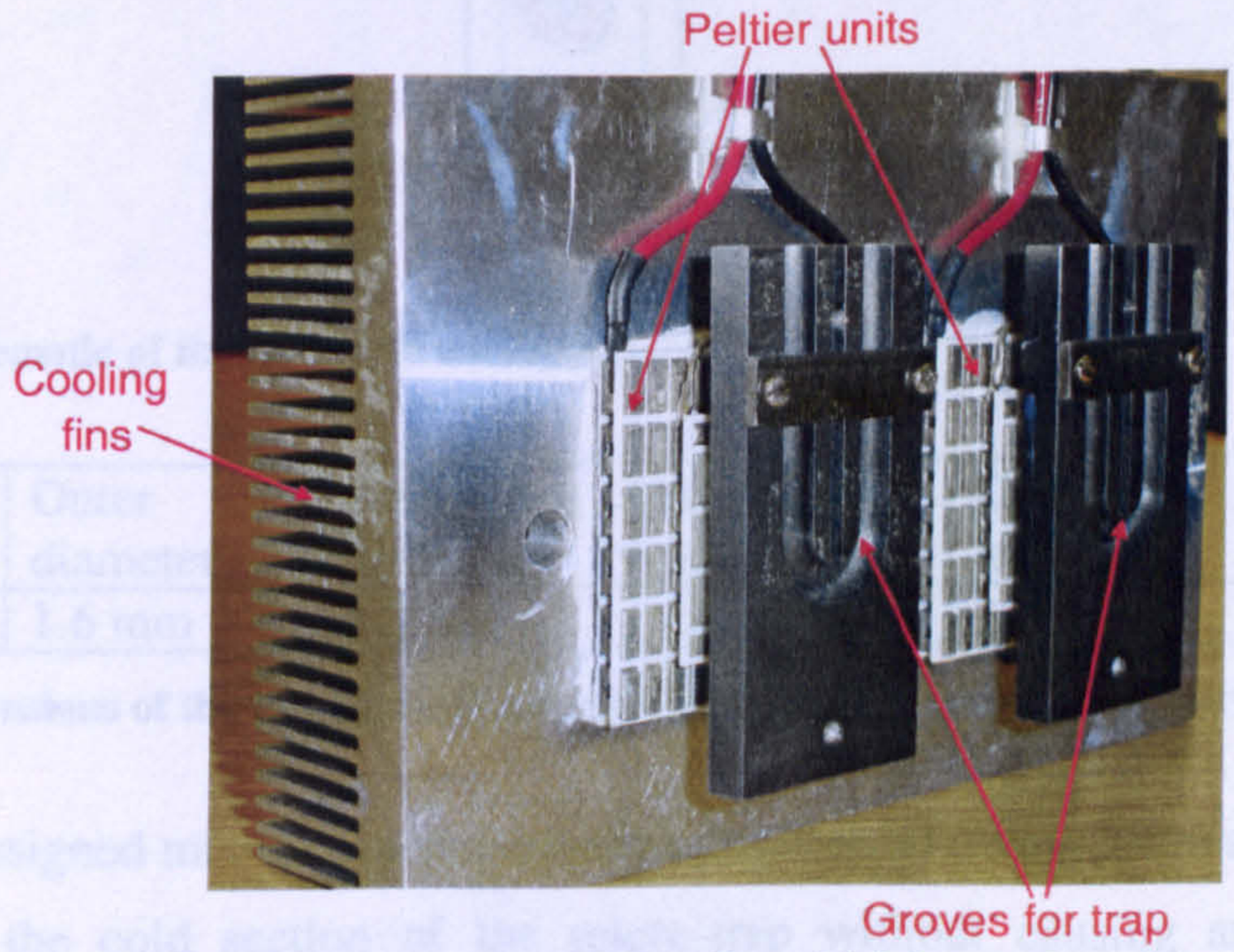

Figure 4.4 Dual Peltier units, cold plates and cooling fins which house the micro-traps.

4.2. Set-up for micro-traps

The design of the micro-traps has been re-thought since the micro-trap design used in chapter 2. The new design of micro-trap uses thinner walled tubing, resulting in a wider internal diameter from the original micro-trap design. This enables a larger amount of adsorbent to be packed into the micro-trap and held at -40 °C with the use of Peltier units. The new trap design is also longer in length, enabling the micro-traps, to be bent by 90 ° and to be connected via a bulkhead union to the valve tubing. The same method, as described in section 2.4.1.1 is used for construction of the new micro-traps. A schematic of the new micro-trap design is given in Figure 4.5 and the dimensions are listed in Table 4.1.

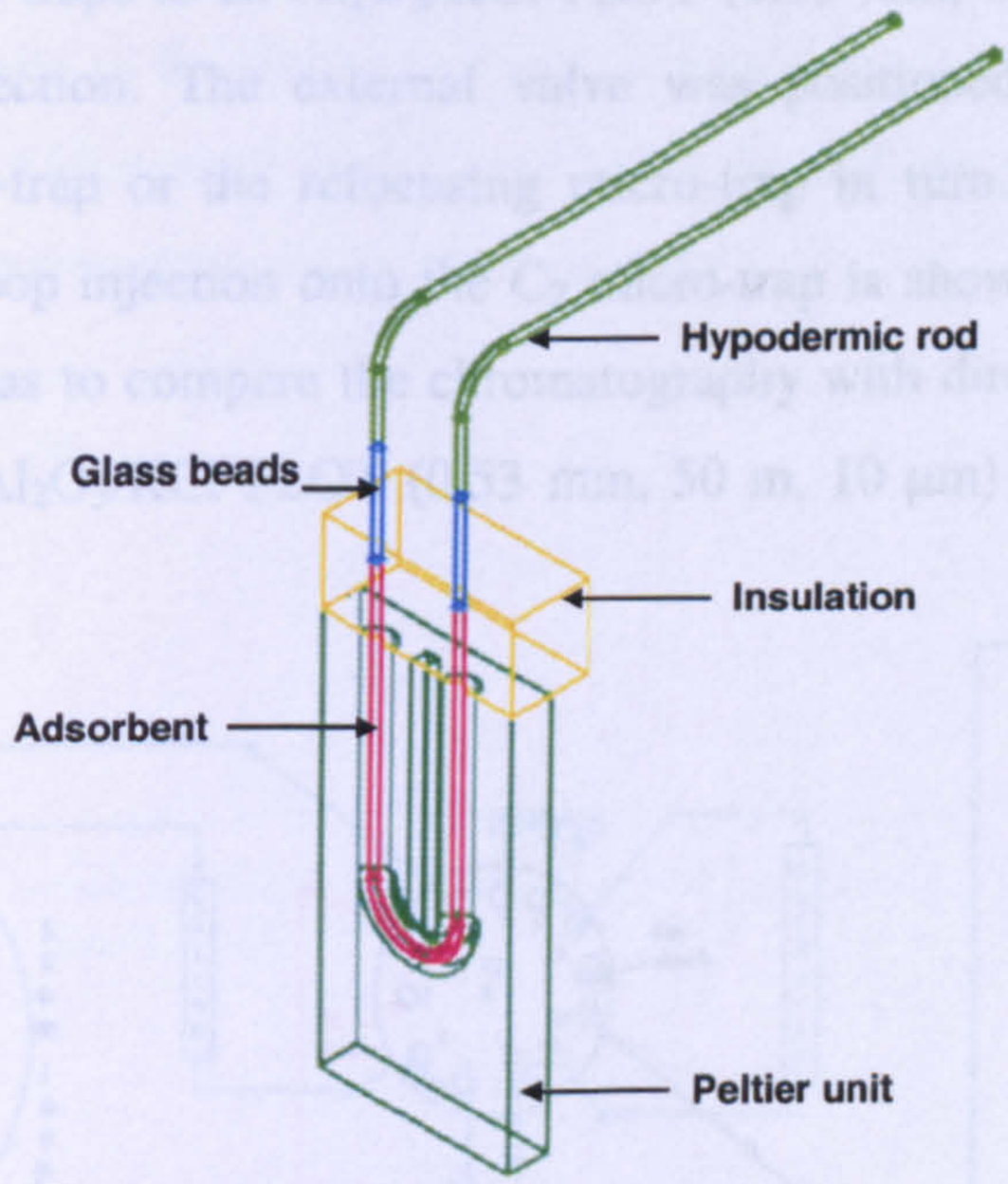

Figure 4.5 Schematic of the new-style micro-trap.

Trap length	Outer diameter	Inner diameter	Adsorbent length	Glass bead length	Hypodermic rod length
332 mm	1.6 mm	1.3 mm	110 mm	2 * 15 mm	2 * 95 mm

Table 4.1 Dimensions of the new-style micro-traps used in the elution BTV experiments.

The newly designed micro-traps proved advantageous, allowing more adsorbent to be packed into the cold section of the micro-trap without causing any significant, negative affects on the chromatography. The result of this improvement allowed larger volumes of gas to be sampled before BTVs were exceeded.

4.3. Set-up for the elution breakthrough volume determination

4.3.1. Procedure

An external Valco 6 port, 2-position valve was used to allow 50 µl loop injections of ppmv concentration hydrocarbon standards to be transferred on to each of the three traps in turn. The micro-traps were cooled to -40 °C and the bulk-trap was held at room temperature. The wiring of the Peltiers and micro-traps is such that cooling of the micro-traps occurs simultaneously but each trap can be heated independently. Desorption from the traps to an Al_2O_3/KCl PLOT (0.53 mm, 50 m, 10 µm) column and a FID for detection. The external valve was positioned either prior to the bulk-trap, C_2 micro-trap or the refocusing micro-trap in turn. An example of the set-up for a 50 µl loop injection onto the C_2 micro-trap is shown in Figure 4.6. The aim of this set-up was to compare the chromatography with direct loop injections of standards onto the Al_2O_3/KCl PLOT (0.53 mm, 50 m, 10 µm) column discussed in chapter 3.

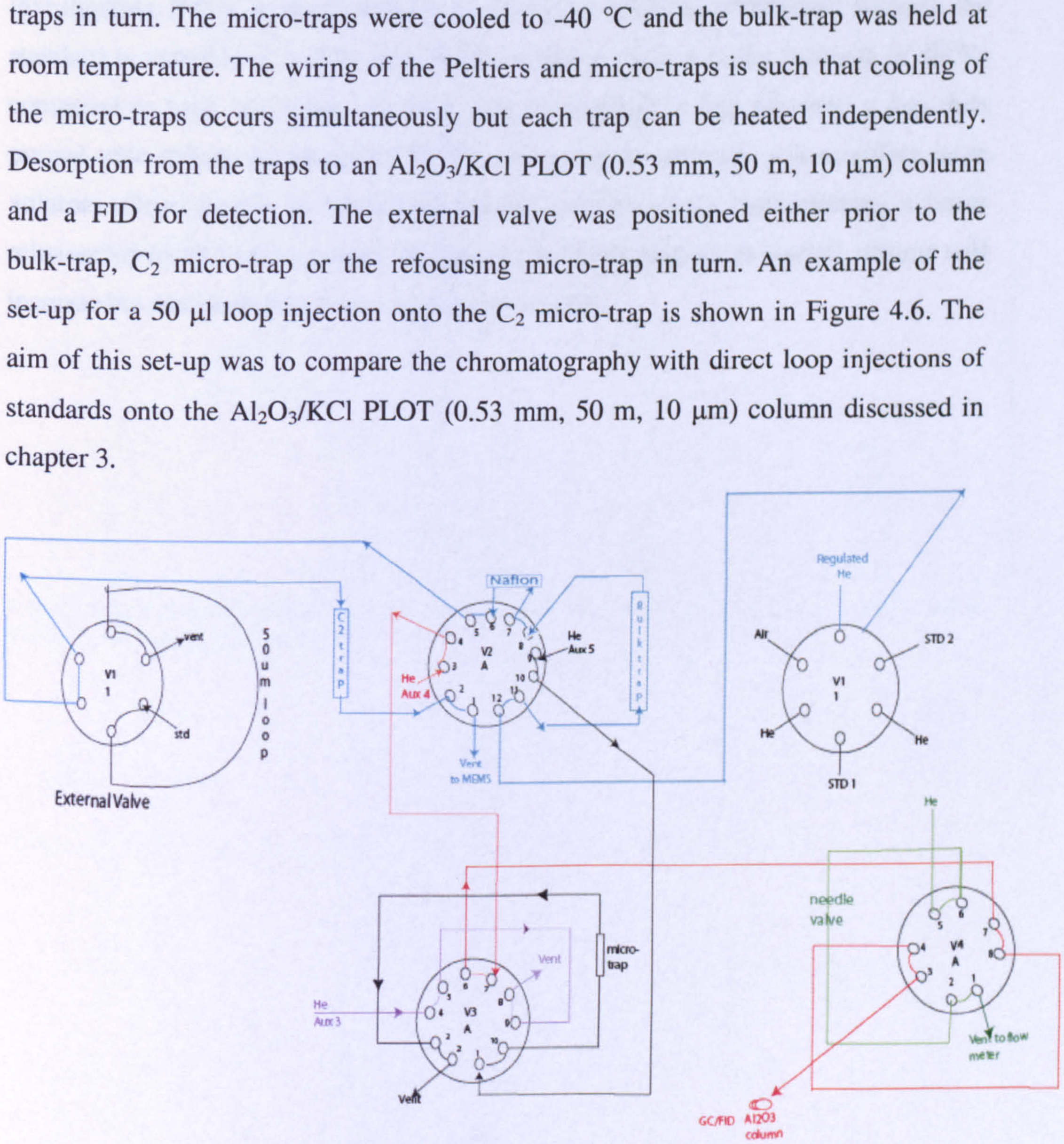

Figure 4.6 Valve diagram allowing 50 µl standard loop injections onto the C_2 micro-trap.

After successfully demonstrating that the previous step worked the next step was to sample varying concentrations of a ppbv concentration Apel-Reimer hydrocarbon standard. The Apel-Reimer standard has a wide range of hydrocarbons in the ppbv concentration range it was used in the previous NMHC instrument at Mace Head as its working standard plumbed directly to valve 1; varying volumes of the Apel-Reimer standard were sampled, to determine BTVs and trap linearity results. Because the Apel-Reimer standard is plumbed direct to valve 1 and does not require loop injections, varying volumes of the standard can be taken. This method for investigating BTVs is more realistic to everyday sampling conditions; because the standard is sampled at a flow rate of 50 ml/min it gives a better estimate of BTVs compared to loop injections, where a plug of standard is injected onto a trap then purged with helium to determine BTVs. Using a ppbv standard and sampling large volumes allows graphs to be plotted; sample volume versus concentration, a linear relationship should be seen, until the point of break-through when sample volume will increase but concentration does not increase linearly.

4.3.2. Standards

Table 4.2 shows the standards used to make loop injections. Table 4.3 lists the contents of the Apel-Reimer hydrocarbon standard.

Standard	Supplier	Contents	Concentration in standard (ppmv)	Affective column concentration after injecting 50 µl loop (ppmv)
Alkane	Supelco	Methane	1002	50.1
		Ethane	989	49.5
		Propane	974	48.7
		n-Butane	976	48.8
		n-Pentane	1025	51.3
		n-Hexane	979	49.0
Alkene	Scientific & Technical Gases	Ethene	1000	50.0
		Propene	998	49.9
		1-Butene	1009	50.5
		1-Pentene	994	49.7
		1-Hexene	1020	51.0
C_4	Scientific & Technical Gases	n-Butane	1032	51.6
		Isobutane	1018	50.9
		Cis-2-butene	1028	51.4
		Trans-2-butene	1018	50.9
		1-Butene	1018	50.9
		Isobutene	1018	50.9
		1,3-Butadiene	1028	51.4
		Ethylacetylene	1028	51.4

Table 4.2 Hydrocarbon standards used to make standard loop injections to examine BTVs. 50 µl Valco stainless steel loops accurate to ± 5%

	Compound	Conc in Std (pptv)		Compound	Conc in Std (pptv)
C2	Ethane	11700	C6	Cyclohexene	1680
C2	Ethene	5510	C6	Benzene	1950
C2	Ethyne (Acetylene)	8700	C7	Toluene	2430
C3	Propane	10480	C7	1,3- dimethylcyclopentane (cis)	3050
C3	Propene	2250	C7	1-heptene	4550
C3	Propyne	5540	C7	Heptane	4790
C4	n-Butane	9490	C7	2,3-dimethyl-2-pentene	940
C4	isobutane (2 methyl propane)	4790	C7	Methylcycloheaxene	840
C4	isobutene	3560	C7	2,4-dimethylpentane	950
C4	1-butene	2310	C8	2,3,4 trimethylpentane	530
C4	t-2-butene	1170	C8	2-methylheptane	460
C4	c-2-butene	2230	C8	3-methylheptane	1170
C4	1,3 butadiene	2210	C8	4-methylheptane	950
C4	1,2 butadiene	5390	C8	Octane	470
C5	n-pentane	7620	C8	o-xylene	390
C5	i-pentane	7170	C8	m-xylene	1340
C5	cyclopentane	960	C8	p-xylene	420
C5	t-2-pentene	910	C8	styrene (ethenylbenzene)	390
C5	c-2-pentene	2240	C9	Indan(e)	1040
C5	1-pentene	1170	C9	Nonane	910
C5	2 methyl-1-butene	1110	C9	I-propylbenzene	190
C5	2 methyl-2-butene	900	C9	Propylbenzene	210
C5	cycopentene	890	C9	1,3,5-trimethylbenzene	570
C5	isoprene	4580	C9	2-ethyltoluene	420
C6	hexane	2960	C9	3-ethyltoluene	200
C6	2-2 dimethyl butane	2540	C9	4-ethyltoluene	390
C6	2-3 dimethyl butane	1710	C9	1,2,4-trimethylbenzene	800
C6	cyclohexane	480	C9	1,2,3-trimethylbenzene	1130
C6	2-methylpentane	960	C10	t-butylbenzene	1510
C6	3-methylpentane	990	C10	Decane	860
C6	2-methyl-1-pentene	910	C10	1,3 dietyhylbenzene	630
C6	t-2-hexene	460	C10	1,4 dietyhylbenzene	790
C6	c-2-hexene	920	C10	Butylbenzene	400
C6	1,3 hexadiene	2150	C11	Undecane	400
C6	methylcyclopentane	950			

Table 4.3 Contents of the Apel-Reimer hydrocarbon standard accurate to ± 2%.

4.4. Results from elution technique

4.4.1. Loop injections of ppm concentration NMHC standards

Comparison of loop injections of standards directly onto the Al_2O_3/KCl (50 m, 0.53 mm, 10 μm) column (discussed in chapter 3) with standards pre-concentrated on a micro-trap, prior to separation on the Al_2O_3/KCl column focused on the respective chromatographic peak shape, resolution and retentions times. Adsorbent traps will affect results if they adsorb too strongly, resulting in peak broadening and asymmetric chromatographic peak shapes; traps may also produce artefacts when desorbed at high temperatures which may interfere with peaks.

Comparing loop injections of standards directly onto the column with loop injections pre-concentrated on the Carbosieve SIII and Hayesep D micro-traps and desorbed onto the Al_2O_3/KCl (50 m, 0.53 mm, 10 μm) column showed promising results. The Peak areas and/or heights for both direct loop injections and injections via the micro-trap were very similar and reproducible. This indicates good recovery from the micro-traps. Figure 4.7 compares the peak areas for the C_4 isomers on the Hayesep D micro-trap and the C_2-C_3 NMHCs on the Carbosieve SIII micro-trap.

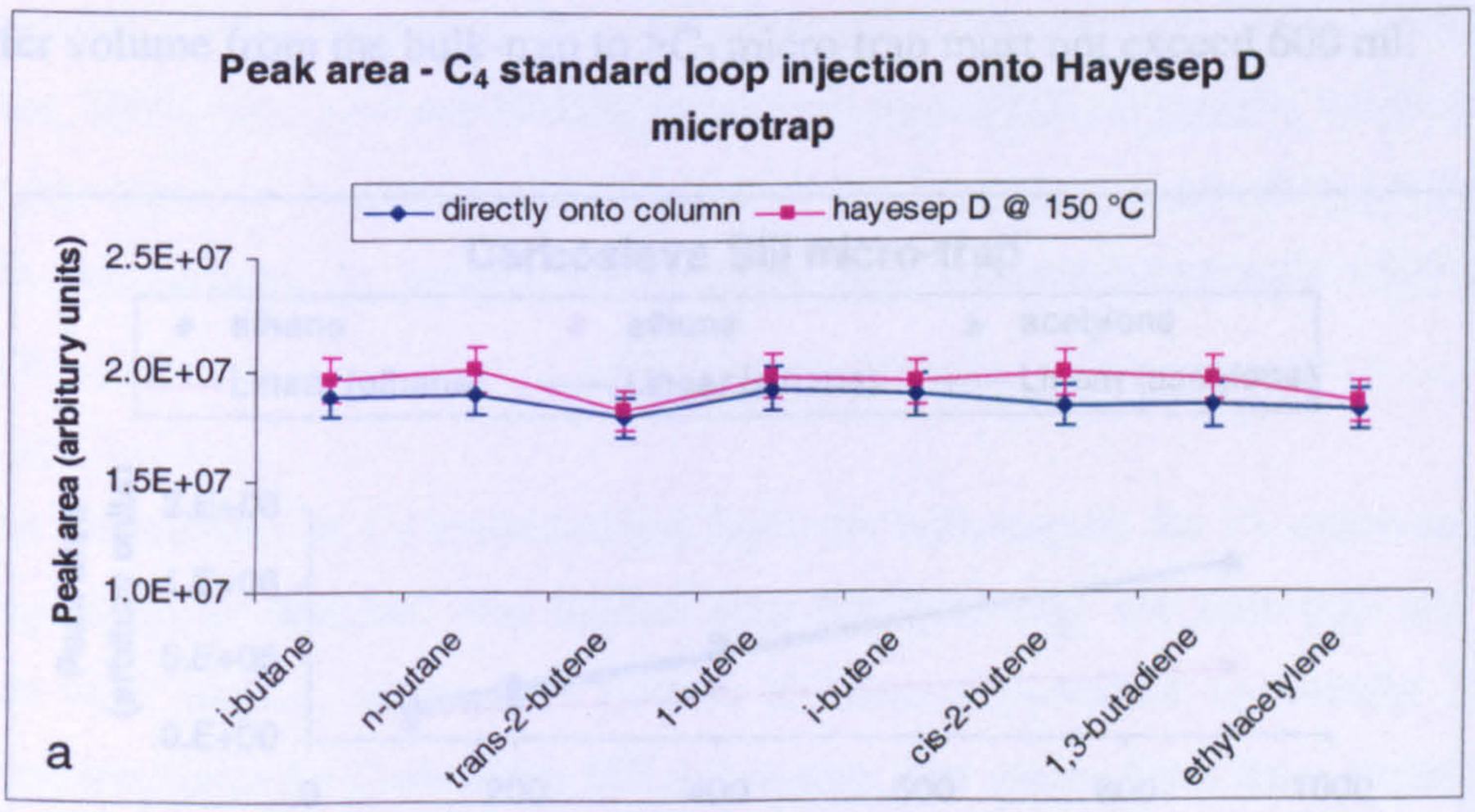

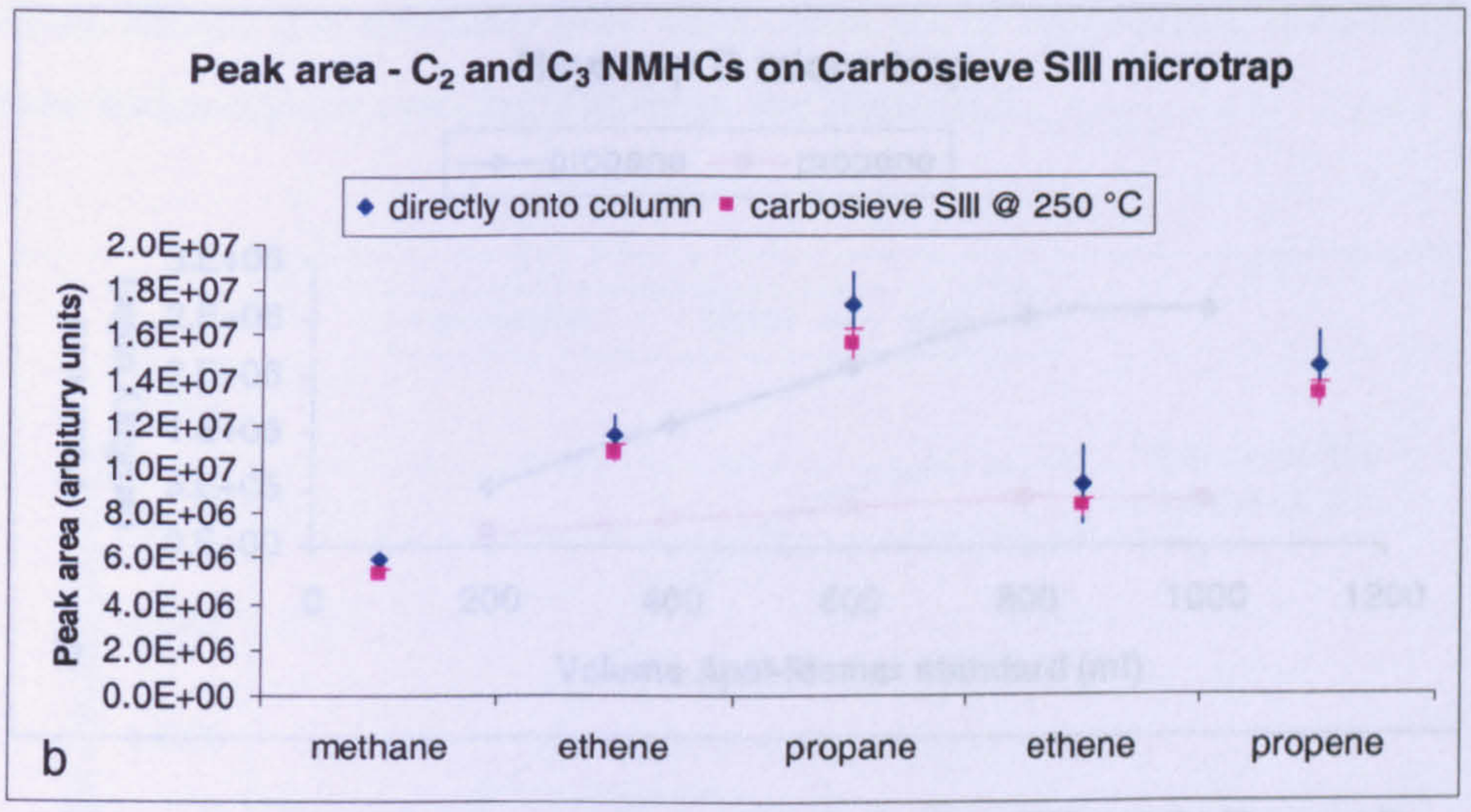

Figure 4.7 Comparing peak areas between direct loop injections onto the column with loop injections onto the (a) Hayesep D and (b) Carbosieve SIII micro-traps to column. (Error bars represent the standard deviation).

4.4.2. Linearity and break-through volumes of micro-traps

Linearity tests using the Apel-Reimer standard indicated the Carbosieve SIII (C_2) micro-trap was linear to over 900 ml for acetylene, ethene and ethane see Figure 4.8(a). The Hayesep D ($\geq C_3$) micro-trap was linear to 600 ml for propane and propene (the most volatile compounds to be analysed by this trap) (Figure 4.8(b)). This means the total sample volume should not exceed 900 ml for the C_2 micro-trap and the transfer volume from the bulk-trap to $\geq C_3$ micro-trap must not exceed 600 ml.

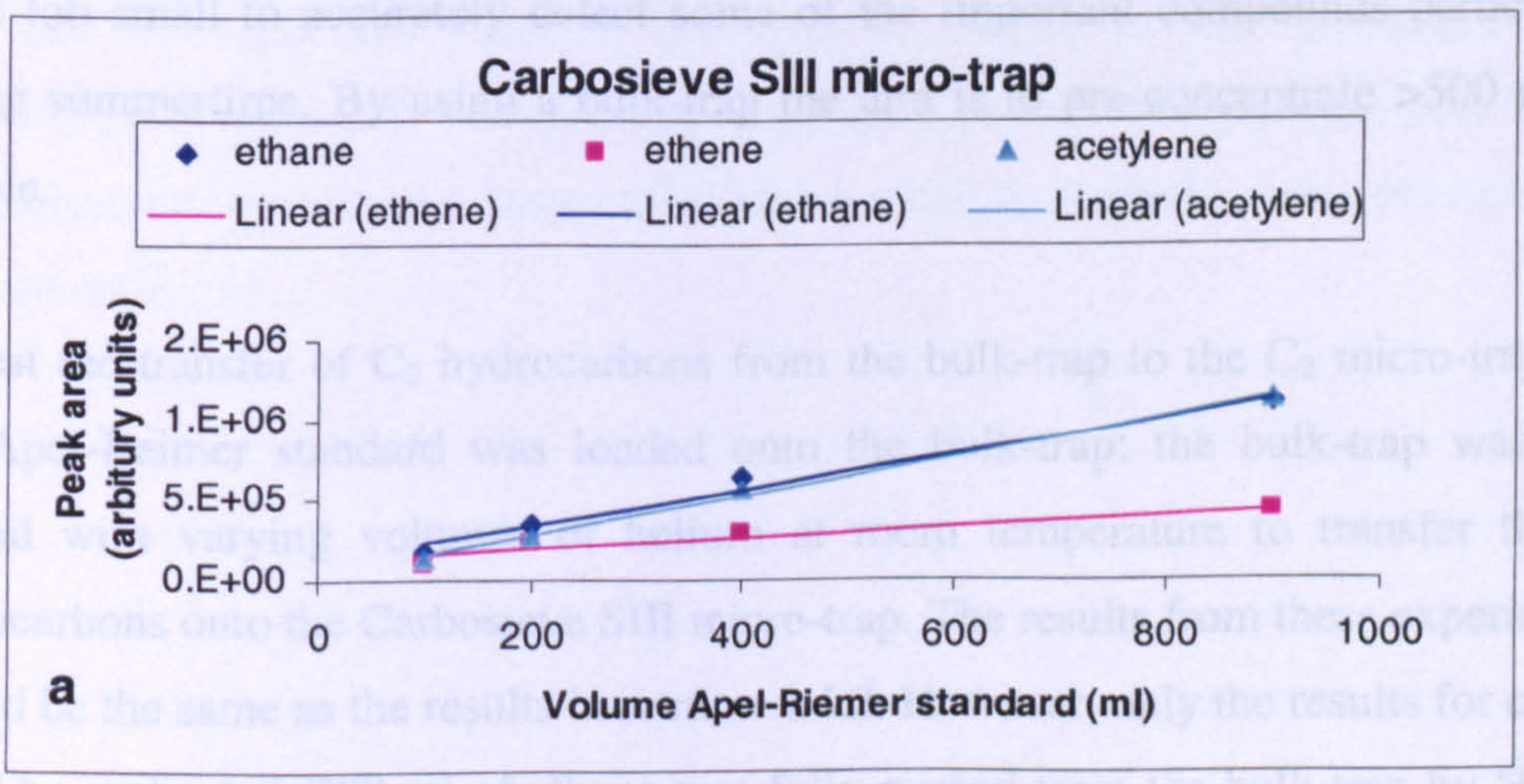

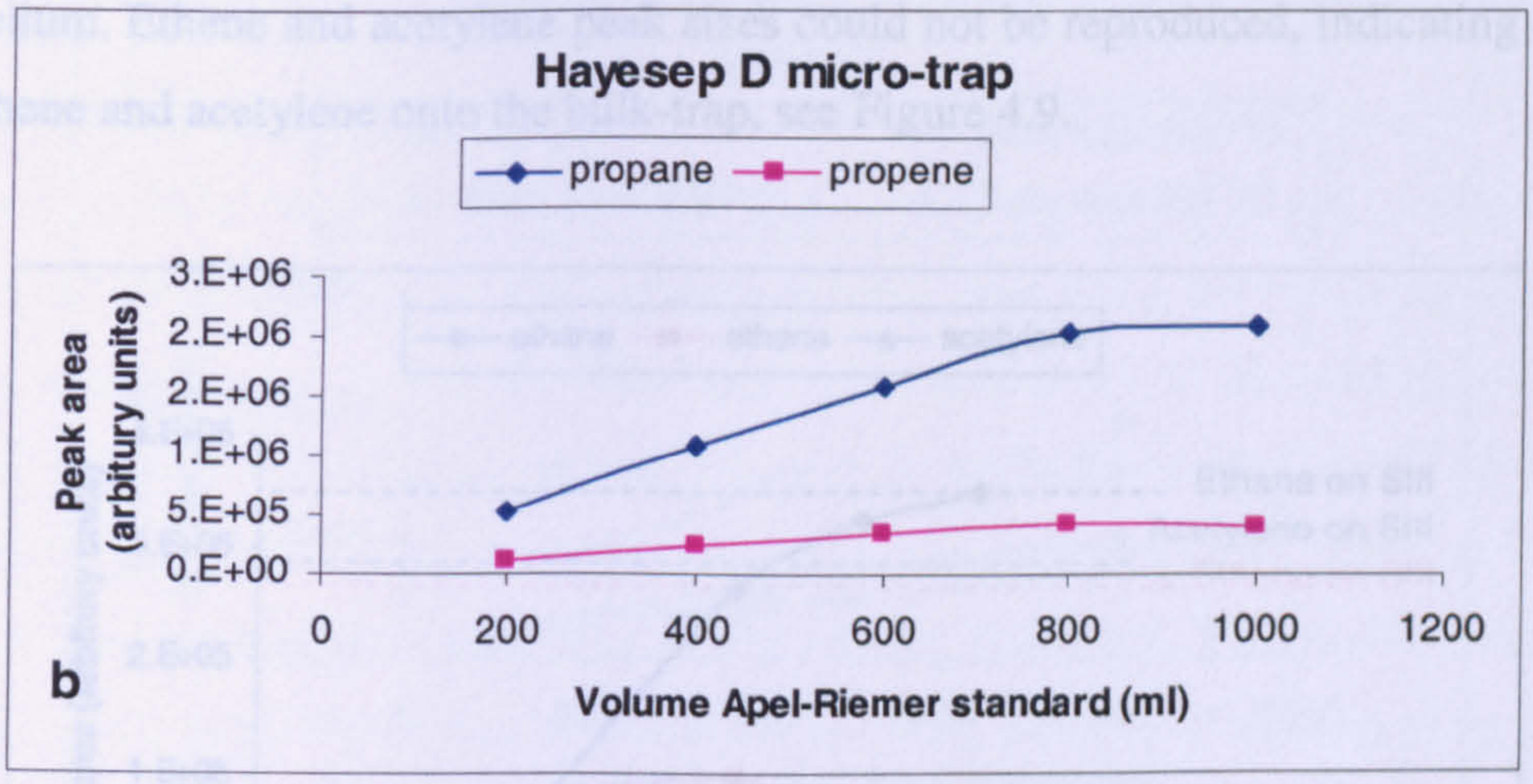

Figure 4.8 Linearity of Apel-Reimer standard on (a) Carbosieve SIII and (b) Hayesep D micro-trap. (a) Includes the linear least squares fit to the data, for ethane R^2=0.9595, ethene R^2=0.9999, acetylene R^2=0.9986.

4.4.3. Purging C_2 hydrocarbons from bulk-trap to C_2 micro-trap

The bulk-trap enables fractionation between the C_2 and C_3 and higher hydrocarbons. The C_2 hydrocarbons and most of the water are purged (with helium) off the bulk-trap at room temperature and sent through the Nafion drier to the Carbosieve SIII micro-trap. The $\geq C_3$ hydrocarbons are then back-flushed (with helium) from the bulk-trap to be re-focused on a Hayesep D micro-trap, avoiding the Nafion drier and its potential artefacts/losses, which were observed in the previous NMHC instrument (Martin, 2002). The previous NMHC instrument took a 500 ml sample, which proved to be too small to accurately detect some of the important compounds particularly during summertime. By using a bulk-trap the aim is to pre-concentrate >500 ml air sample.

To test the transfer of C_2 hydrocarbons from the bulk-trap to the C_2 micro-trap 200 ml, Apel-Reimer standard was loaded onto the bulk-trap; the bulk-trap was then purged with varying volumes of helium at room temperature to transfer the C_2 hydrocarbons onto the Carbosieve SIII micro-trap. The results from these experiments should be the same as the results in section 4.4.2. However, only the results for ethane could be replicated. 200 ml of ethane was fully purged from the bulk-trap by 500 ml

of helium. Ethene and acetylene peak sizes could not be reproduced, indicating a loss of ethene and acetylene onto the bulk-trap, see Figure 4.9.

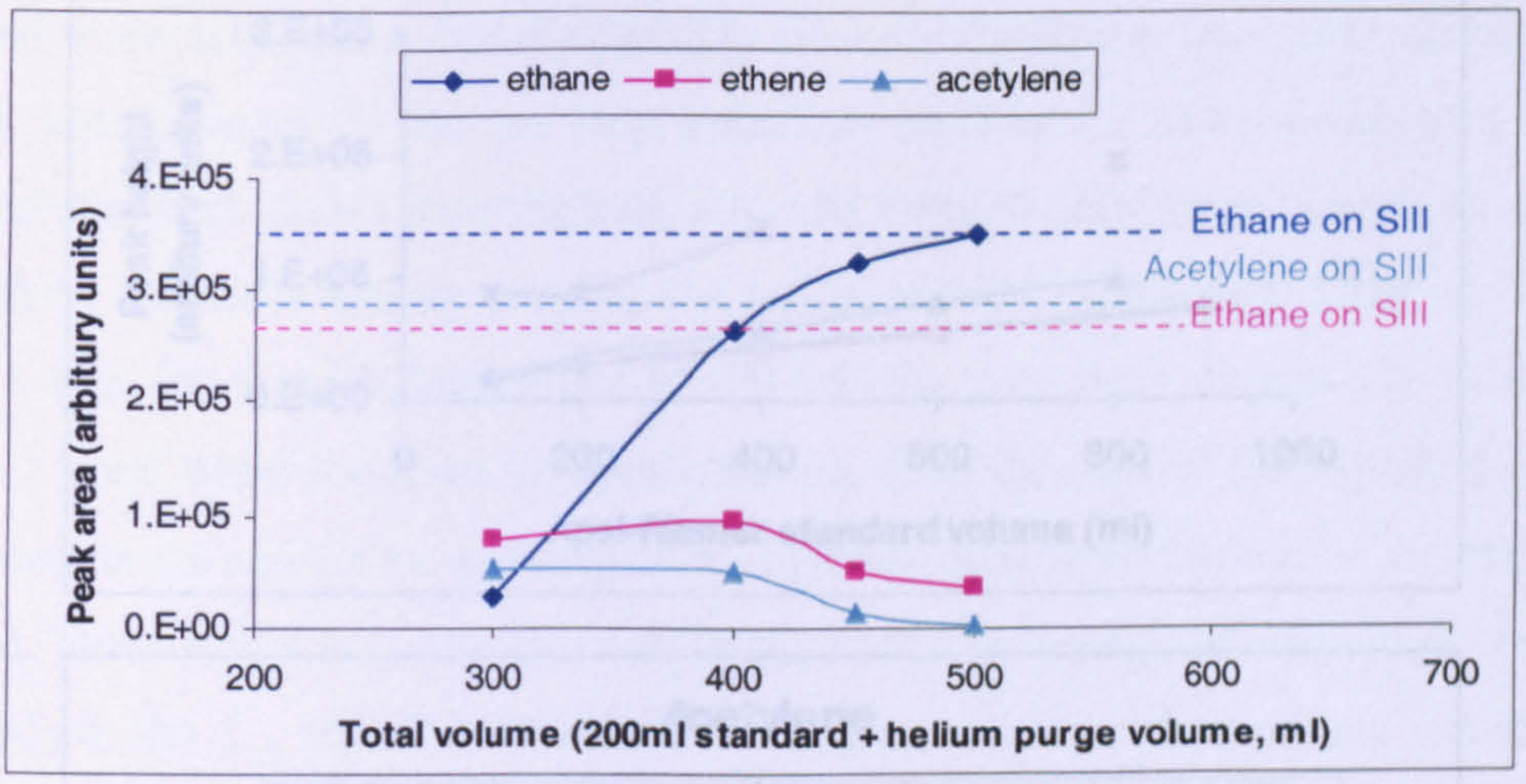

Figure 4.9 200 ml of Apel-Reimer hydrocarbon standard sampled onto the bulk-trap and purged with varying volumes of helium purging the low molecular weight hydrocarbons to the Carbosieve SIII micro-trap.

To investigate the reasons for the losses of ethene and acetylene during transfer from the bulk-trap to micro-trap, the bulk-trap was heated (to varying temperatures) whilst sampling. Heating the bulk-trap means the Apel-Reimer standard should flow straight through the bulk-trap, (without being adsorbed) to the Carbosieve SIII micro-trap, where the hydrocarbons are pre-concentrated at -40 °C. This affectively by-passes the bulk-trap and hence results should replicate those in section 4.4.2. Heating the bulk-trap did increase the ethene and acetylene peak sizes (Figure 4.10). The ethene peak size was replicated when the bulk-trap was heated to 100 °C. However, the acetylene peak could only be replicated when the bulk-trap was heated to 190 °C, but this temperature produced a large ethene blank, indicating ethene desorption artefacts from the bulk-trap.

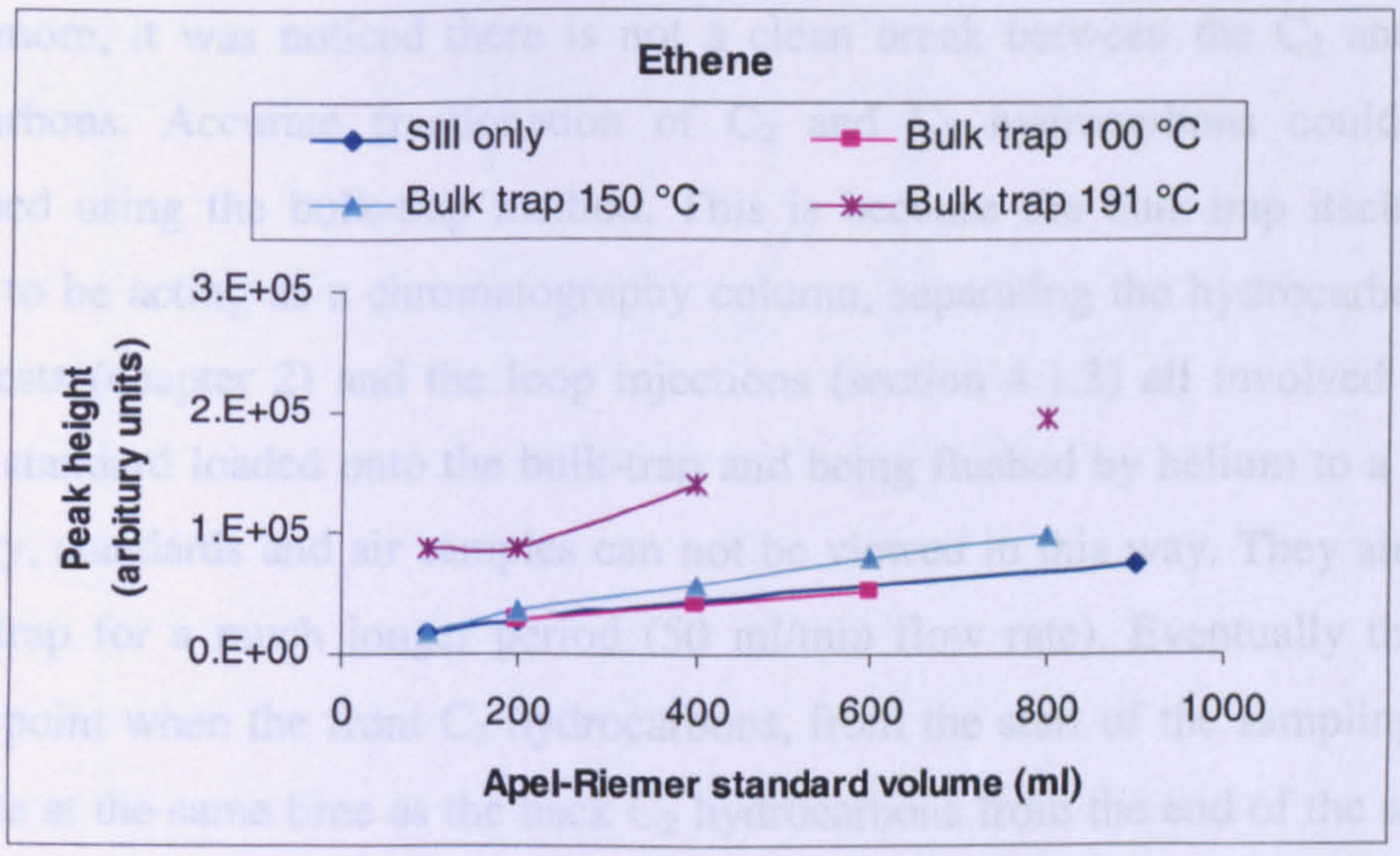

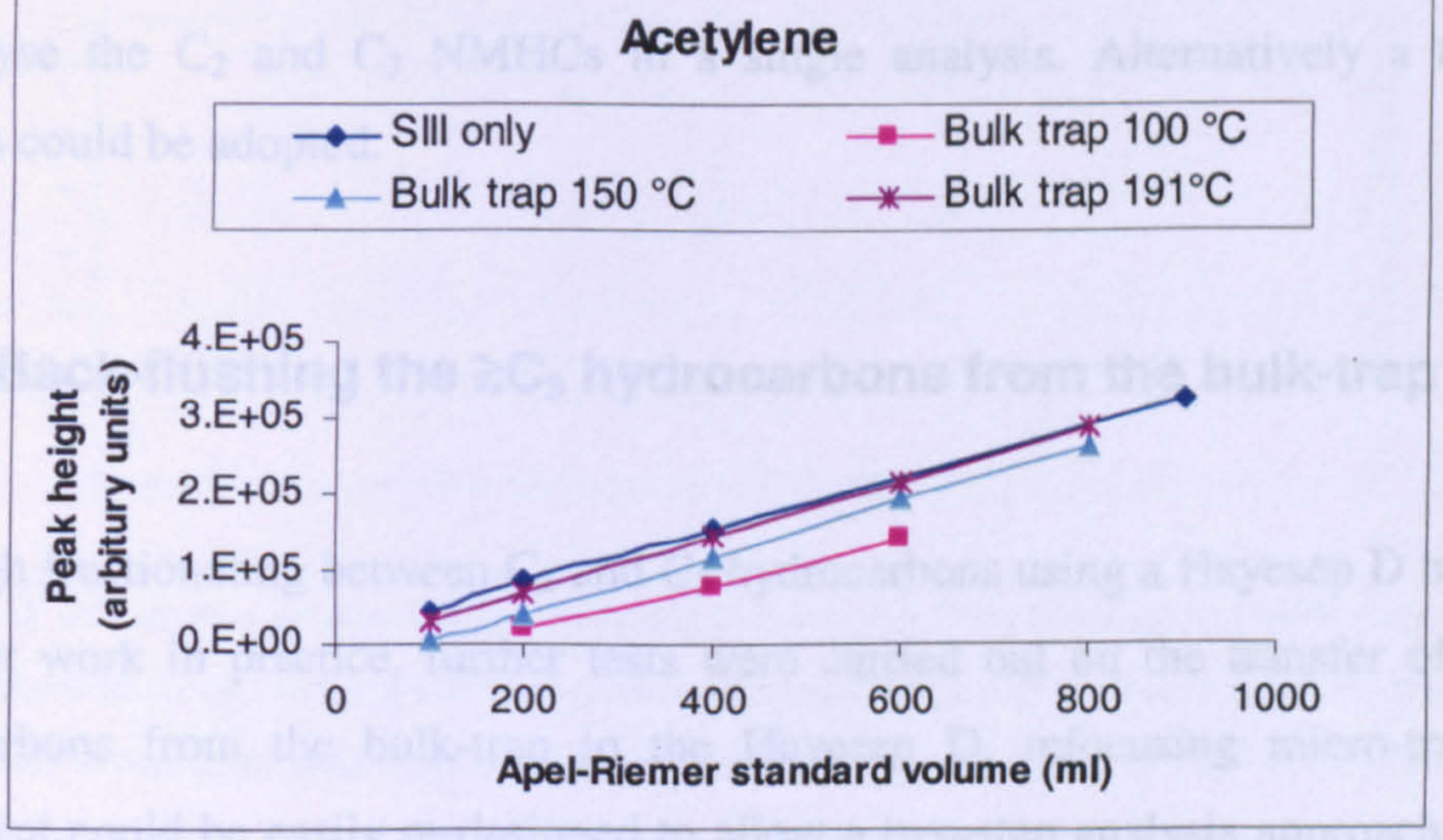

Figure 4.10 Varying volumes of the Apel-Reimer hydrocarbon standard sampled through the bulk-trap at room temperature (100 – 900 ml). Purged with 200 ml helium to the Carbosieve SIII micro-trap whilst heating the bulk-trap.

Furthermore, it was noticed there is not a clean break between the C_2 and the C_3 hydrocarbons. Accurate fractionation of C_2 and C_3 hydrocarbons could not be performed using the bulk-trap method. This is because the bulk-trap itself can be viewed to be acting as a chromatography column, separating the hydrocarbons. The initial tests (chapter 2) and the loop injections (section 4.1.3) all involved a single plug of standard loaded onto the bulk-trap and being flushed by helium to a column. In reality, standards and air samples can not be viewed in this way. They are loaded onto a trap for a much longer period (50 ml/min flow rate). Eventually there will reach a point when the front C_3 hydrocarbons, from the start of the sampling period will elute at the same time as the back C_2 hydrocarbons from the end of the sampling period. These results required that a different sampling strategy be adopted, if one was to analyse the C_2 and C_3 NMHCs in a single analysis. Alternatively a two-step analysis could be adopted.

4.4.4. Back-flushing the ≥C_3 hydrocarbons from the bulk-trap

Although fractionating between C_2 and C_3 hydrocarbons using a Hayesep D bulk-trap does not work in practice, further tests were carried out on the transfer of the C_3 hydrocarbons from the bulk-trap to the Hayesep D, refocusing micro-trap. The instrument could be easily re-designed to allow a two-step analysis approach. First a sample would be taken through the Nafion drier directly onto the Carbosieve SIII micro-trap (which proved to be linear to over 900 ml). This could be analysed inspecting only for the C_2 hydrocarbons. The second step would involve loading a sample on the bulk-trap and back-flushing this with helium to the Hayesep D micro-trap for analysis of ≥C_3 hydrocarbons.

During the back-flush of the C_3 and higher hydrocarbons from the Hayesep D bulk-trap to the Hayesep D micro-trap, the bulk-trap must be heated to displace the higher molecular weight hydrocarbons. Heating the bulk-trap produced desorption artefacts as shown in Figure 4.11.

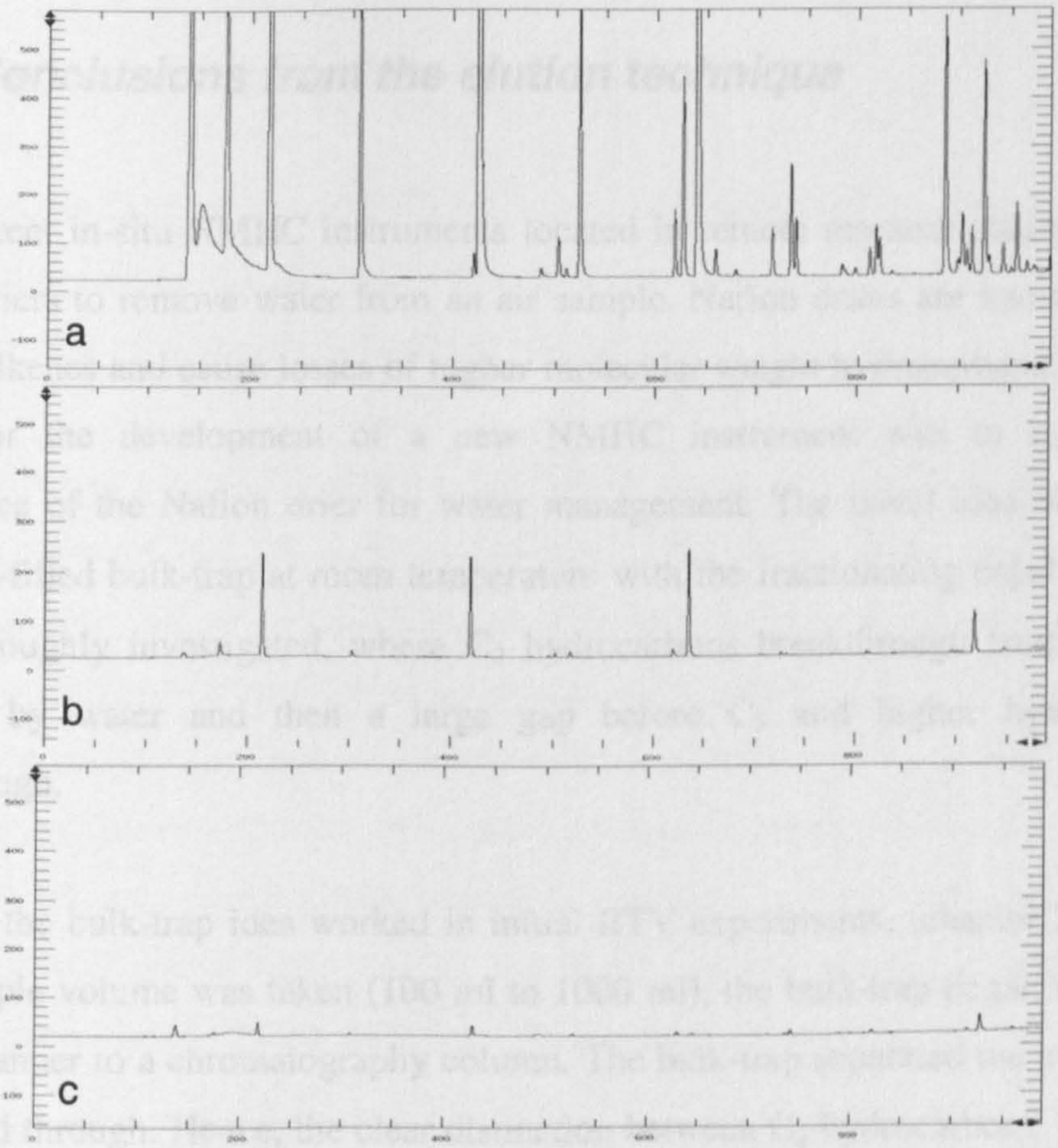

Figure 4.11 Desorption artefacts from sampling 200 ml of helium through the bulk-trap, back-flushing the bulk-trap (varying the temperature) to the Hayesep D re-focusing micro-trap and onto the GC column. (a) bulk-trap desorption at 191 °C (b) desorption at 100 °C (c) desorption at room temperatures.

4.5. Conclusions from the elution technique

Most current in-situ NMHC instruments located in remote research stations rely on Nafion driers to remove water from an air sample. Nafion driers are known to react with C_4 alkenes and cause losses of higher molecular weight hydrocarbons. The main reason for the development of a new NMHC instrument was to remove the dependence of the Nafion drier for water management. The novel idea of using an adsorbent-filled bulk-trap at room temperature with the fractionating capabilities has been thoroughly investigated, where C_2 hydrocarbons breakthrough from the trap, followed by water and then a large gap before C_3 and higher hydrocarbons breakthrough.

Although the bulk-trap idea worked in initial BTV experiments, (chapter 2) when a large sample volume was taken (100 ml to 1000 ml), the bulk-trap began to act in a similar manner to a chromatography column. The bulk-trap separated the standard as it travelled through. Hence, the clear distinction between C_2 hydrocarbons, water and C_3 and higher hydrocarbons as seen in chapter 3 when a single "slug" of standard was sampled could not be replicated.

The system was re-plumbed to investigate a two-step analysis approach. This would involve taking a 900 ml sample directly onto the Carbosieve SIII micro-trap (via the Nafion drier) and analysing this, looking at just the C_2 hydrocarbons. The second step would involve sampling 1000 ml through the bulk-trap to the Hayesep D micro-trap and analysing this sample for C_3 and higher hydrocarbons. This method also proved problematic as the back-flush of the bulk-trap with helium whilst heating to desorb the hydrocarbons to the re-focusing micro-trap produced large amounts of desorption artefacts. The desorption artefacts could not be removed by thorough and lengthy conditioning of the bulk-trap. The two-step analysis method would also increase the sample time considerably, resulting in fewer NMHC measurements per day.

4.6. Instrument re-design

A complete re-think of the NMHC instrument was necessary in order to sample a large sample volume (ideally 1000 ml), with less than 2 hour sample time and to avoid sending the C_4 alkenes through the Nafion drier.

Work by Sive, et al. (2005) utilised a Kleemenko cooler for dual-stage trapping. The first stage consisted of a 1/8 inch stainless steel tube held at -20 °C acting as a water trap. Water from an air sample condenses on the inner walls of the cold tubing, affectively removing water from an air sample without causing it to freeze and block the trap. The second stage housed a glass-bead trap held at -175 °C, providing an inert surface for analyte concentration. Inspired by this publication, a Stirling-cycle cooler (MA-SCUC04, www.stirlingcooler.com) was purchased in order to house a stainless steel tubing loop held at –20 °C to act as a water trap and another Stirling cooler to house the main micro-trap, capable of reaching temperatures as low as -100 °C.

The principle of a Stirling-cycle cooler is the adsorption of heat energy into an expanded gas from the environment or the emission of heat energy from a compressed gas into the environment. The Stirling-cycle cooler operates in four steps (Figure 4.12).

Stage 1 A piston compresses the working gas (helium) causing the temperature to rise, according to the ideal gas law, in the warm area. Heat is deposited in the regenerator, which buffers the flow of heat between the hot and cold ends of the gas chamber; ultimately heat will be removed from the system to the surroundings. The cold area piston is stationary.

Stage 2 Both pistons move together, with compression of the warm area and expansion of the gas in the cold area. Gas flows from the warm area, through the regenerator, where it is cooled to the cold area.

Stage 3 Warm area piston is stationary; gas in the cold area further expands and cools, absorbing heat from the surroundings. The external side of the cold area is housed inside an insulator, thus creating a cold zone.

Stage 4 Both pistons move together, displacing gas from the cold area to the warm area, cooling the regenerator ready to start the cycle again.

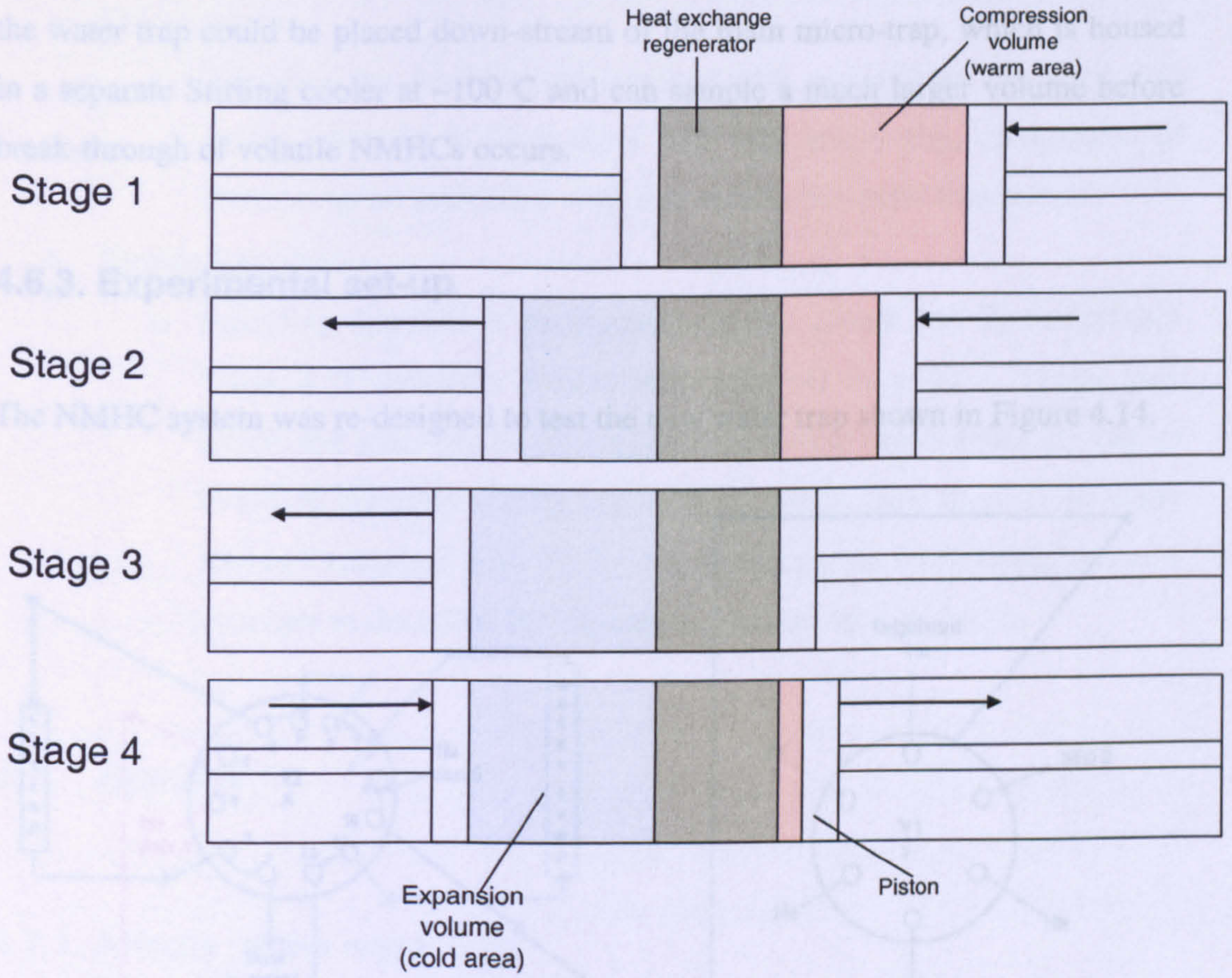

Figure 4.12 Basic operating principle of a Stirling-cycle cooler.

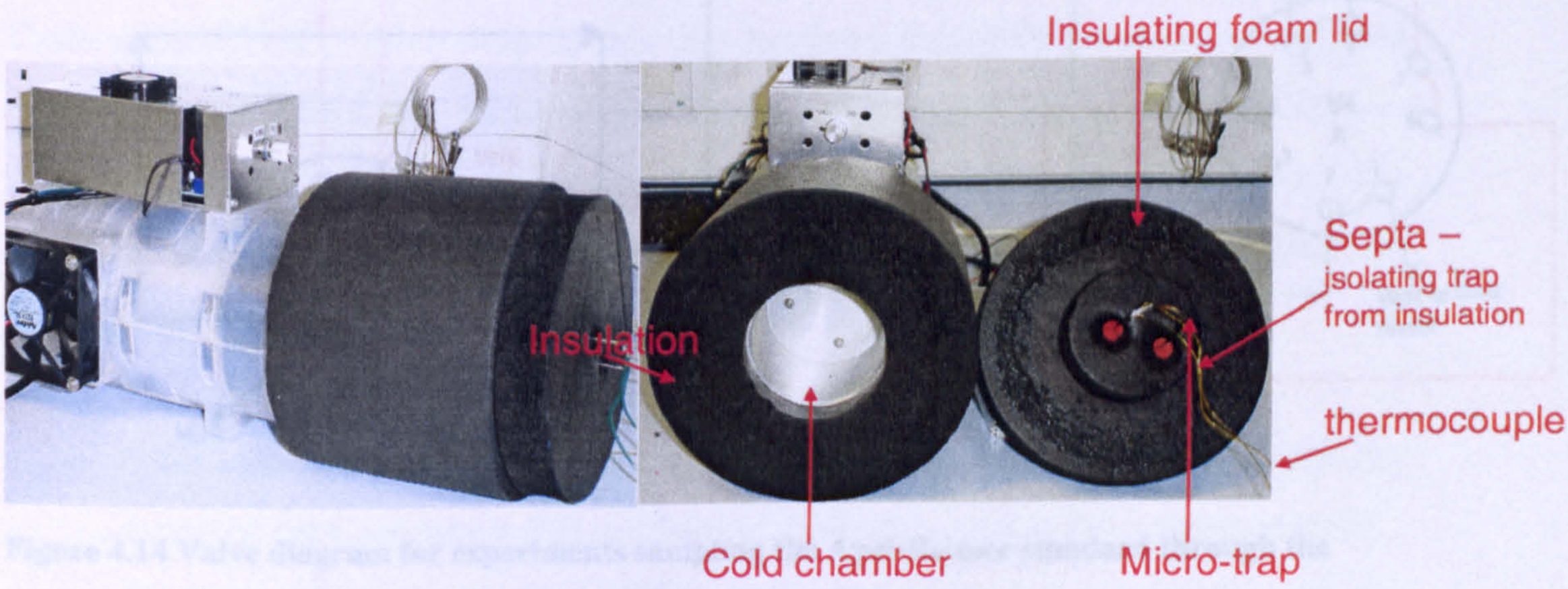

Figure 4.13 Photograph of the Stirling cycle cooler. On the right shows the open chamber with details of the micro-trap insulated by septa's from the foam insulated lid. The left photograph shows the Stirling cycle cooler with the micro-trap housed inside the cooling chamber.

4.6.2. Aims

The aim of the water trap experiment is to allow the assessment of losses of NMHCs; the water trap could be placed down-stream of the main micro-trap, which is housed in a separate Stirling cooler at –100 C and can sample a much larger volume before break-through of volatile NMHCs occurs.

4.6.3. Experimental set-up

The NMHC system was re-designed to test the new water trap shown in Figure 4.14.

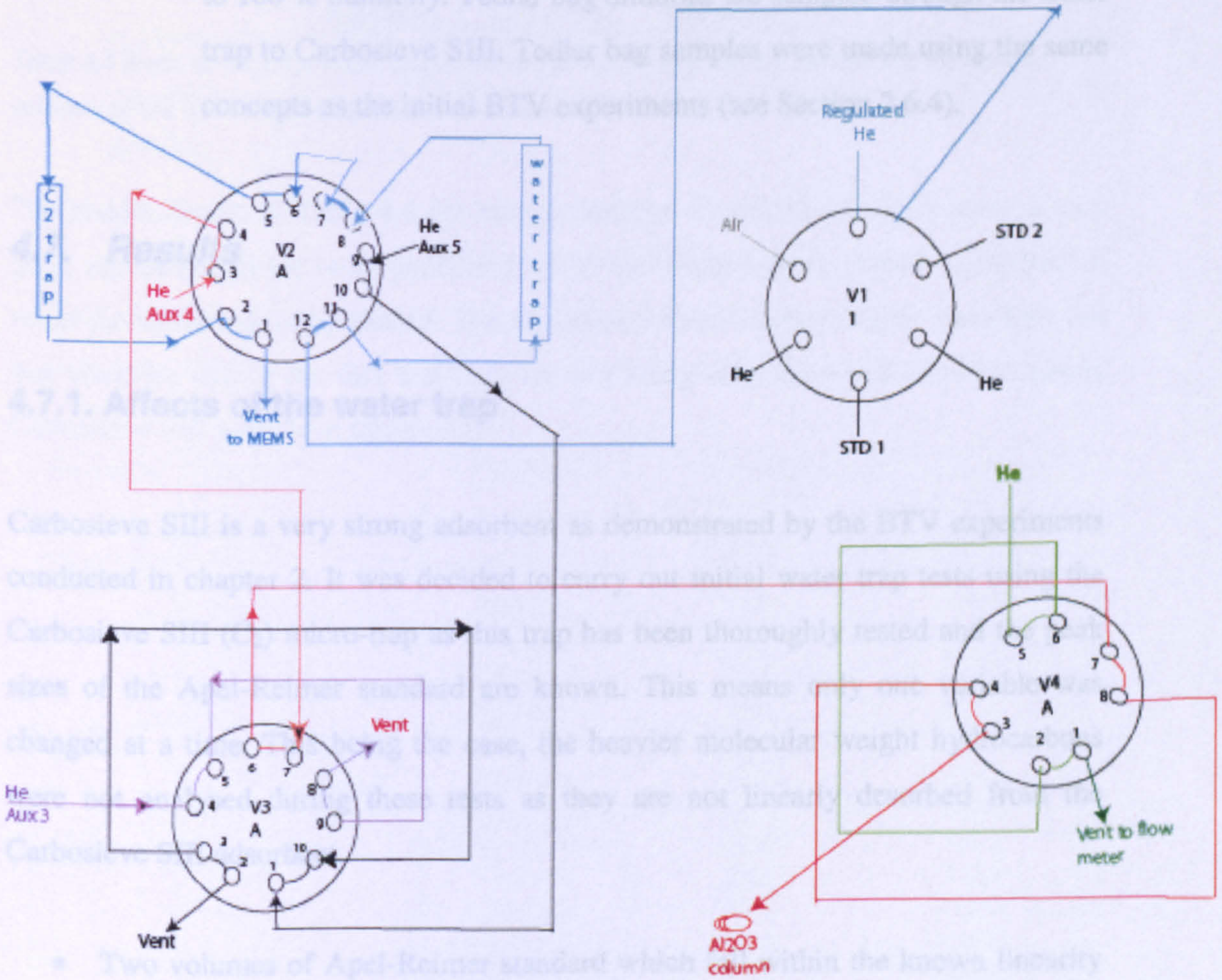

Figure 4.14 Valve diagram for experiments sampling the Apel-Reimer standard through the water trap onto the Carbosieve SIII (C_2) micro-trap.

The following experiments were carried out to test the affect of the water trap and sample humidity:

- The water trap.
    - Sampling the Apel-Reimer standard with and without the water trap in-line, directly to Carbosieve SIII (C_2) micro-trap, comparison of chromatogram peak sizes with and without the water trap present.
- Sample humidity.
    - Sampling dilutions of ppmv-concentration alkene and C_4 isomer (see Table 4.2) standards diluted with zero air in a 10 L Tedlar bag. Deionised water can be injected into the Tedlar bag to make the bag up to 100 % humidity. Tedlar bag dilutions are sampled through the water trap to Carbosieve SIII. Tedlar bag samples were made using the same concepts as the initial BTV experiments (see Section 2.6.4).

4.7. Results

4.7.1. Affects of the water trap

Carbosieve SIII is a very strong adsorbent as demonstrated by the BTV experiments conducted in chapter 2. It was decided to carry out initial water trap tests using the Carbosieve SIII (C_2) micro-trap as this trap has been thoroughly tested and the peak sizes of the Apel-Reimer standard are known. This means only one variable was changed at a time. This being the case, the heavier molecular weight hydrocarbons were not analysed during these tests as they are not linearly desorbed from the Carbosieve SIII adsorbent.

- Two volumes of Apel-Reimer standard which fall within the known linearity range of the Carbosieve SIII micro-trap, (200 ml and 400 ml) were examined.
- Each Apel-Reimer standard volume (200 and 400 ml) was sampled with the water trap in-line and without, to examine the affect of the water trap on standard samples; each set of experiments were repeated at least three times.

Table 4.4 compares the ratio with/without the water trap, for each sample volume for C_2-C_4 hydrocarbons from the Apel-Reimer standard. A ratio of around one suggests the water trap is having little to no affect on the C_3 and C_4 peak sizes, suggesting there are no losses or artefacts created by the water trap.

	200ml	400ml
Ethane	1.00 ± 0.08	0.98 ± 0.02
Propane	1.01 ± 0.05	1.01 ± 0.02
Propene	1.09 ± 0.1	1.00 ± 0.05
Acetylene	-	1.12 ± 0.08
i-Butane	1.03 ± 0.05	1.02 ± 0.02
n-Butane	1.02 ± 0.01	1.01 ± 0.02
t-Butene	1.10 ± 0.01	1.04 ± 0.02
1-Butene	1.14 ± 0.03	1.09 ± 0.02
i-Butene	1.28 ± 0.03	1.12 ± 0.04
c-Butene	1.12 ± 0.01	1.07 ± 0.03

Table 4.4 Ratio of with the water trap/without the water trap for 200 ml and 400 ml sample volumes of the Apel-Reimer hydrocarbon standard.

The results shown in Table 4.4 are very promising. C_2 and C_3 NMHCs show a very good agreement in terms of peak area when the water trap is present compared to when the water trap is by-passed. The C_4 isomers show slightly higher variations but this could be due to the fact that they are not being fully desorbed from the strong Carbosieve SIII adsorbent micro-trap

4.7.2. Affects of sample humidity

The gas standards used for the experiments were made up by injecting 10 μl of ppmv concentration alkene or C_4 isomer standard into a 10 L Tedlar bag filled with zero air, making a ppbv concentration standard. The standard concentration in the 10 L Tedlar bag can be calculated knowing using the following example:

- The concentration of ethene in the alkene standard is 1000 ppmv, which is equivalent to 1×10^{-4} unit volume.
- A 10 μl sample (1×10^{-4} l) of the alkene standard results in an ethene concentration of 1×10^{-8} unit volume.
- A 10 μl alkene standard sample in a 10 l Tedlar bag is equivalent to an ethene concentration of 1×10^{-9} unit volume, equivalent to 1 ppbv. (See Table 4.5 for details).

Zero air was obtained from a Parker Balston TOC generator (a zero air generator suitable for total organic halogen analyses) and was tested prior to use to ensure that there was no contamination from the generator that could compromise the experiment.

Standard	Supplier	Contents	Concentration in standard (ppmv)	Tedlar bag concentration (ppbv)
Alkene	Scientific & Technical Gases	Ethene	1000	1.000
		Propene	998	0.998
		1-Butene	1009	1.009
		1-Pentene	994	0.994
		1-Hexene	1020	1.020
C_4	Scientific & Technical Gases	n-Butane	1032	1.032
		i-butane	1018	1.018
		Cis-2-butene	1028	1.028
		Trans-2-butene	1018	1.018
		1-Butene	1018	1.018
		Isobutene	1018	1.018
		1,3-Butadiene	1028	1.028
		Ethylacetylene	1028	1.028

Table 4.5 Dilutions of an alkene and C_4 standard.

The system set-up is the same as in the previous experiments, which sampled the Apel-Reimer standard onto the Carbosieve SIII; the water trap was in-line during

these experiments. The aim of this experiment was to determine the affect of a humid sample compared to dry samples. Specifically, it was to determine if the water trap can efficiently remove water from an air sample without either blocking the sample flow rate or causing water to elute on the column, in which case a large broad peak would be observed along with a shift in retention times of NMHC peaks.

- The Tedlar bag was connected to the air pump module inlet allowing Tedlar bag gas samples to be taken in the same way an air sample is taken; the air is pumped through the system.
- 200 ml samples of Tedlar bag dilutions were taken for each standard dilution and the chromatogram peak areas were analysed. Samples of each standard dilution were taken at least three times to ensure peak areas were constant.
- To assess the affects of water on the chromatography and peak areas the Tedlar bag standards were humidified to over 100 % by an injection of 150 μl de-ionised water into the Tedlar bag.
- Once again, 200 ml Tedlar bag dilution samples were taken and the chromatography and peak areas produced compared with dry samples. These tests were repeated at least three times.

Compound	Ratio wet/dry	Compound	Ratio wet/dry
Ethane	0.99 ± 0.02	n-Butane	1.10 ± 0.04
Propene	0.99 ± 0.05	t-Butene	1.01 ± 0.3
1-Butene	0.99 ± 0.01	1-Butene	1.03 ± 0.04
1-Pentene	1.02 ± 0.03	c-Butene	1.02 ± 0.02
1-Hexene	0.92 ± 0.3	Butyne	1.00 ± 0.01
i-Butane	1.04 ±0.02	1,3-Butadiene	1.01 ± 0.01

Table 4.6 Ratio 200 ml samples of ppbv concentration dilutions from a humid Tedlar bag sample/dry Tedlar bag sample Ratio wet/dryTedlar bag samples for the alkene standard and the C_4 isomer standard.

Table 4.6 compares the ratio of a wet/dry 200 ml sample of a ppbv concentration standard dilution for alkenes and C_4 isomer standards sampled through the water trap to the Carbosieve SIII micro-trap. A ratio close to one suggests the humidity of the sample is having little to no affect on the alkene and C_4 peak sizes and chromatography. This suggests the water trap can affectively remove water from a

standard sample without blocking either the water trap or micro-trap, which would result in changes in the sample flow rate and volume causing changes in chromatogram peak sizes.

4.8. *Discussion – the affects of the water trap and sample humidity*

The previous experiments compare peak sizes for NMHC standards with and without the water trap present and compare humid and dry standard samples; these showed promising results. No losses or artefacts appear to be generated by the presence of the water trap. Comparisons of 100 % humid standard samples with dry samples show that the water trap affectively removes water from a standard sample without compromising the chromatography and peak areas of C_2-C_6 alkenes and C_4 isomer NMHCs.

Two problem areas still persist: The first is the recovery of heavy molecular weight NMHCs from the micro-trap. Carbosieve SIII is a very strong adsorbent, and > C_4 NMHCs are not fully recovered from the micro-trap during desorption. A new trap is needed which can fully desorb heavy NMHCs without compromising the sample volume that can be concentrated as demonstrated by high BTVs for the most volatile, C_2 hydrocarbons. The second problem is with the chromatography of ethane and ethene on the Alumina PLOT (Al_2O_3/KCl: 50 m, 0.53 mm) column. Ethane and ethene are the first NMHCs to elute on the column and are not fully resolved; they appear as short, broad peaks. This is a known problem with the Alumina PLOT columns and has previously been reported by Martin, 2002 when using the Al_2O_3/KCl (50 m, 0.32 mm 5 μm) column.

In order to solve the remaining problems, the following experiments were carried out:

- BTV experiments of a multi-bed adsorbent micro-trap containing a Carbosieve SIII (a strong adsorbent) and Carboxen 1016 (a weak adsorbent).

- Column experiments to resolve ethane and ethene peaks, using a PoraPLOT chromatography column and the use of a refocusing micro-trap to help resolve the front end of the chromatogram.

4.9. *BTV and linearity of multi-bed adsorbent micro-trap*

More than one type of adsorbent is required to fully concentrate and desorb the full range of C_2- C_8 NMHCs due to their wide range in volatility. The most volatile hydrocarbons require very strong adsorbents to fully trap them and allow a large sample volume (1 L) to be taken before break-through occurs. The least volatile hydrocarbons require a weaker adsorbent to enable full recovery during Desorption. A multi-bed adsorbent micro-trap was made using the same procedures as outlined in chapter 2. The micro-trap contains 20 mg of Carboxen 1016 (weak adsorbent) and 70 mg of Carbosieve SIII (strong adsorbent). The packing order of the adsorbents is also important; during air sampling the weak adsorbent must be first in line and the strong adsorbent second in line. This is so that during sampling only the volatile hydrocarbons, which breakthrough from the Carboxen 1016 (weak) adsorbent will reach the Carbosieve SIII (strong) adsorbent. During desorption the micro-trap is back-flushed, so the helium purges from the strong adsorbent to the weak adsorbent, this way the least volatile, heavy molecular weight hydrocarbons do not come into contact with the strong adsorbent and will be fully desorbed from the micro-trap.

To examine the BTVs and linearity of the multi-bed adsorbent trap varying sample volumes of the Apel-Reimer hydrocarbon standard were analysed. This was carried out in the same manner as the elution BTV tests were carried out on the single-adsorbent Hayesep D and Carbosieve SIII micro-traps. The water trap was in-line and prior to the micro-trap during this experiment.

To take full advantage of the Stirling cycle cooler which is able to reach temperatures of -100 °C, these BTV experiments were carried out with the micro-trap housed inside the chamber of the Stirling cooler. Lower temperatures enable larger sample volumes to be taken before break-through of the volatile hydrocarbons occurs. Another Stirling cycle cooler has been purchased (MA-SCU08) for use as a

micro-trap cooling device, replacing the need for Peltier coolers (which only cool to -40 °C).

4.9.1. Results

Use of the multi-bed adsorbent micro-trap resulted in much poorer peak shapes for ethane and ethene using the Al_2O_3/KCl (50 m, 0.53 mm, 10 μm) column. Poor peak shapes were thought arise from the properties of the pre-concentration trap used, with two main possibilities. First, the use of a multi-bed adsorbent trap uses one weak adsorbent and one strong adsorbent, and the ethane and ethene are split between the two adsorbents during trapping. During desorption the two adsorbents release ethane and ethene at different rates resulting in poor peak shape. Another possibility is that using the Stirling cooler at -100 °C means that the trap takes longer to heat to 200 °C (18 seconds compared to 16 seconds when heating from -40 °C) so compounds desorbed slower than when using Peltier coolers at -40 °C. The peak shape of ethane and ethene is so poor that they have not been quantified during these experiments. The reduction in heating rate does not affect acetylene or the heavier NMHCs. This must be because acetylene is on one adsorbent (strong) and the heavier NMHCs on the weak adsorbent, not split between the two.

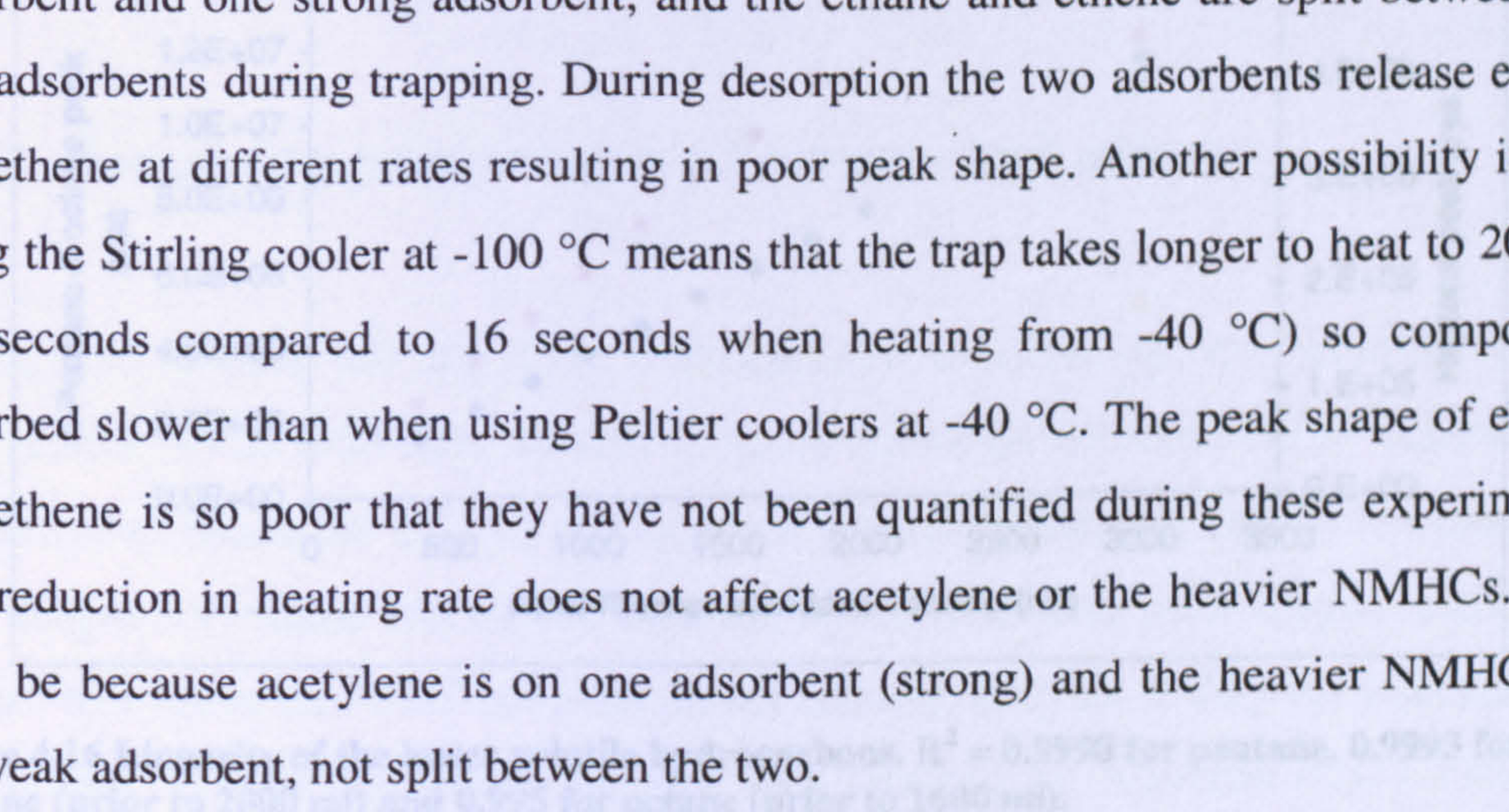

Figure 4.15 Linearity and break-through of the most volatile hydrocarbons. $R^2 = 1$ for propane, propene and i-butane and to acetylene up to 2000 ml.

Acetylene is the most volatile NMHC and is the first to break-through from an adsorbent trap. Ethane and ethene have not been used to assess BTVs given the problems with peak shape and resolution. Figure 4.15 shows the multi-bed adsorbent trap is linear for acetylene to 2000 ml. Acetylene breaks through from the micro-trap between 2–3 L. i-Butane is included in this figure as it has a similar peak area to acetylene in the standard and clearly shoes how the acetylene peak size is not linear from 2-3 L and i-butane, being less volatile, is linear.

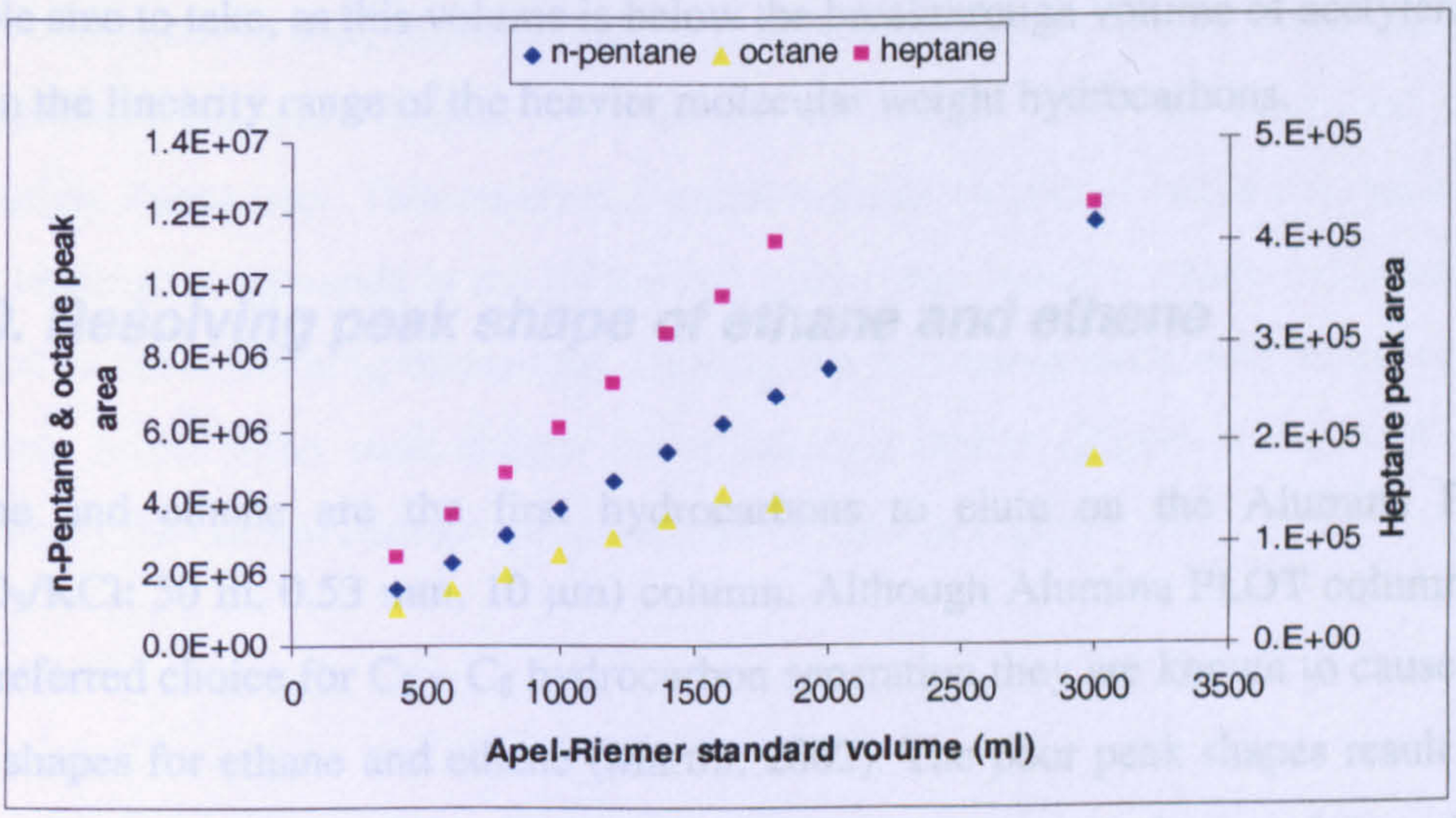

Figure 4.16 Linearity of the lesser volatile hydrocarbons. R^2 = 0.9998 for pentane, 0.9993 for heptane (prior to 2000 ml) and 0.995 for octane (prior to 1600 ml).

Figure 4.16 shows the linearity of the less volatile hydrocarbons. n-Pentane shows a complete linear profile, indicating complete, full recovery from the micro-trap during desorption. Heptane and octane have a linear relationship until 2000 ml and 1700 ml respectively. This suggests that the heptane and octane are fully recovered from the micro-trap until 2000 ml and 1700 ml when they each in turn break-through from the weaker adsorbent and come in contact with the stronger (Carbosieve SIII) adsorbent and are not fully desorbed from the micro-trap.

4.9.2. Discussion

The multi-bed adsorbent trap held at – 100 °C in a Stirling cycle cooler provides an affective mechanism for trapping large sample volumes without break-through of the more volatile hydrocarbons. The trap is limited by the amount of volume which can be sampled before the least volatile hydrocarbons come into contact with the stronger of the two adsorbents. Thus, it can be suggested that a 1 L air sample is an ideal sample size to take, as this volume is below the breakthrough volume of acetylene and within the linearity range of the heavier molecular weight hydrocarbons.

4.10. Resolving peak shape of ethane and ethene

Ethane and ethene are the first hydrocarbons to elute on the Alumina PLOT (Al_2O_3/KCl: 50 m, 0.53 mm, 10 μm) column. Although Alumina PLOT columns are the preferred choice for $C_2 - C_8$ hydrocarbon separation they are known to cause poor peak shapes for ethane and ethene (Martin, 2002). The poor peak shapes result from the fact that Alumina PLOT columns do not refocus analytes as they are injected onto the column. Ethane and ethene are not well retained by Alumina PLOT columns, eluting quickly from these columns; having spent little time refocusing they often have poor peak shape.

The poor peak shape exhibited by ethane and ethene on the Al_2O_3/KCl (50 m, 0.53 mm, 10 μm) column depends largely upon the pre-concentration trap. Ethane and ethene peak shapes from direct, loop injections of NMHC standards onto the Al_2O_3/KCl (50 m, 0.53 mm, 10 μm) column appeared well-resolved and of good, quantifiable shape (see Section 3.3.2). However, the peak shape of ethane and ethene was not as good when NMHC standards were pre-concentrated using an adsorbent trap prior to GC analysis. Ethane and ethene were quantifiable during initial tests using the Carbosieve SIII micro-trap, (Section 4.13) see Figure 4.18(a). The multi-bed adsorbent trap used in Section 4.2.4, produced much worse peak shape for ethane and ethene and as a result they were not quantifiable, see Figure 4.17(b).

To resolve the poor ethane and ethene peak shapes, a much smaller micro-trap containing 20 mg of Carboxen 1016 was constructed and placed down-stream of the multi-bed micro-trap to act as a refocusing trap. Carboxen 1016 was chosen as it is used in the multi-bed adsorbent micro-trap (along with Carbosieve SIII) and the weaker of the two adsorbents. A weak adsorbent is necessary for the refocusing micro-trap to obtain complete desorption of the heavy molecular weight NMHCs and since only a small volume of helium is needed to purge the NMHCs from the micro-trap to the refocusing micro-trap; break-through is not an issue, the refocusing micro-trap needs to fully desorb NMHCs to produce sharp, Gaussian peaks. Adsorbed compounds were back-flushed with helium to transfer from the multi-bed to the refocusing micro-trap. This requires a small volume (8 ml) of helium to back-flush (with heating) compounds to the refocusing micro-trap, hence a weaker adsorbent can be used as the refocusing micro-trap. Heating the refocusing micro-trap to the column produces much better peak shapes for ethane and ethene (Figure 4.17(c)). A valve diagram of the current instrument set-up can be seen in Figure 4.19.

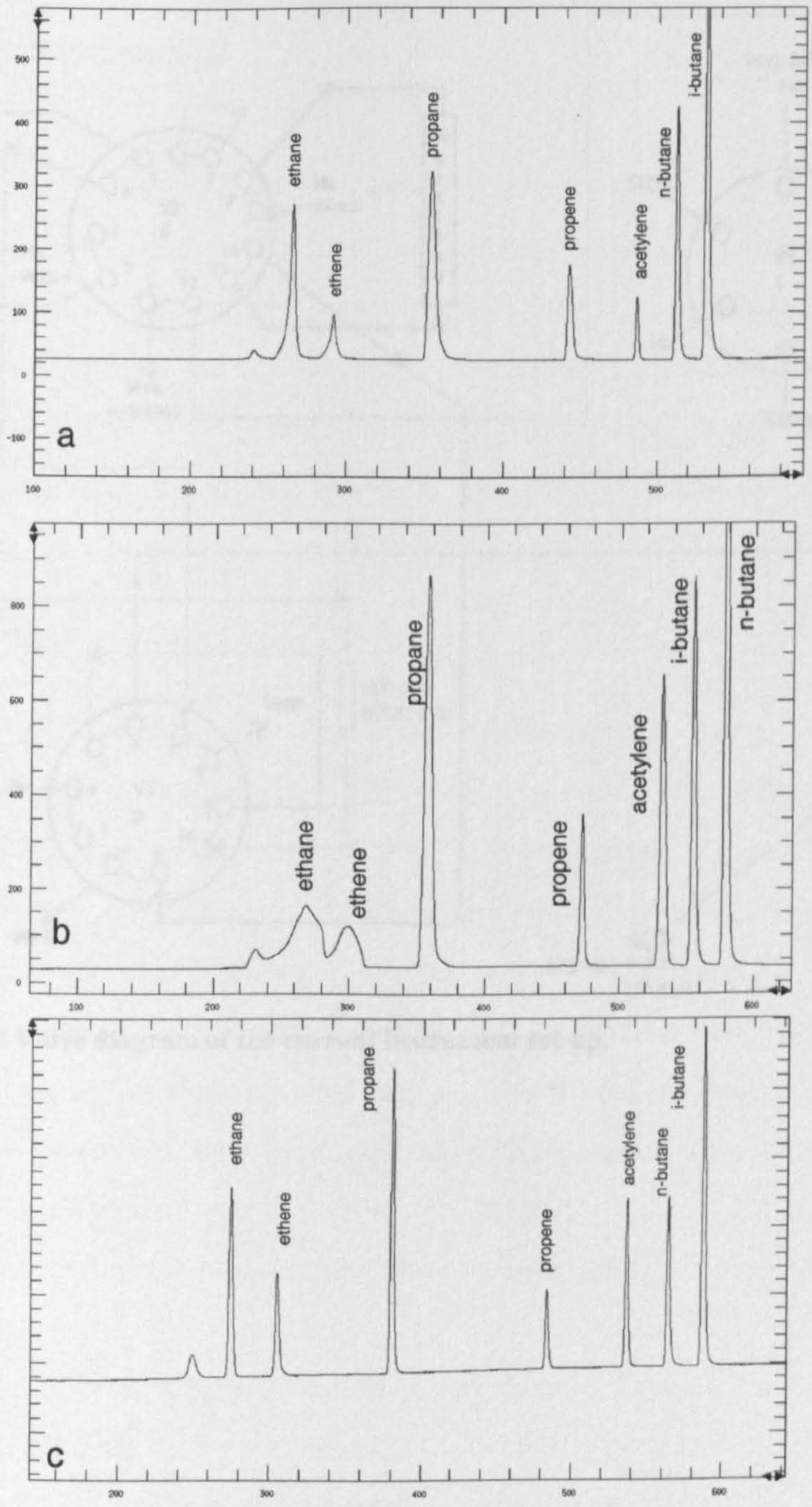

Figure 4.17 Chromatogram showing C_2 and C_3 hydrocarbon peaks from the Apel-Reimer standard on the Alumina PLOT (Al_2O_3/KCl: 50 m, 0.53 mm) column. (a) Carbosieve SIII micro-trap (b) multi-bed micro-trap (c) multi-bed micro-trap + refocusing micro-trap.

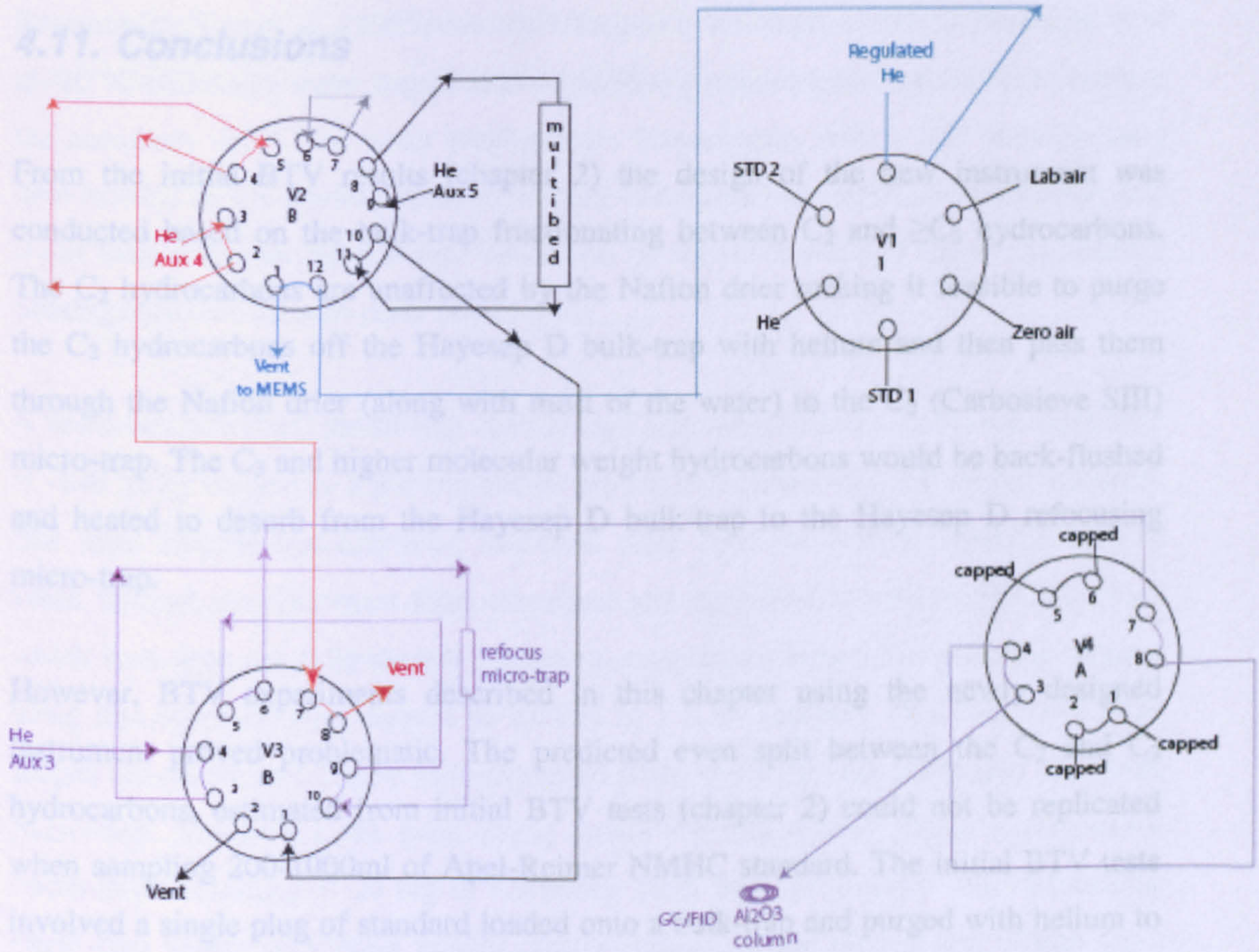

Figure 4.18 Valve diagram of the current instrument set-up.

4.11. Conclusions

From the initial BTV results (chapter 2) the design of the new instrument was conducted based on the bulk-trap fractionating between C_2 and $\geq C_3$ hydrocarbons. The C_2 hydrocarbons are unaffected by the Nafion drier making it feasible to purge the C_2 hydrocarbons off the Hayesep D bulk-trap with helium and then pass them through the Nafion drier (along with most of the water) to the C_2 (Carbosieve SIII) micro-trap. The C_3 and higher molecular weight hydrocarbons would be back-flushed and heated to desorb from the Hayesep D bulk-trap to the Hayesep D refocusing micro-trap.

However, BTV experiments described in this chapter using the newly designed instrument proved problematic. The predicted even split between the C_2 and C_3 hydrocarbons, estimated from initial BTV tests (chapter 2) could not be replicated when sampling 200-1000ml of Apel-Reimer NMHC standard. The initial BTV tests involved a single plug of standard loaded onto a bulk-trap and purged with helium to the column until it eluted from the bulk-trap. In reality standards and air samples cannot be viewed in this way, real samples are loaded onto the trap over a period of minutes (50 ml/min sample flow rate). Over the sampling period the bulk-trap can be viewed as acting like a chromatography column, the clear distinction between the C_2 and C_3 hydrocarbons is compromised by a merging of the C_2 and C_3 hydrocarbons.

A two-step analysis approach was next investigated; firstly a sample would be taken directly through the Nafion drier to the Carbosieve SIII micro-trap (linear to over 900 ml for acetylene). This would be analysed looking at just the C_2 hydrocarbons. The second step involves taking a new sample onto the Hayesep D bulk-trap and back-flushing this with helium to the Hayesep D refocusing micro-trap. This too proved problematic, the back-flush of the NMHCs from the bulk-trap whilst heating produced large desorption artefacts.

A new concept was needed to meet the requirements of a new NMHC instrument, the main ones being: A large sample volume (500-1000ml) and removal of the dependence on the Nafion drier for water management.

Research by Sive et al., (2005) describes the use of an empty stainless steel tube, held at -20 °C to act as a water trap. It was decided to purchase a Stirling cooler to achieve the necessary -20 °C for water management. Experiments with a 1/8" stainless steel tube housed in the Stirling cooler chamber and cooled to -20 °C demonstrated that water from a humidified standard condenses on the inner walls of the tubing without causing losses of the non-polar NMHCs.

A multi-bed adsorbent micro-trap containing Carbosieve SIII and Carboxen 1016 held at -100 °C by the use of a Stirling cooler proved to be linear to 2000 ml for acetylene (the most volatile hydrocarbon); however, after 1600 ml heavier NMHCs start to break through the Carboxen 1016 adsorbent and onto the Carbosieve SIII adsorbent which then does not fully desorb the heavy compounds. Hence the sampling volume using this new technique should be limited to 1 L air samples. However, poor peak shapes for ethane and ethene were observed when using the new multi-bed adsorbent micro-trap. To resolve the peak shape issues for ethane and ethene a refocusing micro-trap consisting of 20 mg of Carboxen 1016 was constructed. The re-focusing micro-trap shows promising results, vastly improving the ethane and ethene peak shapes.

Overall summary of the new NMHC instrument:

- 1/8" stainless steel water trap housed in a Stirling cooler maintained at - 20 °C.
- Use of 1 multi-bed adsorbent micro-trap housed in a Stirling cooler maintained at -100 °C.
- Use of 1 single-bed adsorbent micro-trap housed in the same Stirling cooler as the multi-bed micro-trap, maintained at -100 °C.
- Capable of taking 1 L air sample.
- Alumina Al_2O_3/KCl PLOT (50 m, 0.53 mm, 10 μm) chromatography column for fast analysis of NMHCs.
- Overall runtime 80 minutes.

After several set-backs during the instrument development phase, a number of problems have been addressed, in terms of water management and sample size and the instrument is now producing very promising results. Several steps are required to

fully engineer and integrate the two Stirling coolers into the instrument along with additional testing for optimising the trapping and chromatographic techniques, including:

- BTV and recovery tests using the multi-bed adsorbent trap in-conjunction with the refocusing micro-trap.
- Incorporation of the Stirling coolers into the instrument. The current instrument frame is too small to house the Stirling coolers inside. The Stirling coolers sit on top of the instrument, which is ideal for easy access to the micro-traps. If they are to stay here, the instrument frame could be vastly reduced in size.
- Re-plumbing of the instrument, at present the valves configuration is the same as in the original design. The new design requires fewer valves and could be completely re-configured.
- Running whole air samples whilst at Bristol to test the automatic operation before the instrument can be sent to Mace Head research station, Ireland.

5. NMHC observations at Mace Head

5.1. Background

Mace Head research station has been a site for atmospheric measurements since 1958 (NUI, 2007). Situated on the west coast of Ireland, the atmospheric station at Mace Head, Carna, Co Galway, offers a unique opportunity to study the Northern Hemispheric background atmospheric composition when predominate westerly winds bring clean air to the research site. Polluted air arriving at Mace Head from Europe can then be compared with the baseline measurements and used to assess European emissions. The site is located 53° 20' N 9° 54' W in the path of the mid-latitude cyclones that frequently traverse the North Atlantic. The site is 88 km west of Galway city, 150 km away from the main Atlantic shipping routes and 80 km away from the transatlantic air corridors.

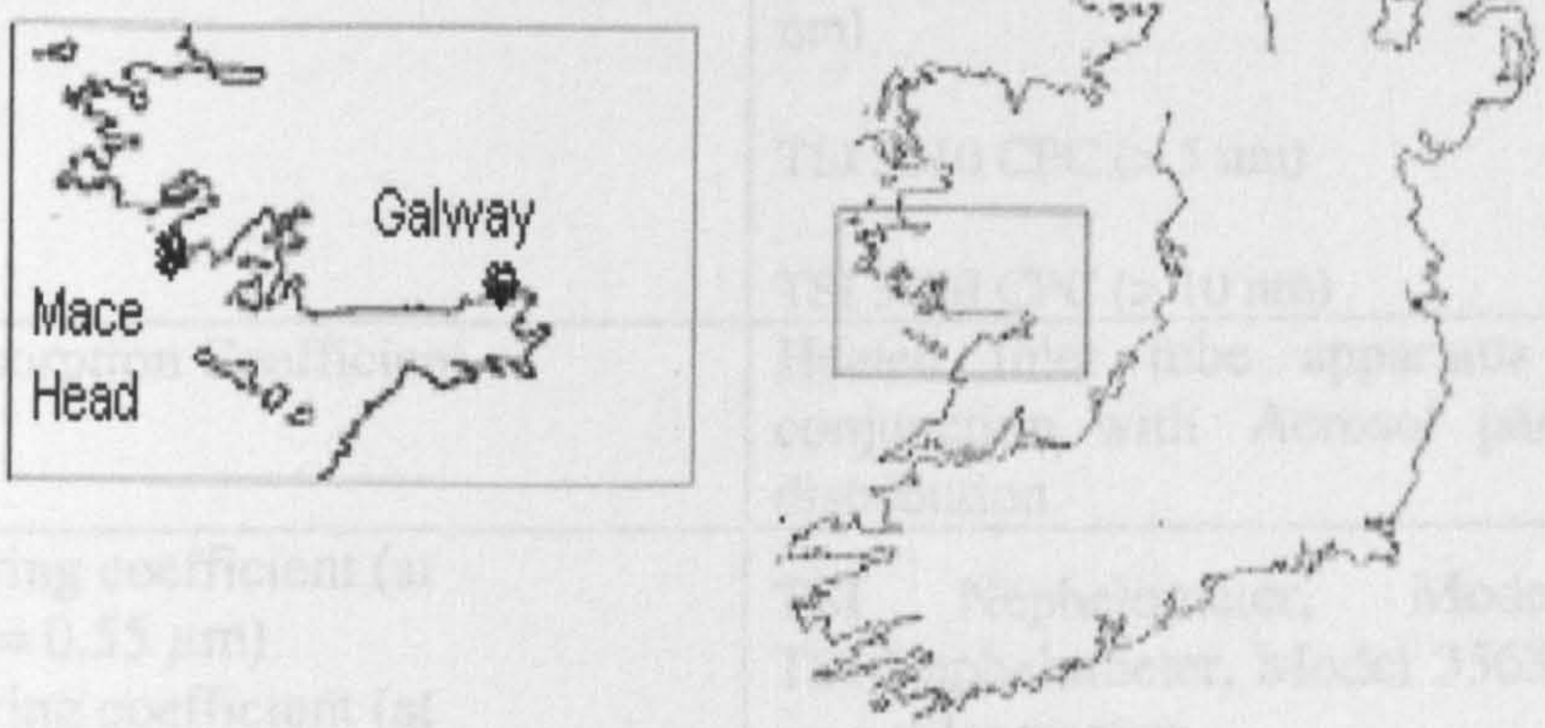

Figure 5.1 Geographical location of Mace Head research station (Martin, manuscript in preparation)

5.2. Instrumentation at Mace Head

Mace Head is used as a background atmospheric research station making routine measurements of a range of atmospheric constituents listed in Tables 5.1, 5.2 and 5.3.

Aerosols	Instrument
Aerosol particle size distribution	Pulse-Height-Analyser Condensation Particle Counter (2-10 nm) Nano Scanning Mobility Particle Sizer (3- 20 nm) Scanning Mobility Particle Sizer (10-400nm) Particle Measuring Systems (PMS) ASASP-X , (0.1 - 3.0μm) Aerodynamic Particle Sizer (0.5 - 30 μm) Electrical Low Pressure Impactor (30 nm - 30 μm)
Cloud Condensation Nuclei, (CCN)	DH Associates, Model M1, CCN counter (Twomey static thermal diffusion chamber)
Condensation Nuclei, (CN)	TSI 3025 Condensation Particle Counter (>3 nm) TSI 3010 CPC (> 5 nm) TSI 3010 CPC (> 10 nm)
Aerosol Absorption Coefficient	Heated inlet tube apparatus used in conjunction with Aerosol particle size distribution
Light scattering coefficient (at wavelength = 0.55 μm) Light scattering coefficient (at wavelengths=0.45,0.55 and 0.7μm)	TSI Nephelometer, Model 3551 TSI Nephelometer, Model 3563 mounted on a solar tracker
Aerosol Optical Depth	World Radiation Centre, Precision Filter Radiometer mounted on a solar tracker
PM2.5 mass concentration	R&P Tapered Element Oscillating Microbalance, Model 1400a
Aerosol Sampling Impactor	Moudi multistage rotating impactor, MD110

Table 5.1 Aerosol measurements made at Mace Head (NUI, 2007).

Gases	Instrument
$CFCl_3$, CF_2Cl_2, $CF_2ClCFCl_2$, $CHCl_3$, CH_3CCl_3, CCl_4, and N_2O	EC/FI/MR-GC, Electron capture detectors
CH_4	EC/FI/MR-GC, Flame Ionisation detector
CO and H_2	EC/FI/MR-GC, Mercuric oxide reduction detector
CO_2	Siemens IR carbon dioxide analyser
PAN	EC-GC, Electron capture detector
OZONE	UV Spectrometer
HFC's, other Halocarbons and NMHCs	GC-MS, gas chromatography mass spectrometer (Medusa)

Table 5.2 Trace gas measurements made at Mace Head (NUI, 2007).

Meterological parameter	Instrument
Wind speed	Munro cup anemometer
Wind direction	Munro wind vane
Air temperature	Vaisala HMD-30YB strain gauge temperature sensor, at 1.5m elevation
Relative Humidity	Vaisala HMD-30YB humidity sensor
Atmospheric pressure	Moudi multistage rotating impactor, MD110
Aerosol Sampling Impactor	Moudi multistage rotating impactor, MD110
Solar Radiation (UVA, UVB, Photopic)	National Radiological Protection Board, Chilton, UK.

Table 5.3 Meteorological measurements made at Mace Head (NUI, 2007).

5.3. Overview of the Medusa-GCMS instrument design

The Medusa-GCMS was developed to measure perflurocarbons and SF_6, very volatile long-lived greenhouse gases. The Medusa-GCMS is part of AGAGE (AGAGE, 2007), a global observing system of all important Montreal Protocol species and all significant non-CO_2 gases in the Kyoto Protocol. AGAGE collaborates with the System of Halogenated Greenhouse Gases in Europe, SOGE (SOGE, 2007) by sharing technology and placing AGAGE and SOGE data on common calibration scales with comparable precisions, accuracy and measurement frequency.

The Medusa-GCMS has been measuring perflurocarbons, SF_6, ethane, propane, benzene and toluene at Mace Head since November 2003. In January 2005 the NMHC list was extended to include; C_2-C_5 alkanes, isoprene, benzene, toluene, m&p-xylene, o-xylene and ethylbenzene. The measurements have been compared with the original Adsorption Desorption System (ADS) GCMS at Mace Head and have shown good precision and accuracy.

The Medusa is a pre-concentration system which, when coupled with a GCMS, allows analysis of very volatile trace gases in the parts per trillion (pptv) range. Central to the Medusa-GCMS design is the `Cryotiger'; its cold end maintains a temperature of -175 °C and conductively cools two traps to -165 °C. The use of dual traps (the first trap being larger than the second trap) allows analytes to be purified from more abundant gases which would otherwise interfere with analysis (including N_2, O_2, H_2O, CH_4). Purification is achieved by fractionation and refocusing from the first trap to the second, smaller trap, at very low temperatures. The Medusa is a fully automated, in-situ instrument which takes a 2 L air sample, a much larger volume than most other in-situ NMHC instruments. This increased sample volume combined with the use of a mass spectral detector provides better sensitivity, better signal to noise and precision. Sample analysis takes 1 hour, and each hour air and reference sample are alternated resulting in 12 air samples per day. A Valve diagram of the Medusa-GCMS is shown in Figure 5.2.

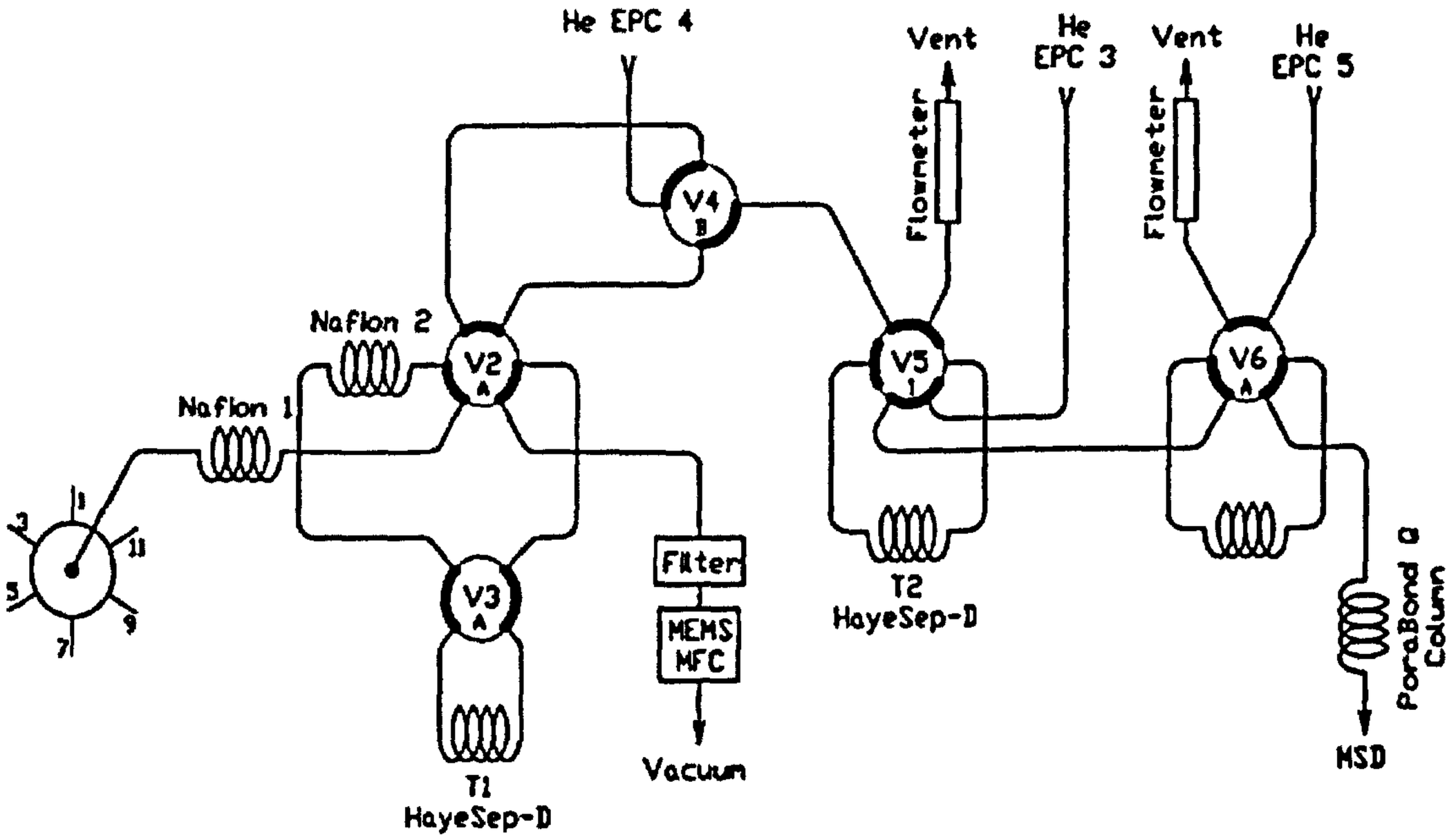

Figure 5.2 Valve diagram of the Medusa-GCMS.

Sample analysis takes place in a number of steps:

- The first valve is a multi-position Valco valve; when selected to take an air sample, the sample flows through two Nafion driers and onto the first trap (T1), held at -65 °C. Analytes are trapped on the Hayesep D adsorbent trap, the rest of the air sample flows through a filter and high precision mass flow controller (MFC) at a rate of 100 scc/min.
- T1 is post-flushed (with helium from EPC4) to remove N_2, O_2, Ar, CH_4
- T1 is heated to 80 °C, CF_4 is transferred to T2.
- T2 is post-flushed at -125 °C to further reduce N_2, O_2, Ar
- T2 heated to 100 °C; CF_4 is back-flushed to the GCMS, through the MS-4A and HiSiv-3000 packed pre-column. This is a micropacked column which separates CF_4 from residual O_2, N_2, N_2O, CO_2, Ar and Kr.
- While CF_4 is analysed, T1 post-flushed at -70 °C to remove CO_2, Xe.
- T1 is heated to 100 °C and back-flushed to transfer analytes to T2, held at -165 °C.
- T2 is post-flushed at -65 °C to further reduce CO_2, Xe.
- T2 is heated to 100 C and back-flushed to transfer analytes to the GCMS (bypassing the pre-column).
- Porabond Q chromatography column programmed from 40 °C to 200 °C at 23 °C/min to separate the flurocarbons, SF_6, halocarbons and NMHCs.
- Custom software under the Linux operating system runs the Medusa and the GCMS in Selective Ion Mode (SIM).

5.4. Hydrocarbon calibration on the Medusa-GCMS

The synthetic standard used to calibrate hydrocarbon measurements on the Medusa-GCMS was a dilution of the ppbv concentration Apel-Reimer hydrocarbon standard, details of which can be seen in Table 5.4. A dilution was necessary to mimic as closely as possible the composition of an air sample. Using a standard containing species in a similar concentration range to those in ambient air samples is the most accurate and reliable calibration method and prevents instrument non-linearity.

A dilution of the Apel Reimer hydrocarbon standard was achieved using a 35 litre electropolished stainless steel canister (Essex Cryogenics Inc., MO, USA). The canister is first cleaned using a static dilution system by evacuating it to 1×10^{-5} mm Hg using an oil pump. Up-stream of the oil pump there is a cold water trap (housed in a Dewar containing liquid nitrogen) which prevents any contamination from the oil pump reaching the dilution system. Second, the evacuated canister is filled with N_2. N_2 travels through an activated charcoal trap cooled by a cryocool II probe to -75 °C to prevent hydrocarbon contamination reaching the canister. The canister is filled to 100 Psi and allowed to equilibrate for at least 2 hours before the process of evacuation was repeated again. The process of evacuation and re-filling is performed three times.

Once the canister was cleaned, the Apel Reimer hydrocarbon standard dilution was made using a Keller pressure transmitter (accurate to 0.01%). The canister was connected to the Apel Reimer standard via a sample loop. The pressure transmitter was connected to the top of the cleaned canister and relayed the pressure inside the canister to a computer. The pressure of the Apel Reimer standard was set to 1 bar, the canister was still closed and the standard was allowed to flow through the lines, to equilibrate the lines with a standard and allowing any leaks to be detected. The canister was then opened and allowed to fill to 2 bar. The Keller pressure transmitter recorded the pressure of the canister during this time. Once complete, the canister was left for 2 hours to equilibrate; the pressure transmitter recorded the pressure of the canister every second. The Apel Reimer standard was diluted by a ratio of 12.9 based on the premise that the target compound, o-xylene should not be below 30 pptv in concentration.

Compound	Conc in primary Std (pptv)	Conc in secondary std (pptv)	Compound	Conc in primary Std (pptv)	Conc in secondary std (pptv)
Ethane	11700	908	cyclohexene	1680	130
Ethene	5510	427	benzene	1950	151
Ethyne (Acetylene)	8700	675	toluene	2430	189
Propane	10480	813	1,3- dimethylcyclopentane (cis)	3050	237
Propene	2250	175	1-heptene	4550	353
Propyne	5540	430	heptane	4790	372
n-Butane	9490	736	2,3-dimethyl-2-pentene	940	73
isobutane (2 methyl propane)	4790	372	methylcycloheaxene	840	65
isobutene	3560	276	2,4-dimethylpentane	950	74
1-butene	2310	179	2,3,4 trimethylpentane	530	41
t-2-butene	1170	91	2-methylheptane	460	36
c-2-butene	2230	173	3-methylheptane	1170	91
1,3 butadiene	2210	171	4-methylheptane	950	74
n-pentane	7620	591	Octane	470	36
i-pentane	7170	556	o-xylene	390	30
cyclopentane	960	74	m-xylene	1340	104
t-2-pentene	910	71	p-xylene	420	33
c-2-pentene	2240	174	styrene (ethenylbenzene)	390	30
1-pentene	1170	91	Indan(e)	1040	81
2 methyl-1-butene	1110	86	nonane	910	71
2 methyl-2-butene	900	70	I-propylbenzene	190	15
cycopentene	890	69	propylbenzene	210	16
isoprene	4580	355	1,3,5-trimethylbenzene	570	44
hexane	2960	230	2-ethyltoluene	420	33
2-2 dimethyl butane	2540	197	3-ethyltoluene	200	16
2-3 dimethyl butane	1710	133	4-ethyltoluene	390	30
cyclohexane	480	37	1,2,4-trimethylbenzene	800	62
2-methylpentane	960	74	1,2,3-trimethylbenzene	1130	88
3-methylpentane	990	77	t-butylbenzene	1510	117
2-methyl-1-pentene	910	71	decane	860	67
t-2-hexene	460	36	1,3 dietyhylbenzene	630	49
c-2-hexene	920	71	1,4 dietyhylbenzene	790	61
1,3 hexadiene	2150	167	butylbenzene	400	31
methylcyclopentane	950	74	undecane	400	31

Table 5.4 Dilution of the Apel Reimer hydrocarbon standard. The primary standard is accurate to ± 2%. The secondary standard relies on accurate setting of the pressure regulators and errors associated with volumes, pressures and temperatures of primary and secondary standards.

The dilution of the Apel Reimer hydrocarbon standard was sent to Mace Head and sampled by the Medusa-GCMS. The standard was sampled eleven times against a known, tertiary standard (Figure 5.3). The sequence of analysis was standard-tertiary-standard-tertiary etc with two blanks at the end of the eleven samples to check for hydrocarbon carry over. The NMHC concentrations in the Apel Reimer dilution standard are known (listed in Table 5.4), and by comparing the dilution to a tertiary standard allowed concentrations to be ascribed to the tertiary and so propagate through as with other AGAGE gases (O'Doherty, et al., 2004; Prinn, et al., 2000).

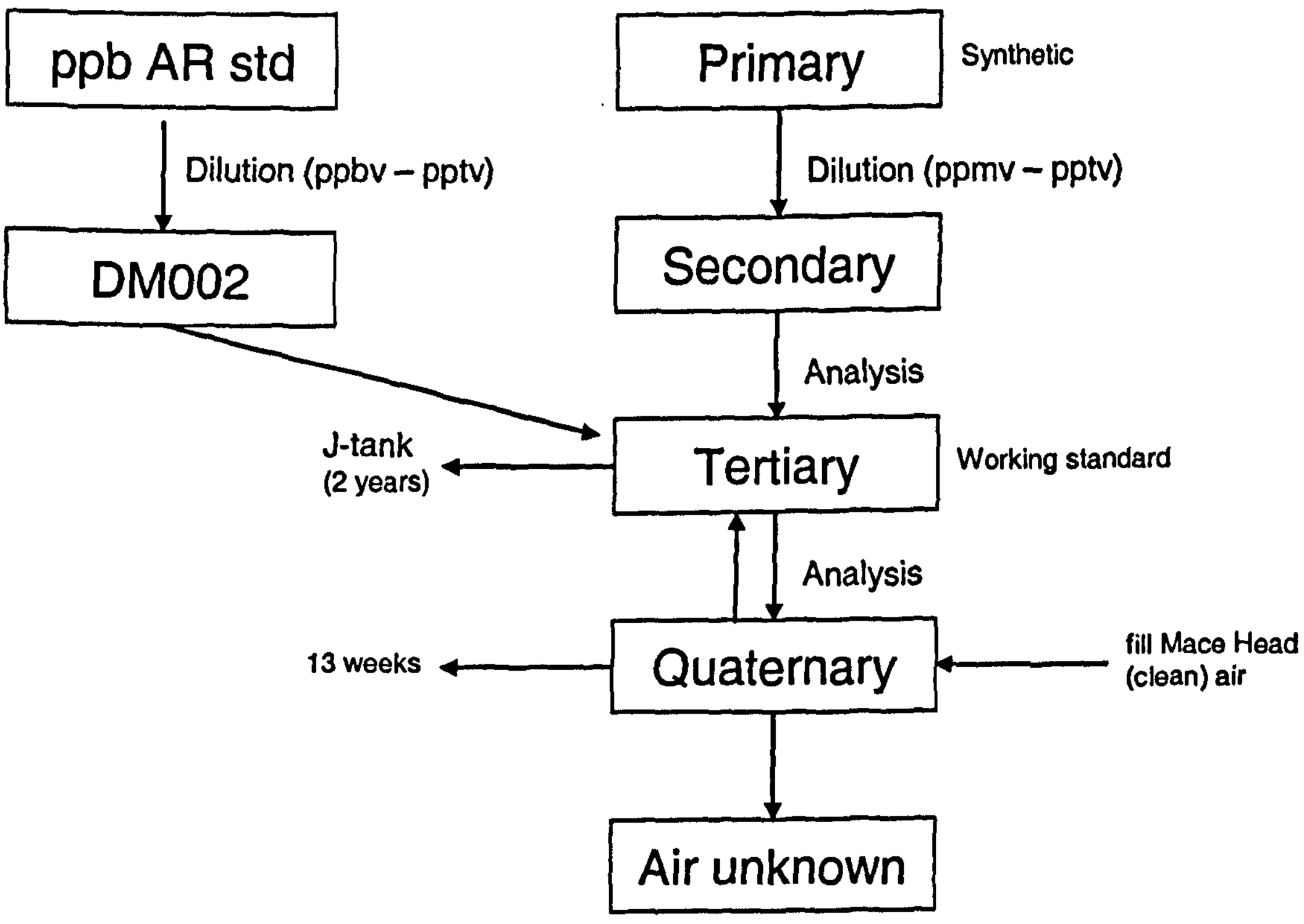

Figure 5.3 Calibration of the AGAGE Medusa-GCMS.

5.5. Mass spectrum detection

5.5.1. SIM and TIC analysis

The Medusa-GCMS is run in selective ion monitoring (SIM) mode, only looking at a few ions at any given time. The retention time along with a target ion (and possibly one or two qualifying ions) are used to identify each species. Because SIM analysis only looks at a few characteristic ions in each retention window it is a more sensitive than when the mass spectrum is operated in total ion chromatogram (TIC) mode. TIC analysis performs a full scan over all ions in a selected mass range; although it is less sensitive it does allow ion ratios for each compound to be calculated. The Medusa-GCMS is run in TIC mode once a week (after the blank run routine) producing a full ion spectrum for each peak which can be compared with mass spectra available from http://webbook.nist.gov/ (an example is shown in Figure 5.4). This enables any co-elution or incorrect peak assignment to be identified. Detailed analysis of ion spectrums obtained from TICs has been performed in both air and standard samples, confirming NMHC peak assignments on the Medusa-GCMS.

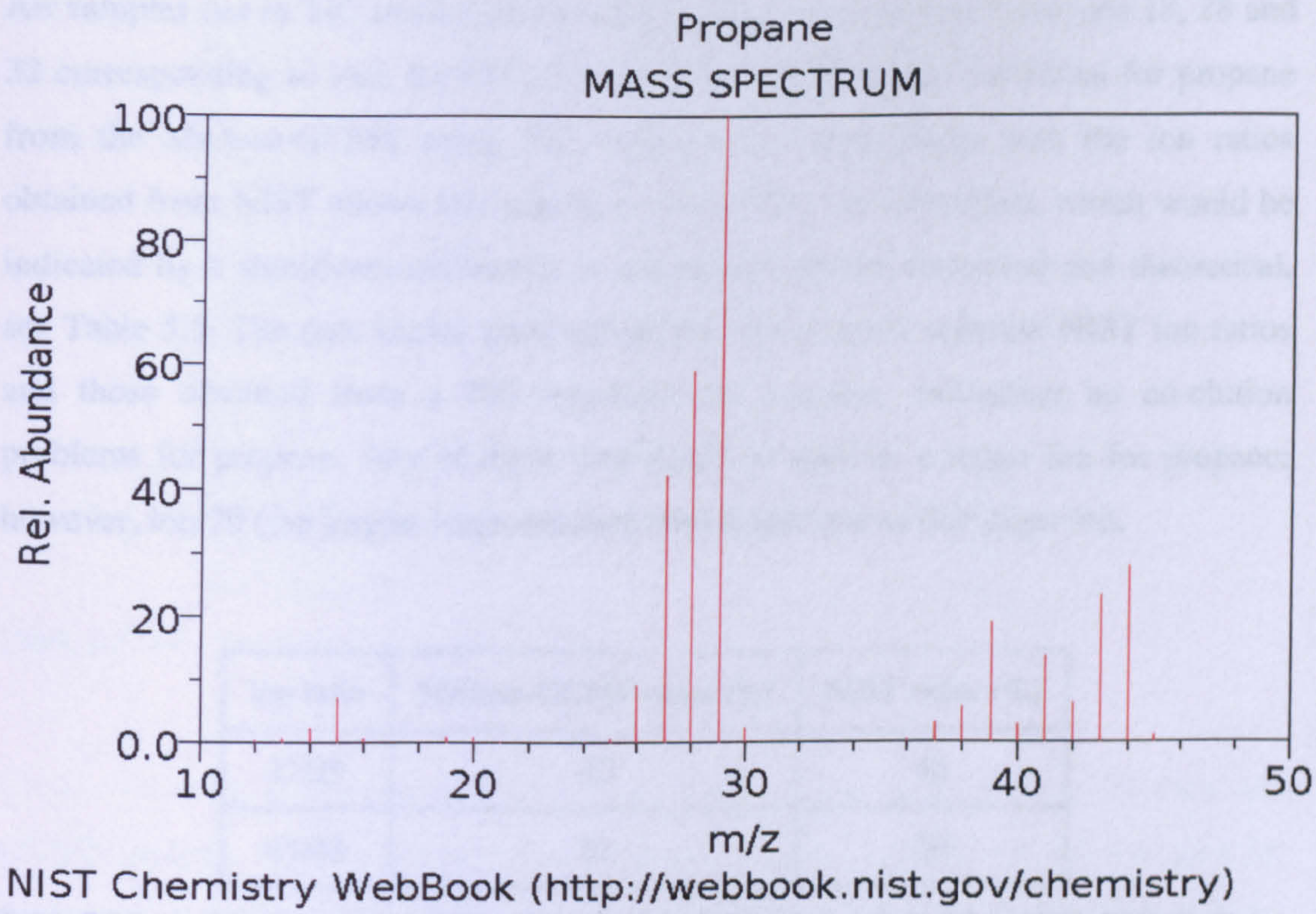

Figure 5.4 Ion spectrum for propane obtained from NIST, 2007.

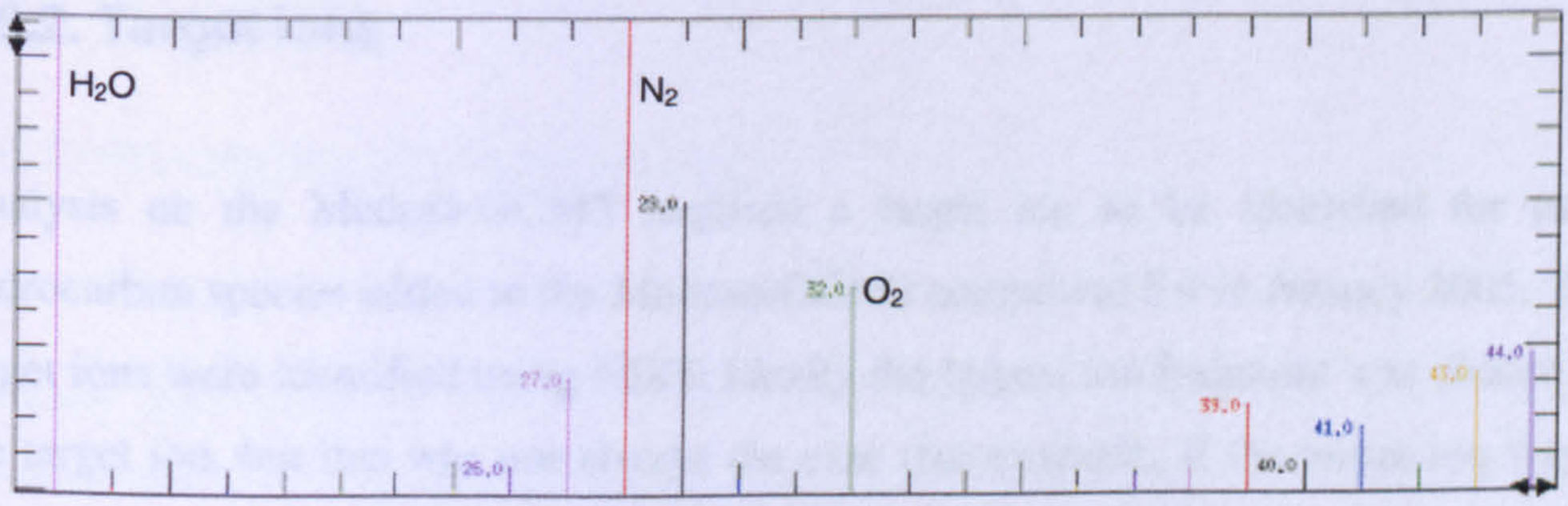

Figure 5.5 Ion spectrum for propane obtained from TIC analysis with the Medusa-GCMS.

Air samples run in TIC mode include large background peaks for m/z ions 18, 28 and 32 corresponding to ions for H_2O, N_2 and O_2. Examining the ion ratios for propane from the Medusa-GCMS using TIC analysis and comparison with the ion ratios obtained from NIST allows any potential co-elution to be identified, which would be indicated by a significant difference in ion ratios between measured and theoretical, see Table 5.5. The data shows good agreement between the reported NIST ion ratios and those obtained from a TIC spectrum for propane, indicating no co-elution problems for propane. Any of these ions could be used as a target ion for propane; however, ion 29 (the largest fragmentation ion) is selected as the target ion.

Ion ratio	Medusa-GCMS value (%)	NIST value (%)
27/29	42	42
41/43	52	50

Table 5.5 Ion ratios for propane TIC mode compared with data values from NIST, 2007. Both the GCMS and NIST values are approximate values taken directly from observation of the mass spectrums from TIC analysis and downloaded from NIST.

5.5.2. Target ions

Analysis on the Medusa-GCMS required a target ion to be identified for each hydrocarbon species added to the Medusa-GCMS compound list in January 2005. The target ions were identified using NIST; ideally the largest ion fragment was chosen as the target ion, but this was not always the case (for example, if the target ion was a major component of background air). Table 5.6 shows a list of target ions, and qualifying ion used to identify NMHCs.

NMHC	NIST major ion	Target ion	Qualifying ion
Ethane	28	26	-
Propane	29	41	29
i-Butane	43	42	43
n-Butane	43	43	42
i-Pentane	43	43	-
n-Pentane	43	43	-
Isoprene	68	67	-
Benzene	78	78	-
Toluene	91	91	92
m&p-Xylene	91	91	106
o-Xylene	91	91	106
Ethylbenzene	91	91	106

Table 5.6 List of NMHCs and their target ions.

Cases when the major ion fragment is not used as the target ion by the Medusa-GCMS include: ethane, propane and i-butane. The M^+ ion 28 can not be used for analysis due to N_2 interference. It was decided to use ion 41 for propane as the propane peak for ion 29 appeared on the tail of a very large peak which interfered with propane measurements during summer months.

5.5.3. Resolving i-butane issues

i-Butane concentrations were only recorded since September 2005 due to initial measurement problems. Ion 43 was originally used as the target ion for i-butane and in the summer months, when i-butane concentrations are low, a co-eluting peak was noticed. Although much work was done to try to identify the peak, it still remains elusive. The co-eluting peak could be present all year round, being swamped by the large i-butane peak during winter months, or it could have a significant biogenic source only present in summer. The influences of the co-eluting peak can be seen in Figure 5.6. Since a mass spectrum in SIM mode is used for analysis, the co-eluting peak is only a problem if it has the same ion in its ion fragment spectrum as the target ion for i-butane. Since the Porabond Q chromatography column separates compounds by boiling points the co-eluting peak must have a similar boiling point to i-butane

(262.0 K). Various compounds with similar boiling points and a 43 ion in their mass spectrums (data obtained from NIST) were investigated to identify the co-eluting peak. OVOCs such as ethylene oxide (285.0 K) and acetaldehyde (293.9 K) and butene isomers, i-butene (266.7 K) and 1-butene (266.8 K), were investigated. All were found to elute after i-butane on the Porabond Q column and hence could not be the co-eluting peak, which still remains unknown.

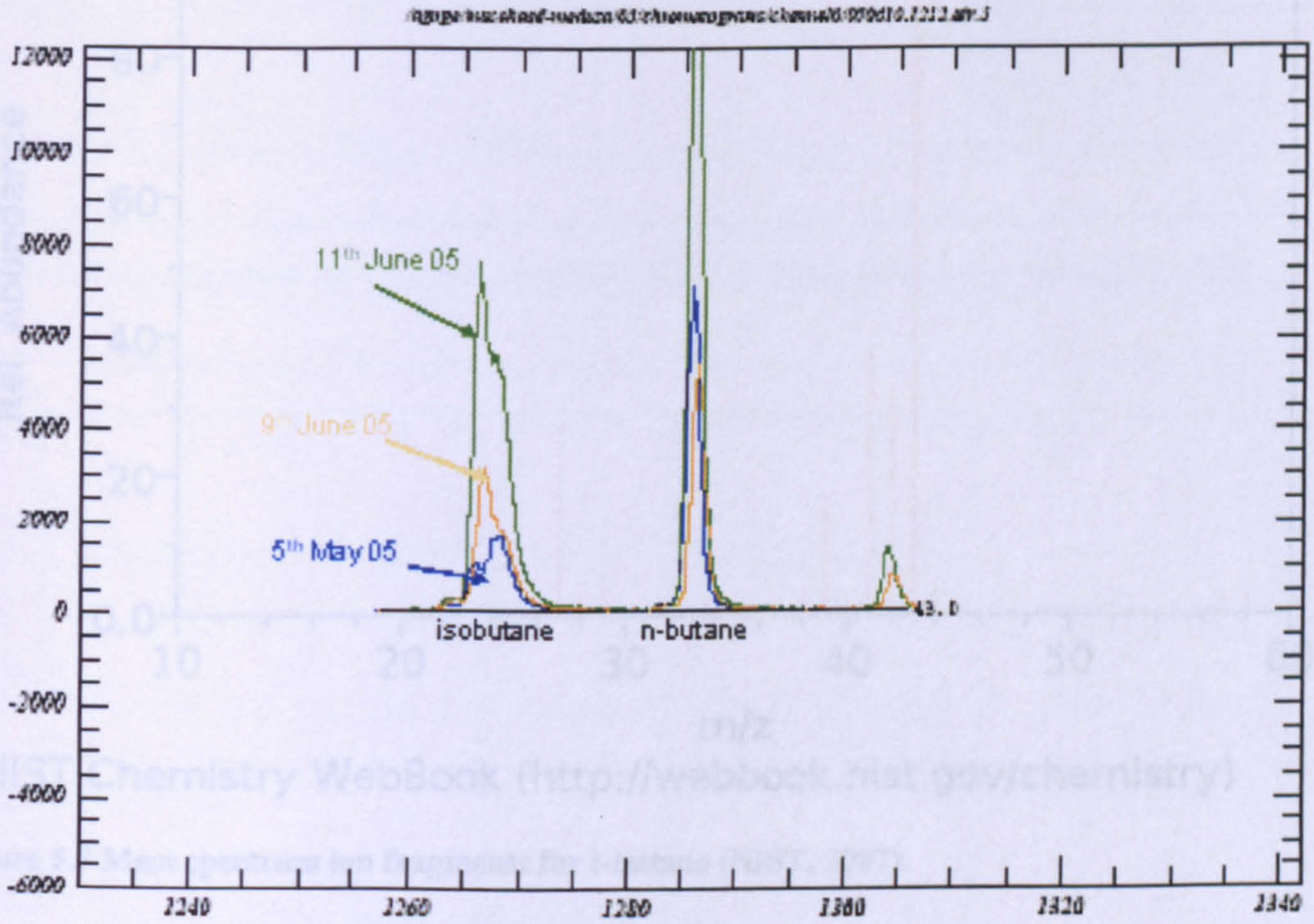

Figure 5.6 Chromatogram showing the co-eluting peak eluting prior to i-butane and growing during summer months.

Since the relationship between i-butane and n-butane is well characterised by a large number of data sets and has been shown to be robust, the data from Mace Head should replicate these data sets. Derwent, (2000) found the urban relationship of i-butane vs. n-butane of 0.46 in 1996 and 0.5 in 1998. Plotting the i-butane/n-butane ratio against n-butane should show, at high n-butane concentrations (corresponding to a pollution event), a ratio similar to the urban ratio; and at low n-butane concentration (aged/clean air sampled) the ratio should increase due to the preferential removal of n-butane compared with i-butane by reaction with the hydroxyl radical. Using ion 43 as the target ion for i-butane could not replicate this well-established trend, because

the i-butane/n-butane ratio is low at low concentrations due to an under-estimation of i-butane concentrations caused by the co-eluting peak (which must contain ion 43 fragment) being incorrectly integrated as i-butane.

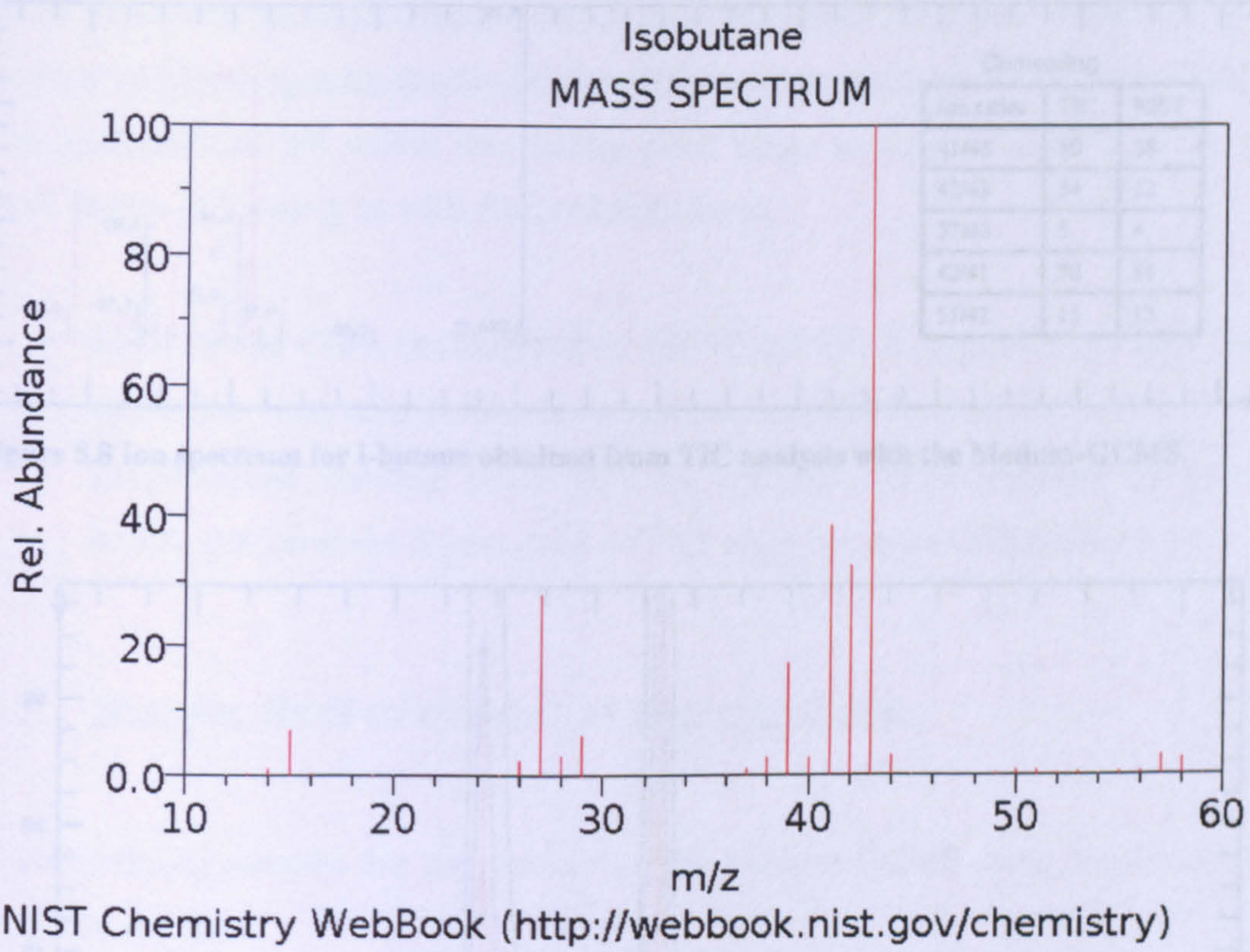

Figure 5.7 Mass spectrum ion fragments for i-butane (NIST, 2007).

In order to resolve this i-butane interference three alternative ions 57, 41 and 42 were investigated. It was decided that ion 42 should be used as the target ion for i-butane. Ion 57 was discarded as the 57 fragment is very small (at about 0.04% of the base peak, ion 43). Using ion 41 as the target ion for i-butane also caused a decrease in i-butane/n-butane ratio at low concentrations indicating the co-eluting compound also contains an ion 41 fragment. Using ion 42 as the i-butane target ion resolved the issues with measuring i-butane, giving the correct relationship between i-butane and n-butane. Thus, it appears that the co-eluting compound does not have an ion fragment of 42, and hence by switching the target ion for i-butane we can effectively resolve the co-eluting compounds. Figure 5.8 shows the ion spectrum for i-butane when the mass spectrometer is run in TIC mode. The ion ratios for TIC are compared with reported NIST ratios, ion 42 and 57 give the correct ratios. This means the co-eluting peak either doesn't have an ion 42 or 57, or it has both ions in the same ratio

as i-butane, the assumption made here is that the co-eluting compound does not have an m/z 42 or 57. Figure 5.9 shows the i-butane chromatographic peak, using ion 42 as the target ion.

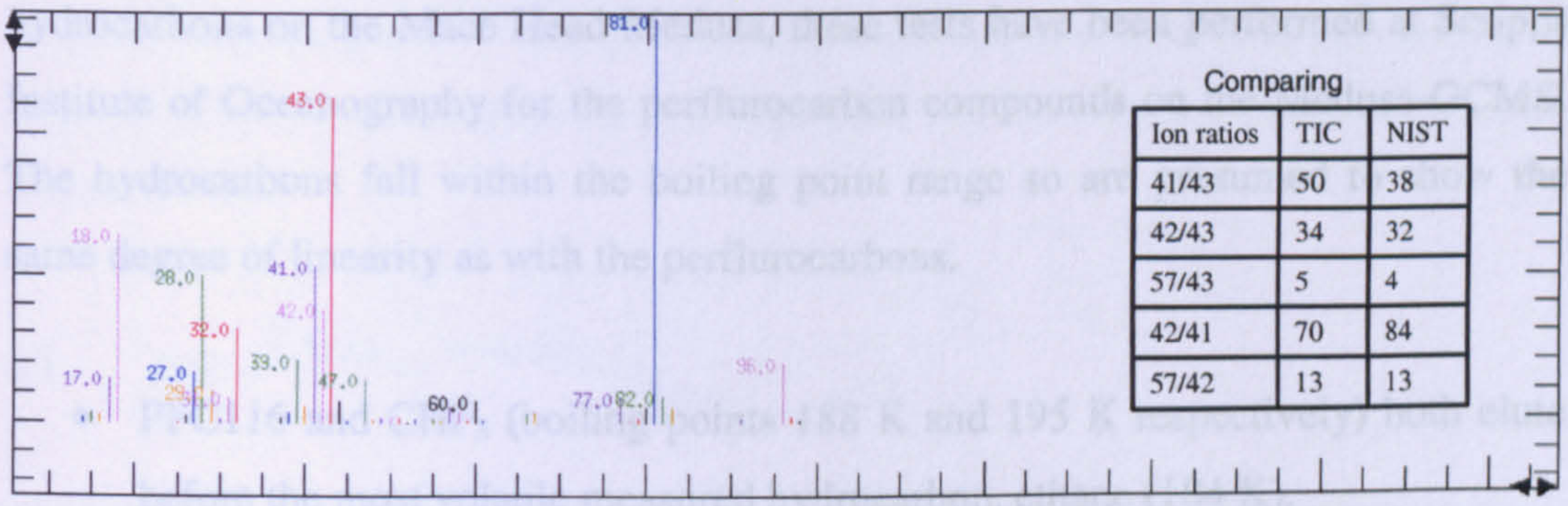

Ion ratios	TIC	NIST
41/43	50	38
42/43	34	32
57/43	5	4
42/41	70	84
57/42	13	13

Figure 5.8 Ion spectrum for i-butane obtained from TIC analysis with the Medusa-GCMS.

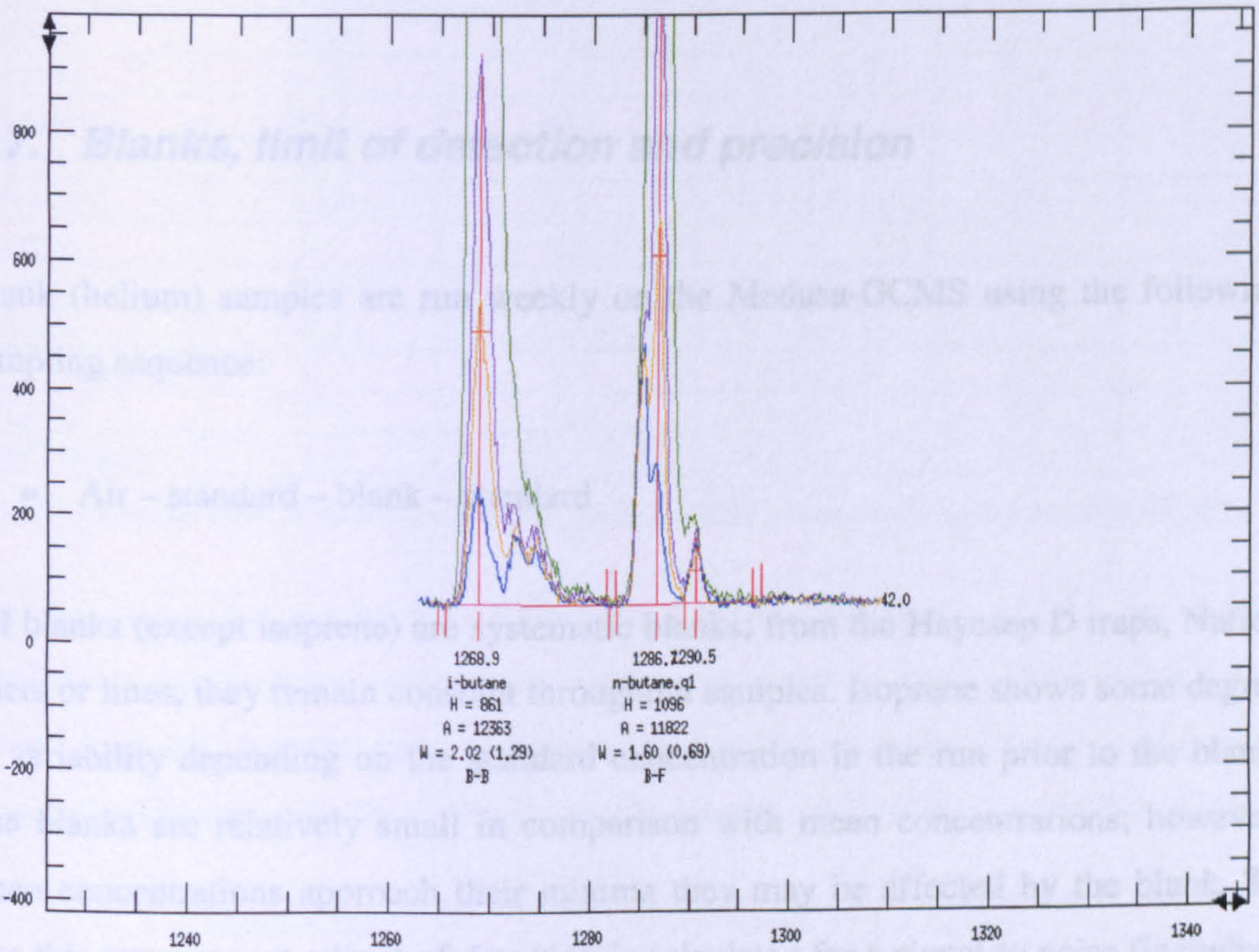

Figure 5.9 Chromatogram showing the i-butane peak during pollution event and clean summertime air.

5.6. Breakthrough & Linearity

Although no direct linearity and breakthrough tests have been carried out for the hydrocarbons on the Mace Head Medusa, these tests have been performed at Scripps Institute of Oceanography for the perflurocarbon compounds on the Medusa-GCMS. The hydrocarbons fall within the boiling point range so are presumed to show the same degree of linearity as with the perflurocarbons.

- PFC116 and CHF_3 (boiling points 188 K and 195 K respectively) both elute before the most volatile measured hydrocarbon, ethane (184 K).
- Ethylbenzene (boiling point 409 K) and the xylene isomers (m-xylene 412 K, p-xylene 411 K, o-xylene 417 K) elute just after $CHBr_3$ (422 K).

5.7. Blanks, limit of detection and precision

Blank (helium) samples are run weekly on the Medusa-GCMS using the following sampling sequence:

- Air – standard – blank – standard

All blanks (except isoprene) are systematic blanks; from the Hayesep D traps, Nafion driers or lines, they remain constant throughout samples. Isoprene shows some degree of variability depending on the standard concentration in the run prior to the blank. The blanks are relatively small in comparison with mean concentrations; however, when concentrations approach their minima they may be affected by the blank. To take this into account a limit of detection is calculated for a signal to noise (including the blank concentration) of 3.

Instrument precision is an indicator of the detectors response over a period of time. Precision is calculated from the standard-standard ratios (SSR) using Equation 5.1. The range in precision is obtained depending on the NMHC concentration in the bracketing standard. The Medusa-GCMS uses a synthetic standard as the original

reference, to which standard air samples are referenced and concentrations determined as shown in Figure 5.3. An explanation for the large variability in isoprene's precision is when the bracketing standard was filled during winter months, the concentration of isoprene is very low and so the standard-standard ratio is high, due to poor integration of small isoprene peaks. When the standard was filled in summer months, during an isoprene biogenic event, isoprene is a large peak and the standard-standard precision is much better.

5.1. $$SSR = {(Area_{run1} + Area_{run2})}/{(Area_{run2} \times 2)}$$

Compound	2006 Winter minimum (pptv)	2006 Summer minimum (pptv)	Mean blank (pptv)	Limit of detection (pptv)	Precision (%)
Ethane	1105.3	240.0	0.9 (± 0.2)	2.8	0.6 – 1
Propane	168.6	<0.4	0.3 (± 0.2)	1.2	1 – 3
i-Butane	15.8	<0.4	0.5 (± 0.1)	1.4	2 – 5
n-Butane	54.6	<0.2	0.2 (± 0.1)	0.6	3 – 5
i-Pentane	12.8	0.4	0.3 (± 0.2)	1.2	3 – 9
n-Pentane	12.4	0.3	0.2 (± 0.1)	1.0	3 – 9
Isoprene	0.1	0.3	-	-	7 – 60
Benzene	56.9	6.7	0.5 (± 0.1)	1.6	0.6 – 1
Toluene	6.8	0.6	0.4 (± 0.1)	1.3	0.6 – 2
m&p-Xylene	2.1	1.0	0.8 (± 0.3)	2.3	3 - 10
o-Xylene	1.0	<0.3	0.3 (± 0.1)	0.9	3 – 15
Ethylbenzene	1.3	0.1	0.1 (± 0.1)	0.3	2 - 10

Table 5.7 Blanks, limit of detection and precision of NMHCs measured by the Medusa-GCMS.

The isoprene blank is variable (2006 blanks vary between 0.1 and 1.1 pptv). The blank is an insignificant percentage of the large biogenic events observed at Mace Head (50 to 250 ppt) and large winter isoprene pollution events (20 pptv). However, lower winter/summer isoprene measurements may be affected by the variable blank.

Month (2006)	Isoprene mean Blank (pptv)	Standard deviation
January - February	0.2	0.1
March – April	0.4	0.1
May – June	0.4	0.3
July – August	0.5	0.1
September – October	0.1	0.1
November - December	0.1	0.1

Table 5.8 Isoprene's variable blanks.

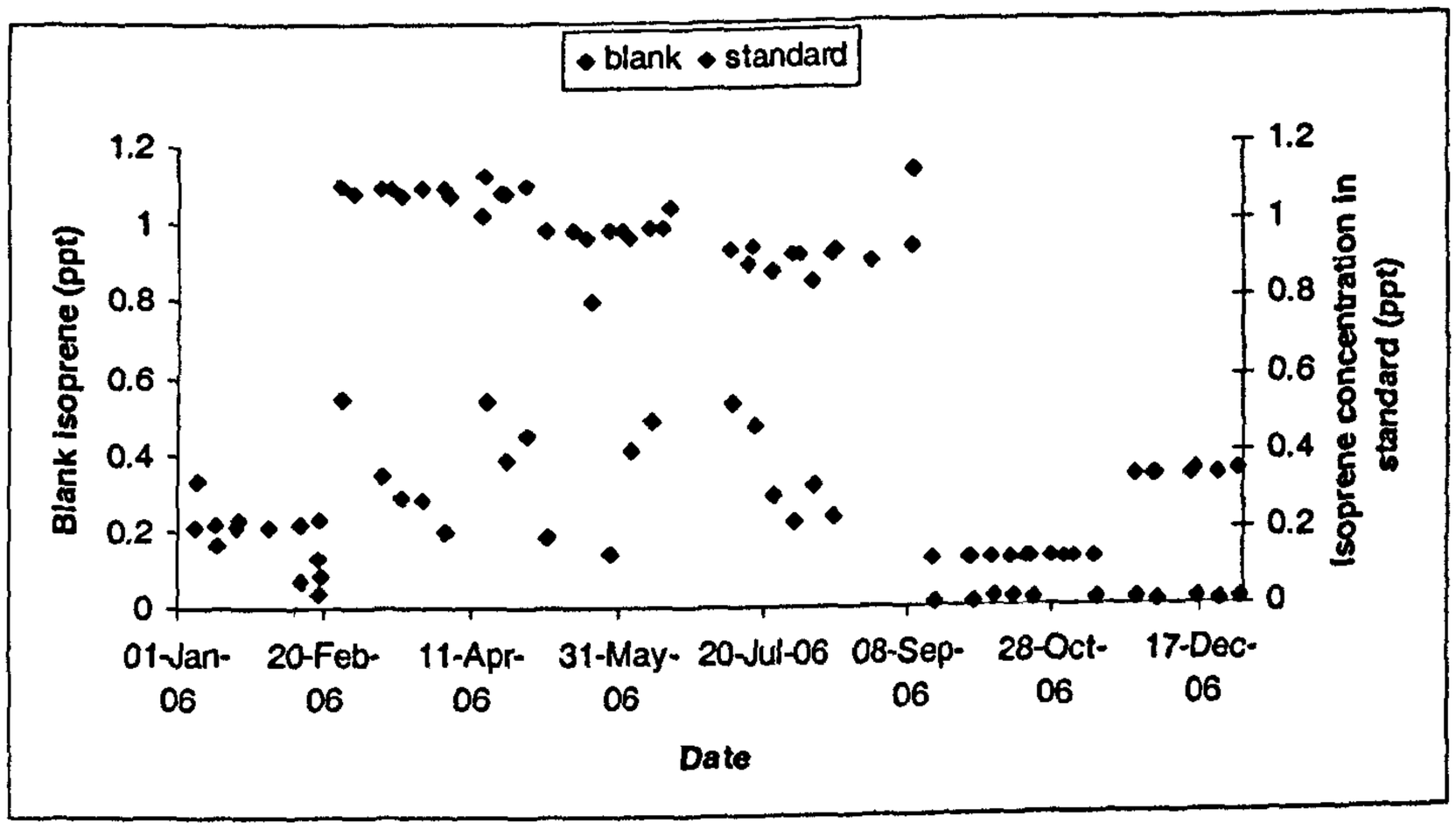

Figure 5.10 The variable isoprene blank plotted with standard concentrations.

5.8. NMHC measurements made at Mace Head

NMHC species measured by the Medusa-GCMS include; ethane, propane, i-butane, n-butane, i-pentane, n-pentane, isoprene, benzene, toluene, m,p-xylene, o-xylene and ethylbenzene. The monthly mean concentrations for each NMHC species measured by the Medusa-GCMS can be seen in Table 5.9.

	Ethane	Propane	I-Butane	n-Butane	i-Pentane	n-Pentane	Isoprene	Benzene	Toluene	m,p-Xylene	o-Xylene	Ethylbenzene
Jan-05	1750.4	544.6	-	248.2	74.4	71.4	0.4	122.7	48.1	23.7	10.8	6.4
Feb-05	2123.4	762.4	-	312.0	94.6	88.5	0.9	178.8	68.1	56.9	25.1	14.1
Mar-05	1858.8	469.4	-	201.3	67.8	48.5	0.6	132.1	57.7	44.8	20.9	10.2
Apr-05	1864.3	395.3	-	145.8	47.4	36.3	0.6	110.8	39.8	33.6	15.0	7.3
May-05	1402.8	126.7	-	35.8	13.0	11.8	0.7	55.2	15.6	15.7	7.1	2.7
Jun-05	780.6	22.3	-	18.5	10.4	6.8	2.2	21.5	10.9	9.0	5.5	2.0
Jul-05	655.1	33.0	-	3.4	11.1	7.5	2.9	18.8	13.2	16.1	7.0	2.3
Aug-05	681.5	38.6	-	16.9	7.4	6.5	2.0	33.4	12.9	13.7	5.8	2.1
Sep-05	878.7	91.6	5.5	60.3	26.6	7.4	4.2	48.2	19.5	14.8	7.7	2.9
Oct-05	1117.7	223.7	49.9	121.8	15.4	10.7	2.1	70.2	39.4	10.1	18.2	5.8
Nov-05	1400.7	397.2	42.6	177.7	61.4	55.9	0.6	108.5	61.0	46.4	22.8	8.4
Dec-05	1827.6	650.3	102.5	285.9	97.9	82.9	0.4	153.8	69.0	68.6	29.9	12.5
Jan-06	1990.0	753.2	132.3	341.3	122.2	98.1	0.5	182.6	100.6	91.7	36.8	15.0
Feb-06	2062.8	744.7	128.5	314.5	102.5	87.0	0.4	180.1	77.8	53.2	25.3	12.3
Mar-06	2087.0	681.5	98.4	268.1	82.9	74.8	1.2	161.5	64.2	42.9	14.3	9.6
Apr-06	1702.5	279.3	26.4	75.5	15.8	16.5	0.5	79.9	6.9	5.2	1.3	0.9
May-06	1293.7	106.8	14.7	36.3	14.0	11.4	1.0	55.1	12.4	7.0	3.0	1.7
Jun-06	922.1	45.0	10.3	30.4	17.4	11.6	4.3	32.5	12.4	7.2	3.0	1.6
Jul-06	708.7	42.5	9.6	30.2	21.7	14.3	8.3	35.6	21.4	14.3	6.4	2.6
Aug-06	659.6	43.1	7.9	22.3	11.4	7.9	3.1	21.0	9.3	7.0	4.0	1.7
Sep-06	818.0	76.3	9.6	29.7	11.2	10.4	3.8	30.1	13.3	9.1	2.7	2.4
Oct-06	1061.7	225.9	38.8	107.3	40.7	32.7	0.1	58.5	36.3	26.0	12.5	5.2
Nov-06	1321.0	358.6	44.8	137.9	41.7	39.8	0.0	81.3	29.6	16.3	8.1	4.2
Dec-06	1722.0	615.5	87.7	259.6	89.2	73.2	0.1	131.0	70.2	13.8	8.5	7.9

Table 5.9 Monthly mean NMHC concentrations at Mace Head during 2005 and 2006.

5.8.1. Ethane and propane measurements

Atmospheric measurements of ethane and propane are generally derived from natural gas leakage, with a negligible ethane source from motor vehicles. Prior to the implementation of catalytic converters, propane had a significant motor vehicle source which is steadily being reduced (Dollard, et al., 2007).

5.8.1.1. Composite cycle of ethane and propane

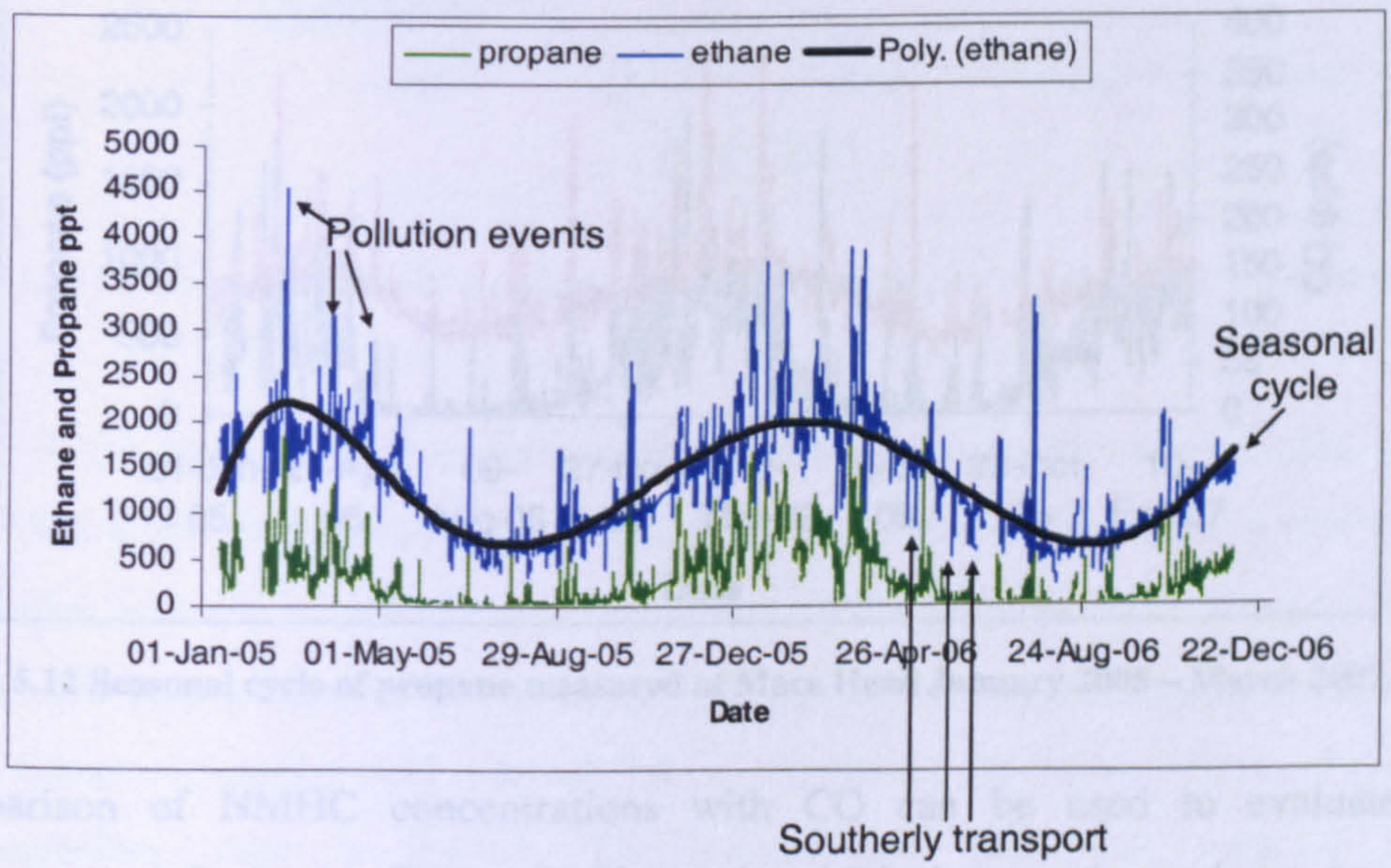

Figure 5.11 Seasonal cycle of ethane measured at Mace Head January 2005 – January 2007.

A seasonal variation in the background concentrations of ethane and propane is observed, with an increase in baseline concentrations during winter months and a decrease in summer. This seasonal cycle is mainly due to increased oxidation of NMHCs by reaction with the hydroxyl radical during summer months (caused by increased photolysis of O_3 and increased evaporation of H_2O; see chapter 1); as a result, the amplitude of the annual cycle is driven by atmospheric removal rates. Westerly winds bring clean, Atlantic air to Mace Head and are used to determine the background, or baseline atmospheric concentrations. Above baseline concentrations indicate pollution events, when air parcels arrive at Mace Head from European trajectories. During southerly transport events, ethane and propane show sharp

reductions in concentration. This is in part due to lower levels of anthropogenic trace gases in the Southern Hemisphere compared with the Northern Hemisphere and because transport from southerly latitudes results in more photochemical processing and reaction with the OH radical, further reducing NMHC concentrations.

5.8.1.2. Comparison of propane's seasonal cycle with CO

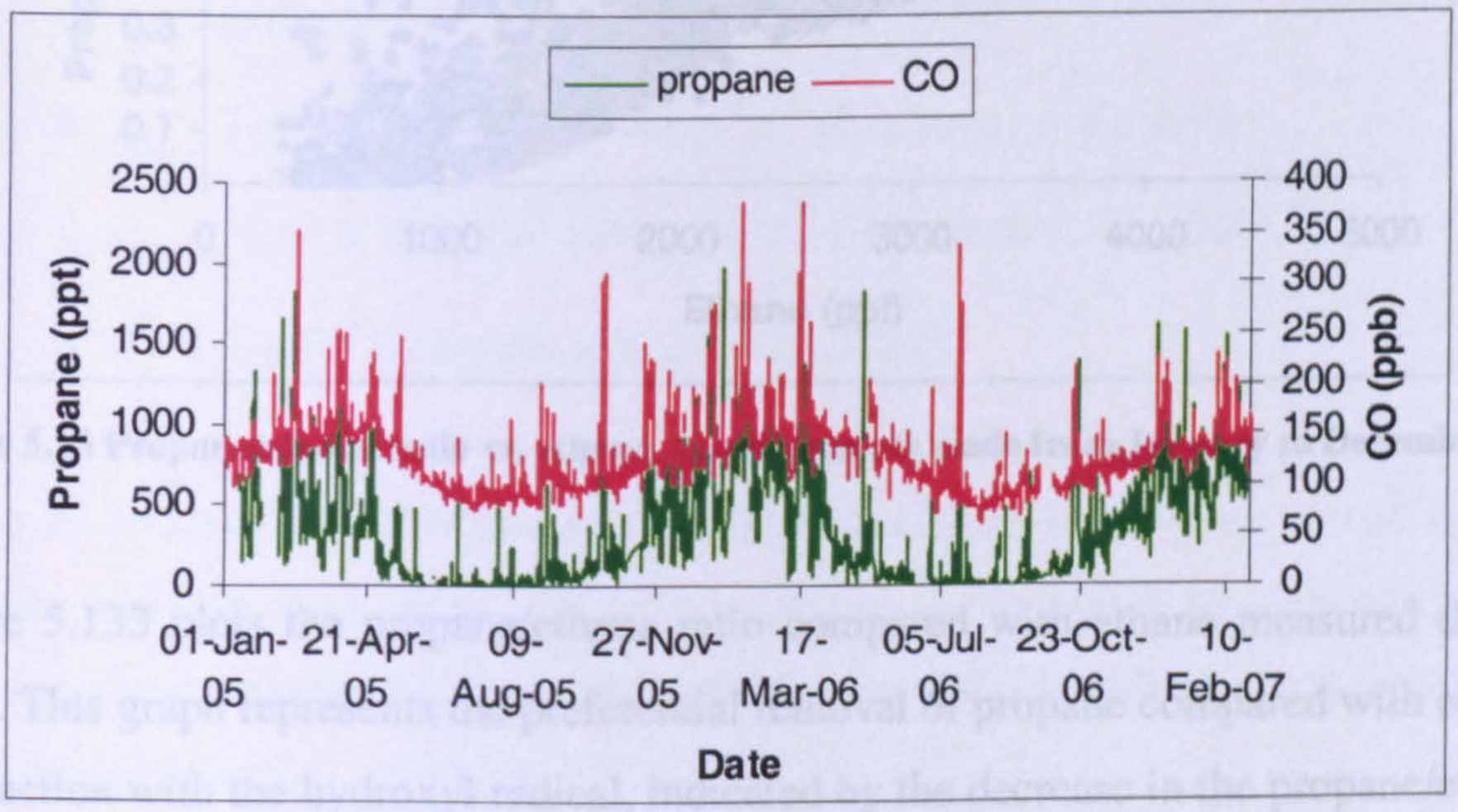

Figure 5.12 Seasonal cycle of propane measured at Mace Head January 2005 – March 2007.

Comparison of NMHC concentrations with CO can be used to evaluate the instruments performance. Figure 5.122 shows a high degree of correlation between propane and CO measurements, with all pollution events well emphasised. Propane baseline concentrations begin to decrease prior to that of CO due to propane's much shorter atmospheric lifetime, which varies between 1–4 months: 1 month in the tropics to 4 months in mid-latitude spring/autumn (Seinfeld and Pandis, 1998). This is also highlighted by the amplitude of the seasonal cycles, which is much larger for propane than CO.

5.8.1.3. Ethane and propane ratios

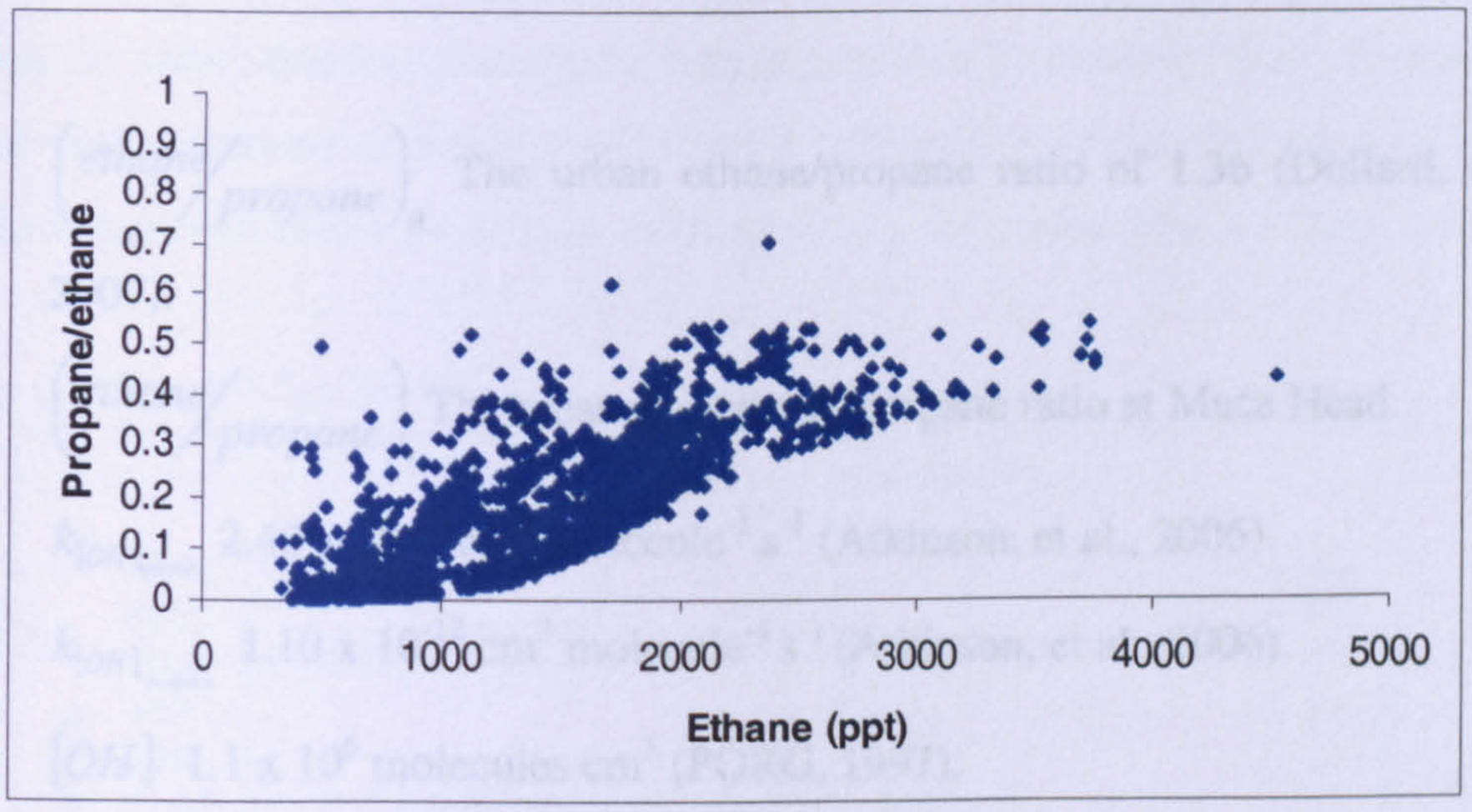

Figure 5.13 Propane/ethane ratio vs. ethane. Measurements made from January to December 2005.

Figure 5.133 plots the propane/ethane ratio compared with ethane measured during 2005. This graph represents the preferential removal of propane compared with ethane by reaction with the hydroxyl radical, indicated by the decrease in the propane/ethane ratio at low ethane concentrations which correspond to very clean/aged air samples. High ethane concentrations correspond to European pollution events; here the propane/ethane ratio is 0.4-0.5. This corresponds well with reported urban background propane/ethane ratios of 0.7, the urban industrial ratio of 0.8 and rural UK ratio of 0.6 (Dollard, et al., 2007).

Due to the long atmospheric lifetimes of ethane and propane, the ratio of ethane/propane remains distinct from background for several days. The ethane/propane ratio can be used to estimate the air mass age or transport time, τ_{OH} using equation 5.2.

5.2. $$\tau_{OH} = \frac{\ln\left(ethane/propane\right)_0 - \ln\left(ethane/propane\right)_t}{\left(k_{[OH]_{ethane}} - k_{[OH]_{propane}}\right)[OH]}$$

- $\left(ethane/propane\right)_0$ The urban ethane/propane ratio of 1.36 (Dollard, et al., 2007).
- $\left(ethane/propane\right)_t$ The measured ethane/propane ratio at Mace Head.
- $k_{[OH]_{ethane}}$ 2.40 x 10^{-13} cm^3 $molecule^{-1}$ s^{-1} (Atkinson, et al., 2006).
- $k_{[OH]_{propane}}$ 1.10 x 10^{-12} cm^3 $molecule^{-1}$ s^{-1} (Atkinson, et al., 2006).
- $[OH]$ 1.1 x 10^6 molecules cm^3 (PORG, 1997).

Figure 5.144 shows how the relationship between ethane and propane can be used to estimate transport time. High ethane/propane ratios correspond to photochemically aged air where propane has been preferential removed over ethane by reaction with the hydroxyl radical.

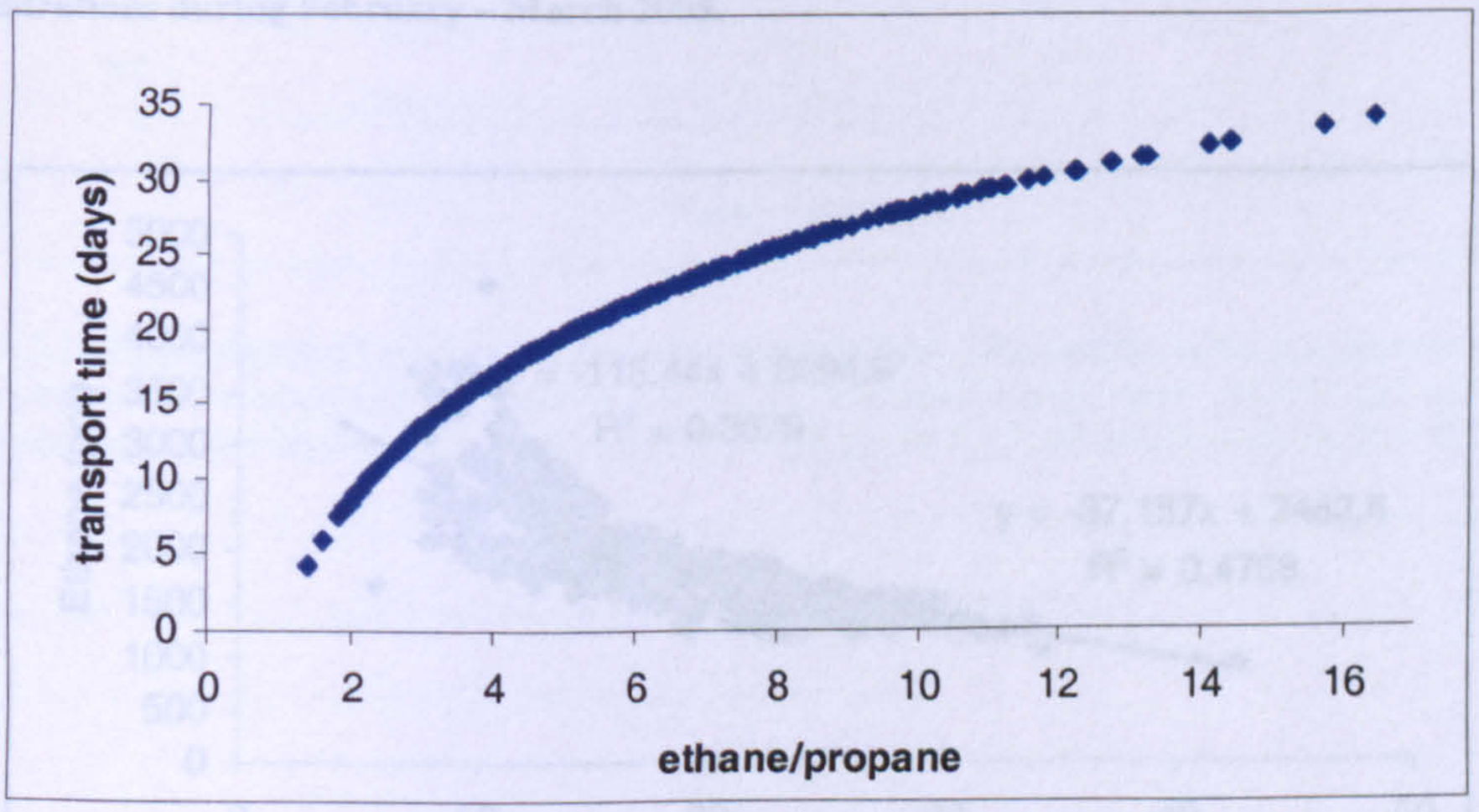

Figure 5.14 Estimated photochemical transport time based on the ethane/propane ratio January - May 2005.

Plotting the estimated transport time against absolute ethane concentrations shows an anti-correlation between ethane and transport times. During pollution events, when ethane concentrations are high the transport time is low indicating fresh emissions into an air mass. Southerly transport events can also be seen by sharp decreases in ethane concentrations coinciding with sharp increases in transport time to 25 days. Baseline concentrations of ethane correspond to approximately 15 days transport time.

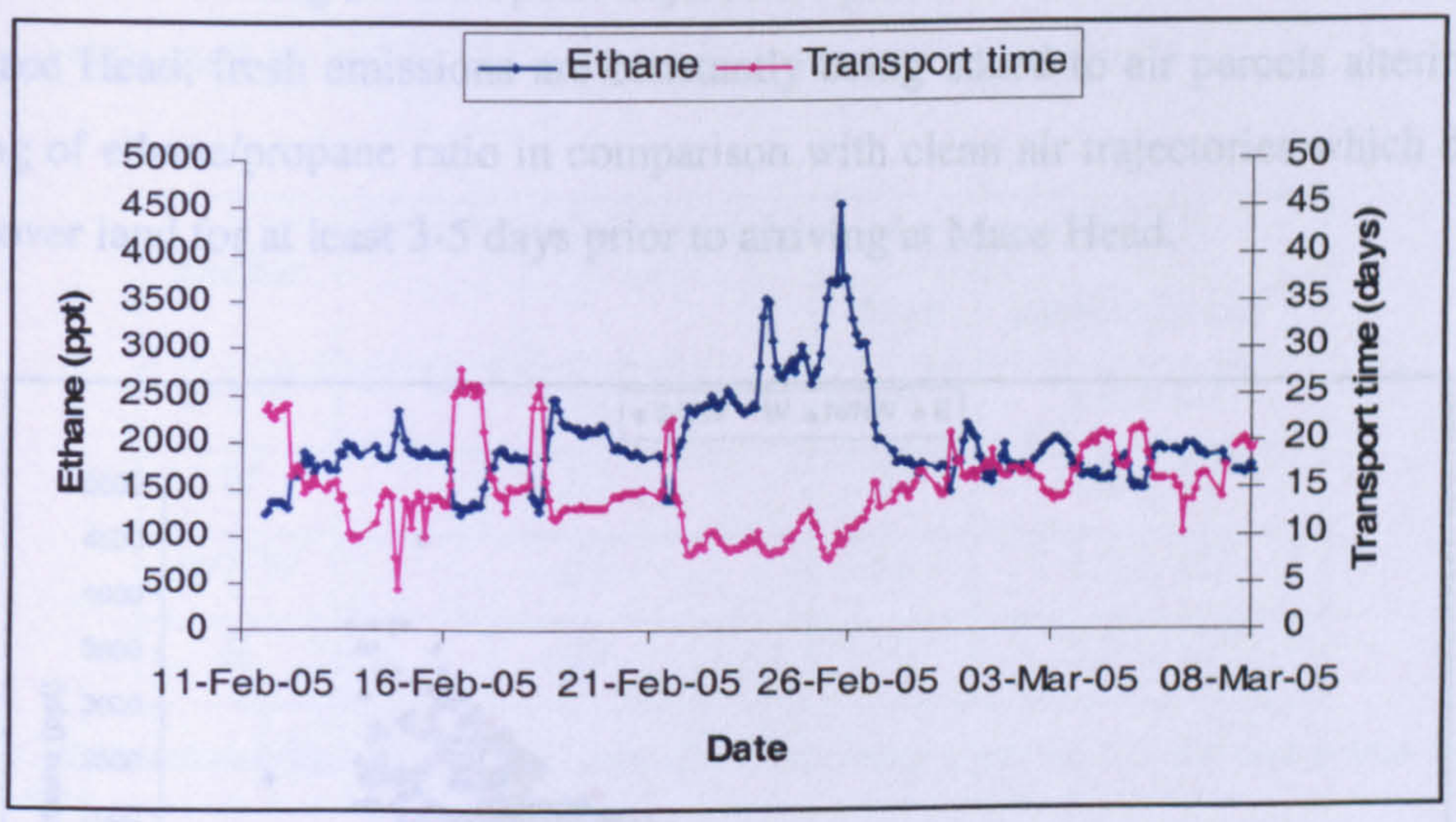

Figure 5.15 Estimated transport time based on the ethane/propane ratio compared with ethane concentrations during February – March 2005.

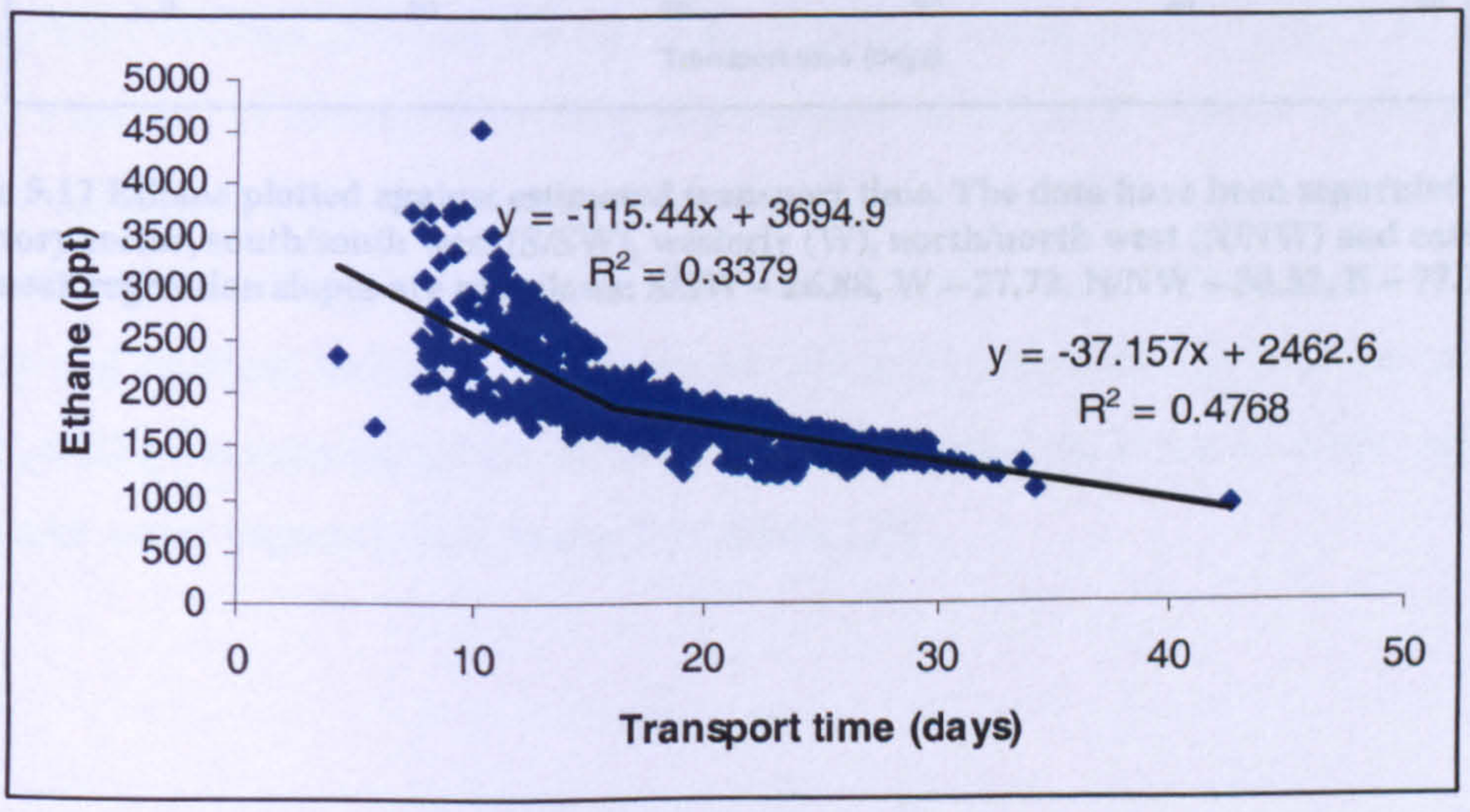

Figure 5.16 Ethane plotted against the calculated estimated transport time January – May 2005. Graph appears like a 'broken stick'

Figure 5.166 appears as a broken stick, rather than the predicted linear relationship between decreasing concentrations of ethane and increasing transport time. To investigate why the graph appears as a broken stick, 5-day back trajectories from Nilu, 2007 were viewed and a trend emerged, the high values of ethane correspond to emissions from European trajectories. When the same data set is re-plot by trajectory sector, Figure 5.177 is produced, showing the clear distinction between clean air trajectories (S/SW, W, N/NW) and European trajectories (E). This difference can be explained considering the European trajectories pass over a lot of land before arriving at Mace Head; fresh emissions are constantly being added to air parcels altering the ageing of ethane/propane ratio in comparison with clean air trajectories which do not pass over land for at least 3-5 days prior to arriving at Mace Head.

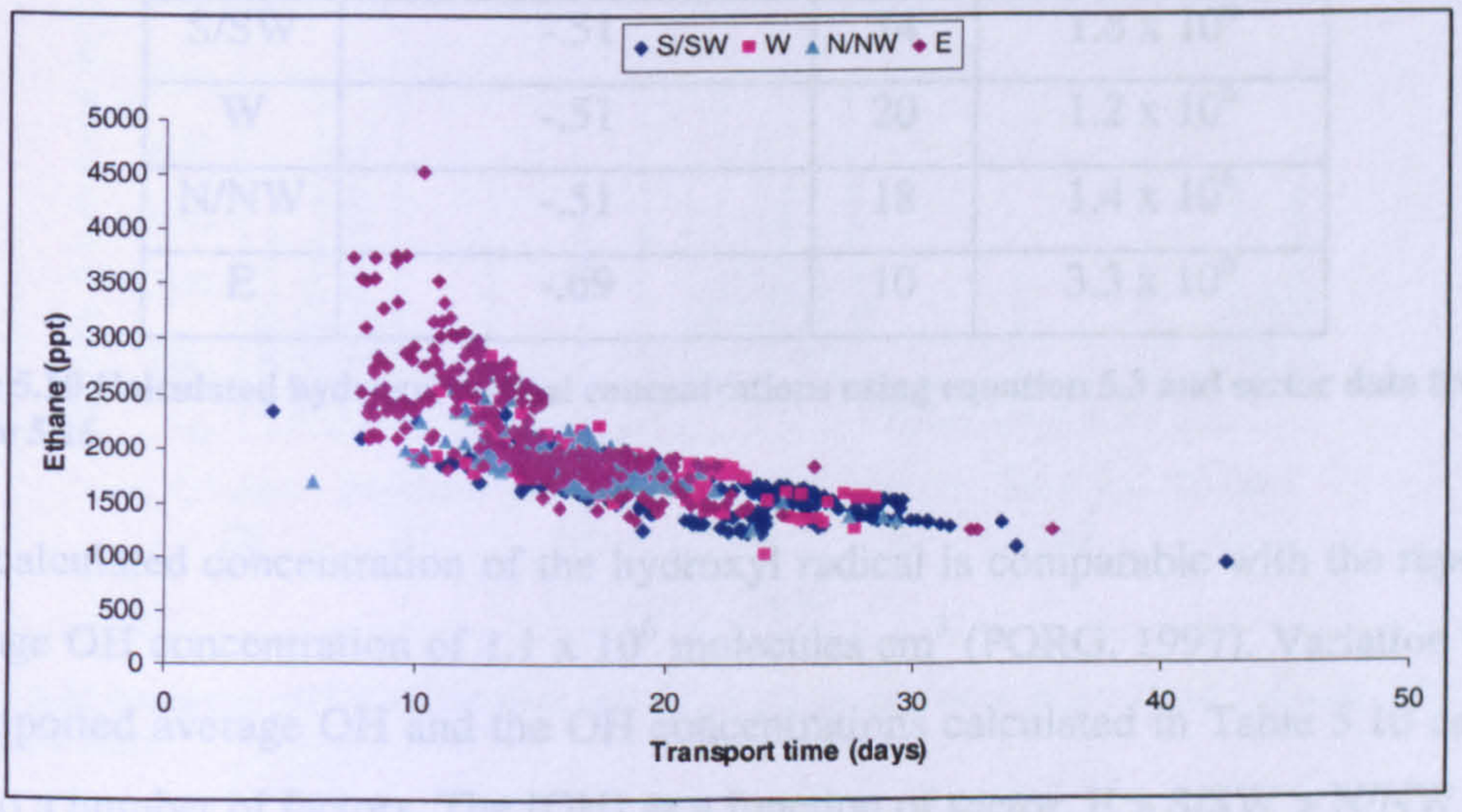

Figure 5.17 Ethane plotted against estimated transport time. The data have been separated by trajectory sector, south/south west (S/SW), westerly (W), north/north west (N/NW) and easterly (E). linear regression slopes are as follows: S/SW – 26.88, W – 27.72, N/NW – 30.52, E – 77.74.

The concentration of the hydroxyl radical [OH] can be calculated from data obtained from the ethane vs. transport time plot in Figure 5.17 using equation 5.3:

5.3 $$[OH] = \ln\{\frac{[ethane]_t}{[ethane]_0}\} \Big/ -k_{ethane(OH)} \times t$$

$k_{ethane(OH)}$ 2.4 x 10^{-13} cm^3 $molecule^{-1}$ s^{-1} (Atkinson, et al., 2006).

t is the difference in transport time in days between $[ethane]_0$ and $[ethane]_t$ multiplied by 86400 (24 x 60 x 60) to convert into seconds

Sector	ln $[ethane]_t/[ethane]_0$	t days	[OH] molecule cm^{-3}
S/SW	-.51	14	1.8 x 10^6
W	-.51	20	1.2 x 10^6
N/NW	-.51	18	1.4 x 10^6
E	-.69	10	3.3 x 10^6

Table 5.10 Calculated hydroxyl radical concentrations using equation 5.3 and sector data from Figure 5.16.

The calculated concentration of the hydroxyl radical is comparable with the reported average OH concentration of 1.1 x 10^6 molecules cm^3 (PORG, 1997). Variation from the reported average OH and the OH concentrations calculated in Table 5.10 can be due to a number of factors. The [OH] as a function of sector, E > S/SW > N/NW > W is reasonable. Air from the easterly sector is likely to be polluted and contain higher levels of ozone and hence higher OH. For the southerly sector, higher levels of water vapour and incident radiation will increase OH levels even though it is the cleanest sector, whilst the remaining two sectors have lower pollution, lower incident radiation and lower water vapour levels, hence the lowest OH.

5.8.2. i-Butane and n-butane measurements

The isomers of butane principally arise from extraction and distribution of fossil fuels, in particular the evaporation of motor spirit (Dollard, et al., 2007). i-Butane and n-butane account for the twelfth and the single largest contribution to photochemical ozone production respectively according to Derwent, et al. (2003).

5.8.2.1. Composite cycle of i-butane and n-butane

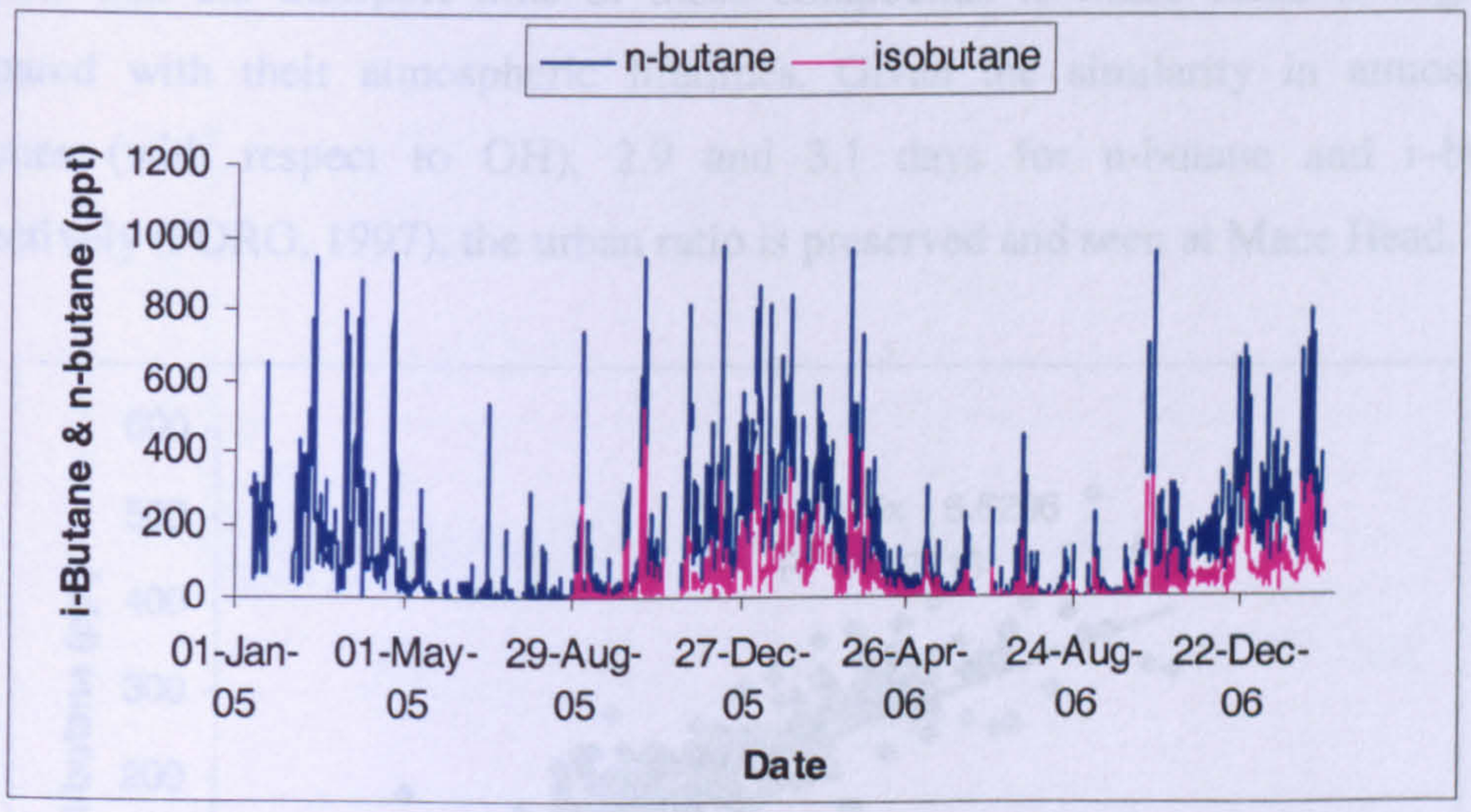

Figure 5.18 Seasonal cycles of i-butane and n-butane measured at Mace Head January 2005 – February 2007.

Unfortunately, reliable and accurate measurements of i-butane are only reported from September 2005. i-Butane and n-butane show a high degree of correlation, with pollution events clearly visible. A ratio of 2:1 n-butane to i-butane appears to be consistent throughout these data.

5.8.2.2. i-Butane and n-butane ratios

The ratio of i-butane to n-butane can be used to observe the effects of transport. The reported urban ratio of i-butane/n-butane is well characterised over a number of data sets and although the isomers have disparate sources they show a high degree of consistency. The mean urban i-butane/n-butane ratio is 0.45 (Derwent, 2000). Figure 5.199 shows the i-butane/n-butane ratio measured at Mace Head over 2005 and 2006. The Mace Head i-butane/n-butane ratio of 0.41 is in close agreement with the reported urban value of 0.45. The close agreement between Mace Head and urban data suggests that the transport time of these compounds to Mace Head is negligible compared with their atmospheric lifetimes. Given the similarity in atmospheric lifetimes (with respect to OH), 2.9 and 3.1 days for n-butane and i–butane, respectively (PORG, 1997), the urban ratio is preserved and seen at Mace Head.

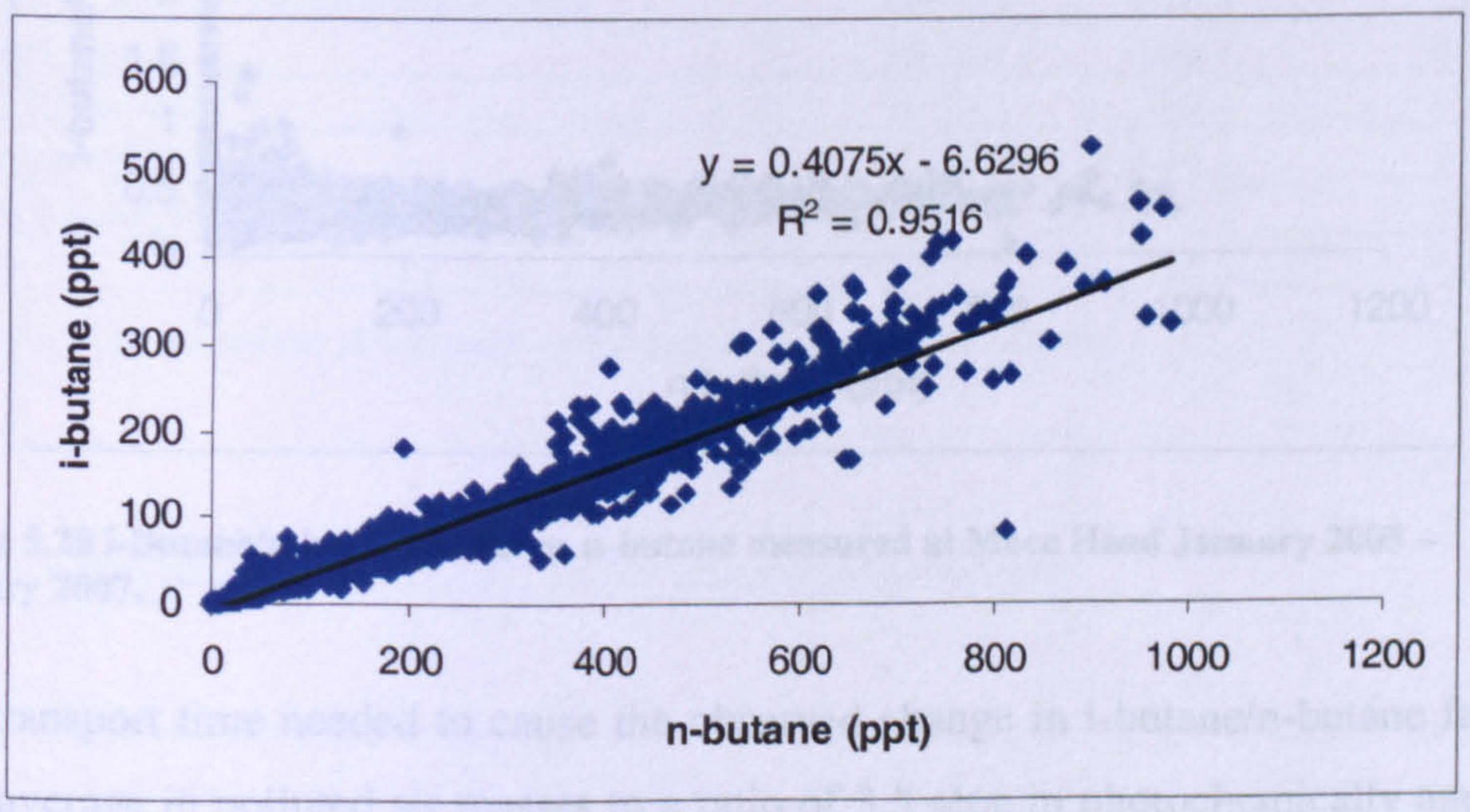

Figure 5.19 i-Butane/n-butane ratio measured at Mace Head January 2005 – January 2007.

To view the effects of photochemical ageing on the butane isomers, i-butane/n-butane must be plotted against n-butane concentrations as seen in Figure 5.2020. At greater than 150 ppt of n-butane the i-butane/n-butane ratio is consistent with urban data sets. As the concentrations fall below these values a general increase in the ratio with lowering n-butane is observed. Lower concentrations correlate with more photochemically aged air, the increase in ratio at low n-butane concentrations is mainly due to the preferential removal of n-butane compared with i-butane with respect to the OH radical (Seinfeld and Pandis, 1998).

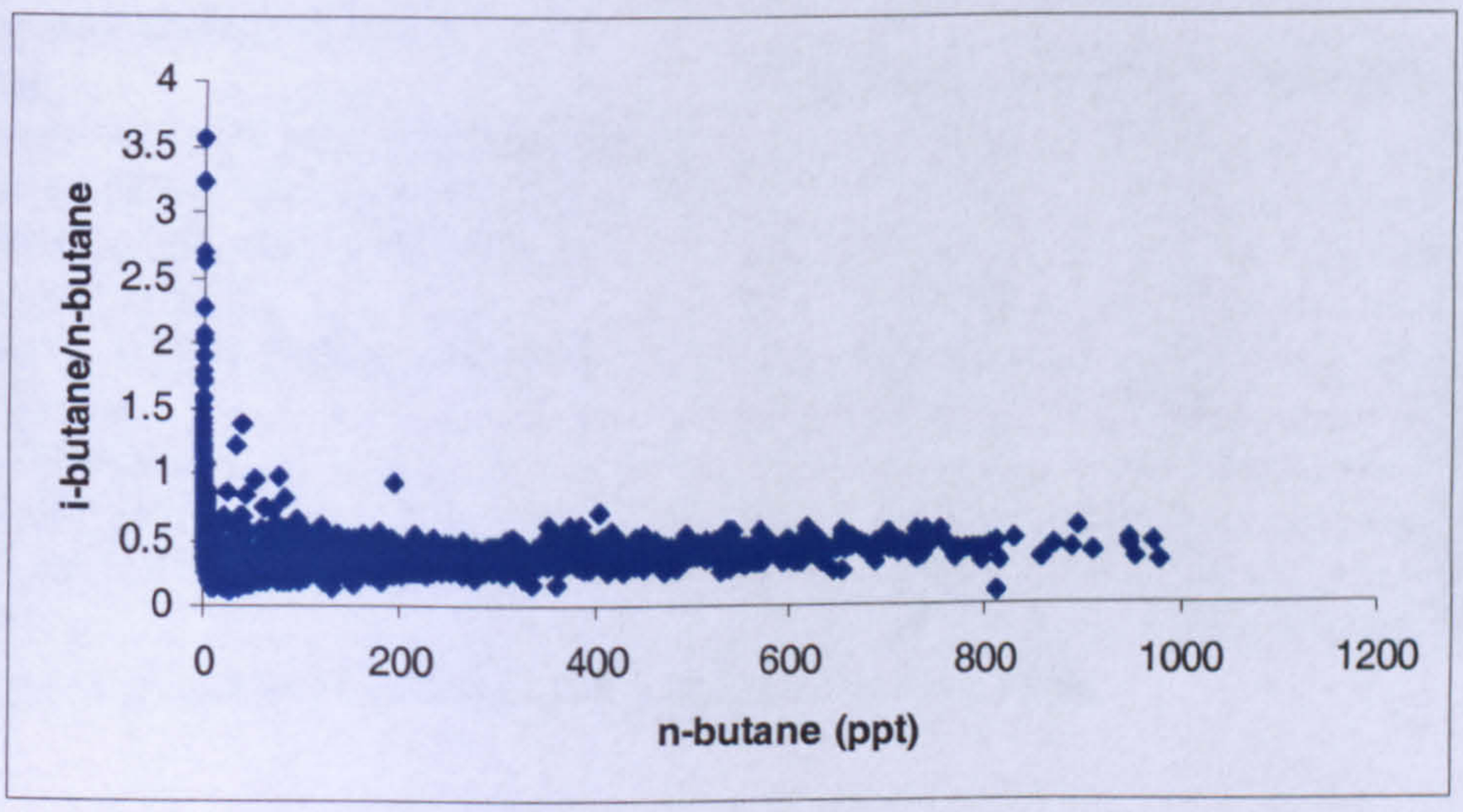

Figure 5.20 i-Butane/n-butane ratio vs. n-butane measured at Mace Head January 2005 – January 2007.

The transport time needed to cause the observed change in i-butane/n-butane from a 0.41 average in polluted air masses to a ratio of 3.5 seen in photochemically aged air (Figure 5.2020), given an average OH concentration of 1.1 x 10^6 molecules cm^3 (PORG, 1997) and butane isomer rate constants from Atkinson (2003), can be calculated using equation 5.4. Solving equation 5.4 results in a transport time of 94 days. Given the average lifetimes of n-butane and i-butane with respect to the OH radical are 2.9 and 3.1 days, respectively, the change in ratio can not be explained by OH chemistry alone. In polluted air masses automotive sources are the dominant butane isomer sources, in clean air different sources are being sampled, such as extraction and distribution of fossil fuels and solvent use (see Table 5.11) and possibly oceanic emissions (Broadgate, et al., 1997).

5.4 $$\tau_{OH} = \frac{ln\left(i-butane/n-butane\right)_0 - ln\left(i-butane/n-butane\right)_t}{\left(k_{[OH]_{i-butane}} - k_{[OH]_{n-butane}}\right)[OH]}$$

$\left(i-butane/n-butane\right)_0$ urban ratio, 0.41

$\left(i-butane/n-butane\right)_t$ photochemically aged ratio, 3.5

$k_{[OH]_{i-butane}}$ 2.12 x10-12 cm^3 $molecule^{-1}$ s^{-1} (Atkinson, 2003).

$k_{[OH]_{n-butane}}$ 2.36 x 10-12 cm^3 $molecule^{-1}$ s^{-1} (Atkinson, 2003).

$[OH]$ 1.1 x 10^6 molecules cm^3 (PORG, 1997).

Mass emissions (Ktonnes)			
Source	**n-butane**	**i-butane**	**iso/n-butane**
stationary combustion (energy production)	0.25	0.01	0.04
stationary combustion (commercial & resid'n)	1.36	0.41	0.30
stationary combustion (industrial)	0.38	0.01	0.03
production process	4.69	0.23	0.05
extraction and distribution fossil fuels	69.49	12.6	0.18
Solvent use	19.14	0.92	0.05
Road transport	10.71	4.9	0.46
other transport	0.47	0.21	0.45
waste treatment	0.02	0.01	0.50
Total	**107**	**19**	**0.18**

Table 5.11 UK emissions of i-butane and n-butane (Dore, et al., 2006).

5.8.3. i-Pentane and n-pentane measurements

The pentane isomers are important constituents in evaporating motor spirit (Dollard, et al., 2007). i-Pentane and n-pentane account for the seventh and fifth largest contributions to photochemical ozone formation. (Derwent, et al., 2003).

5.8.3.1. Composite cycle of i-pentane and n-pentane

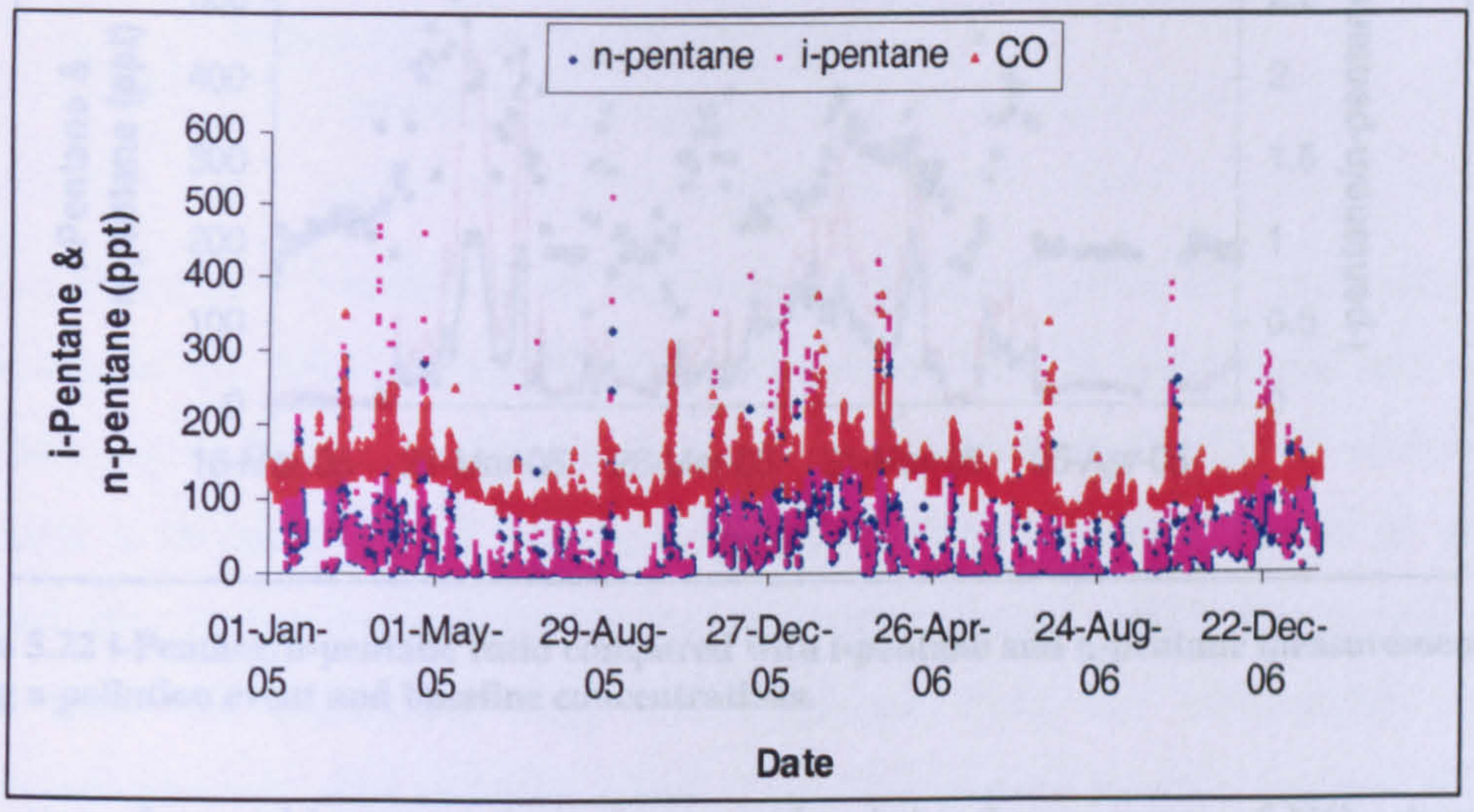

Figure 5.21 i-Pentane and n-pentane measured at Mace Head January 2005 – January 2007.

Figure 5.211 plots the seasonal cycles for i-pentane and n-pentane observed at Mace Head. Pollution episodes are clearly evident and are well correlated with CO measurements. Figure 5.222 looks at the i-pentane and n-pentane relationship in more detail. The i-pentane/n-pentane ratio in baseline air masses is 1:1, increasing to 2:1 during pollution events. The reported urban mean ratio of i-pentane/n-pentane is 2:1 Hopkins, et al., 2002. This urban ratio is preserved and seen at Mace Head due to the similar lifetimes of the pentane isomers of 1.9 and 1.8 days with respect to reaction with the hydroxyl radical (PORG, 1997). Due to the similarity of the lifetimes, the change in ratio from 2:1 to 1:1 can not be due to OH chemistry alone. This change in ratio could be due to NO_3 or Cl chemistry or due to a difference in sources.

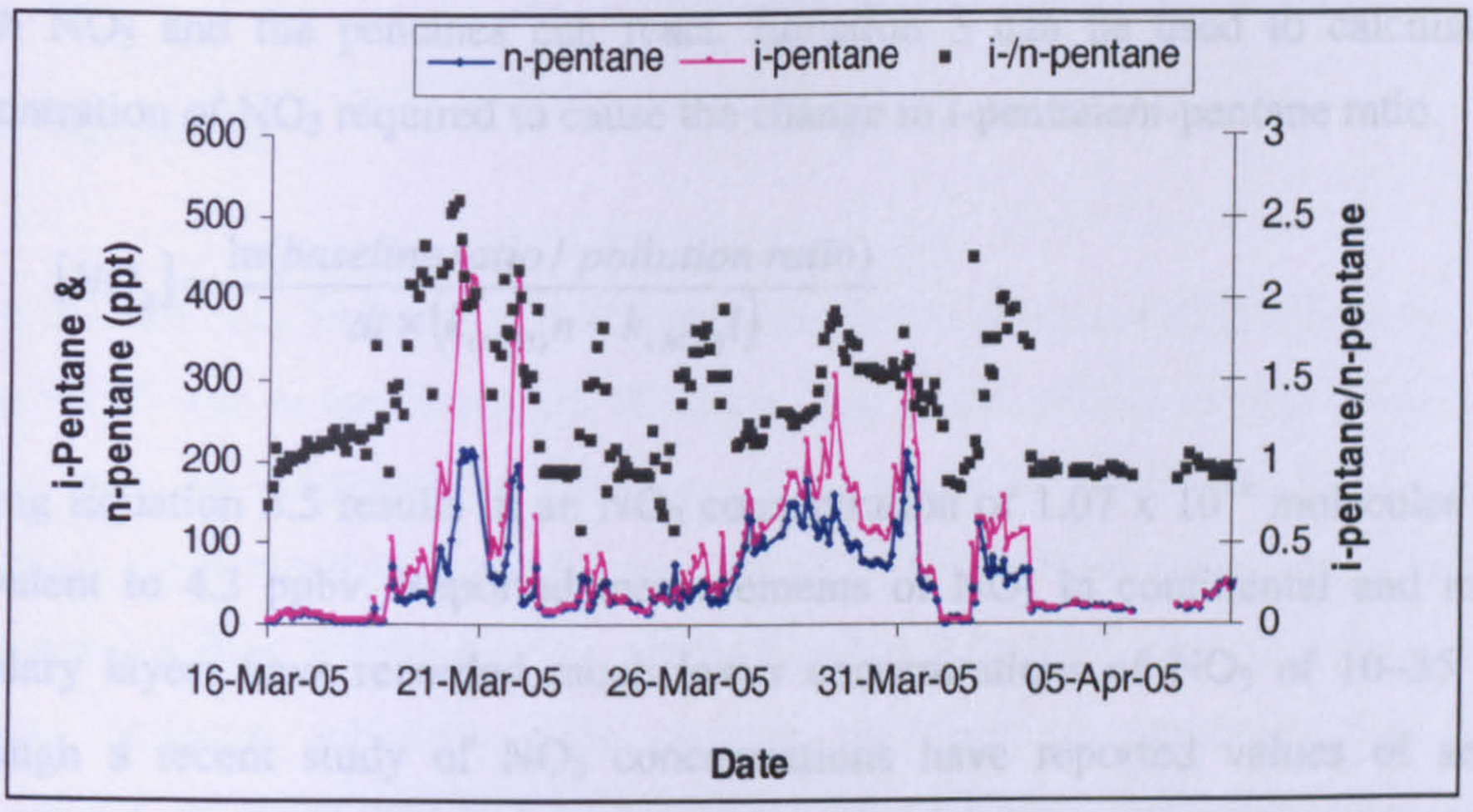

Figure 5.22 i-Pentane/n-pentane ratio compared with i-pentane and n-pentane measurements during a pollution event and baseline concentrations.

The ratios of n- and i-pentane have been used to infer the presence of NO_3 chemistry (Lewis, et al., 1997, Penkett, et al., 2007) due to the large difference in reactivity between n-pentane and i-pentane with NO_3 as shown in Table 5.12.

	k(OH)	k(Cl)	$k(NO_3)$
n-Pentane	3.80×10^{-12} [a]	2.80×10^{-10} [b]	8.1×10^{-17} [d]
i-Pentane	3.60×10^{-12} [a]	2.20×10^{-10} [b]	1.56×10^{-16} [c]

Table 5.12 Rate coefficients (cm^3 $molecule^{-1}$ s^{-1}) for OH, Cl and NO_3 reaction with n- and i-pentane at 298K. [a] Atkinson, 2003 [b] Atkinson, 1997 [c] Atkinson, 1991 [d] Atkinson, 1991.

Given the similarity in rate constants for i-pentane and n-pentane with OH and Cl, the change in i-pentane/n-pentane ratio between pollution events and baseline air cannot be explained by OH or Cl chemistry. NO_3, however, shows a large difference in reactivity between i-pentane and n-pentane. NO_3 reacts faster with i-pentane than n-pentane and would result in the i-pentane/n-pentane ratio decreasing in aged air masses, a trend which could be used to explain the differences in the i-pentane/n-pentane ratio falling from 2:1 in polluted air masses to 1:1 in baseline air samples.

NO_3 is only present in significant quantities during night time as it is rapidly photolysed by sunlight to form NO or NO_2. Given a transport time of 3 days from UK to Mace Head, a night time of 8 hours a day will result in 24 hours (86400 seconds) in

which NO_3 and the pentanes can react. Equation 5 can be used to calculate the concentration of NO_3 required to cause the change in i-pentane/n-pentane ratio.

$$5.5. \quad [NO_3] = \frac{\ln(baseline\,ratio\,/\,pollution\,ratio)}{dt \times \left(k_{(NO3)}n - k_{(NO3)}i\right)}$$

Solving Equation 5.5 results in an NO_3 concentration of 1.07 x 10^{11} molecules cm^{-3}, equivalent to 4.3 ppbv. Reported measurements of NO_3 in continental and marine boundary layers have recorded much lower concentrations of NO_3 of 10–35 pptv. Although a recent study of NO_3 concentrations have reported values of several hundred pptv in the upper boundary layer (Penkett, et al., 2007) this is still much lower than the calculated NO_3 concentrations from the differences in the i-pentane/n-pentane ratio at Mace Head. Thus, the change in ratio can not be fully explained by NO_3 chemistry alone. It is likely that the change in ratio can be explained by a change in emissions.

The urban air ratio is dominated by road transport which gives a ratio of 2:1; however, other sources such as solvent use and production processes give much lower ratios, often below 1:1. Dollard, et al. (2007) recently suggested evidence of a significant source of n-pentane and i-pentane with a ratio of 1:1 in urban-industrial sites (Liverpool, Middlesbrough and Southampton) which they presumed to be from refinery sources. It has also been reported that there is a significant marine source of the pentane isomers which results in an i-pentane/n-pentane ratio of 0.6 (Plass-Dulmer, et al., 1995). It is likely that the varying ratio of i-pentane/n-pentane is observed as background air is more strongly influenced by typically non-urban sources of pentane isomers.

Mass emissions (Ktonnes)			
Source	**n-Pentane**	**I-Pentane**	**I-/n-Pentane**
stationary combustion	1.51	1.98	1.31
production process	1.90	1.01	0.53
extraction and distribution fossil fuels	11.75	9.52	0.81
Solvent use	0.44	0.05	0.11
road transport	5.91	12.13	2.05
other transport	0.29	0.74	2.55
waste treatment	0.03	0.02	0.67
Total	21.83	25.45	1.17

Table 5.13 UK emissions of i-pentane and n-pentane Dore, et al., 2006.

5.8.4. Isoprene

Isoprene is the only biogenic NMHC measured by the Medusa-GCMS. Isoprene plays an important role in the formation of ozone. The global annual isoprene flux is of a similar order of magnitude as methane, but isoprene is more than four orders of magnitude more reactive than methane (Hewitt, 1999). Plant emissions of isoprene are in general from woody species, although some ferns and vines are also isoprene emitters. Isoprene emission rates depend on light, temperature, the growth environment of plants and leaf development. The function and role of isoprene in plants is poorly understood. Isoprene has also been measured in seawater, with concentrations often supersaturated relative to the atmosphere, suggesting an oceanic source of isoprene. Other biogenic sources of isoprene include: exhaled breath in humans and some animals, bacteria present in soils and some fungi and a variety of ground cover have all been reported as isoprene sources (Hewitt, 1999).

Anthropogenic sources of isoprene include industrial processes and motor vehicular sources. Dollard et al. (2007) measured isoprene at urban UK sites and from 1993 to 2004 and reported that the motor vehicle source of isoprene has reduced dramatically over the study period, particularly during wintertime, whilst summertime emissions have remained similar. The reported urban isoprene/benzene ratio is 0.128 ± 0.030

5.8.4.1. Composite cycle of isoprene

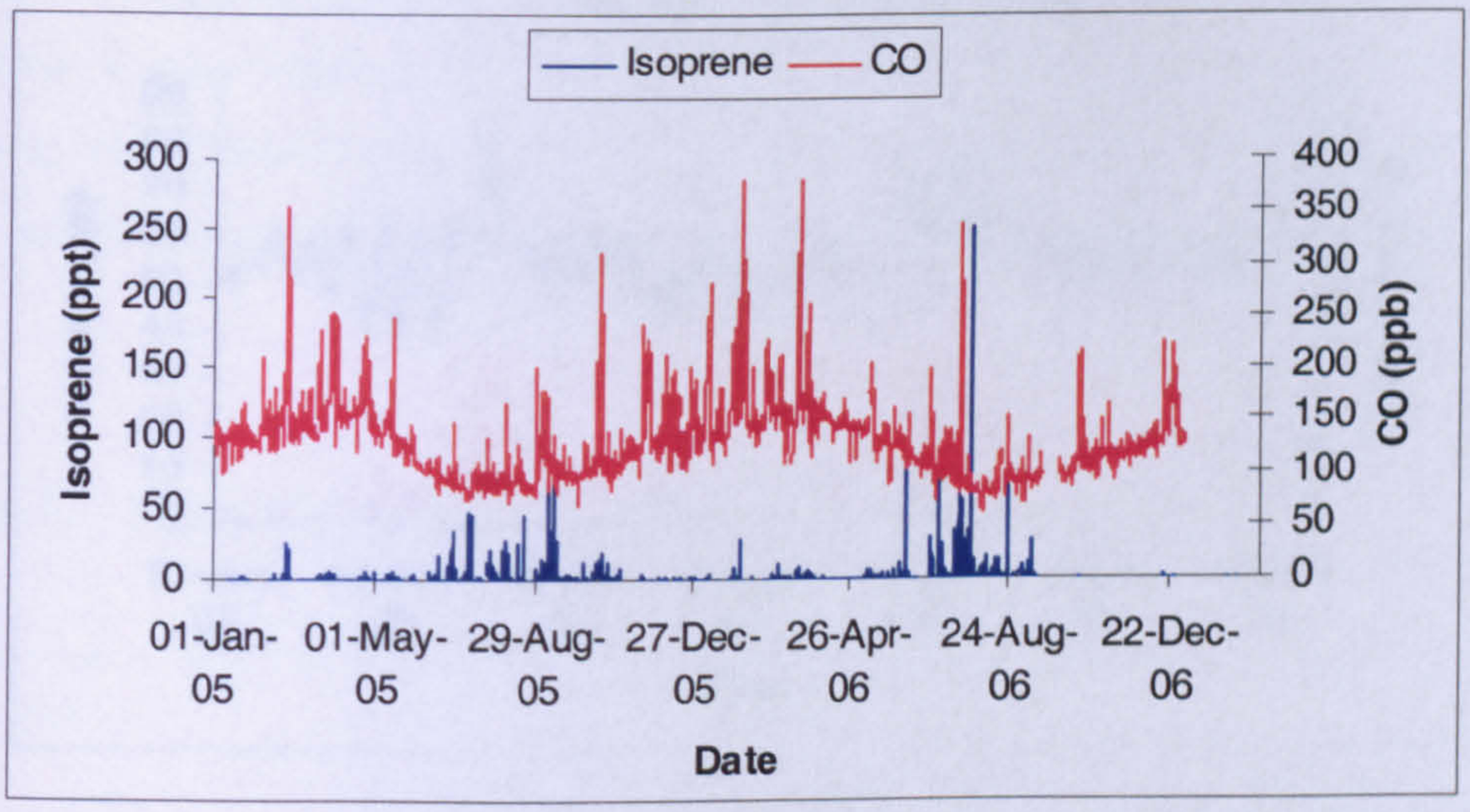

Figure 5.23 Seasonal cycle of isoprene and CO measured at Mace Head January 2005 – March 2007.

Figure 5.233 plots the seasonal cycle of isoprene measured at Mace Head compared with CO. Isoprene reaches a maximum during summer months when CO is at a minima; this suggests that the isoprene is derived from biogenic emissions. Larger biogenic isoprene events were recorded during summer 2006 than 2005. During wintertime isoprene is mainly below the limit of detection. Although some wintertime isoprene events do occur during which they are correlated with peaks in CO concentrations. Given the short atmospheric lifetime of isoprene of 0.2 days (Hewitt, 1999) any isoprene measured at Mace Head must be from local sources.

5.8.4.2. Isoprene production

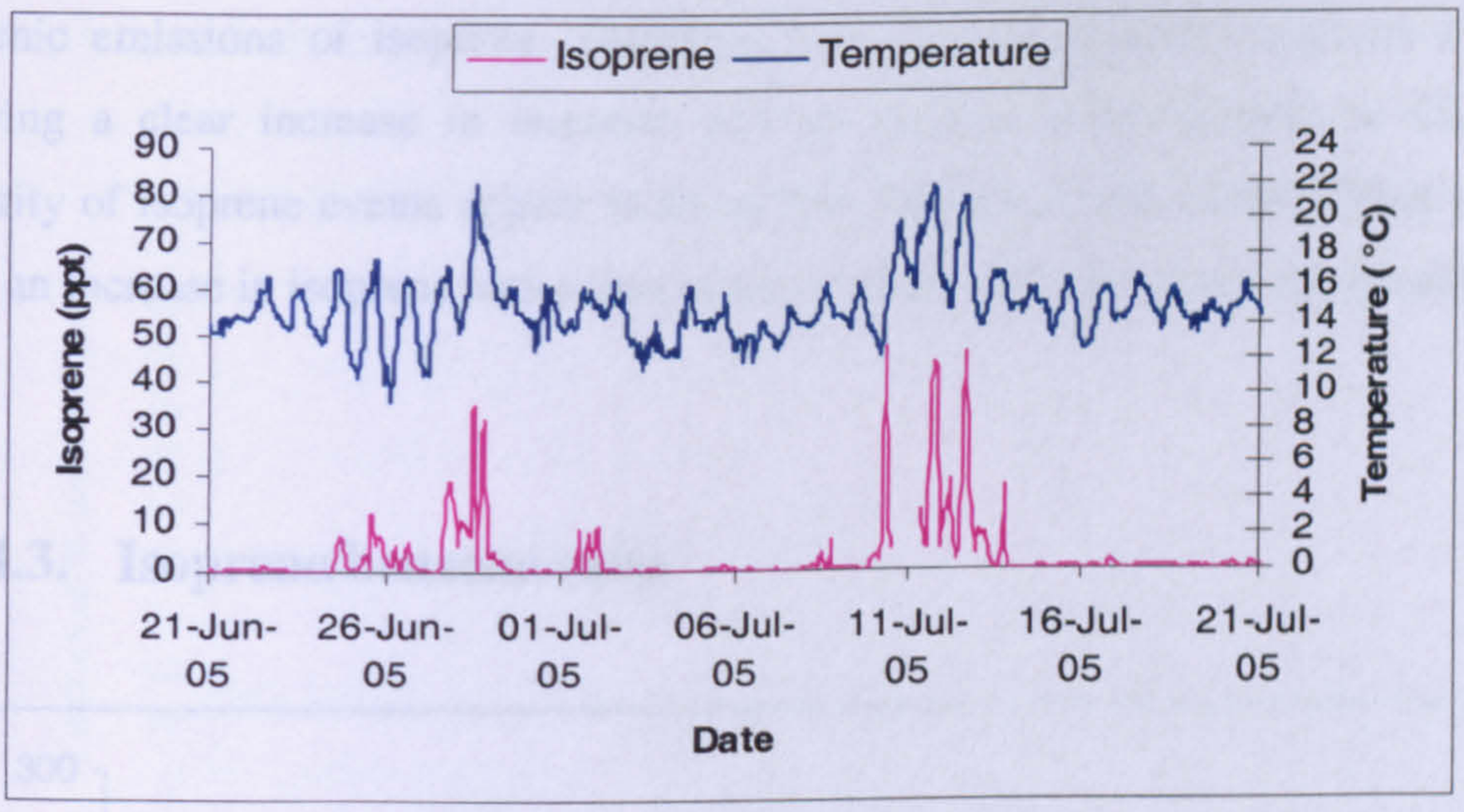

Figure 5.24 Isoprene concentrations compared with temperature recorded at Mace Head during summer 2005.

Figure 5.244 shows one month of summertime isoprene and temperature data. Isoprene emissions and temperature are well correlated with isoprene production occurring on relatively warm days. However, isoprene production is not dependent upon temperature alone, since there are days when temperature is high enough for isoprene production but no isoprene emissions are observed. Other factors, such as wind direction and speed will determine if isoprene is measured at Mace Head.

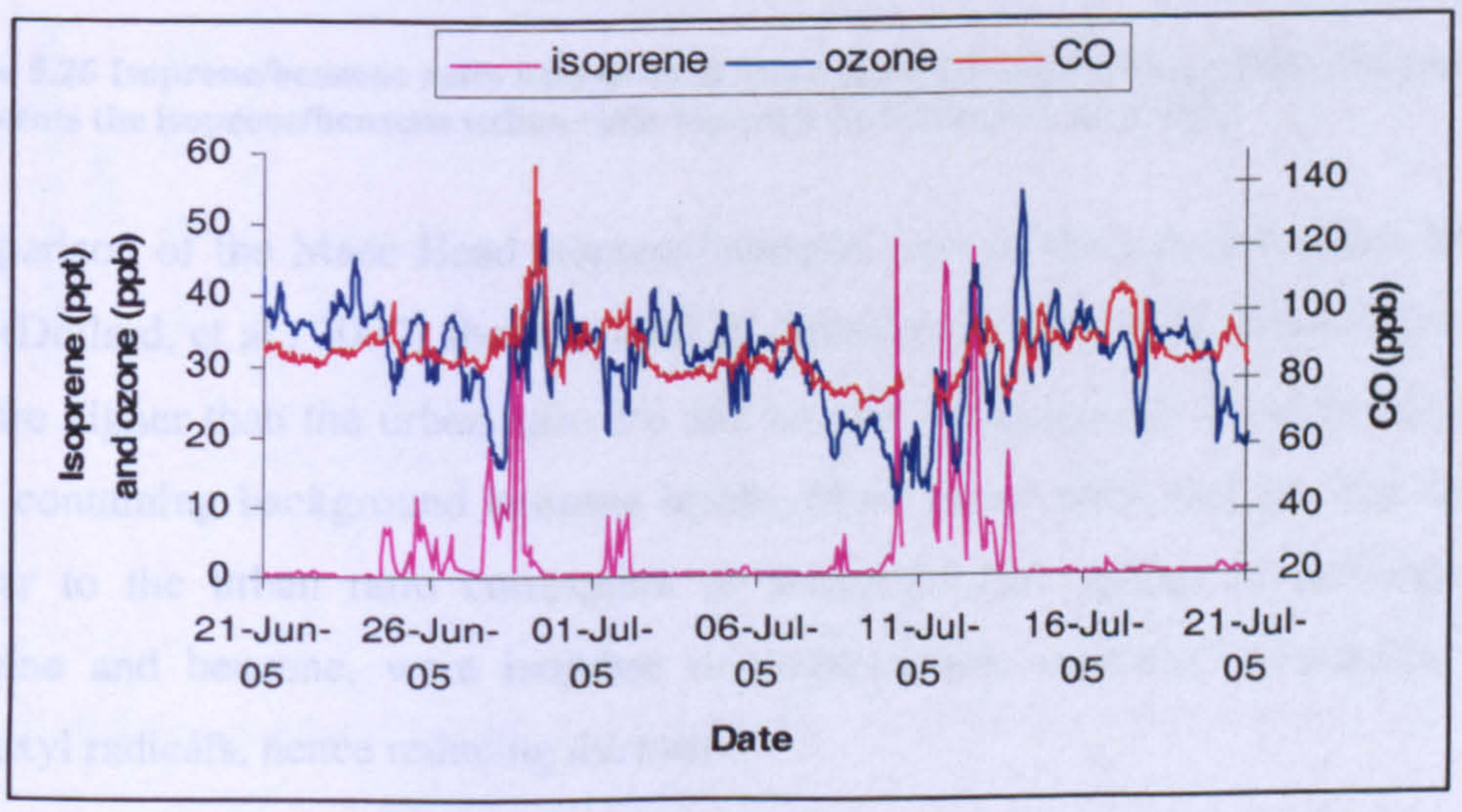

Figure 5.25 Isoprene concentrations compared with ozone and CO measured at Mace Head during summer 2005.

Figure 5.255 plots isoprene compared with CO and ozone measurements at Mace Head. As an anthropogenic marker, CO is useful to compare to isoprene to assess the biogenic emissions of isoprene. There are a number of biogenic isoprene events, showing a clear increase in isoprene and no corresponding increase in CO. the majority of isoprene events appear to be an anti-correlated with ozone. Those events were an increase in isoprene and ozone occur coincide with elevated concentrations of CO.

5.8.4.3. Isoprene/benzene ratio

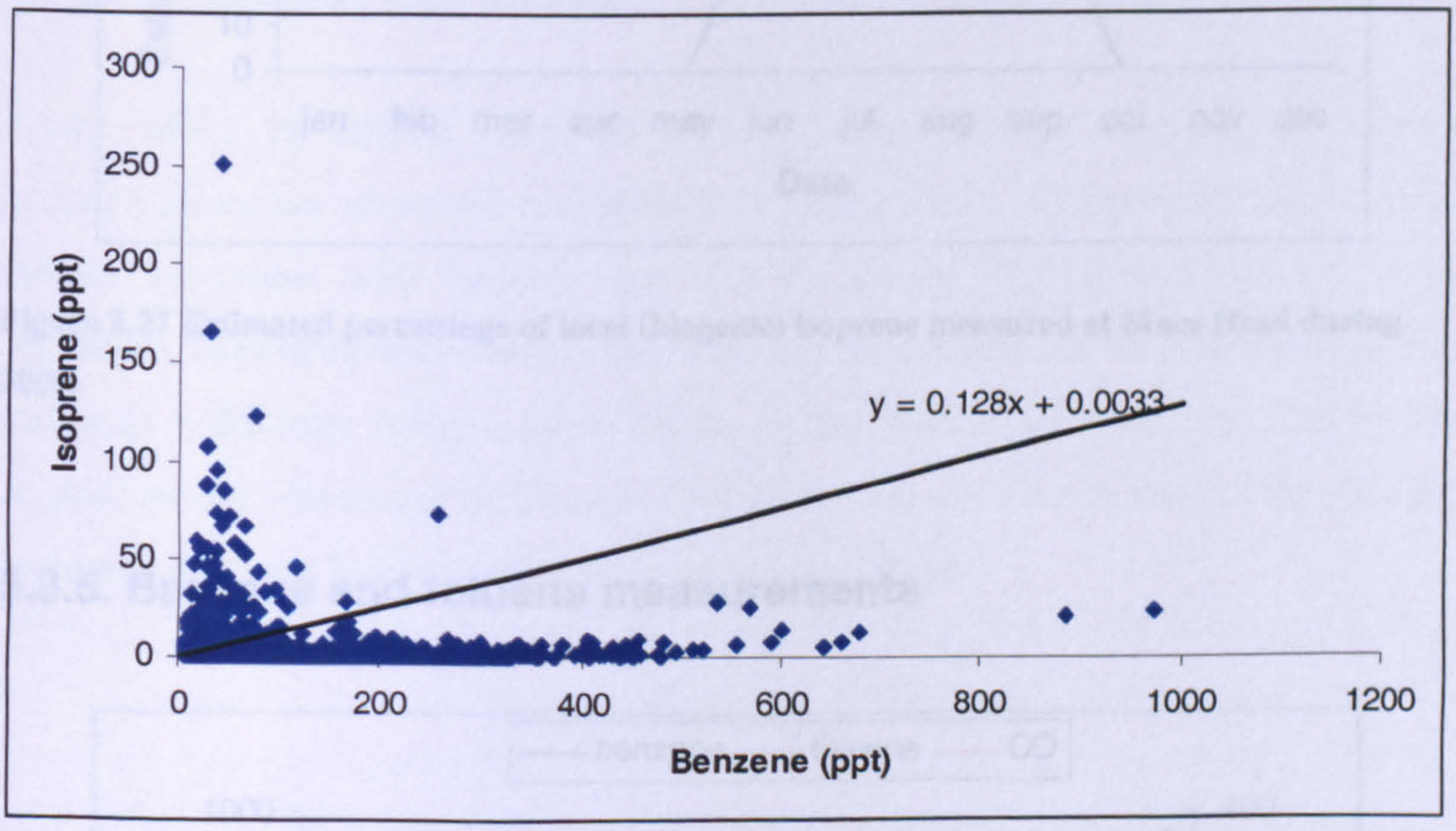

Figure 5.26 Isoprene/benzene ratio measured at Mace Head during 2005 and 2006. The line represents the isoprene/benzene urban ratio reported by Dollard et al., (2007).

Comparison of the Mace Head isoprene/benzene ratio to the reported urban ratio of 0.13 (Dollard, et al., 2007) shows a marked difference as expected. Mace Head ratios that are higher than the urban ratio are due to local emissions of isoprene into an air mass containing background benzene levels. Mace Head ratios that are less than or similar to the urban ratio correspond to photochemical ageing of anthropogenic isoprene and benzene, were isoprene is preferentially removed by reaction with hydroxyl radicals, hence reducing the ratio.

The differences in isoprene/benzene ratio at Mace Head to the reported urban value (Dollard, et al., 2007) can be used to estimate the percentage of local, presumably biogenic isoprene observed at Mace Head as shown in Figure 5.277.

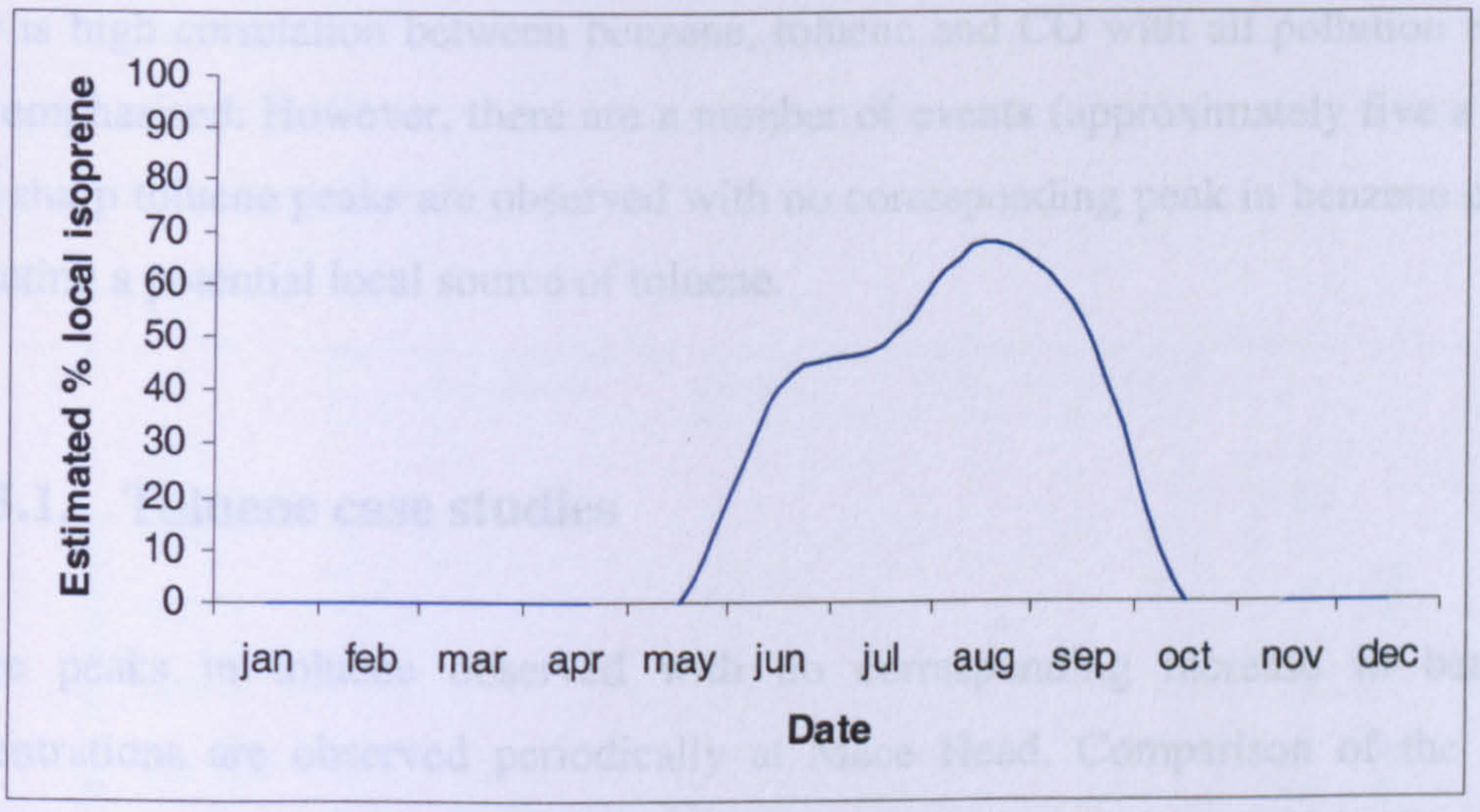

Figure 5.27 Estimated percentage of local (biogenic) isoprene measured at Mace Head during 2005.

5.8.5. Benzene and toluene measurements

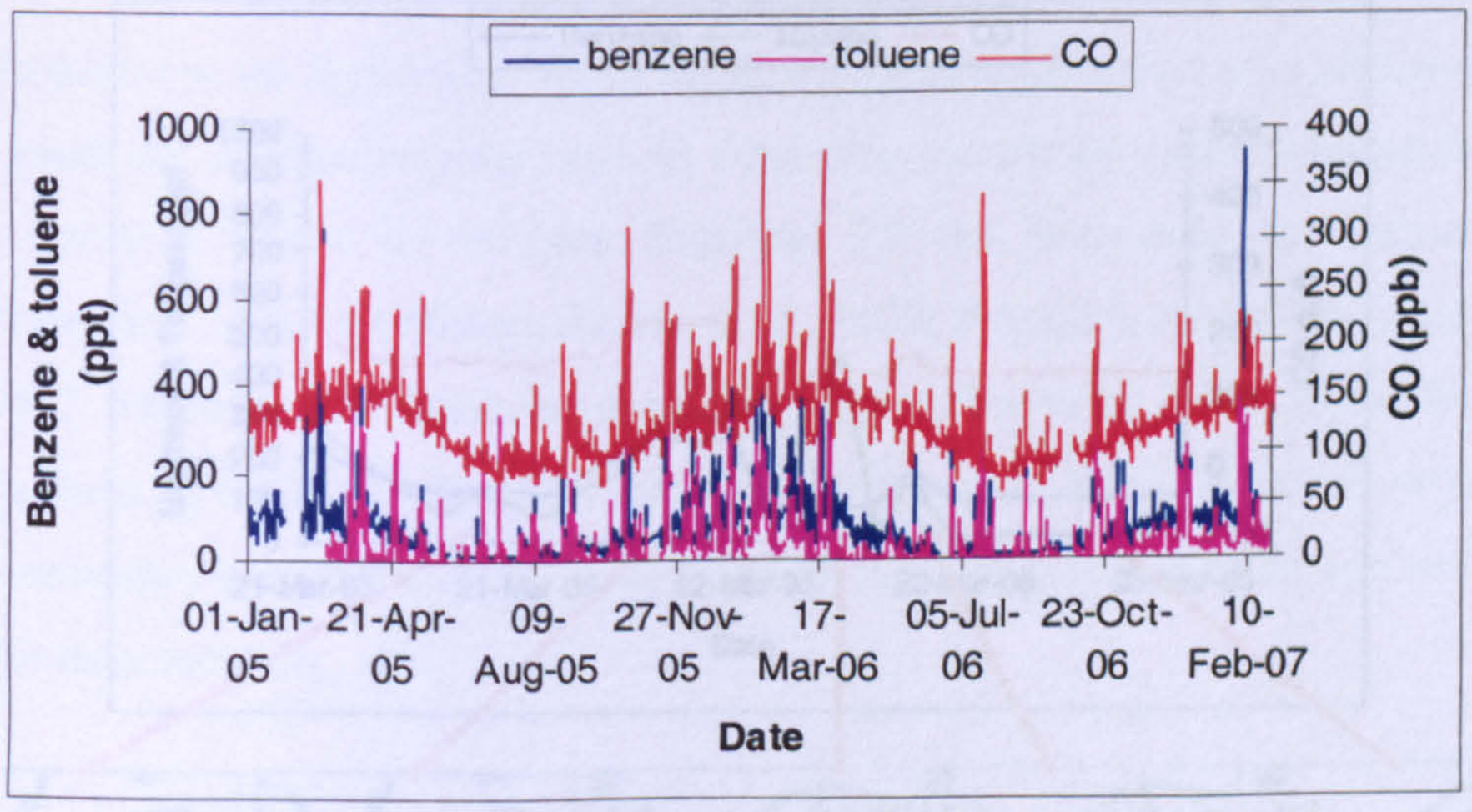

Figure 5.28 Benzene, toluene and CO measured at Mace Head January 2005 – March 2007.

Figure 5.288 shows benzene and toluene data measured at Mace Head since January 2005 compared with CO measurements. The seasonal cycles for the two aromatic compounds can be easily observed in the baseline data, with increasing concentrations during wintertime due to the lack of processing by the hydroxyl radical. In general there is high correlation between benzene, toluene and CO with all pollution events well emphasised. However, there are a number of events (approximately five a year) were sharp toluene peaks are observed with no corresponding peak in benzene or CO indicating a potential local source of toluene.

5.8.5.1. Toluene case studies

Large peaks in toluene observed with no corresponding increase in benzene concentrations are observed periodically at Mace Head. Comparison of the large toluene emissions with benzene and CO are shown in Figure 5.299. Co is an important anthropogenic marker and that fact that there are no increases in CO indicates a different toluene point source. 5 day back trajectories provided by the NAME model (discussed in Chapter 6) indicate the air masses travel over Europe, including southern Ireland before arriving at Mace Head.

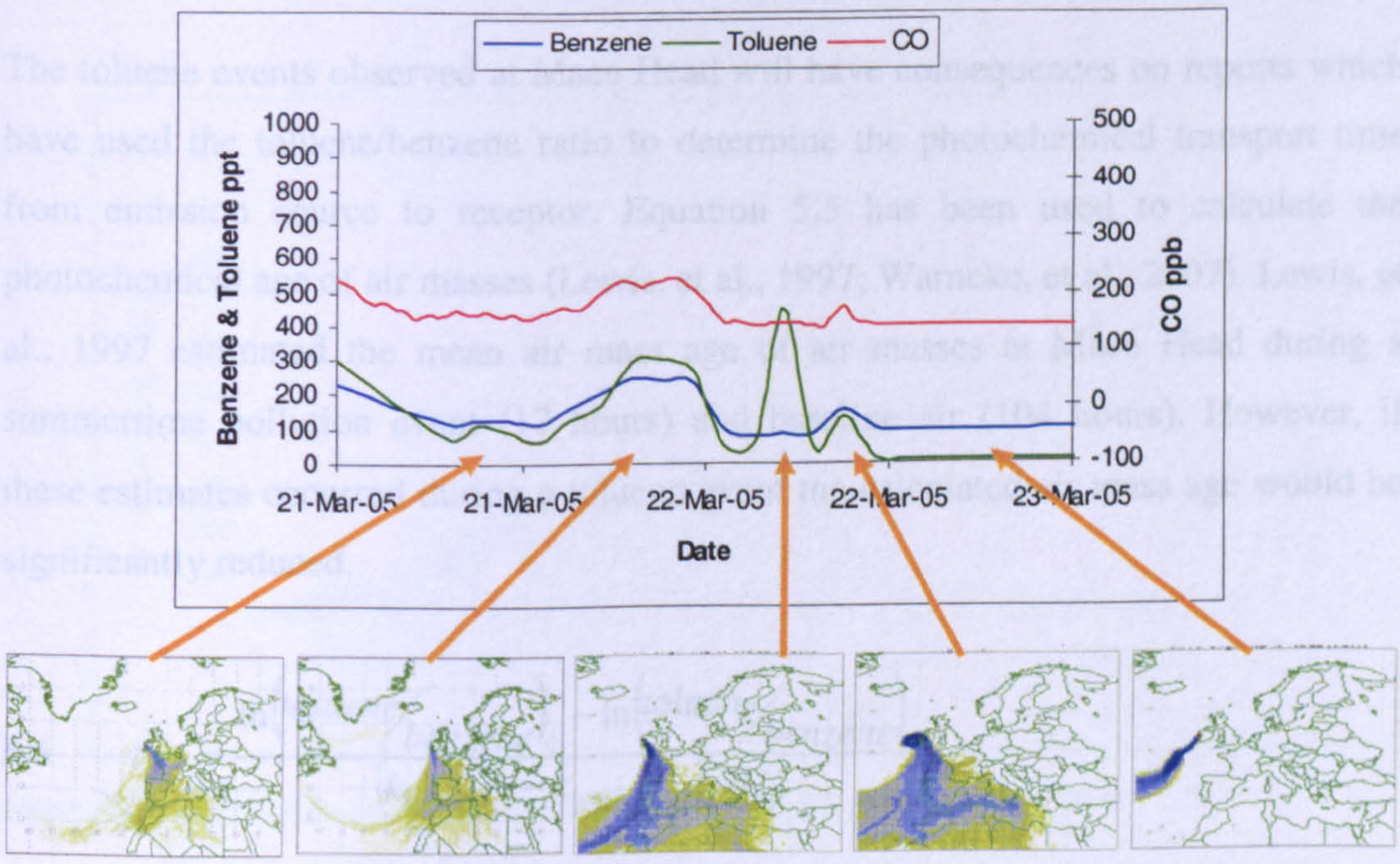

Figure 5.29 Toluene event during March 2005 compared with benzene, CO and back trajectory.

The toluene events have been compared with TCE (trichloroethene) and PCE (Tetrachloroethene (perchloroethene)) measurements. Atmospheric lifetimes of TCE and PCE are 4.8 and 97 days respectively ([OH] = 9.7×10^5 molecules cm^{-3}). TCE and PCE are used as anthropogenic markers indicating solvent emissions (Dimmer, et al., 2001). The fact that TCE and PCE concentrations are above baseline concentrations during the majority of toluene events further confirms a local toluene solvent source is sampled at these times see Figure 5.30.

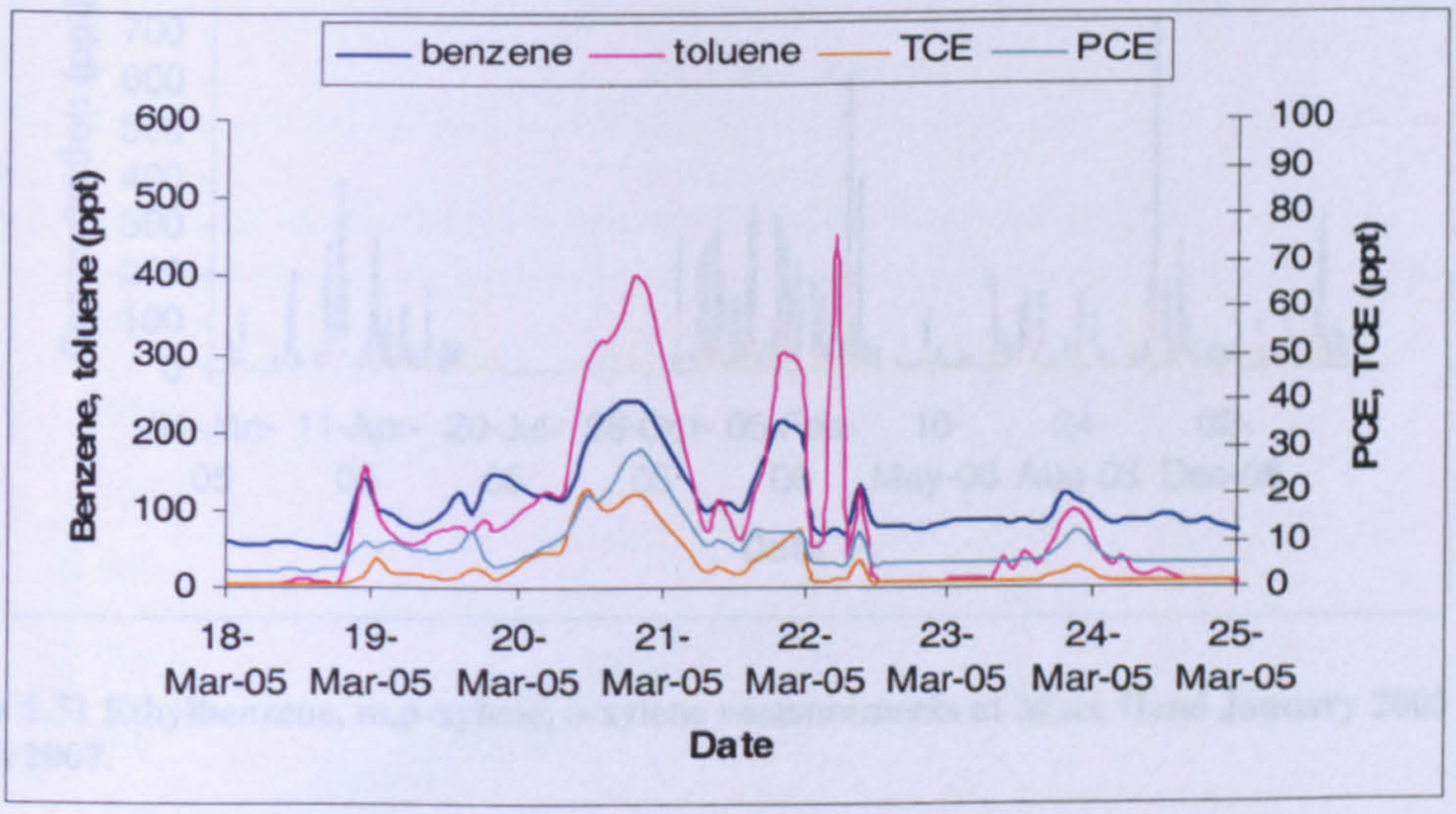

Figure 5.30 Benzene, toluene, TCE and PCE measured at Mace Head during a `toluene event'.

The toluene events observed at Mace Head will have consequences on reports which have used the toluene/benzene ratio to determine the photochemical transport time from emission source to receptor. Equation 5.5 has been used to calculate the photochemical age of air masses (Lewis, et al., 1997; Warneke, et al., 2007). Lewis, et al., 1997 estimated the mean air mass age of air masses at Mace Head during a summertime pollution event (17 hours) and baseline air (104 hours). However, if these estimates occurred during a toluene event the calculated air mass age would be significantly reduced.

$$\textbf{5.6} \qquad \tau_{OH} = \frac{\ln\left(toluene/benzene\right)_0 - \ln\left(toluene/benzene\right)_t}{\left(k_{[OH]_{toluene}} - k_{[OH]_{benzene}}\right)[OH]}$$

5.8.6. Ethylbenzene and xylene isomer measurements

5.8.6.1. Composite cycle

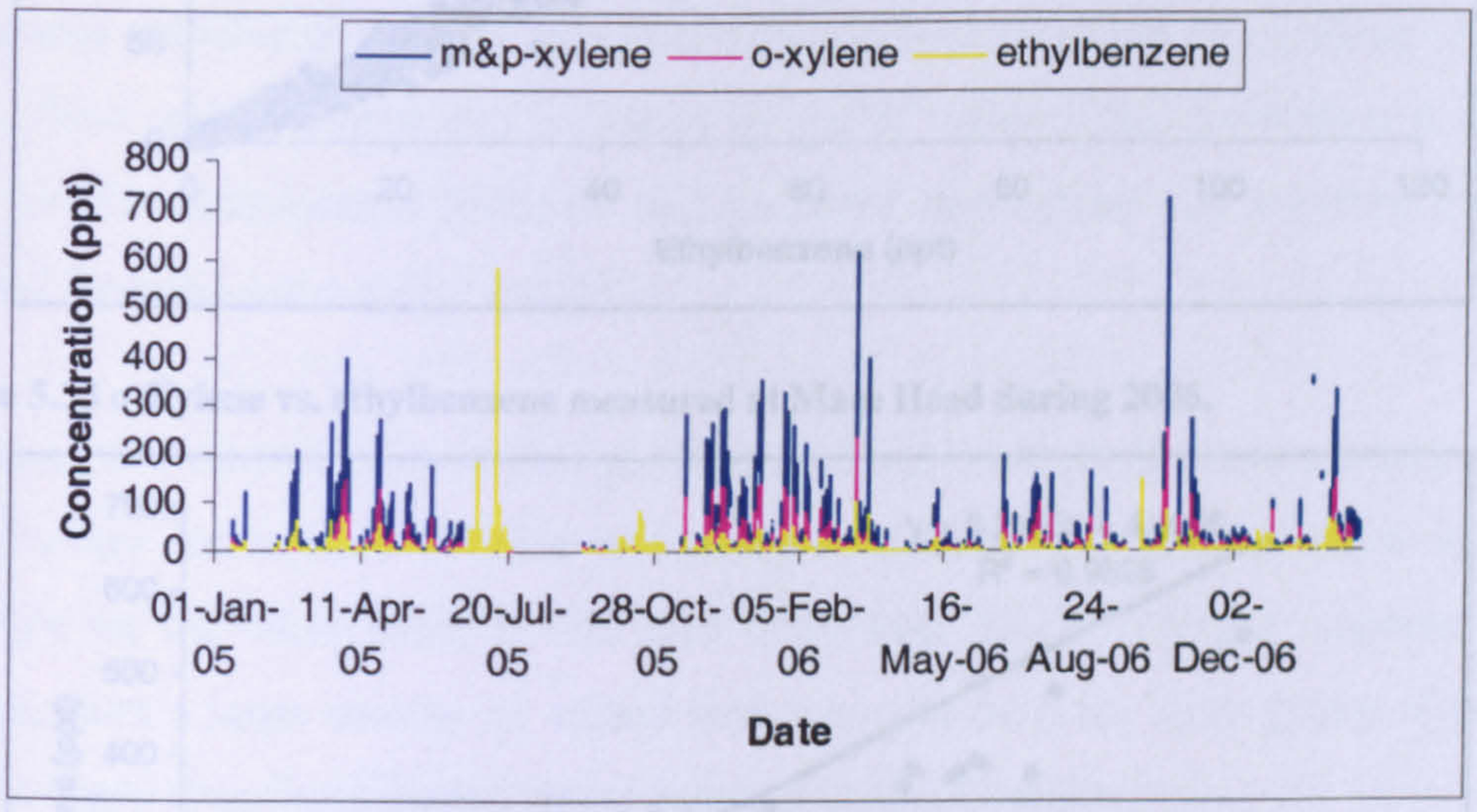

Figure 5.31 Ethylbenzene, m,p-xylene, o-xylene measurements at Mace Head January 2005 – March 2007.

5.8.6.2. Comparisons of BTEX compounds with ethylbenzene

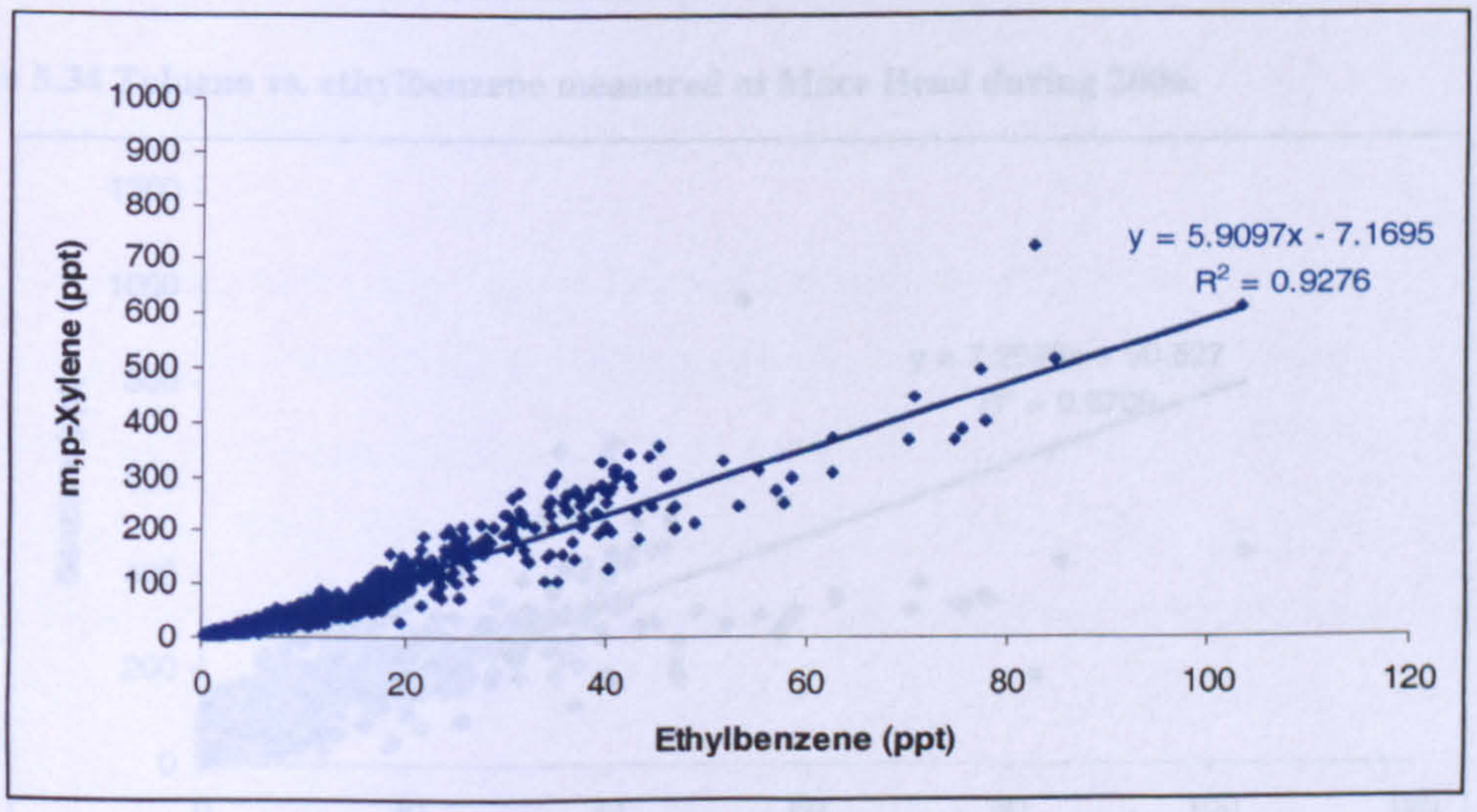

Figure 5.32 m,p-Xylene vs. ethylbenzene measured at Mace Head during 2006.

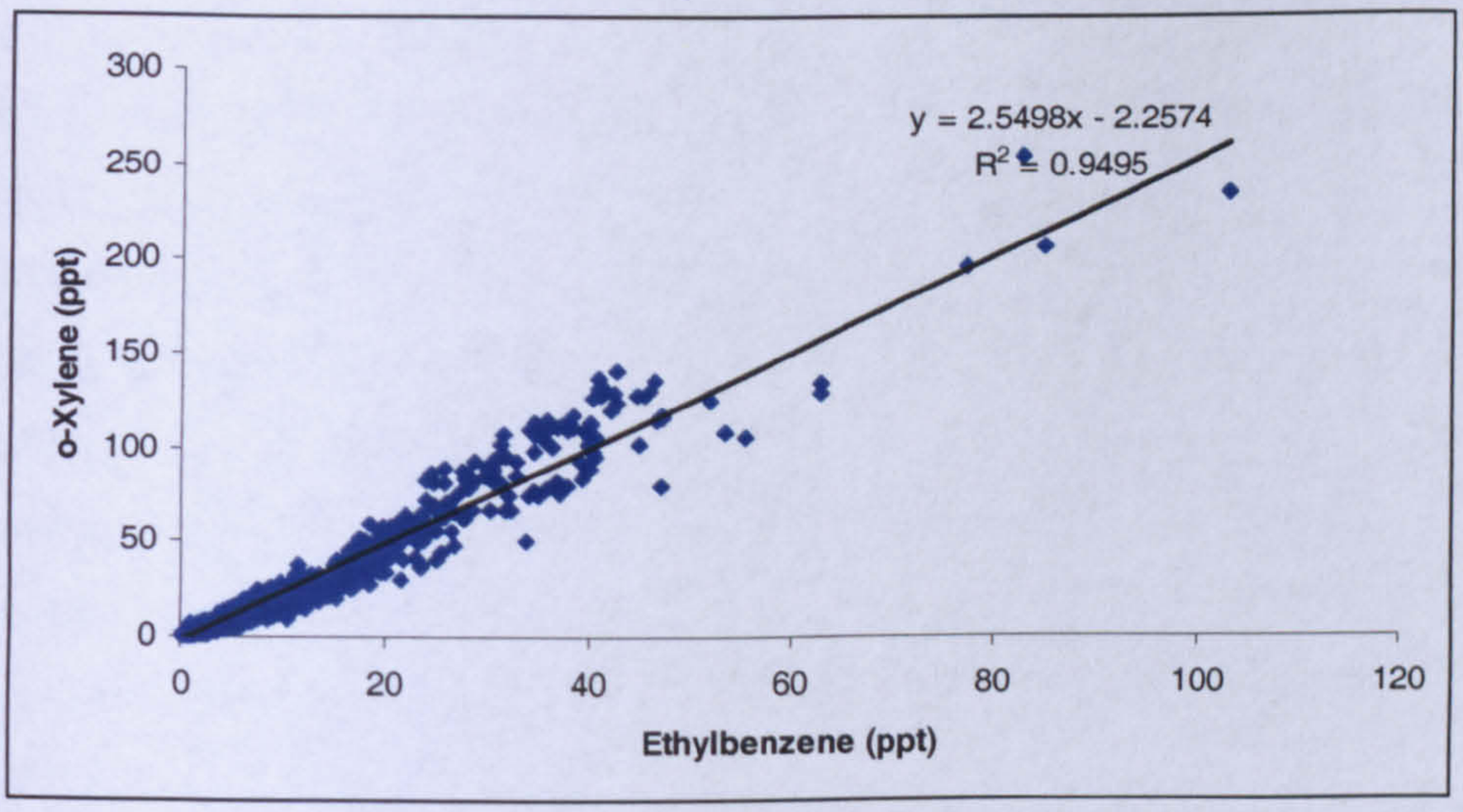

Figure 5.33 o-Xylene vs. ethylbenzene measured at Mace Head during 2006.

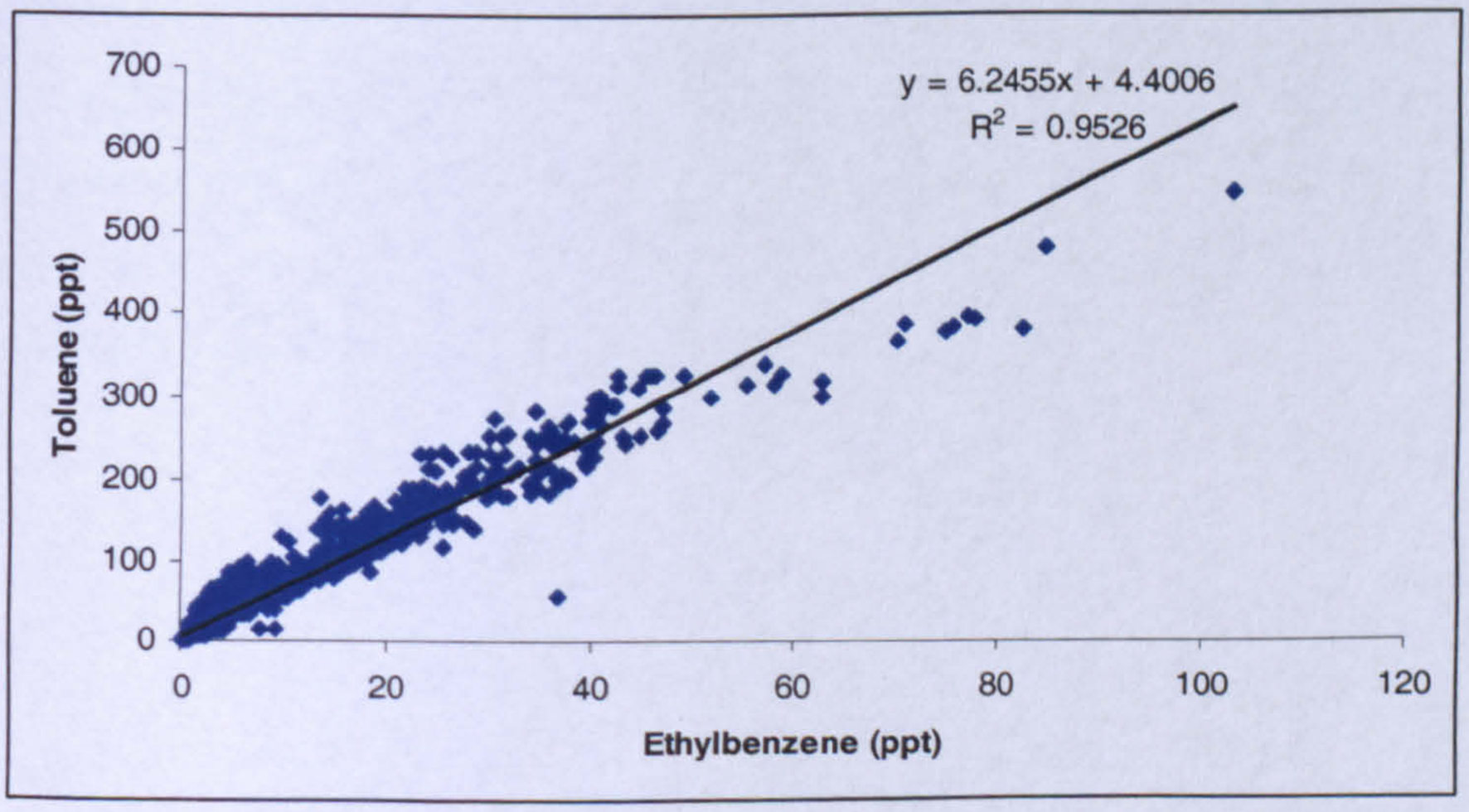

Figure 5.34 Toluene vs. ethylbenzene measured at Mace Head during 2006.

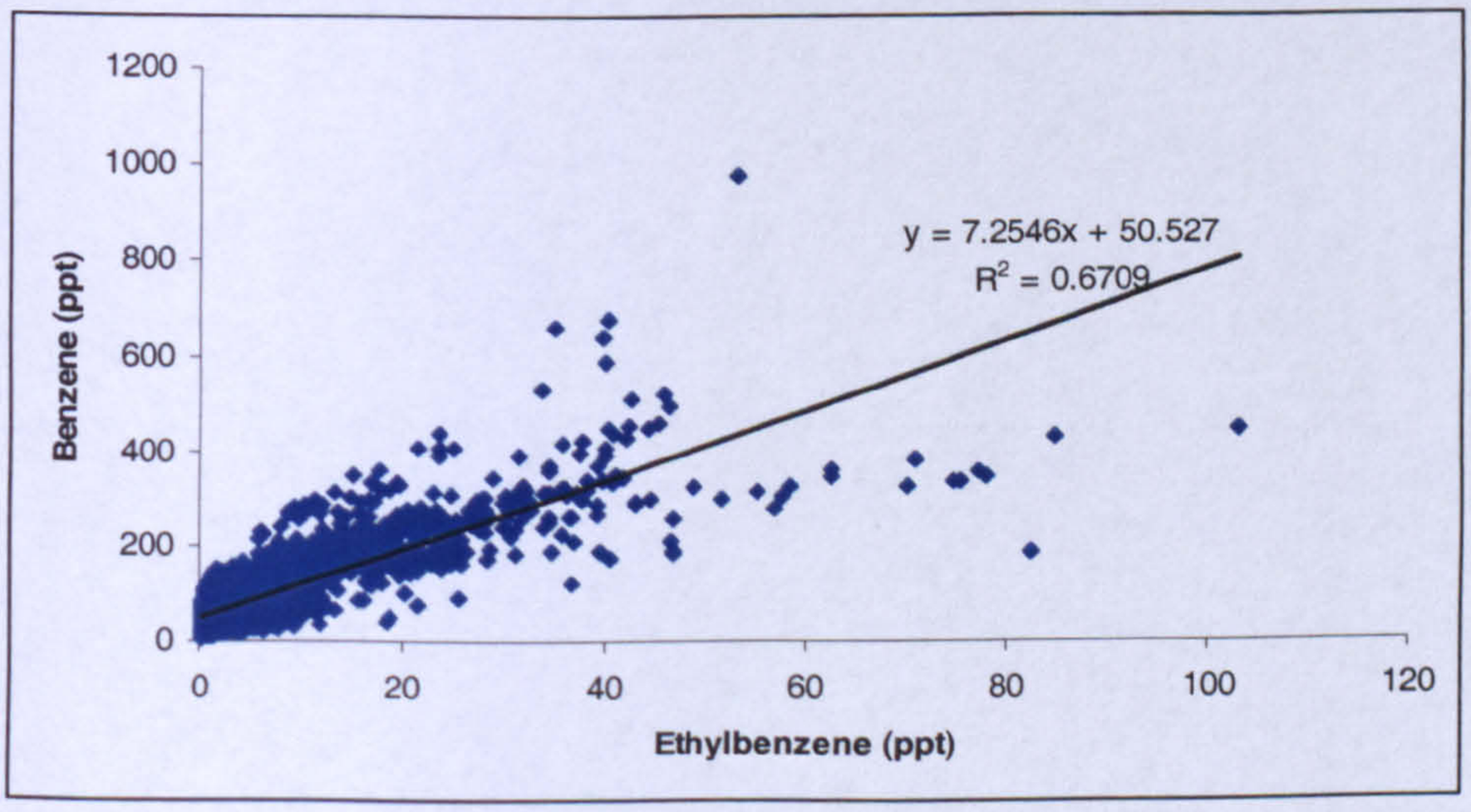

Figure 5.35 Benzene vs. ethylbenzene measured at Mace Head during 2006.

Monod, et al., (2001) reported the average m,p-xylene/ethylbenzene ratio equal to 3.5 ± 0.5. This ratio is constant throughout different sources (vehicle exhaust, solvent petrol and fuel evaporation) but spreads out over a larger range in sites far from urban influence, with ratios of 1.3 to 4.5 reported Monod, et al., (2001). Figure 5.32 shows that the measured Mace Head m,p-xylene/ethylbenzene ratio is 5.9, which is higher than the ratio reported by Monod, et al., 2001. This could be due to other sources such as solvent emissions. There is excellent correlation observed at Mace Head between m,p-xylene and ethylbenzene, indicated by the R^2 value. This correlation is due to their similar atmospheric lifetimes and indicates m,p-xylene and ethylbenzene are emitted from the same major sources.

o-Xylene and toluene both exhibit good correlations with ethylbenzene; partly due to their similar atmospheric lifetime and partly an indication of similar major sources. Benzene on the other hand, is less well correlated. The scatter plot appears to be diffuse, with a large number of values well removed from the main group of points. This is likely to indicate significant separate sources of benzene

5.9. Conclusions

Measurements of NMHCs have been carried out at the Mace Head research station, Ireland (53^0 20' N, 9^0 54' W) using the AGAGE Medusa-GCMS since January 2005. The Medusa-GCMS is a fully automated pre-concentration system attached to a gas chromatograph and quadrupole mass selective detector. The Medusa has been adapted from its primary role of recording halocarbon measurements to also measure a limited number of NMHCs, specifically C_2–C_5 alkanes, isoprene, benzene, toluene, m,p-xylene, o-xylene and ethylbenzene. Medusa-GCMS precision, calculated from standard-standard ratios ranges from 0.6% for ethane, benzene and toluene to 1-15% for the other NMHCs (excluding isoprene). Isoprene has a variable blank which depends on the concentration of isoprene in the working standard, which has not been accounted for and is an insignificant percentage of an isoprene biogenic event.

Seasonal cycles of NMHCs are presented for a two year period (January 2005–January 2007). All NMHCs recorded, except isoprene which is predominately from biogenic sources, exhibit an increase in baseline concentration during winter months and a decrease during summer months. The amplitude of the seasonal cycle is controlled by OH radical concentrations; an increase in photochemical processing during summer months results in a decrease in NMHC baseline concentration. NMHC data, excluding isoprene, are generally well correlated with CO indicating the predominately anthropogenic sources of NMHCs.

The i-butane/n-butane ratio can be used to validate the analytical integrity of NMHC instruments. i-Butane/n-butane ratio exhibit a robust relationship that is well characterised by a large number of urban and rural/remote data sets (Derwent, 2000; Swanson, et al., 2003; Hopkins, et al., 2002). The i-butane/n-butane ratio observed at Mace Head (0.4075 (r^2=0.916)) is consistent with literature reported values. When i-butane/n-butane is plotted against n-butane an increase in the i-butane/n-butane ratio is observed in clean/aged air (low n-butane concentrations) which represents the preferential removal of n-butane (compared to i-butane) by photochemical reaction with the OH radical. However, the change in i-butane/n-butane ratio from 0.4 in pollution events to 3.5 in extremely clean air cannot be explained by OH chemistry

alone. Two possible explanations for this change in ratio are; change in emission sources with different i-butane/n-butane ratios or the presence of Cl chemistry (this is further examined in chapter 6).

The Mace Head ratio of i-pentane/n-pentane is 2 in pollution events and 1 in baseline air. The ratio during pollution events is in good agreement with reported UK urban i-pentane/n-pentane ratios. The decrease in ratio observed during baseline air can be explained by changes in sources emissions. Sources of pentane isomers in UK urban air are dominated by road transport, with an i-pentane/n-pentane ratio of 2 (Dollard, et al., 2007). However the pentane isomers have a number of other sources, such as extraction of fossil fuels and solvent which give much lower i-pentane/n-pentane ratios (Dollard, et al., 2007). NO_3 chemistry will also cause the ratio to decrease alongside changes in source emissions, although NO_3 alone cannot explain the changes.

Isoprene is the only predominately biogenic NMHC measured at Mace Head. Isoprene concentrations are usually below the limit of detection during winter months, except for the occasional wintertime pollution event. These pollution events must be from local sources, given isoprene's short atmospheric lifetime of 1.7 hours with respect to OH (PORG, 1997). Biogenic isoprene events are observed during summer months which are well correlated with increased temperatures. Estimates of the percentage biogenic isoprene contribution during summer months have been made using the reported UK urban isoprene/benzene ratio by Dollard, et al. (2007).

Benzene, toluene, o-xylene and ethyl benzene all show very strong correlations with each other and also with carbon monoxide in European pollution events confirming their anthropogenic origin. Sporadic toluene events are present throughout the data, where there is a sharp increase in toluene with no corresponding increase in benzene. These toluene events are likely to be due to solvent emissions; given that the back trajectories indicate European air masses which pass over southern Ireland before arriving at Mace Head and the correlation between TCE, PCE (predominately solvent sources) and toluene in most events. The toluene events would have a dramatic influence on estimating the age of an air mass using the toluene/benzene ratio, which is frequently used in literature data (Lewis, et al., 1997).

6. Trajectory analysis and transport modelling

6.1. Introduction

Air mass trajectory classification is particularly useful for remote research sites, such as Mace Head as the composition of an air mass measured at any one time is heavily dependent upon where it originated from. Concentrations of NMHCs with atmospheric lifetimes in the order of days (such as alkanes, acetylene and benzene) are dependent on air mass origin. Shorter lived NMHCs (alkenes, isoprene, xylene isomers) are more influenced by local conditions and not entirely dependent on air mass origin. This chapter discusses a trajectory classification technique used to identify air mass origins.

6.2. Air mass classification

Five-day back trajectories downloaded from the British Atmospheric Data Centre (BADC) in three-hourly intervals were obtained from January 2005 – January 2007. The BADC uses the European Centre for Medium-Range Weather Forecasting (ECMWF) reanalysed wind fields to compare data with real meteorological measurements. The trajectory is derived from a grid with horizontal resolution of $2.5^{\circ} \times 2.5^{\circ}$ and a vertical domain extending up to 10 mb. A trajectory sorting program developed by Gray (2002) was used to give each trajectory a point score, depending upon its location, between -9 and +9 as shown in Figure 6.1.

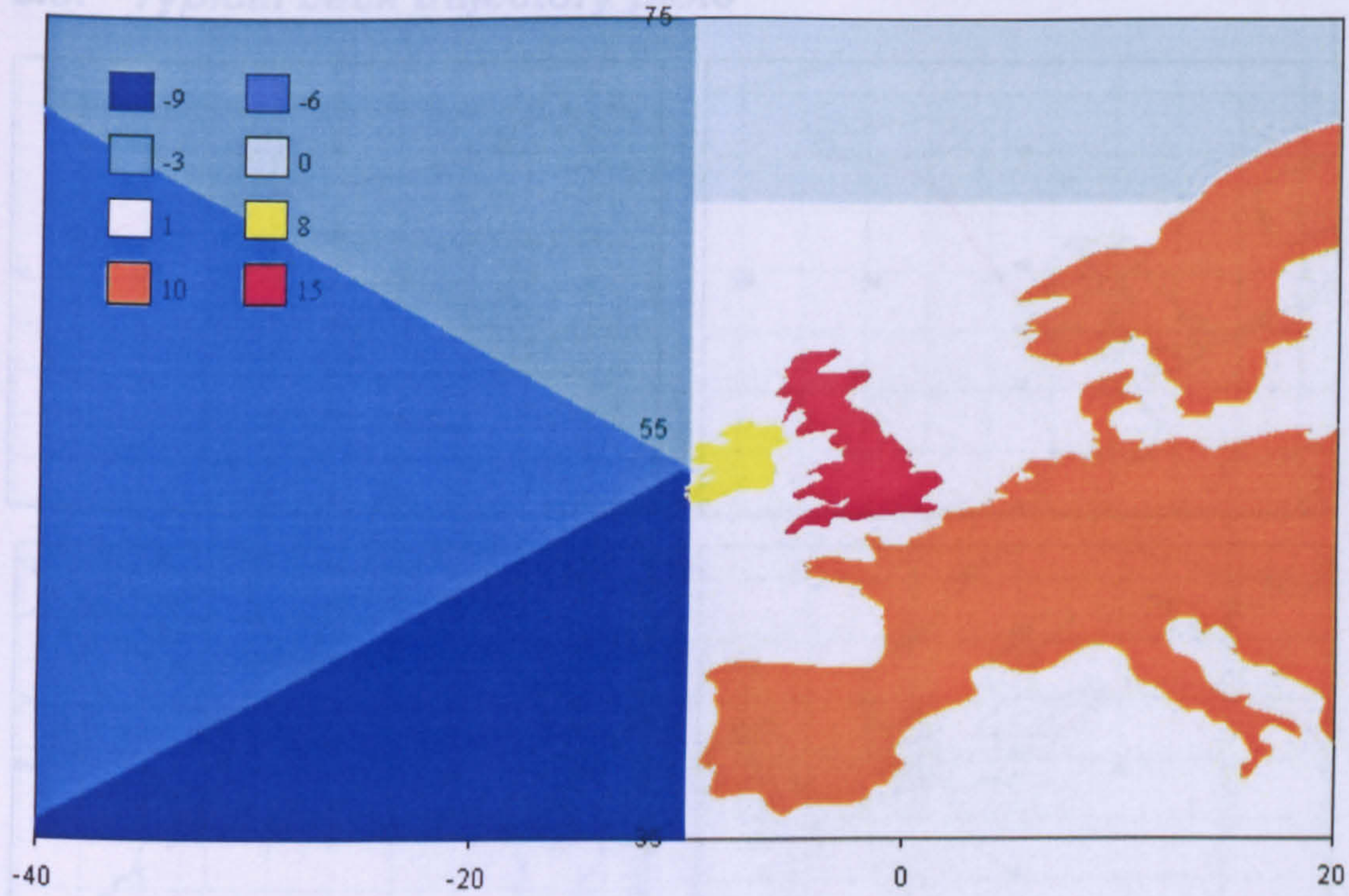

Figure 6.1 Trajectory scoring system used in the trajectory classification program. (Gray 2002).

Trajectories were then binned into one of six classes depending on their final trajectory score as shown in Table 6.1. Trajectory scores of 0 to +9 can be grouped into one category indicating European air masses.

Trajectory score	Trajectory classification
-9 to -6	Ultra clean Atlantic air from the south or south west.
-6 to -3	Clean Atlantic air may receive emissions from the USA.
-3 to 0	Generally clean air from high (polar) latitudes.
0 to +3	Background Northern Hemispheric air.
+3 to +6	Air masses passing over Europe.
+6 to +9	European air masses, having spent the majority of their 5 day trajectories over land

Table 6.1 Trajectory air mass classifications for Mace Head.

6.3. Typical back trajectory plots

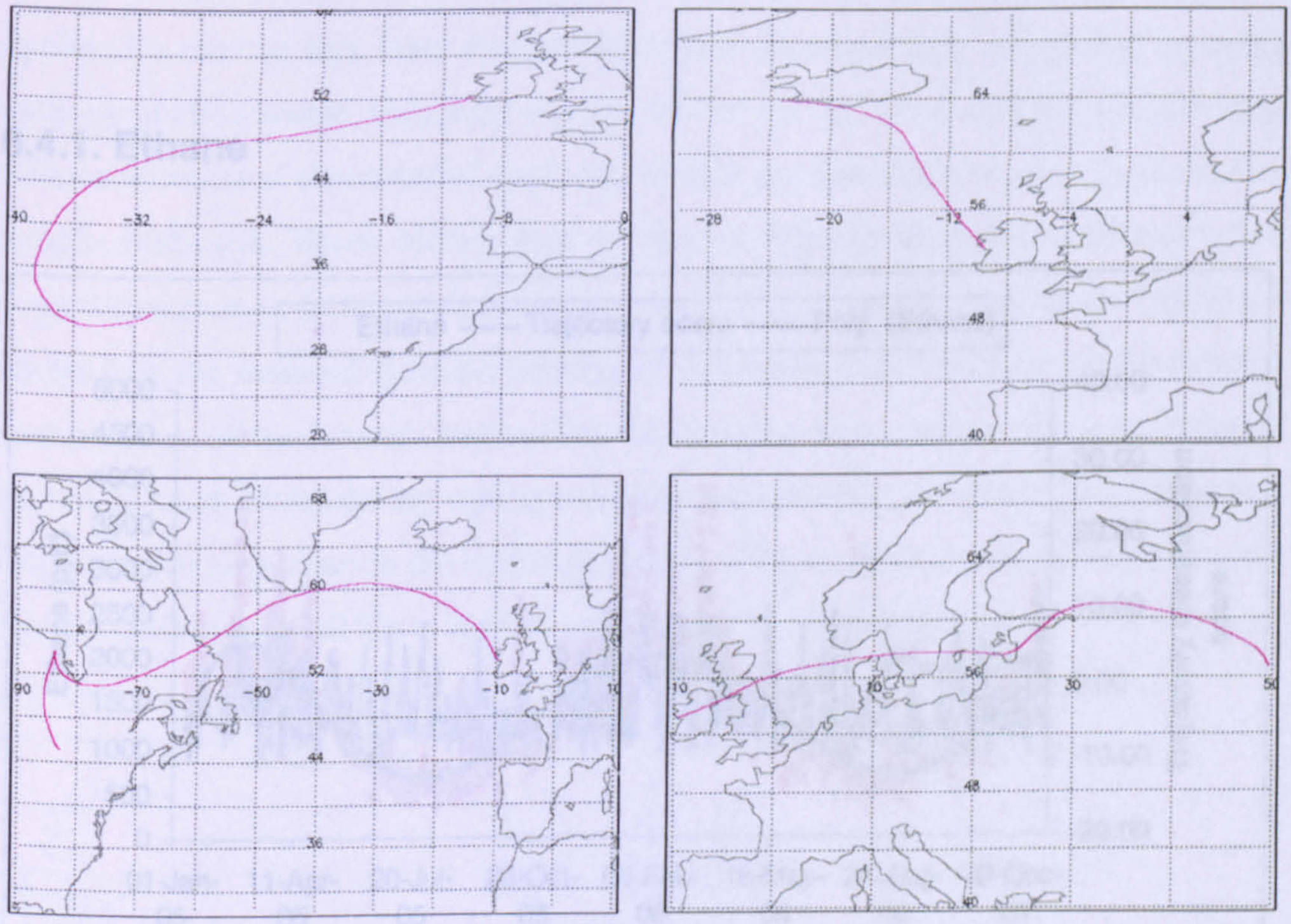

Figure 6.2 Typical 5-day trajectory plots downloaded from www.badc.nerc.ac.uk. From top left clockwise: southerly, high latitude, European and westerly trajectories.

6.4. Trajectory classification results

6.4.1. Ethane

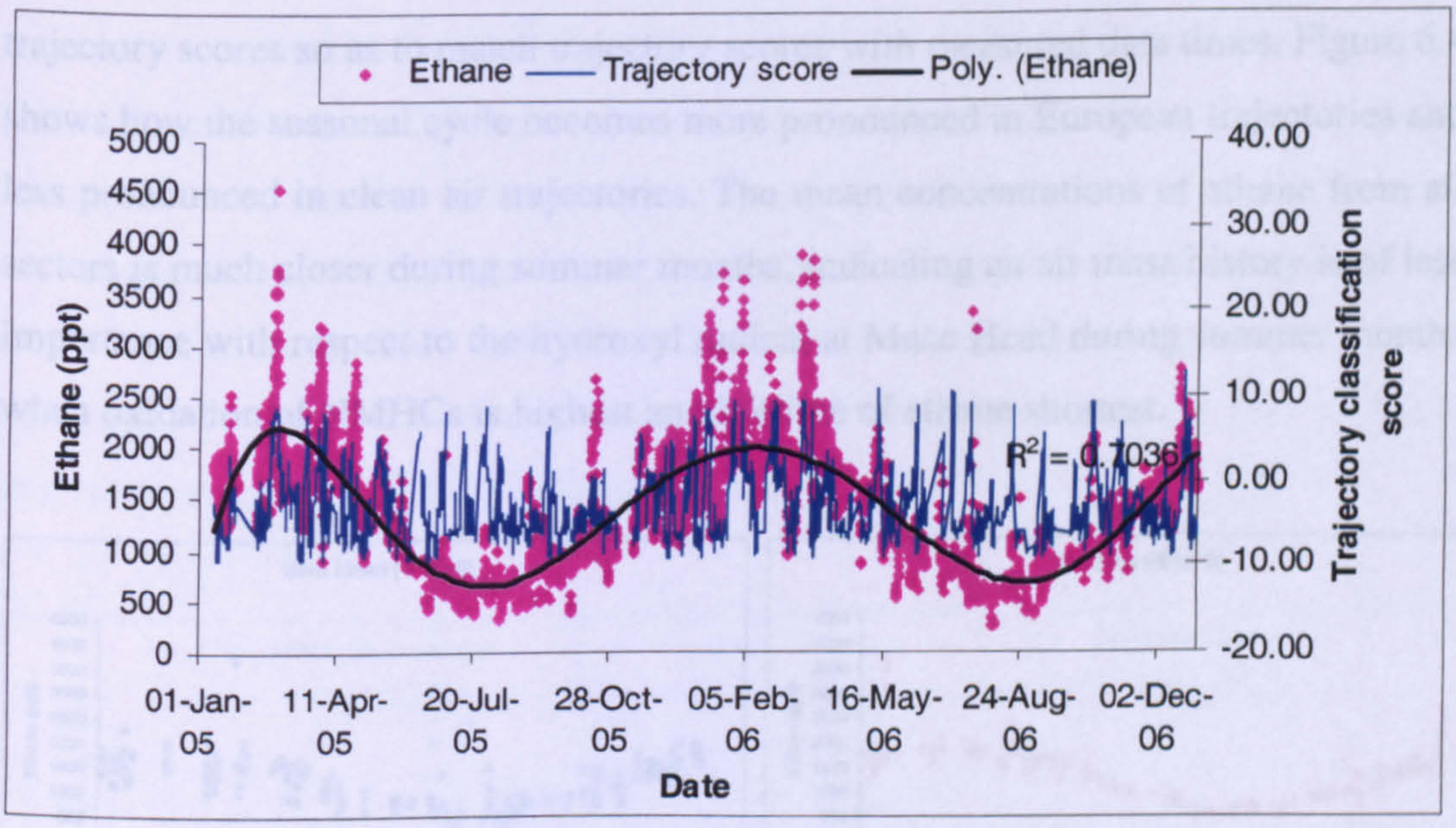

Figure 6.3 Mace Head 2005 – 2006 ethane and trajectory score time series.

Figure 6.3 highlights the general seasonal cycle observed for most trace tropospheric gases measured at Mace Head. 6th-Order polynomial lines of best fit were added to the ethane data to highlight the general trend which has a R^2 value of 0.703. During winter months species exhibit the longest atmospheric lifetimes due to low photochemical activity thus tropospheric species can be transported further in winter months than summer. This is shown in Figure 6.3 by the differences in the magnitude of pollution events between summer and winter and by the high correlation between high trajectory scores (European trajectories) and pollution events. The summer minimums and winter maximums for ethane measured over 2005 and 2006 are in good agreement, with winter maximums of approximately 5000 pptv and a summer minima of approximately 400 pptv this is in good agreement with previous NMHC studies at Mace Head (Lewis, et al., 1997; Martin, manuscript in preparation).

The variation in trajectory scores arriving at Mace Head are not distributed evenly throughout the year. This can introduce a form of bias when looking at seasonal cycles. To remove this bias, data are separated into trajectory categories, grouping data by their average trajectory scores, -9 to -6, -6 to -3 and so on. Because measurements and downloaded back trajectories are not taken at even frequency, a simple Microsoft Excel Macro was written to linearly extrapolate between two trajectory scores so as to match trajectory scores with measured data times. Figure 6.4 shows how the seasonal cycle becomes more pronounced in European trajectories and less pronounced in clean air trajectories. The mean concentrations of ethane from all sectors is much closer during summer months, indicating an air mass history is of less importance with respect to the hydroxyl radical at Mace Head during summer months when oxidation of NMHCs is highest and lifetime of ethane shortest.

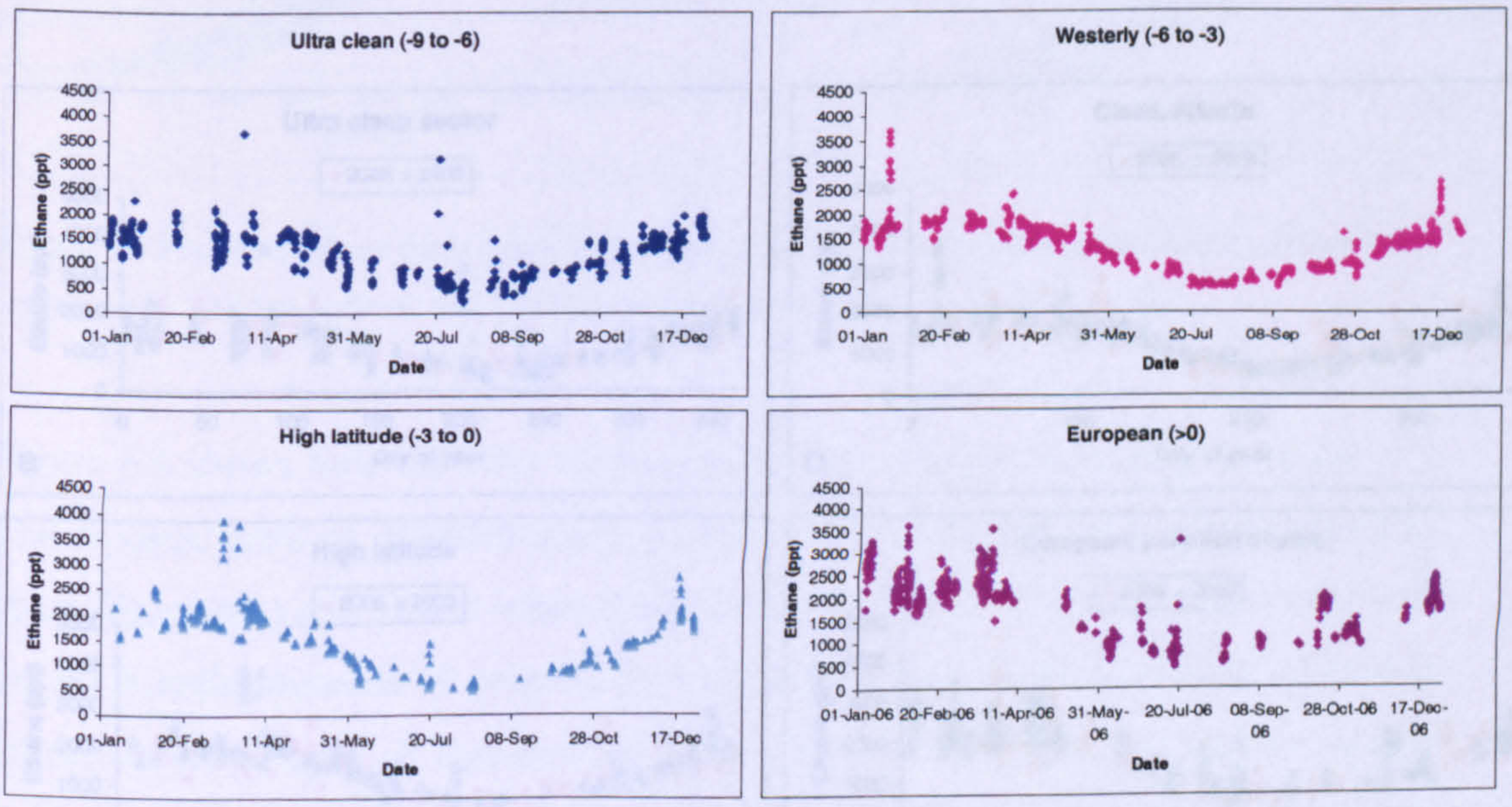

Figure 6.4 Ethane measurements at Mace Head during 2006 segregated by trajectory score. (a) Ultra clean sector, (b) westerly trajectories, (c) high latitude and (d) all European trajectories.

Also of interest are the high values of ethane occasionally observed in the ultra clean (-9 to -6), clean (-6 to -3) Atlantic and high latitude (-3 to 0) trajectories. This is clearly indicated in Figure 6.5, where 2005 and 2006 ethane data have been overlaid and plotted by day of year to allow comparisons between years. The sporadic high concentrations of ethane measured in the ultra clean, clean Atlantic and high latitude sectors could be due to the influence of local ethane emissions as they pass over land to reach Mace Head or from an ethane point source (for example, North Sea oil rigs). Back trajectories show the high values of ethane found in the -9 to -6, ultra clean sector pass over southern Ireland before reaching Mace Head, and so would pick up fresh emissions on route. High ethane concentrations in the -3 to 0 high latitude sector have a similar explanation with influences from Northern Ireland. Interestingly the high ethane concentrations found in the -6 to -3, clean Atlantic sector may indicate long-range transport of ethane from the USA to Ireland.

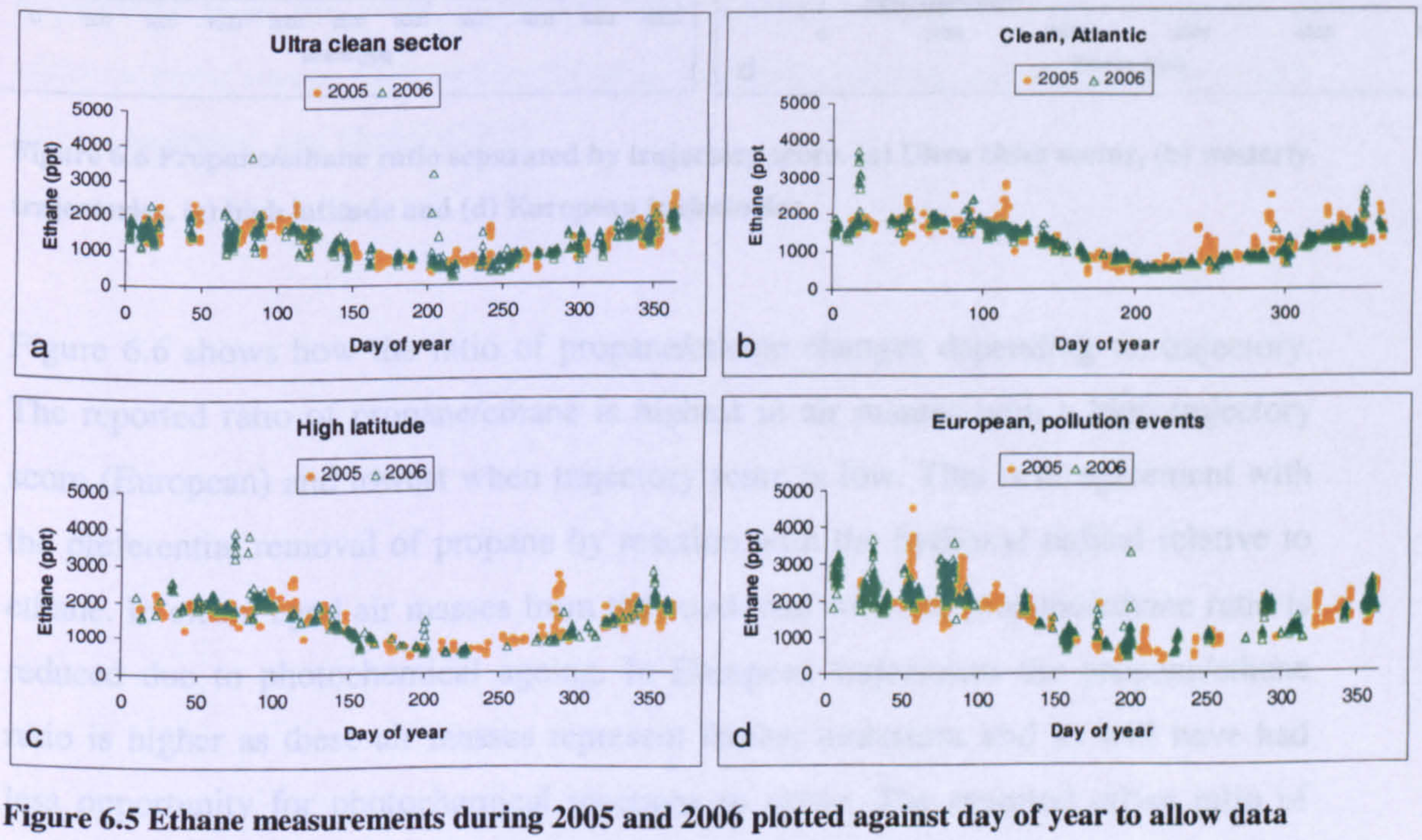

Figure 6.5 Ethane measurements during 2005 and 2006 plotted against day of year to allow data to be overlaid and used for comparison between years. (a) Ultra clean sector, (b) westerly trajectories, (c) high latitude and (d) all European trajectories.

6.4.2. Ethane and propane ratio

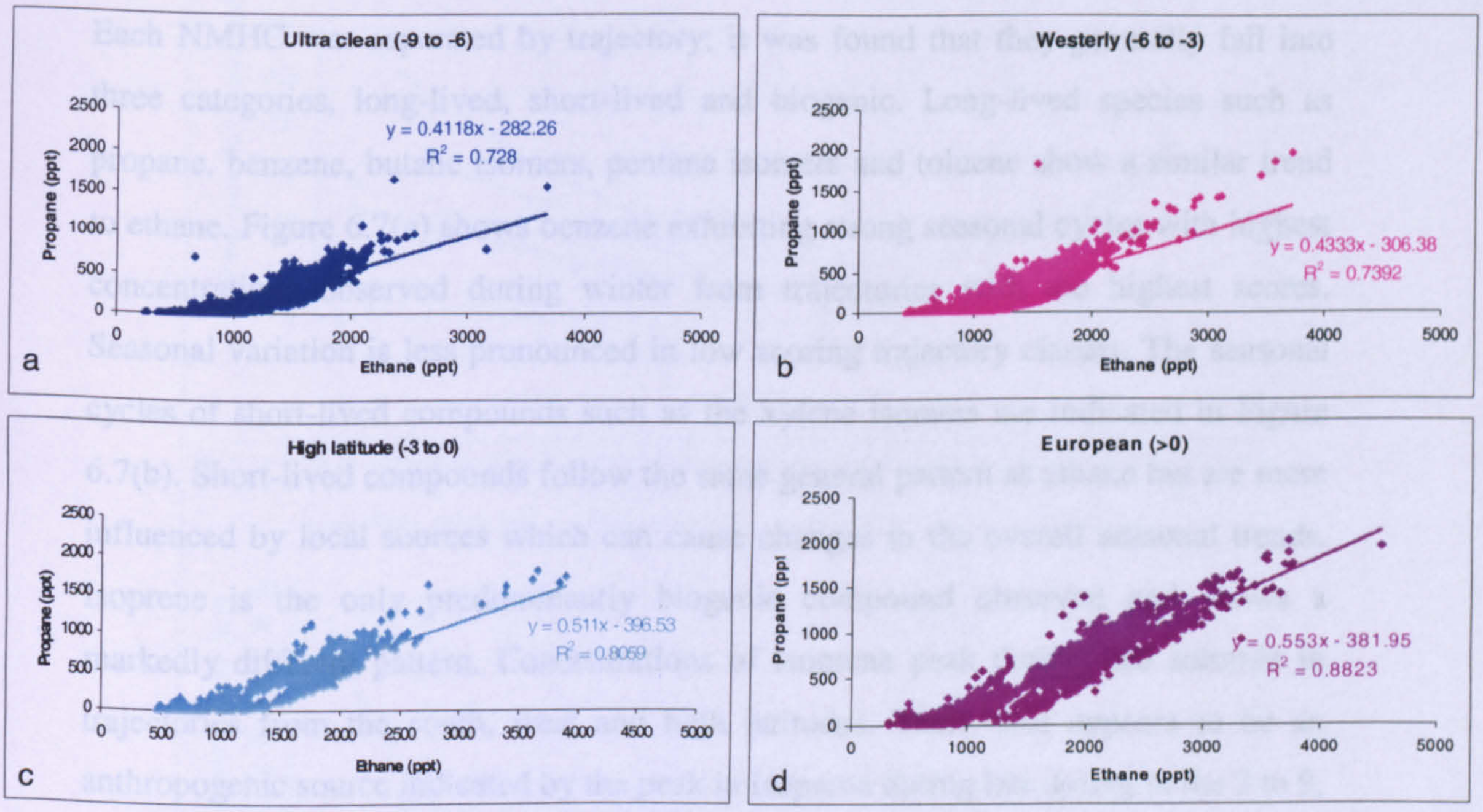

Figure 6.6 Propane/ethane ratio separated by trajectory score. (a) Ultra clean sector, (b) westerly trajectories, (c) high latitude and (d) European trajectories.

Figure 6.6 shows how the ratio of propane/ethane changes depending on trajectory. The reported ratio of propane/ethane is highest in air masses with a high trajectory score (European) and lowest when trajectory score is low. This is in agreement with the preferential removal of propane by reaction with the hydroxyl radical relative to ethane. In clean, aged air masses from the south and west the propane/ethane ratio is reduced due to photochemical ageing. In European trajectories the propane/ethane ratio is higher as these air masses represent fresher emissions and so will have had less opportunity for photochemical reactions to occur. The reported urban ratio of propane/ethane in UK sites away from sources such as oil refining and petrochemical industries is 0.49-0.66. The propane/ethane ratio for UK sites influenced by industrial sources is 1.0-2.15 Derwent, 2000. The propane/ethane ratio at Mace Head from European air masses is 0.55, which is in close agreement with the reported UK urban (non-industrial) values.

6.4.3. Data separation for other NMHCs

Each NMHC was separated by trajectory; it was found that they generally fall into three categories, long-lived, short-lived and biogenic. Long-lived species such as propane, benzene, butane isomers, pentane isomers and toluene show a similar trend to ethane. Figure 6.7(a) shows benzene exhibiting strong seasonal cycles with highest concentrations observed during winter from trajectories with the highest scores. Seasonal variation is less pronounced in low scoring trajectory classes. The seasonal cycles of short-lived compounds such as the xylene isomers are indicated in Figure 6.7(b). Short-lived compounds follow the same general pattern as ethane but are more influenced by local sources which can cause changes in the overall seasonal trends. Isoprene is the only predominantly biogenic compound observed and shows a markedly different pattern. Concentrations of isoprene peak during late summer in trajectories from the south, west and high latitudes. There also appears to be an anthropogenic source indicated by the peak in isoprene during late spring in the 3 to 9, European sector, see Figure 6.7(c).

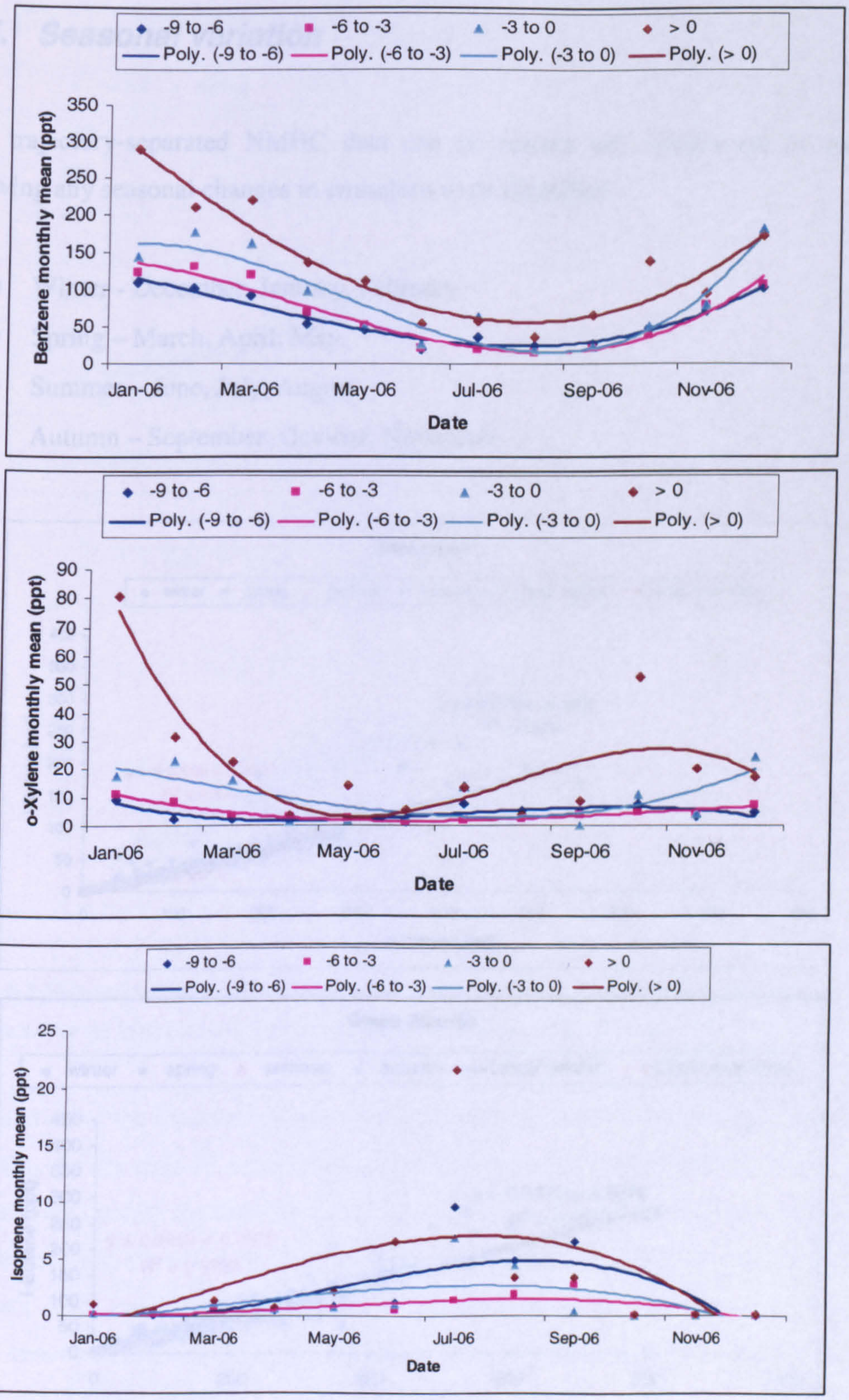

Figure 6.7 Monthly mean concentrations of (a) benzene (b) o-xylene (c) isoprene measured at Mace Head during 2006. 3rd-Order polynomial lines of best fit have been added to highlight general trends.

6.5. Seasonal variation

The trajectory-separated NMHC data can be further sub categorised by season, allowing any seasonal changes in emissions to be identified.

- Winter - December, January, February.
- Spring – March, April, May.
- Summer – June, July, August
- Autumn – September, October, November.

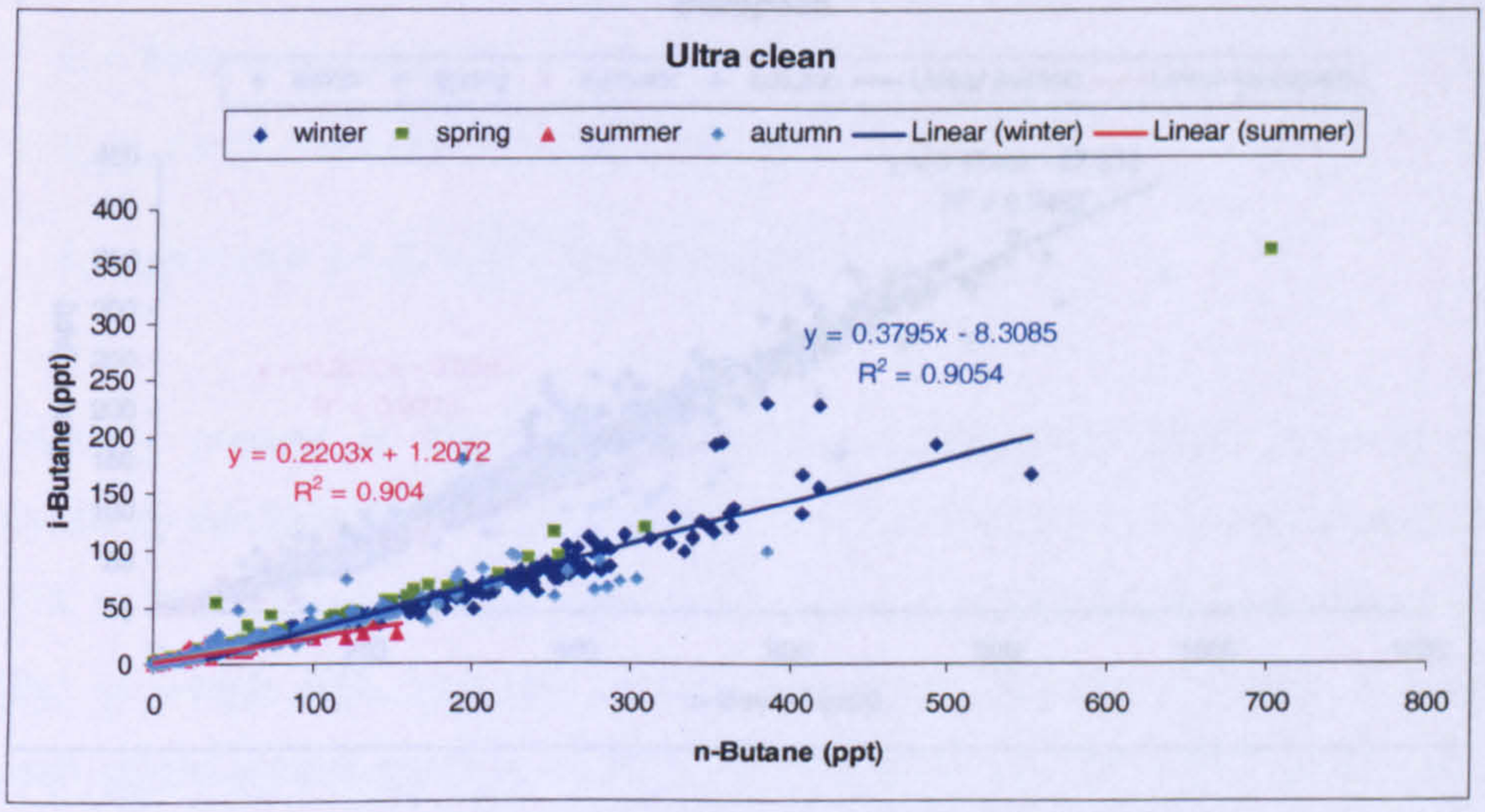

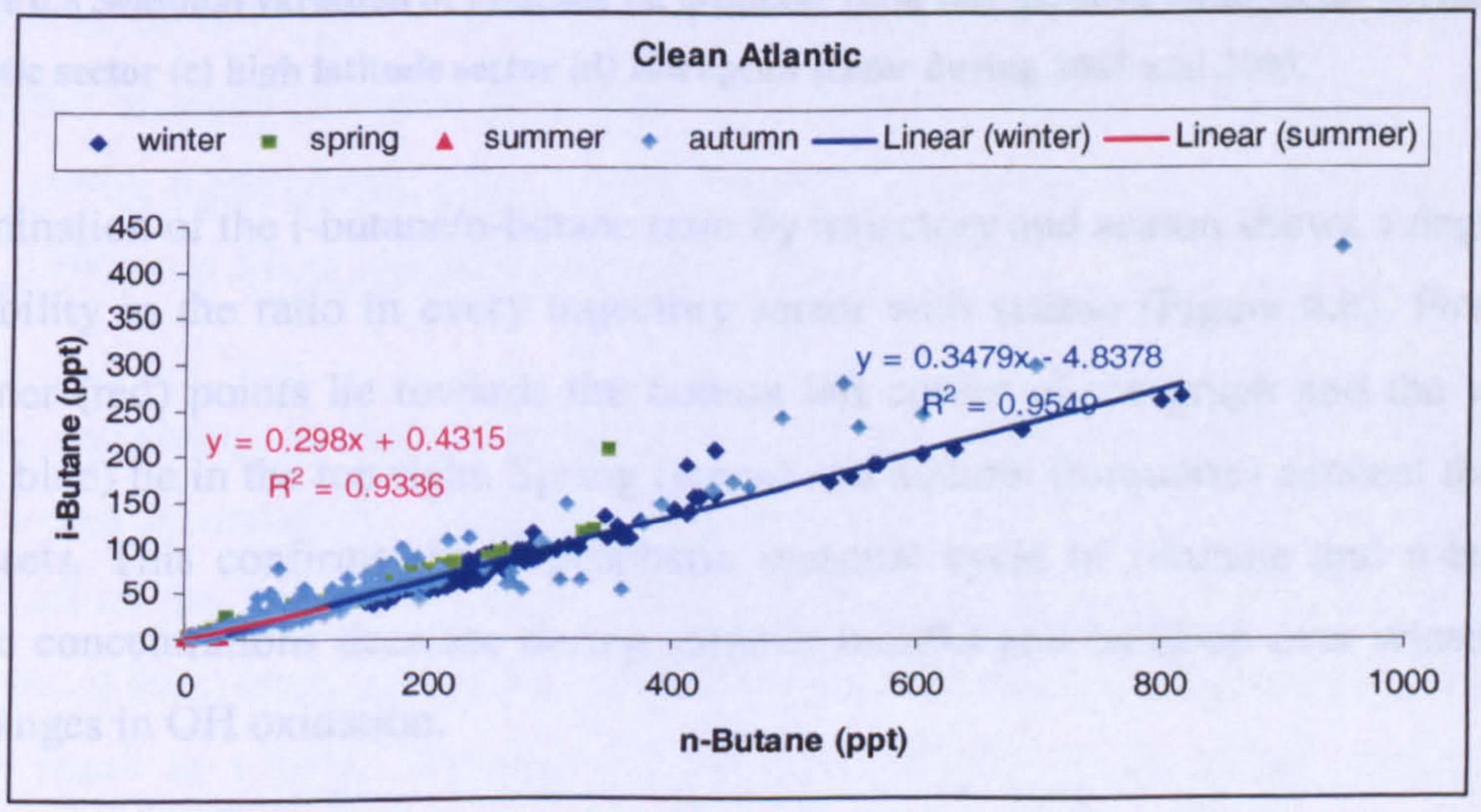

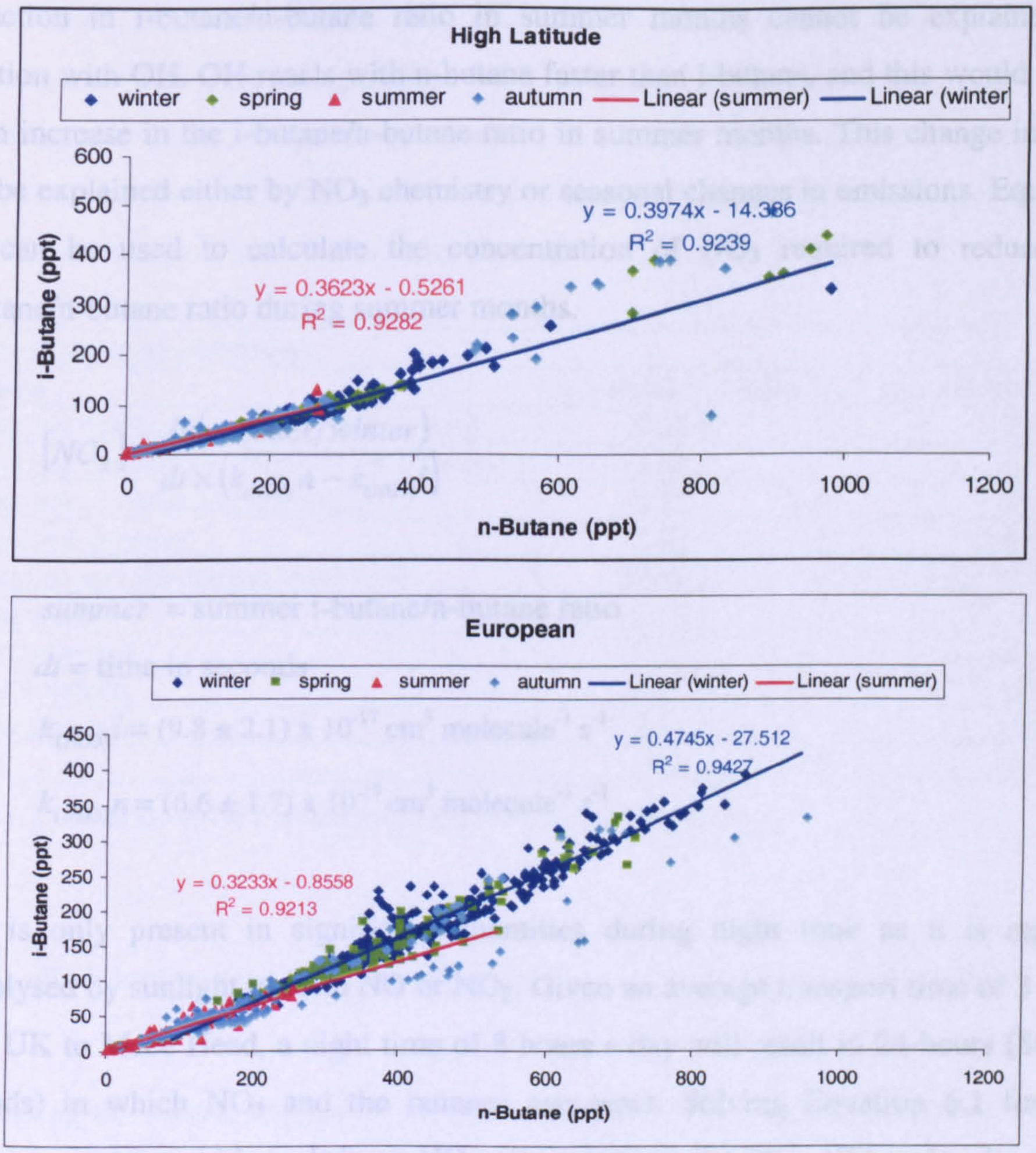

Figure 6.8 Seasonal variation of i-butane vs. n-butane ratio for; (a) ultra clean sector (b) clean, Atlantic sector (c) high latitude sector (d) European sector during 2005 and 2005.

Examination of the i-butane/n-butane ratio by trajectory and season shows a degree of variability in the ratio in every trajectory sector with season (Figure 6.8). First, the summer (red) points lie towards the bottom left corner of the graph and the winter (dark blue) lie in the top right. Spring (green) and autumn (turquoise) connect the two data sets. This confirms the tropospheric seasonal cycle of i-butane and n-butane, where concentrations decrease during summer months and build-up over winter due to changes in OH oxidation.

Figure 6.8 also shows a decrease in the i-butane/n-butane ratio in summer months, particularly evident in the ultra clean and European sectors. For example, in the European sector i-butane/n-butane is 0.47 in winter and 0.32 in summer. The

reduction in i-butane/n-butane ratio in summer months cannot be explained by reaction with OH. OH reacts with n-butane faster than i-butane, and this would result in an increase in the i-butane/n-butane ratio in summer months. This change in ratio can be explained either by NO_3 chemistry or seasonal changes in emissions. Equation 6.1 can be used to calculate the concentration of NO_3 required to reduce the i-butane/n-butane ratio during summer months.

6.1. $$[NO_3] = \frac{ln(summer/winter)}{dt \times (k_{(NO3)}n - k_{(NO3)}i)}$$

$summer$ = summer i-butane/n-butane ratio

dt = time in seconds

$k_{(NO3)}i = (9.8 \pm 2.1) \times 10^{-17}$ cm^3 molecule^{-1} s^{-1}

$k_{(NO3)}n = (6.6 \pm 1.7) \times 10^{-17}$ cm^3 molecule^{-1} s^{-1}

NO_3 is only present in significant quantities during night time as it is rapidly photolysed by sunlight to form NO or NO_2. Given an average transport time of 3 days from UK to Mace Head, a night time of 8 hours a day will result in 24 hours (86400 seconds) in which NO_3 and the butanes can react. Solving Equation 6.1 for the European sector would result in an NO_3 concentration of 1.39×10^{11} molecules cm^{-3}, equivalent to 5.55 ppbv. This is much too high a value for atmospheric NO_3. Examples of reported nighttime average NO_3 concentrations include; 7.8 ppt (Heintz, et al., 1996), 6 ppt (Allan, et al., 1999), 10 ppt in winter and 6 ppt in summer (Allan, et al., 1999) and 14-48 ppt (McLaren, et al., 2004).

Instead, the change in i-butane/n-butane ratio from winter to summer can be explained by changes in emissions. Biogenic emissions of butanes, such as oceanic emissions could affect the i-butane/n-butane ratio. Oceanic alkane emissions produce higher amounts of the n-isomer compared to the i-isomer (for butanes and pentanes), and this would result in a lower i-butane/n-butane ratio (Riemer, et al., 2000). Variation in anthropogenic sources could also alter the butane ratio. Table 6.2 shows the varying UK sources and emissions of i-butane and n-butane. For example, increased solvent evaporation during summer months could perturb the i-butane/n-butane ratio to a

lower value. To further examine the causes for the change in ratio, extra information is needed, such as monitoring of other NMHCs (particularly alkenes which are highly reactive with NO_3 compared to alkanes) NO_X and acetyl nitrates. Direct flux measurements from different butane sources would also help to establish the reasons behind the change in butane ratio with season.

Mass emissions (Ktonnes)			
Source	**n-butane**	**i-butane**	**iso/n-butane**
stationary combustion (energy production)	0.25	0.01	0.04
stationary combustion (commercial & resid'n)	1.36	0.41	0.30
stationary combustion (industrial)	0.38	0.01	0.03
production process	4.69	0.23	0.05
extraction and distribution fossil fuels	69.49	12.6	0.18
Solvent use	19.14	0.92	0.05
Road transport	10.71	4.9	0.46
other transport	0.47	0.21	0.45
waste treatment	0.02	0.01	0.50
Total	**107**	**19**	**0.18**

Table 6.2 UK emissions of i-butane and n-butane (Dore, et al., 2006).

6.6. Evidence for Cl chemistry

Comparing the natural logarithms of n-butane/ethane with i-butane/ethane ratios and n-butane/ethane with propane/ethane can be used to determine the photochemical age of an air mass and the importance of OH oxidation (Parrish, et al., 1992, Swanson, et al., 2003). The analysis of three alkanes eliminates the dependence on the hydroxyl radical concentration (found when comparing the ratios of two hydrocarbons) in determining the photochemical age of an air mass. The analysis is based on the assumption that three species, A, B and C are emitted simultaneously into an air mass and they are removed by photochemical reactions, following first-order kinetics. The relationship between three alkanes can be expressed as:

$$\ln([A]/[C]) = M\{\ln([B]/[C])\} + D \qquad \textbf{6.2.}$$

In equation 6.2 the slope, M is given by:

$$\mathbf{6.3.} \qquad M = {(k_a - k_c)}/{(k_b - k_c)}$$

The intercept, D is given by:

$$\mathbf{6.4.} \qquad D = \ln([A]_0/[C]_0) - M\ln([B]_0/[C]_0)$$

Parrish, et al. (1992) and Swanson, et al. (2003) compared the natural logarithms of n-butane/ethane with propane/ethane and i-butane/ethane with n-butane/ethane with the calculated kinetic slopes. Kinetic slopes are calculated for reaction with OH radical only using equation 6.3 and the rate coefficients, k(OH) given in Table 6.3. Kinetic slope for n-butane/ethane with propane/ethane is 2.47 (for $(k_{n\text{-butane}}-k_{ethane})/(k_{propane}-k_{ethane})$ at 298 K). The kinetic slope for i-butane/ethane with n-butane/ethane is 0.89 (for $(k_{i\text{-butane}}-k_{ethane})/(k_{n\text{-butane}}-k_{ethane})$ at 298 K). It has been suggested that observed ratios falling below the kinetic value can be accounted for due to the effects of Cl chemistry and/or dilution of air masses.

	k(OH)	k(Cl)	k(NO3)
Ethane	2.4×10^{-13} [a]	5.90×10^{-11} [a]	$<1.00 \times 10^{-17}$ [a]
Propane	1.10×10^{-12} [a]	1.40×10^{-10} [a]	$<7.00 \times 10^{-17}$ [a]
i-Butane	2.12×10^{-12} [b]	1.43×10^{-10} [c]	9.8×10^{-17} [d]
n-Butane	2.36×10^{-12} [b]	2.18×10^{-10} [c]	4.60×10^{-17} [e]

Table 6.3 Rate coefficients for OH, Cl and NO_3 reactions with ethane, propane and butane isomers quoted in $cm^{-3}molecule^{-1}\ s^{-1}$. [a] Atkinson, et al., 2005 [b] Atkinson, 2003 [c] Atkinson, 1997 [d] Atkinson, 1991 [e] Atkinson, et al., 2006

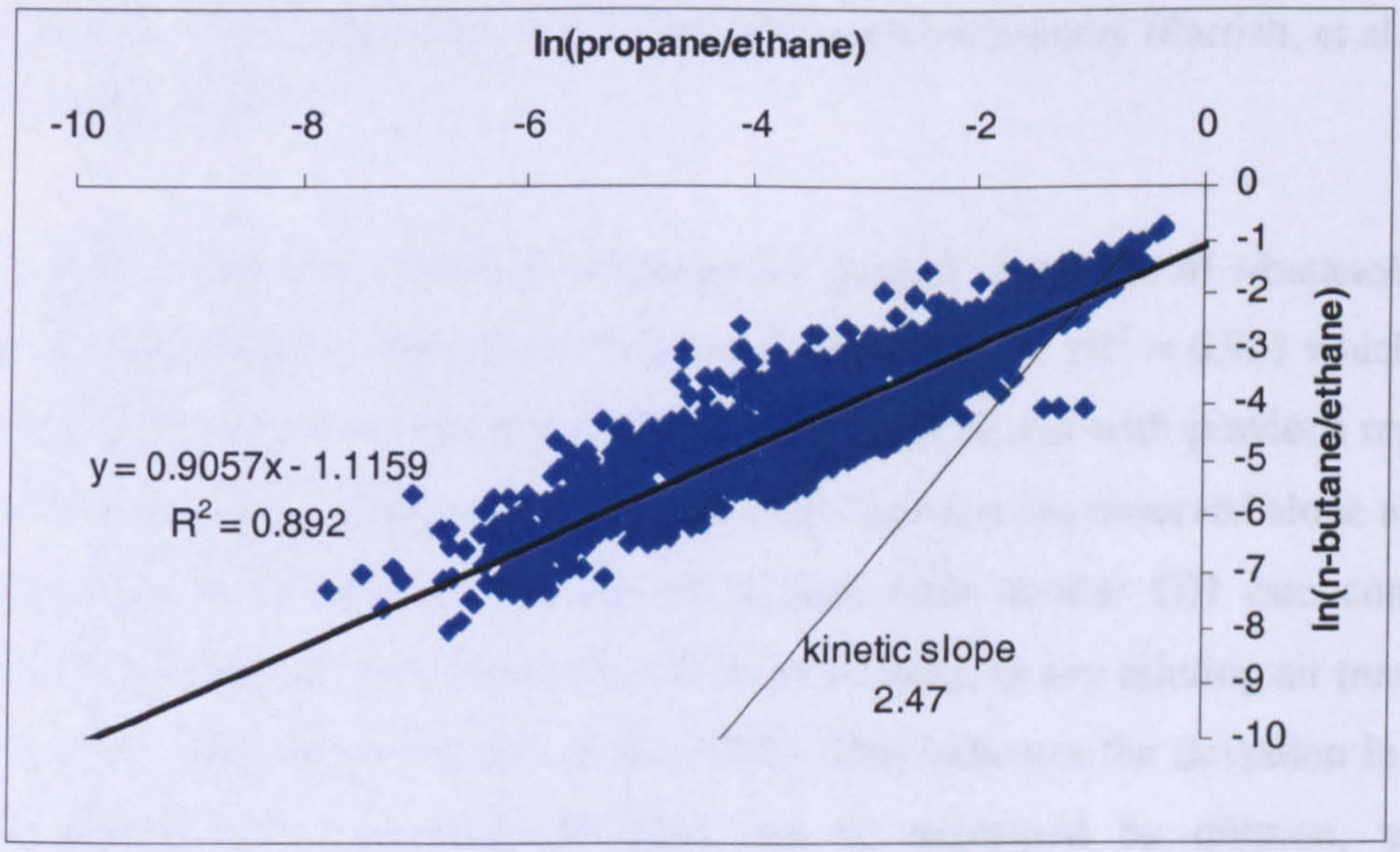

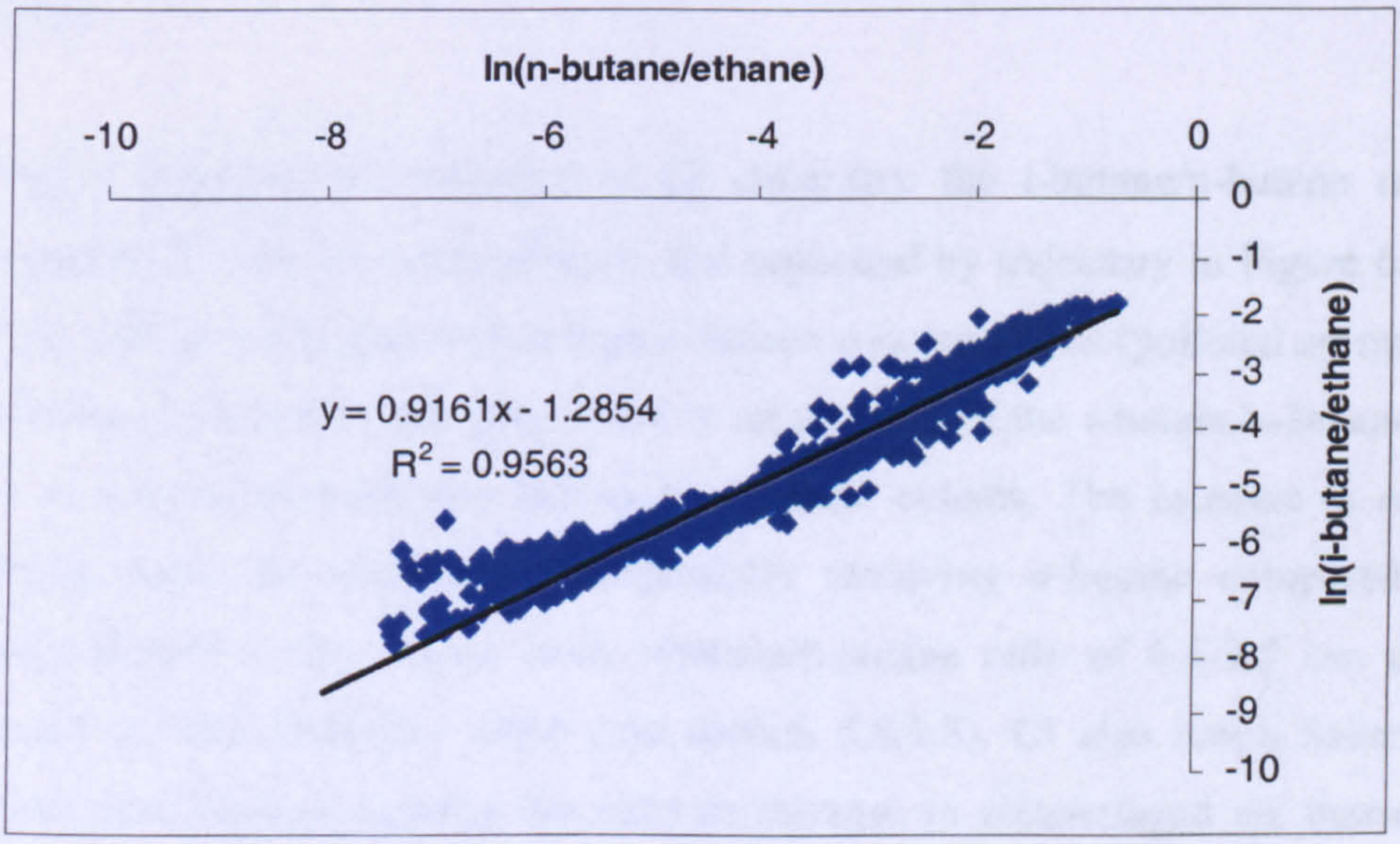

Figure 6.9 Correlation of the natural logarithms of (a) n-butane/ethane with propane/ethane and (b) i-butane/ethane with n-butane/ethane measured during 2006. The bold line in each plot represents the linear least squares fit to the data. The dashed line in plot (a) represents the calculated kinetic slope using equation 6.2.

Figure 6.9a plots the correlation between the natural logarithm of n-butane/ethane with propane/ethane. The slope of the correlation is 0.91 (R^2 = 0.89) in good agreement with previous reported data by Swanson, et al. (2003) and references therein. The observed slope falls below the calculated kinetic slope of 2.47. This observation is consistent with dilution effects of air masses. The observed curvature in

these data has been suggested to be an indication of Cl chemistry (Parrish, et al., 1992 and Rudolph, 1997).

Figure 6.9b shows the correlation between the natural logarithm of i-butane/ethane versus n-butane/ethane. The slope of the correlation is 0.91 (R^2 = 0.95) which is in good agreement with the calculated kinetic value of 0.89 and with previous reported data (Swanson, et al., 2003). The good agreement between the observed slope and the kinetic slope is because comparison of alkanes with similar OH rate constants (n-butane and i-butane) minimizes the effects of dilution, as any diluting air mass will maintain the same ratio Swanson, et al. (2003). This indicates the deviation in slope for n-butane/ethane with propane/ethane can be explained by dilution, not Cl chemistry.

To further examine the evidence of Cl chemistry the i-butane/n-butane ratio is compared with n-butane measurements and separated by trajectory in Figure 6.10. A constant ratio of 0.5 is observed at high n-butane concentrations (polluted air masses). As n-butane falls below 100 pptv. there is an increase in the i-butane/n-butane ratio which is seen in all trajectory sectors to different extents. The increase in ratio is consistent with OH chemistry, preferentially removing n-butane compared with i-butane. However, the change from i-butane/n-butane ratio of 0.5-3.5 can not be explained by OH chemistry alone (see section 5.8.1.5). Cl also reacts faster with n-butane than i-butane causing the ratio to increase in cleaner/aged air masses. Cl chemistry is considered to be an important reaction for NMHC removal in the marine boundary layer. Pszenny, et al. (2007) estimated that reactions with Cl increase the NMHC kinetic reactivity by 16-30 % depending on air mass transport sectors.

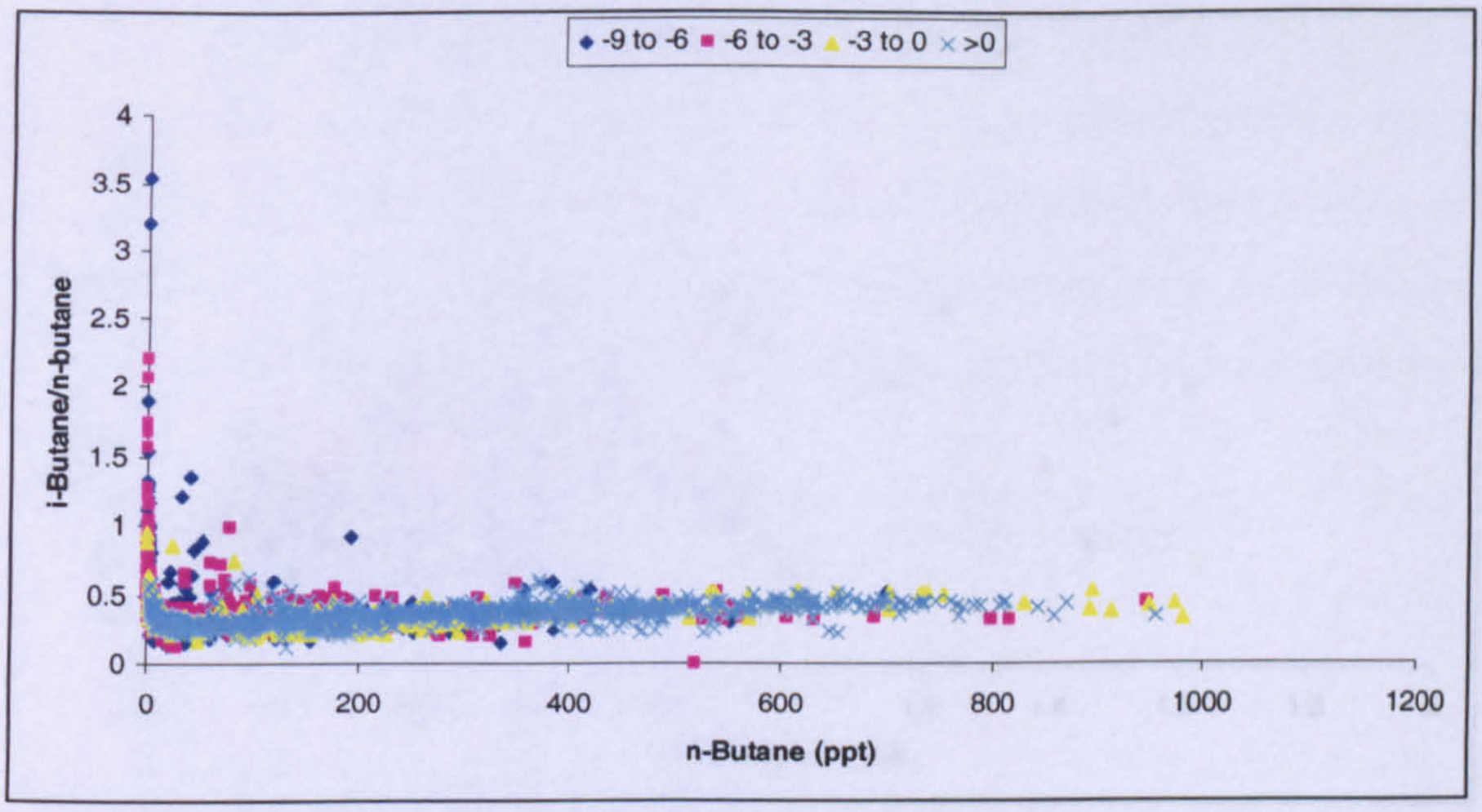

Figure 6.10 i-/n-Butane compared with n-butane separated by trajectory during 2005 and 2006.

Hopkins, et al. (2002) reported the effects of Cl in the marine boundary layer by comparing i-butane/n-butane ratio with i-butane/propane. From Table 6.3 it can be deduced that the rates of removal for i-butane, n-butane and propane by reaction with OH is 2:2:1 respectively. For Cl the comparative rates of removal are 1:2:1. If OH is the dominant removal mechanism the i-butane/n-butane ratio will remain constant and the i-butane/propane will increase. If Cl is the major removal mechanism the i-butane/n-butane ratio would increase and i-butane/propane remain constant. Figure 6.11 shows i-butane/n-butane compared with i-butane/propane separated by trajectory. There appears to be a lot of information in this graph with a wide spread of values in some trajectory sector. To aid analysis of these data Figure 6.12 plots i-butane/n-butane with i-butane/propane for the clean, Atlantic trajectory sector and European air masses. The clean air sectors show an almost linear correlation between i-butane/n-butane and i-butane/propane, possibly indicating removal by both OH and Cl reactions. The European sector is less spread out and appears to fork into two reaction pathways. One where the i-butane/n-butane ratio is constant and i-butane/propane increases and one where i-butane/propane remains relatively constant as i-butane/n-butane increases. Again this could suggest the possibility of Cl along with OH chemistry.

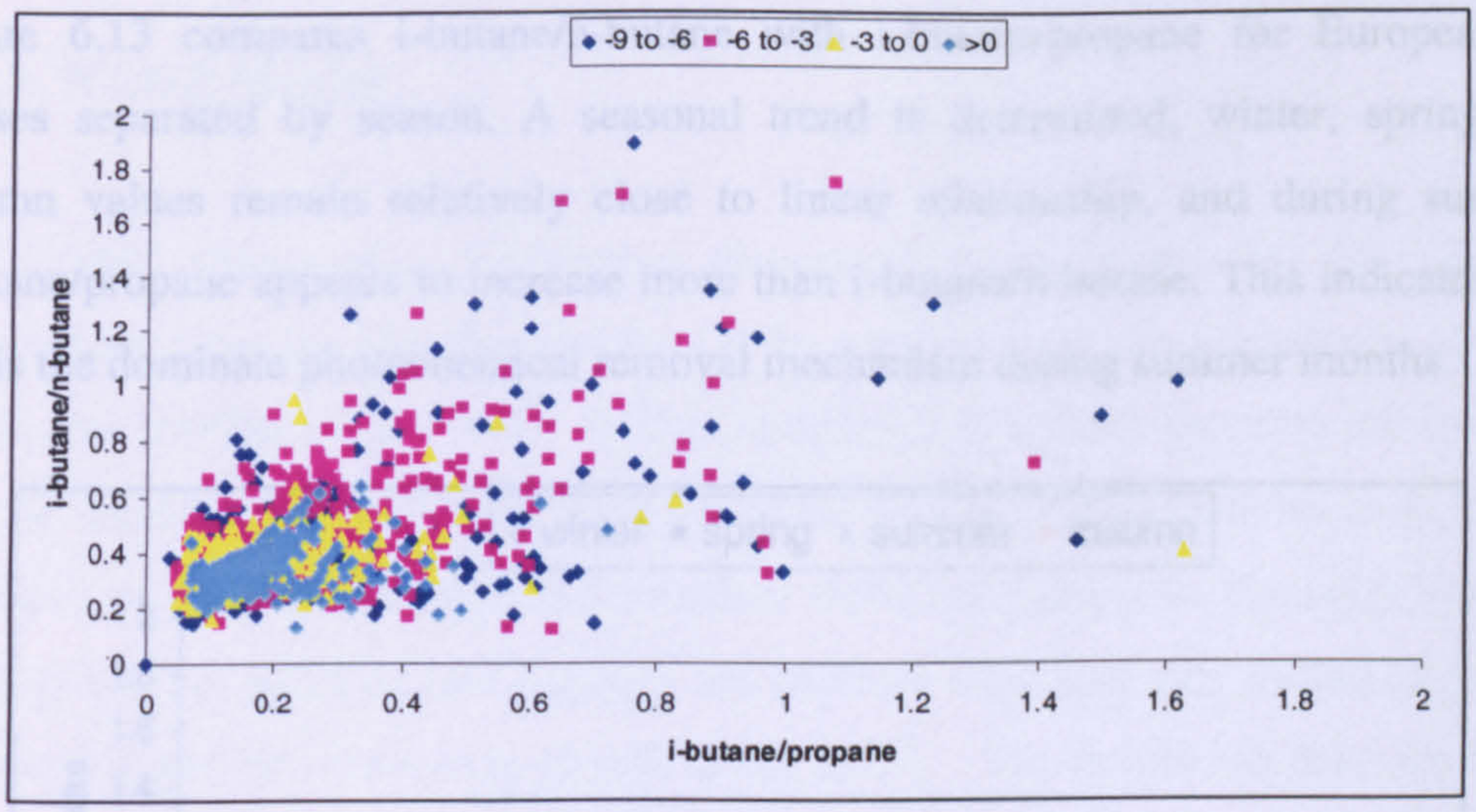

Figure 6.11 i-Butane/n-butane compared with i-butane/propane measured during 2005 and 2006.

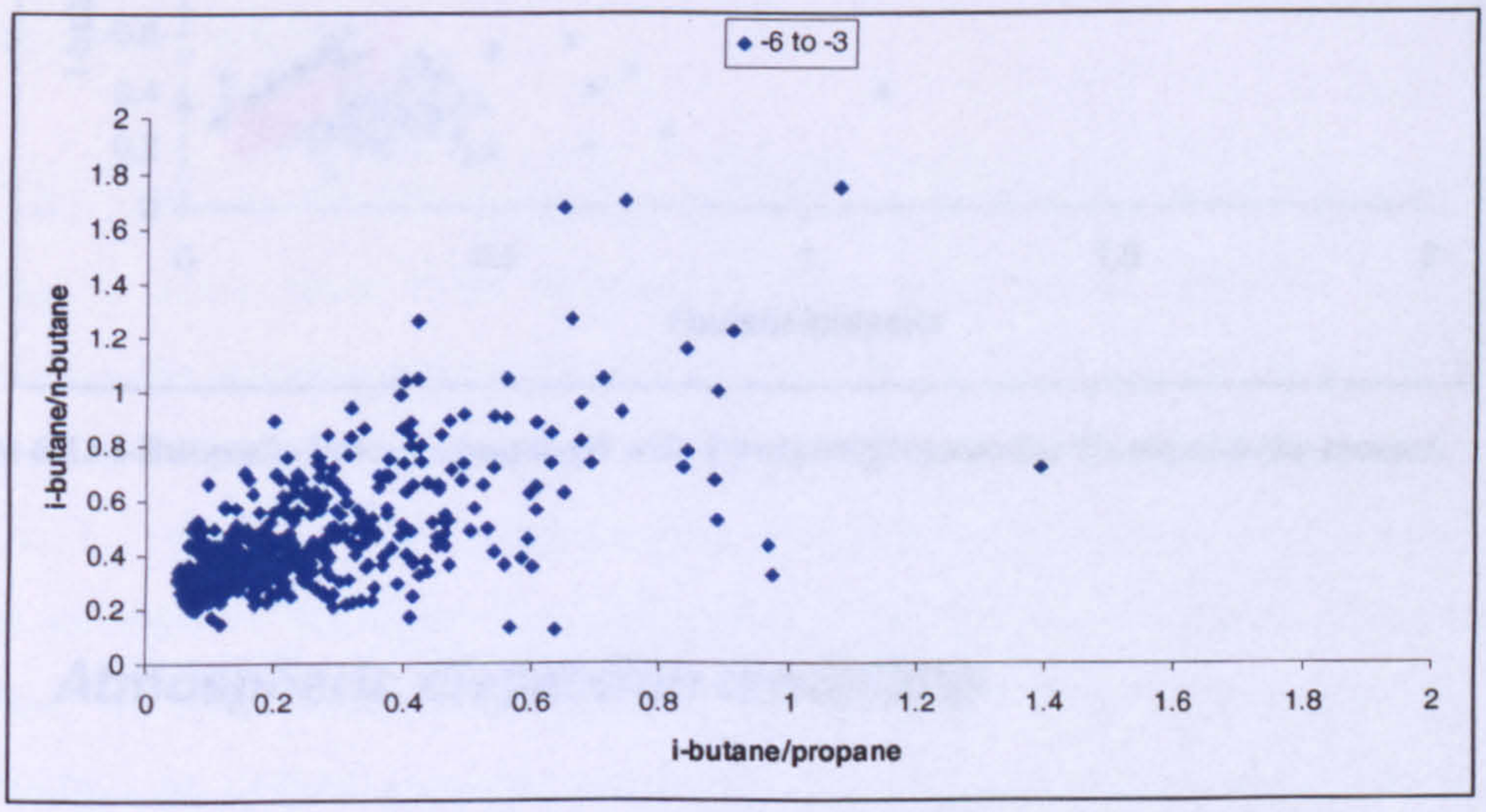

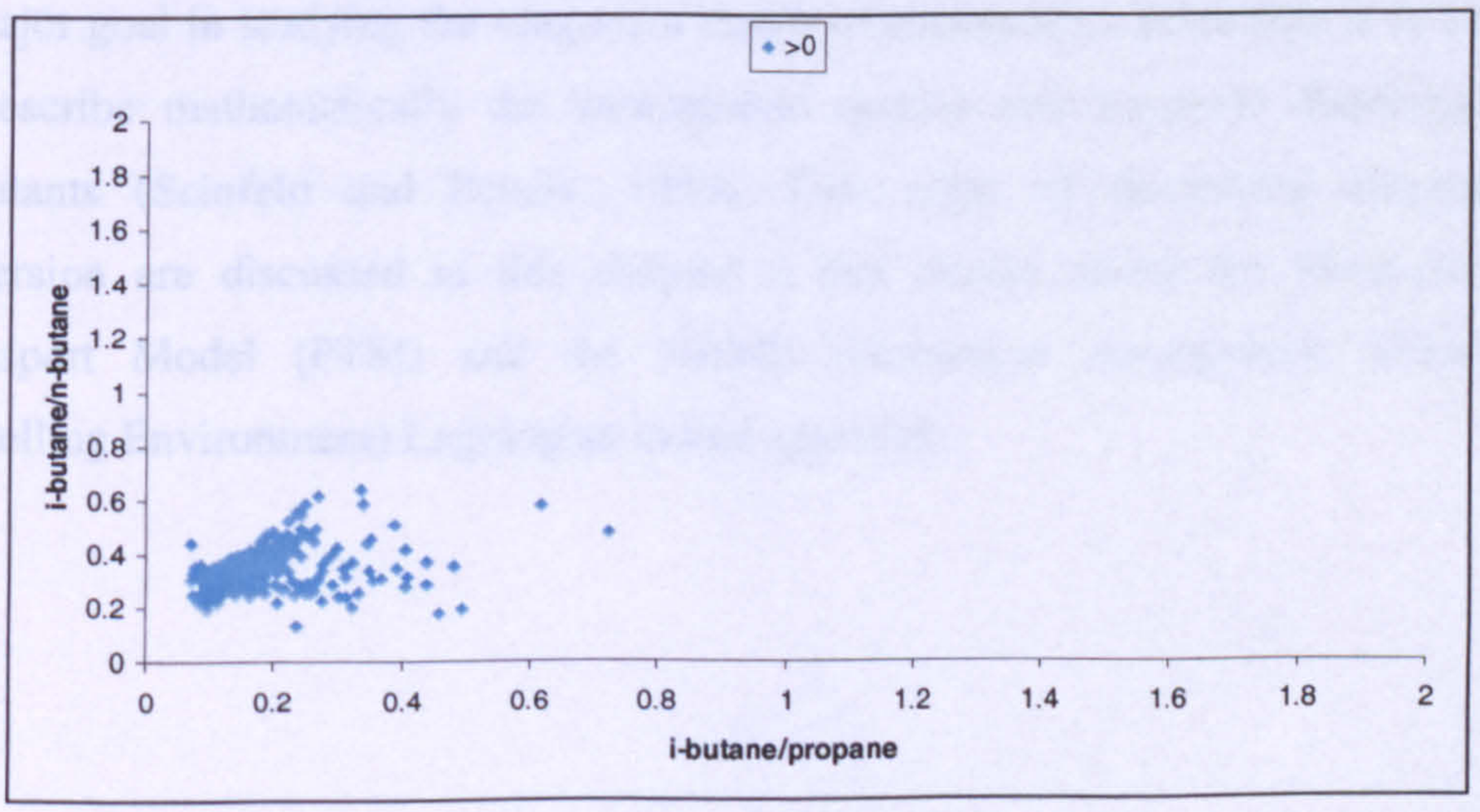

Figure 6.12 Plots of i-butane/n-butane with i-butane/propane in (a) clean, Atlantic sector (b) European sector.

Figure 6.13 compares i-butane/n-butane with i-butane/propane for European air masses separated by season. A seasonal trend is determined, winter, spring and autumn values remain relatively close to linear relationship, and during summer i-butane/propane appears to increase more than i-butane/n-butane. This indicates that OH is the dominate photochemical removal mechanism during summer months.

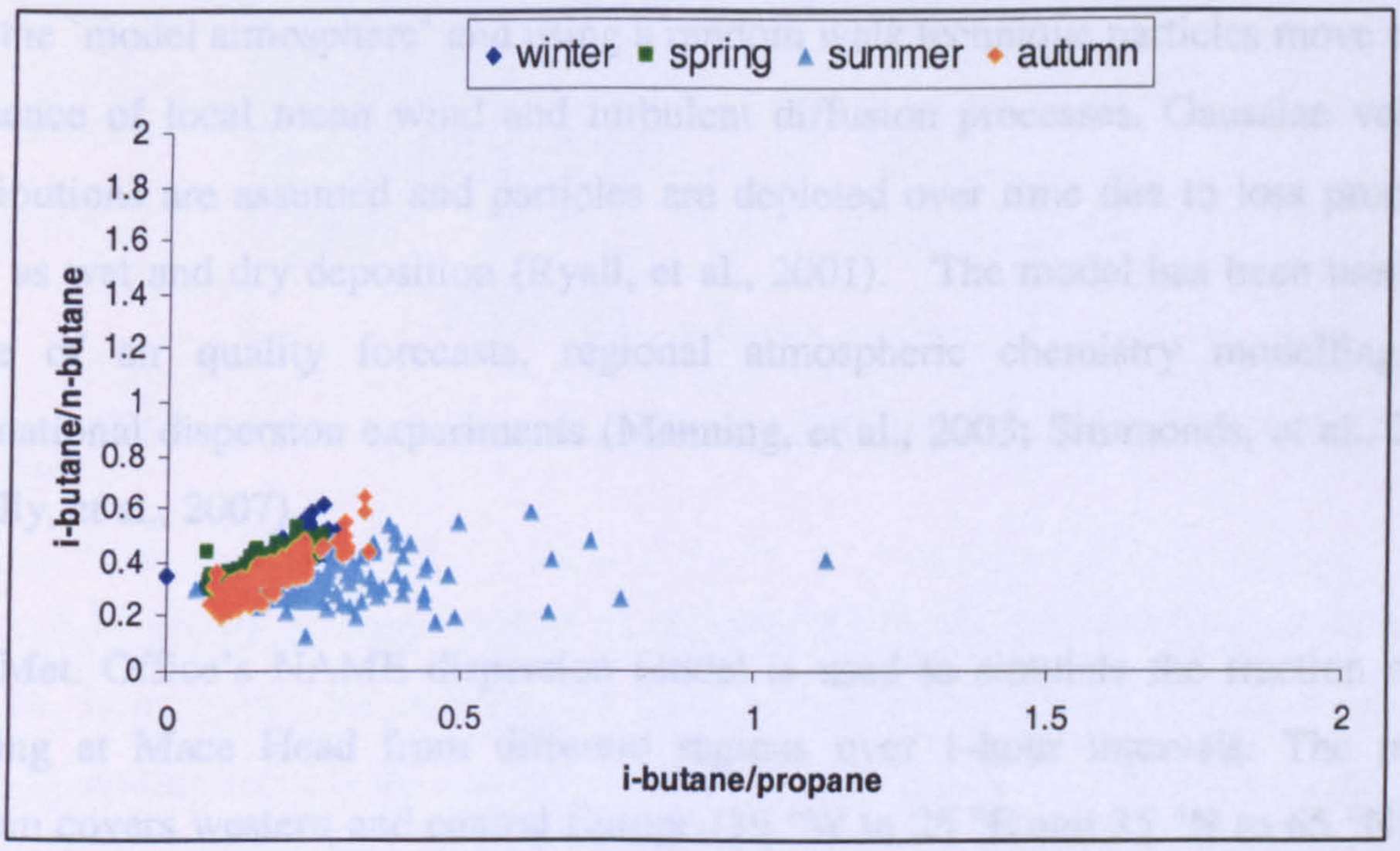

Figure 6.13 i-Butane/n-butane compared with i-butane/propane for European air masses.

6.7. Atmospheric dispersion modelling

A major goal in studying the long-term trends of atmospheric pollutants is to be able to describe mathematically the atmospheric special and temporal distribution of pollutants (Seinfeld and Pandis, 1998). Two ways of describing atmospheric dispersion are discussed in this chapter; a box model called the Photochemical Transport Model (PTM) and the NAME (Numerical Atmospheric Dispersion Modelling Environment) Lagrangian model approach.

6.7.1. NAME model

The NAME model is a Lagrangian dispersion model driven by 3D synoptic meteorology from the UK Meteorology Office complex numerical weather prediction model, the Unified Model (UN). A large number of imaginary particles are released into the `model atmosphere' and using a random walk technique particles move by the influence of local mean wind and turbulent diffusion processes. Gaussian velocity distributions are assumed and particles are depleted over time due to loss processes such as wet and dry deposition (Ryall, et al., 2001). The model has been used in a range of air quality forecasts, regional atmospheric chemistry modelling and international dispersion experiments (Manning, et al., 2003; Simmonds, et al., 2006; Greally, et al., 2007).

The Met. Office's NAME dispersion model is used to simulate the fraction of air arriving at Mace Head from different regions over 1-hour intervals. The model domain covers western and central Europe (19 °W to 25 °E and 35 °N to 65 °N) and is split into a number of grid cells (0.833° × 0.555° × 0-200 m resolution). A constant release (1 g m^{-2} s^{-1}) of inert particles are emitted from grid cells into the lowest 40 m of the atmosphere. Meteorological data, taken from the Met. Office's UM, is used to simulate dilution, with Mace Head as the receptor. Every time step (15 min) information on emitted particles within the grid cell over Mace Head are recorded (including each particles source location and emission time). The model output is presented in 3-hourly attribution maps, showing the spread of emitted particles arriving at Mace Head, a typical example can be seen in Figure 6.14 (Manning, et al., 2003).

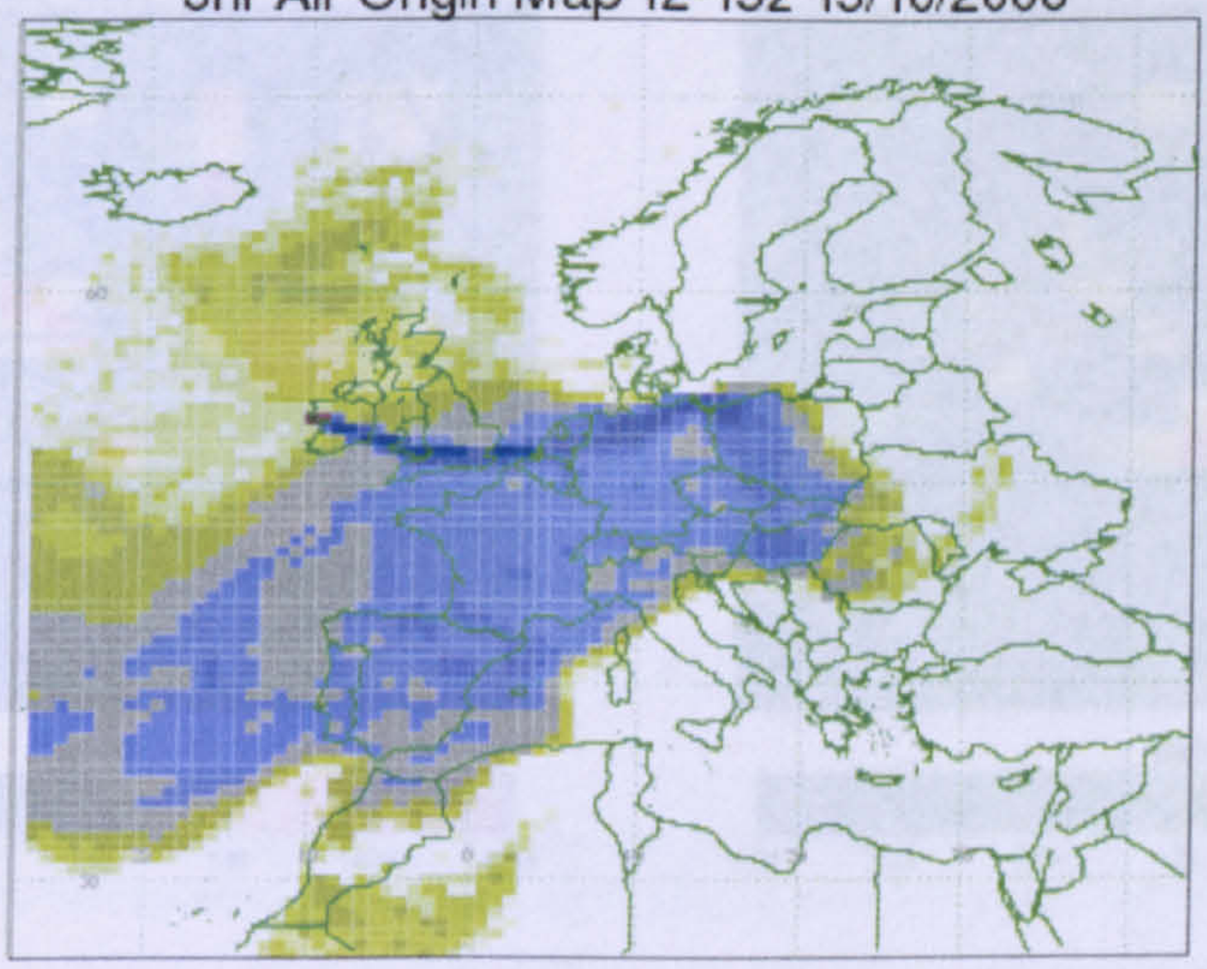

Figure 6.14 Example of an attribution map showing a pollution event (15 October 2006, 1200-1500 GMT).

Figure 6.14 shows a large number of regions which can be identified as emission sources. Long-term data sets can be used to further investigate emission sources. Back-attribution records the number of times each grid cell contributes to Mace Head and the magnitude of the contribution. The closer the grid cells are to Mace Head the more they contribute to Mace Head air masses and are resolved with a higher degree of accuracy than distant grid cells (Manning, et al., 2003). Using this technique emission maps have been derived for ethane and benzene, shown in Figure 6.15. The emission maps of ethane and benzene show a similar pattern, with strong emission sources for both compounds in northern Italy, Germany, France and southern UK. A potential source is indicated in the North Sea, which could suggest a source of ethane and benzene from off-shore oil and gas fields. However, this could be an artefact of the method, so no direct conclusions can yet be drawn from this event; more data are needed to draw any conclusions from this.

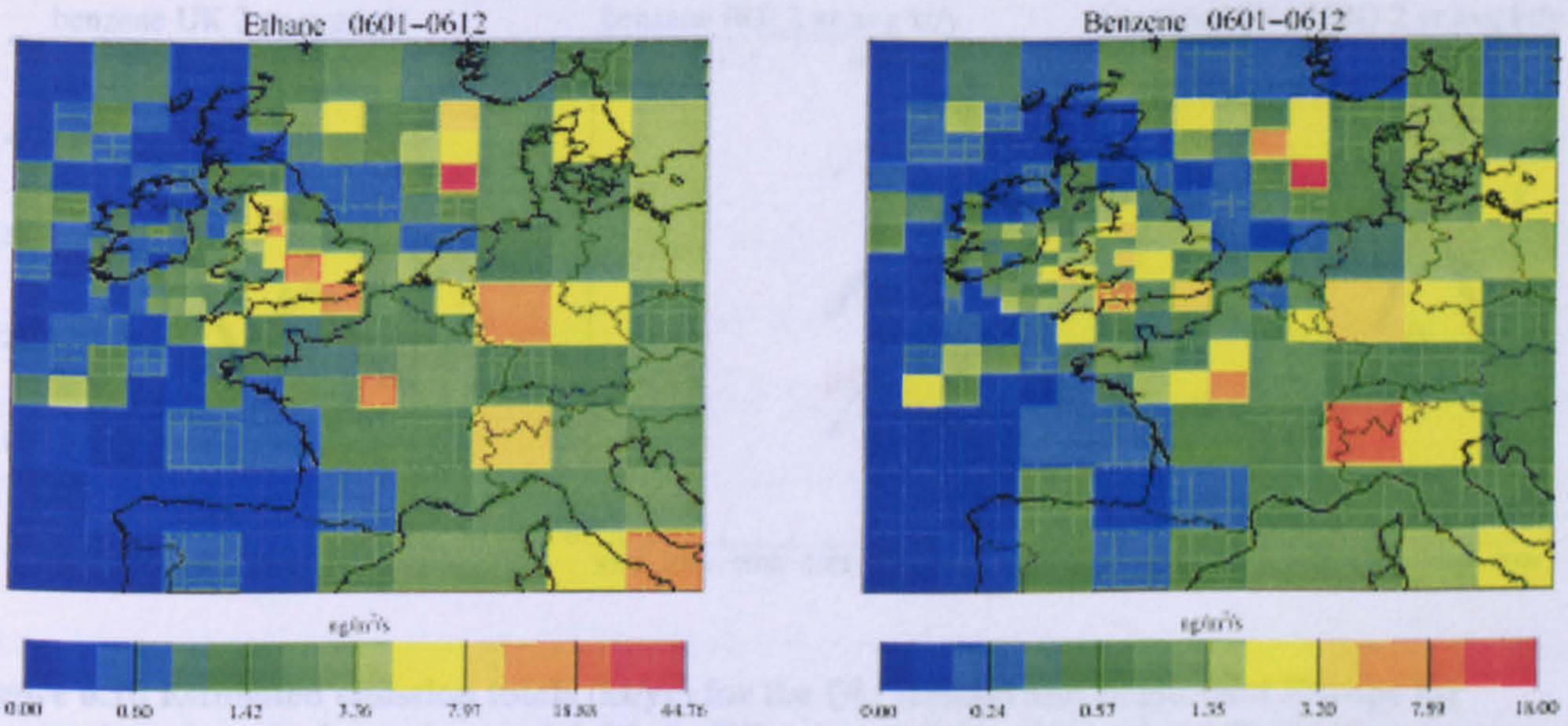

Figure 6.15 NAME inversion model used to estimate the annual average emission distribution of (a) ethane and (b) benzene in 2006.

Another method of calculating emissions is the CO ratio method, benzene emissions have been calculated in this way. First, a filter is applied to define baseline and above baseline benzene and CO at Mace Head. The baseline is removed from the data to generate a ratio of above baseline benzene to above baseline CO. Annual benzene emissions are estimated by multiplying the benzene/CO annual (mass) ratio by the reported annual CO emissions (Greally, et al., 2007). This is the weaker of the two NAME methods as the ratio between hydrocarbons and CO will vary depending upon season and lifetimes. The method is more useful for compounds such as HFCs which show little annual variation.

Two year estimated emission totals (kt/yr) for the UK, Ireland and north west Europe (UK, Ireland, France, Germany, Denmark, Belgium, Luxemburg, Netherlands) for benzene based on the inversion model (blue), and CO ratio method (red) and the reported UK NAEI inventory (black) are shown in Figure 6.16. Benzene data from Mace Head has been run through the NAME model (the inversion and CO ratio) dating back to 2001. 2001–2004 benzene data is taken from the old NMHC ADS-GCFID instrument, 2005–2006 from the Medusa-GCMS. The agreement between the estimated benzene emissions from the NAME model with the UK NAEI inventory is encouraging, see Figure 6.16.

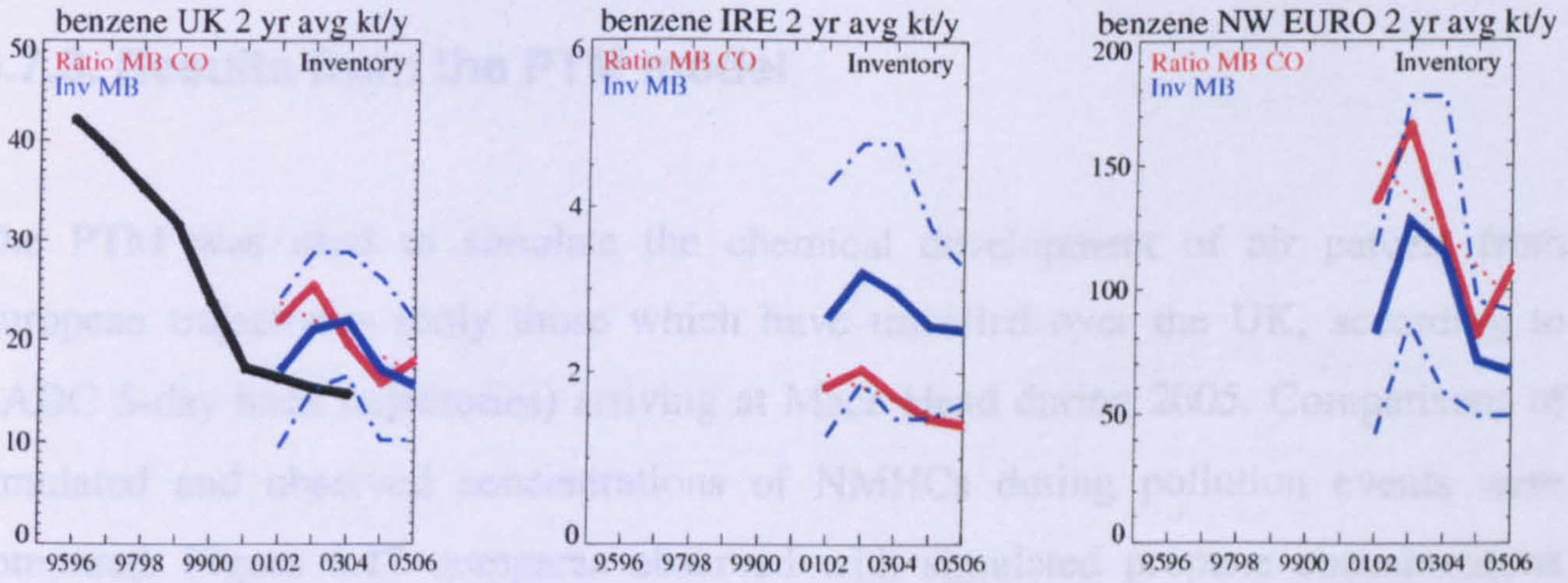

Figure 6.16 Estimated emission totals (kt/yr) for the Uk, Ireland and north west Europe for benzene based on the inversion model (blue), CO ratio methd (red) and the UK NAEI inventory (black).

6.7.2. PTM

The PTM is a Lagrangian model consisting of a single layer model, an air parcel extends from the earths surface to the top of the boundary layer with 10 km x 10 km horizontal dimensions. Diurnal variation of the boundary layer is represented by a variation in boundary layer height from 300 m at night to a maximum of 1300 m in the afternoon. The model follows the chemical development of an air parcel as it travels over emission grids. An air parcel will pick up emissions of NO_x, CO, SO_2, methane and NMHCs details of emission inventories employed in the model are described by Derwent, et al., 1996. Chemical processing is described by the Common Representative Intermediates (CRI) mechanism which was developed from the Master Chemical Mechanism (MCM) version 2.0, the details of which are reported in Jenkin, et al. (2002). This model was used to simulate the chemical development over 5-days along trajectories obtained from BADC website (www.badc.nerc.ac.uk) arriving at Mace Head. Model runs were carried out with the FACSIMILE for Windows kinetics integration package, version 3.5 (MCPA Software). Integrations were performed with an hourly time-step.

6.7.3. Results from the PTM model

The PTM was used to simulate the chemical development of air parcels from European trajectories (only those which have travelled over the UK, according to BADC 5-day back trajectories) arriving at Mace Head during 2005. Comparisons of simulated and observed concentrations of NMHCs during pollution events were compared. Figure 6.17 compares observed with simulated propane concentrations from Mace Head during May 2005. Back-trajectories show air masses travelling over Europe, including the UK before arriving at Mace Head. From 8th May to 10th May air masses originate from the north and Scandinavia then travel over the North Sea before arriving at Mace Head. PTM results over these trajectories give an excellent correlation for propane. PTM results from trajectories which pass over the UK before arriving at Mace Head result in an over-prediction of propane compared to observations.

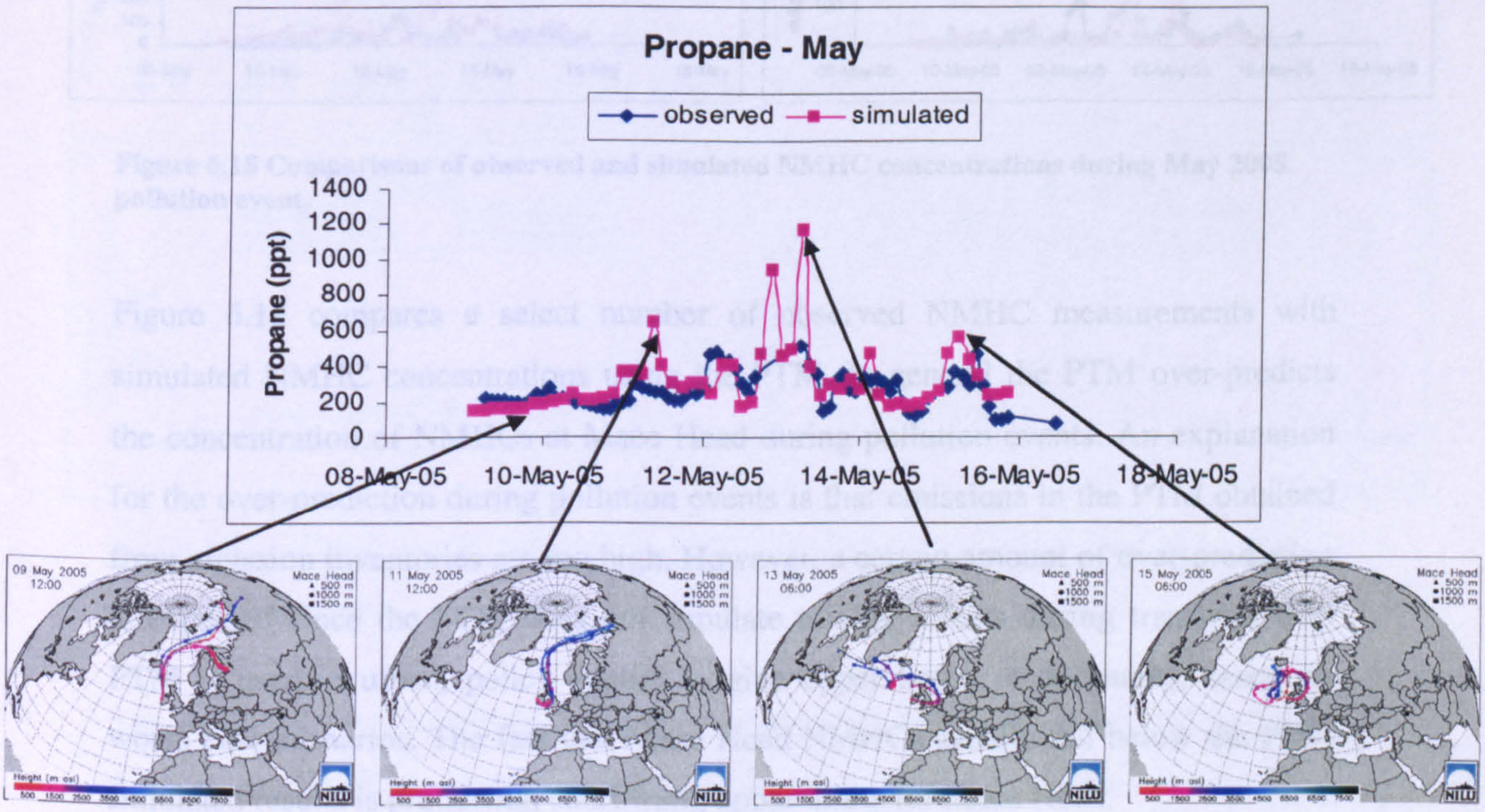

Figure 6.17 Comparison of observed and simulated propane concentrations during a pollution event in May 2005. 5-day back-trajectories downloaded from NIST, 2007 are included for comparison.

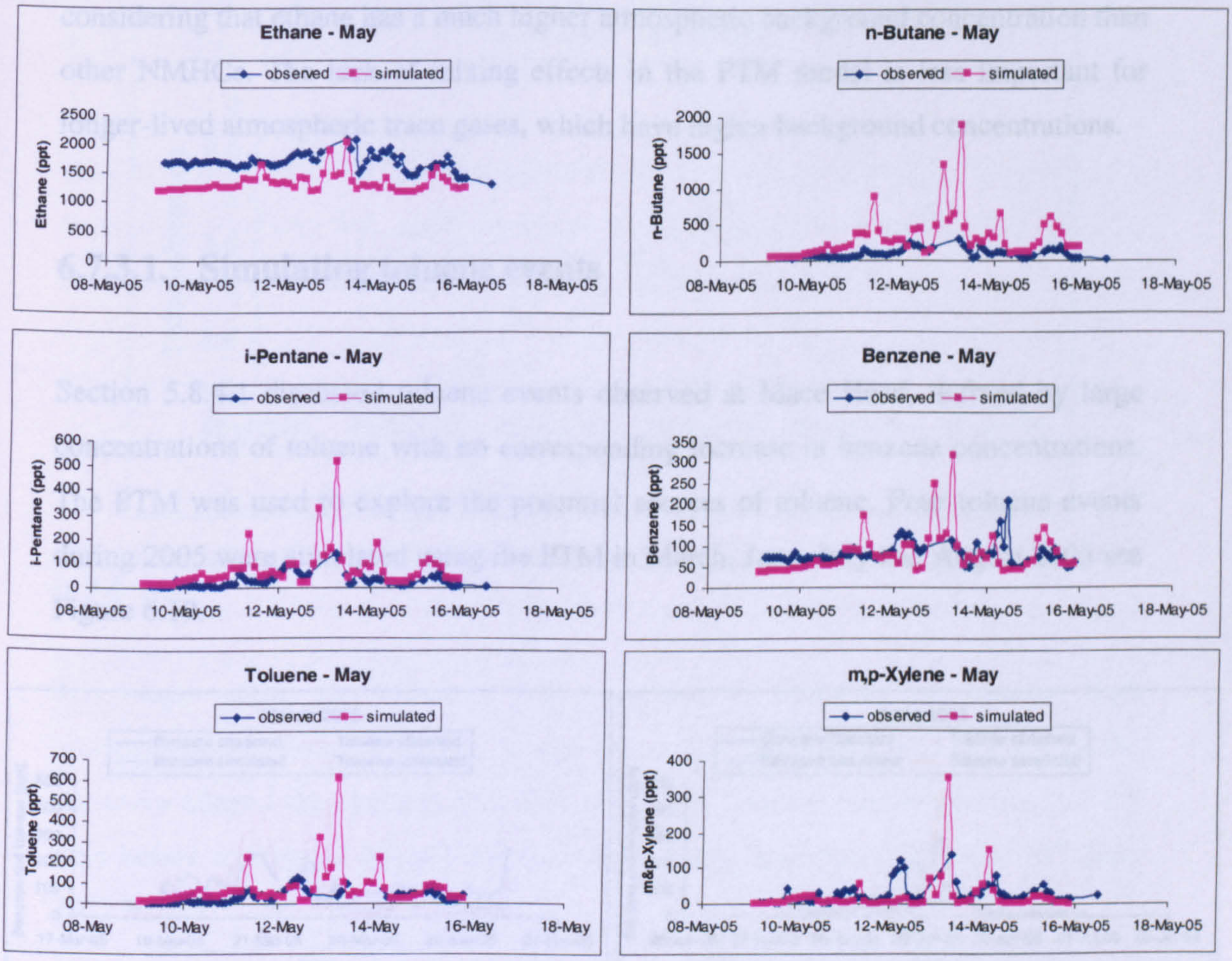

Figure 6.18 Comparisons of observed and simulated NMHC concentrations during May 2005 pollution event.

Figure 6.18 compares a select number of observed NMHC measurements with simulated NMHC concentrations using the PTM. In general the PTM over-predicts the concentration of NMHCs at Mace Head during pollution events. An explanation for the over-prediction during pollution events is that emissions in the PTM obtained from emission inventories are too high. However, a certain amount of over-prediction is expected since the PTM does not simulate mixing effects during transport. The PTM is used in urban, policy studies to give upper limits of pollutants, based on worse case scenarios. The fact that Mace Head NMHCs usually fall below the PTM simulated results is promising, confirming upper limits for Mace Head.

Comparison of the PTM with observed measurements of ethane shows a different case, the PTM is closely correlated with observed data and ethane is not over-predicted by the PTM during the May, 2005 pollution event. This can be explained

considering that ethane has a much higher atmospheric background concentration than other NMHCs. The lack of mixing effects in the PTM model is less important for longer-lived atmospheric trace gases, which have higher background concentrations.

6.7.3.1. Simulating toluene events

Section 5.8.4.1 discussed toluene events observed at Mace Head, defined by large concentrations of toluene with no corresponding increase in benzene concentrations. The PTM was used to explore the potential sources of toluene. Four toluene events during 2005 were simulated using the PTM in March, June, July and August 2005 see Figure 6.19.

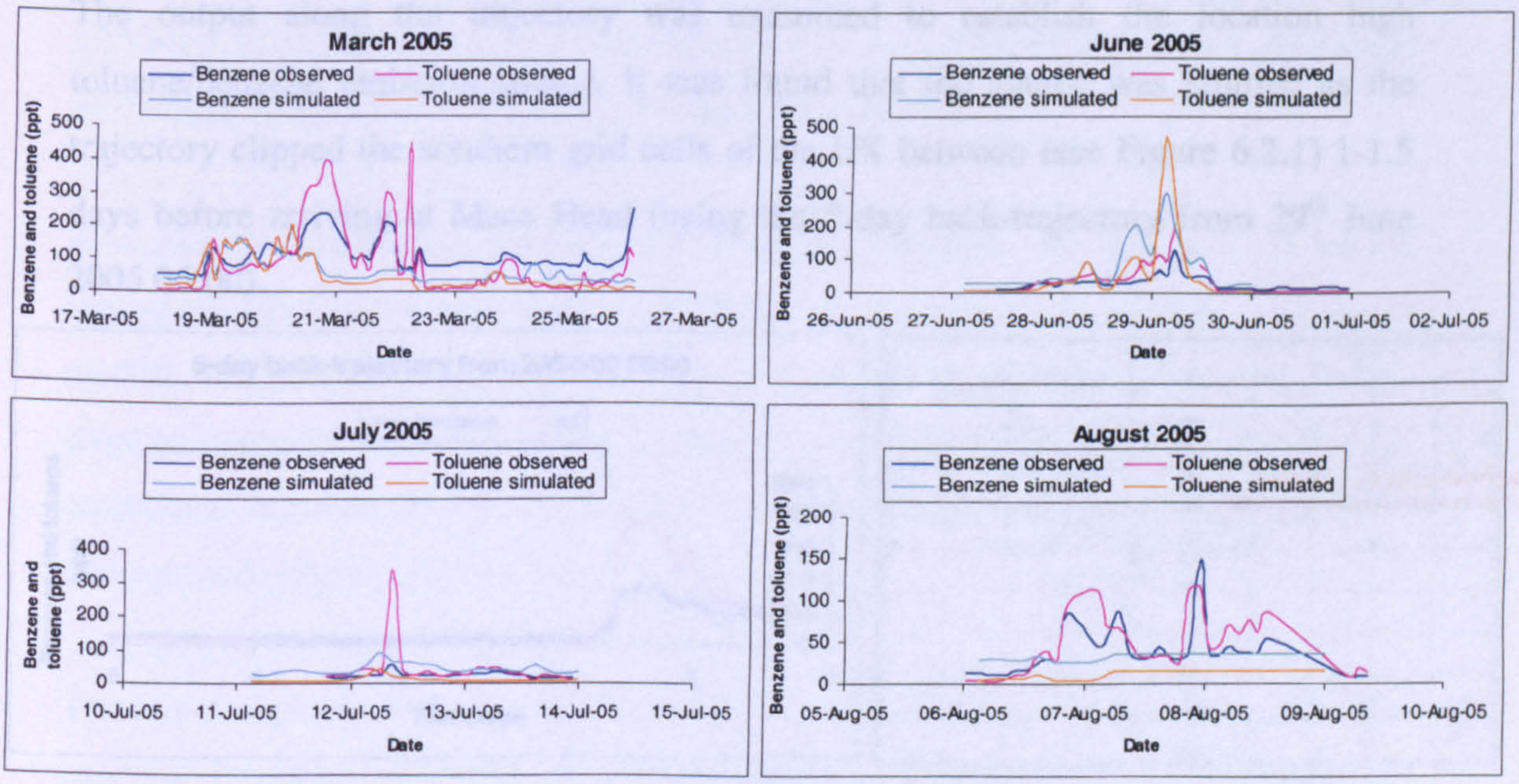

Figure 6.19 Comparison between observed and simulated benzene and toluene during four toluene events in 2005.

The observed high toluene/benzene ratio was replicated in the June 2005 toluene event using the PTM, as seen in Figure 6.19. Although the actual concentrations of benzene and toluene are over-predicted using the PTM, the ratio of toluene/benzene is a reasonable representation, see Figure 6.20.

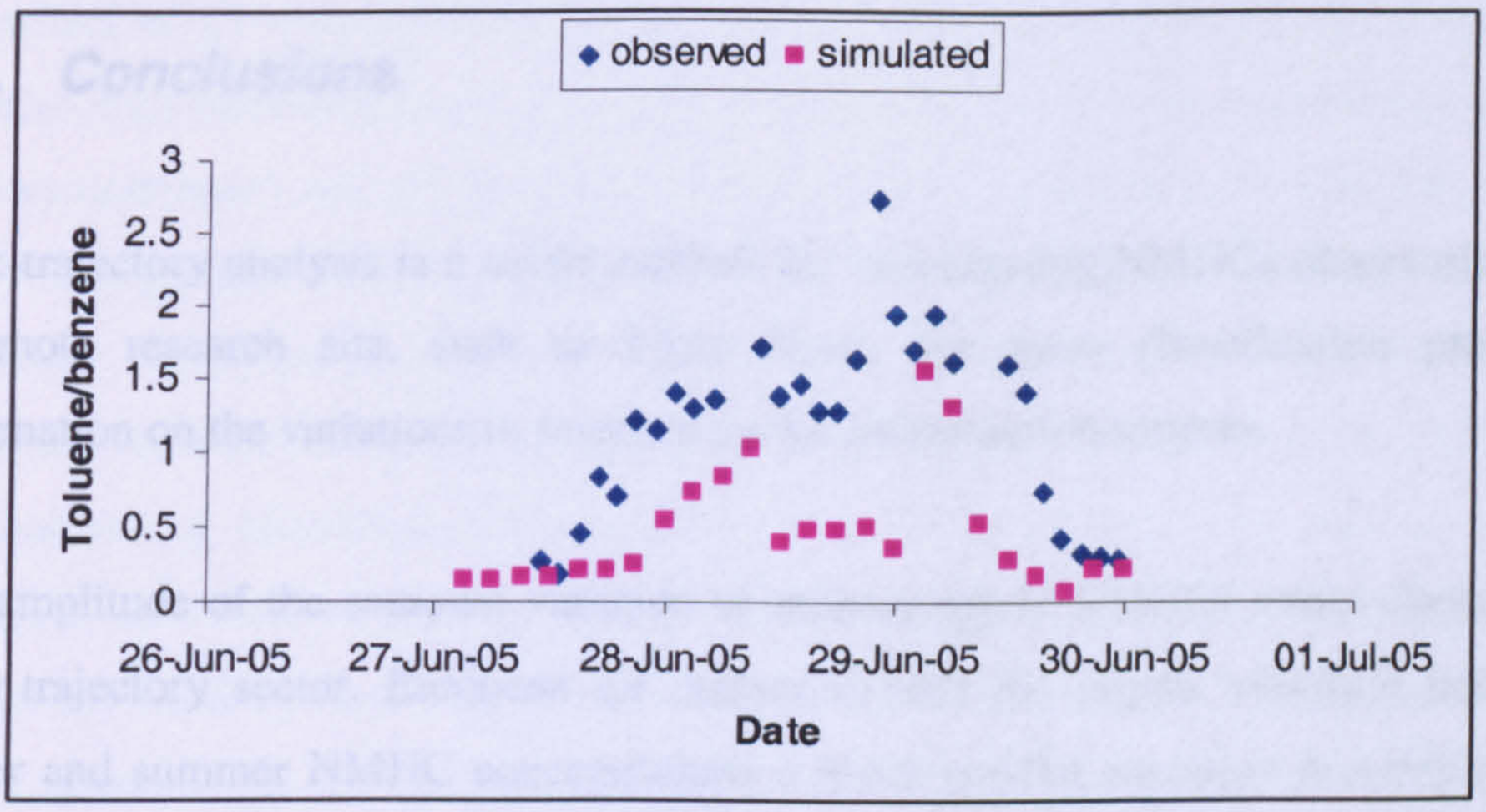

Figure 6.20 Comparing the observed and simulated toluene/benzene ratio during a toluene event in July 2005.

The output along the trajectory was examined to establish the location high toluene/benzene emission source. It was found that the source was emitted as the trajectory clipped the southern grid cells of the UK between (see Figure 6.2.1) 1-1.5 days before arriving at Mace Head (using the 5-day back-trajectory from 29th June 2005 06:00).

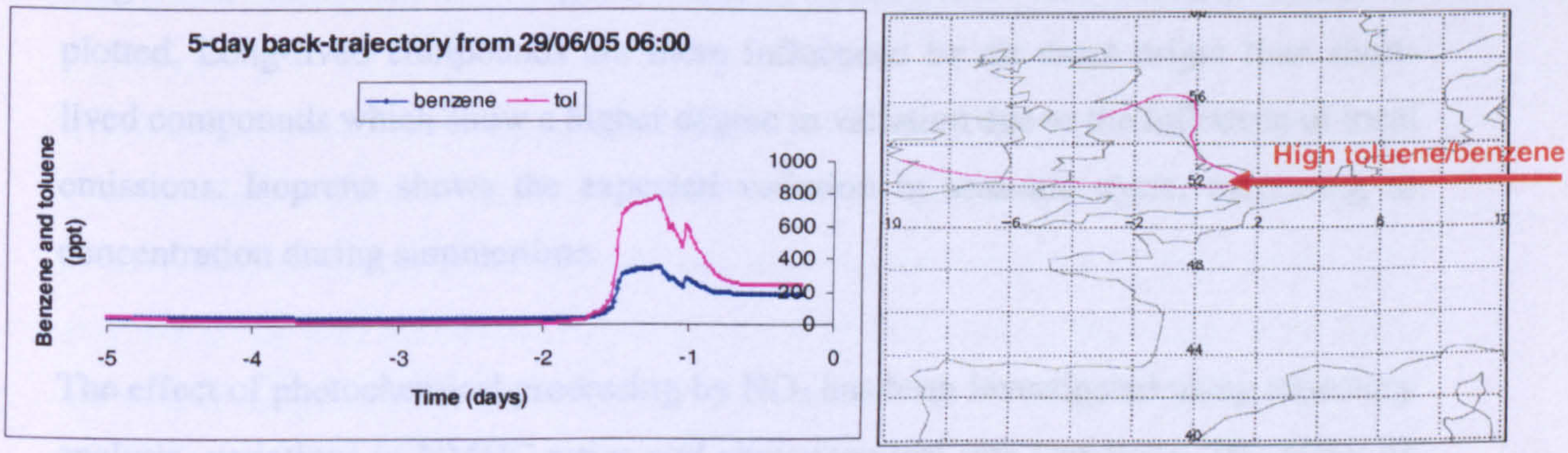

Figure 6.21 Locating the source of the high toluene/benzene emission during the Mace Head, June 2005 toluene event.

6.8. Conclusions

Back-trajectory analysis is a useful method for investigating NMHCs observations in a remote research site, such as Mace Head. Air mass classification provides information on the variations in seasonal cycles and emission sources.

The amplitude of the seasonal variation of anthropogenic NMHCs varies depending upon trajectory sector. European air masses exhibit the largest variation between winter and summer NMHC concentrations a much smaller variation is exhibited in clean air masses, particularly the ultra clean (-9 to -6) sector. This is expected due to the increased NMHC concentrations observed at Mace Head during wintertime pollution events, when OH concentrations are low. During summer the concentrations of NMHCs from all sectors are more closely matched, indicating sampled air masses are well processed photochemically by reaction with OH.

A significant difference between the seasonal variation, by trajectory sector of long-lived, short-lived and biogenic NMHCs is observed when monthly means are plotted. Long-lived compounds are more influenced by air mass origin than short-lived compounds which show a higher degree in variation due to the influence of local emissions. Isoprene shows the expected variation in seasonal cycle, increasing in concentration during summertime.

The effect of photochemical processing by NO_3 has been investigated using trajectory analysis, variations in NMHC ratios and photochemical rate equations. The effect of NO_3 was investigated by analysing the i-butane/n-butane ratio by sector and season. In all sectors, a decrease in the i-butane/n-butane ratio was observed during summer months. This change in i-butane/n-butane cannot be explained by OH chemistry. Photochemical reaction with NO_3 could explain the change in butane isomer ratio, as reaction with NO_3 preferentially removes i-butane relative to n-butane causing a decrease in butane isomer ratio. However the change in i-butane/n-butane between summer and winter is too large a change to be fully explained by NO_3 chemistry. Thus this observation is explained by a change in butane isomer sources between summer and winter or a combination of both emissions and NO_3 chemistry.

The effect of Cl chemistry has been investigated by comparing the ratios of three alkanes; ln(n-butane/ethane) versus ln(propane/ethane), ln(n-butane/ethane) versus ln(i-butane/ethane) and ln(i-butane/n-butane) versus i-butane/propane (Parrish, et al., 1992). Comparison of ln(n-butane/ethane) versus ln(propane/ethane) produced a slope consistent with previous reports (Parrish, et al., 1992; Swanson, et al., 2003) and below the calculated kinetic slope, consistent with effects of dilution or Cl chemistry. Comparison of ln(n-butane/ethane) versus ln(i-butane/ethane) was carried out to minimise the effect of dilution by examining the correlation between i-butane and n-butane, NMHCs with similar lifetime with respect to OH, since diluting air will be of the same butane isomer ratio. This slope is in good agreement with the kinetic slope and suggests the variation in observed slope and kinetic slope of ln(n-butane/ethane) versus ln(propane/ethane) is due to dilution, not Cl chemistry. The effect of Cl was further examined using a method utilised by Hopkins, et al., 2002, examining the i-butane/n-butane versus i-butane/propane correlation. The linear correlation suggests that both OH and Cl play a role in the photochemical aging of NMHCs. Examining the seasonal variation in this ratio for European air masses suggest the effects of Cl to be less significant during summer months, when OH concentrations are high, OH is the dominant removal pathway during summertime.

The Met Office's NAME dispersion model was used to estimate source regions for NMHC observations at Mace Head. The NAME inversion method was used to produce emission maps for ethane and benzene. Ethane and benzene were selected for analysis given they are two of the longer-lived NMHCs (emission maps for propane are also to be generated) hence they are less influenced by local sources near Mace Head. The emission maps present a picture for 2006, however more years data is needed to generate a more complete image of the source regions, and to identify and rule out any possible artefacts generated from the model itself. The NAME inversion method and CO ratio method were used to compare estimated ethane and benzene emissions for the UK, Ireland and Europe. The results presented here are promising, with benzene estimated closely related to the UK inventory for benzene.

The PTM was used to simulate the transport of European emissions to Mace Head. Simulated results have been compared with observations during Mace Head pollution events. The model was found, in general to over-predict the concentrations of

NMHCs during pollution events. This could suggest the emissions in the model are too high; however given that the NAME model benzene emission estimates agree with the UK inventory used in the PTM model this is unlikely. Over-prediction is an inherent problem with the PTM since it is an urban model and does not account for mixing during transport and the PTM relies on single emission trajectories, multi-emission trajectories (as used in the NAME analysis) is much better as the trajectory won't miss an emission grid and a range of emissions and concentrations are averaged giving a more realistic output. However, this is a useful tool; the PTM is an urban model utilised to simulate the worse case scenario, giving upper limits in terms of pollutant concentrations. The PTM can be used for the analysis of worse case scenarios for the transport of emissions from Europe to Mace Head.

The PTM was utilised to model the benzene and toluene concentrations during toluene events (discussed in Section 5.8.4.1 and 6.4.4.1). Out of the four toluene events chosen for analysis, the PTM simulates high toluene/benzene ratio during one event, in June 2005. Although concentrations of toluene and benzene are over-predicted, the ratio of toluene/benzene matches quite well the observed toluene/benzene ratio. This has proved to be a useful tool in identifying where the high toluene/benzene emission occurred, located from tracking the emissions along a trajectory and following latitudes and longitudes in the trajectory. The simulated emission could be an artefact of the trajectory, since it is shown to "clip" the emission grids covering London. However, there is certainly a lot more scope for research in this area, there are preliminary results to see how the PTM performed simulated a remote environment.

7. Conclusions and recommendations

7.1. Overall conclusions

7.1.1. Chapter 2: Retention of analytes on selected adsorbents

- The new NMHC instrument aims to solve the issue of water management with the use of a bulk-trap, at ambient temperature to fractionate between C_2 hydrocarbons and $\geq C_3$ NMHCs.
- BTVs using the elution technique suggest a 3 g Hayesep D bulk-trap has the fractionating ability to separate C_2 hydrocarbons and water from $\geq C_3$ NMHCs. C_2 hydrocarbons and water can be sent through a Nafion drier to a C_2 hydrocarbon micro-trap. While $\geq C_3$ NMHCs are back-flushed and heated to transfer them to a refocusing micro-trap.
- Carbosieve SIII was the strongest adsorbent tested making it an ideal adsorbent for use in a micro-trap specifically targeting C_2 hydrocarbons.
- A weaker, less retentive adsorbent was needed to act as a refocusing micro-trap for the $\geq C_3$ NMHCs, Hayesep D was chosen for this purpose.

7.1.2. Chapter 3: Chromatographic separation of NMHCs

- The Alumina PLOT (both Al_2O_3/KCl and Al_2O_3/Na_2SO_4) were the only columns tested that reasonably resolve C_2-C_8 hydrocarbons.
- The CarboBOND, Carboxen 1016 and Gaspro columns exhibit reasonable resolution of the volatile NMHCs (C_2-C_3 hydrocarbons). These columns could be used to target analysis of volatile NMHCs.

7.1.3. Chapter 4: NMHC instrument design

- BTVs using the Frontal technique and analysing large samples (200-1000 ml) performed on the 3 g Hayesep D bulk-trap proved problematic. The predicted fractionation between the C_2 and $\geq C_3$ hydrocarbons could not be replicated. This is because over a long sampling period (50 ml/min sample flow rate) the bulk-trap was acting in a similar way to a chromatography column, causing the C_2 and C_3 hydrocarbons to merge.
- Back-flushing the bulk-trap with helium and heating to transfer $\geq C_3$ NMHCs to the refocusing trap produced large desorption artefacts.
- New concept for water management involves using an empty stainless steel tube housed at -20 °C, using a Stirling cooler to act as a water trap.
- Another Stirling cooler has been utilised to house an adsorbent micro-trap at -100 °C, decreasing the pre-concentration temperature and hence increasing the sampling size.
- A multi-bed adsorbent micro-trap (Carbosieve SIII and Carboxen 1016) is used to target the pre-concentration of C_2-C_8 hydrocarbons, with a sample capacity of 1 L at -100 °C.
- Problems with the poor peak shape of ethane and ethene on the Al_2O_3/KCl (50 m, 0.53 mm, 10 μm) have been resolved using a 10 mg Carboxen 1016 refocusing micro-trap, held at -100 °C in the same Stirling cooler as the multi-bed adsorbent micro-trap.

7.1.4. Chapter 5: NMHC observations at Mace Head

- Analysis of two years of NMHC data from Mace Head research station using the Medusa-GCMS. The Medusa has been adapted to measure C_2–C_5 alkanes, isoprene, benzene, toluene, m,p-xylene, o-xylene and ethylbenzene.
- Seasonal cycles of NMHCs are presented. All anthropogenic NMHCs exhibit an increase in concentration during winter and decrease in summer months. The amplitude of this cycle controlled by the OH radical and are closely

correlated with CO. Isoprene, being predominately from biogenic sources shows the reverse, increasing in summer months.

- NMHC ratios have been used to identify the possibility of photochemical aging due to Cl and NO_3 (butane and pentane ratios). The changes in ratios of butane and pentane isomers can be explained by changes in emission sources; however Cl and NO_3 chemistry may also play a role. (This idea is explored further in chapter 6).
- NMHC ratios have been used to identify changes in emission sources (toluene/benzene). The observation of periodic 'toluene events' at Mace Head, presumably from solvent emissions has important consequences on using the toluene/benzene ratio to estimate transport time and chemical age of an air mass. (This idea is explored further in chapter 6).

7.1.5. Chapter 6: Trajectory analysis and transport modelling

- Variations in the seasonal cycles of NMHCs with trajectory sector have been identified, with the largest variation present in European trajectories. NMHC seasonal cycles also vary depending upon the relative atmospheric lifetimes; long-lived NMHCs are more influenced by air mass origins than short-lived NMHCs which are influenced by local emissions.
- The effect of NO_3 on the photochemical processing of NMHCs has been investigated using trajectory analysis and the seasonal variation in the i-butane/n-butane ratio. The change in i-butane/n-butane between summer and winter can not be explained by NO_3 alone, it is more likely to be caused by changes in emissions. However, the possibility of NO_3 chemistry cannot be ruled out, extra information is required such as measurements of the nitrate radical, PAN and analysis of butane isomer ratios in other European sites to determine if the observations are local effects.
- The effect of Cl has been investigated comparing the ratios of three alkanes. Some evidence of Cl photochemical processing has been seen, however this is of less importance during summer months, when OH concentrations are high. To draw any definite conclusions of Cl chemistry extra evidence is needed;

measurements of Cl-containing compounds and comparison of NMHC measurements in other European sites.

- The NAME model has been used to identify source regions, producing emission maps for ethane and benzene. The NAME inversion method has also been used to estimate emissions for UK, Ireland and Europe, with benzene estimates in close agreement with the UK inventory.
- The PTM was used to simulate NMHC concentrations during pollution events at Mace Head based on 5-day back-trajectories. PTM over-predicts NMHC concentrations but could provide a useful tool to predict upper limits of NMHCs at Mace Head based on European emissions and to predict emission sources, use of high toluene/benzene ratios have been used as a case study.

7.2. Suggestions for future research

The instrumental set backs encountered during the course of this research mean there are several steps still required to fully engineer an NMHC instrument to the state where it can be deployed to Mace Head for routine NMHC measurements. Additional testing is required to optimise and refine the trapping and chromatographic conditions.

The first tests that need to be carried out are BTV experiments investigating the transfer of NMHCs from the multi-bed adsorbent trap to the refocusing trap. The use of the Apel-Reimer standard and following the same experimental procedures as in Section 4.9.1 can be used for analysis of BTVs and linearity.

The re-design and development of a completely new concept for water management has resulted in the current set-up being dramatically different from the initial instrument lay-out. For testing purposes the instrument was re-structured and re-plumbed around the existing instrument frame and valve configuration. However, since these results are looking promising the frame and valve lay-out needs to be re-considered. It would be advantages to have the Stirling coolers situated outside the instrument frame, allowing easy access to the traps, as these are likely to be the parts that need changing in the instrument. In this case, the Stirling coolers can be placed on top of the instrument (similar to how present), with holes drilled into the top of the

valve enclosure to allow tubing to and from the traps. The instrument frame can be made much smaller to consist of a valve enclosure (same as the current set-up) and a much smaller electronics enclosure to house power supplies, Valco valve actuators and display flow meters and thermocouple temperature displays (omegas). The valve configuration can be simplified to decrease the number of Valco valves to three, a suggested valve configuration is shown in Figure 7.1.

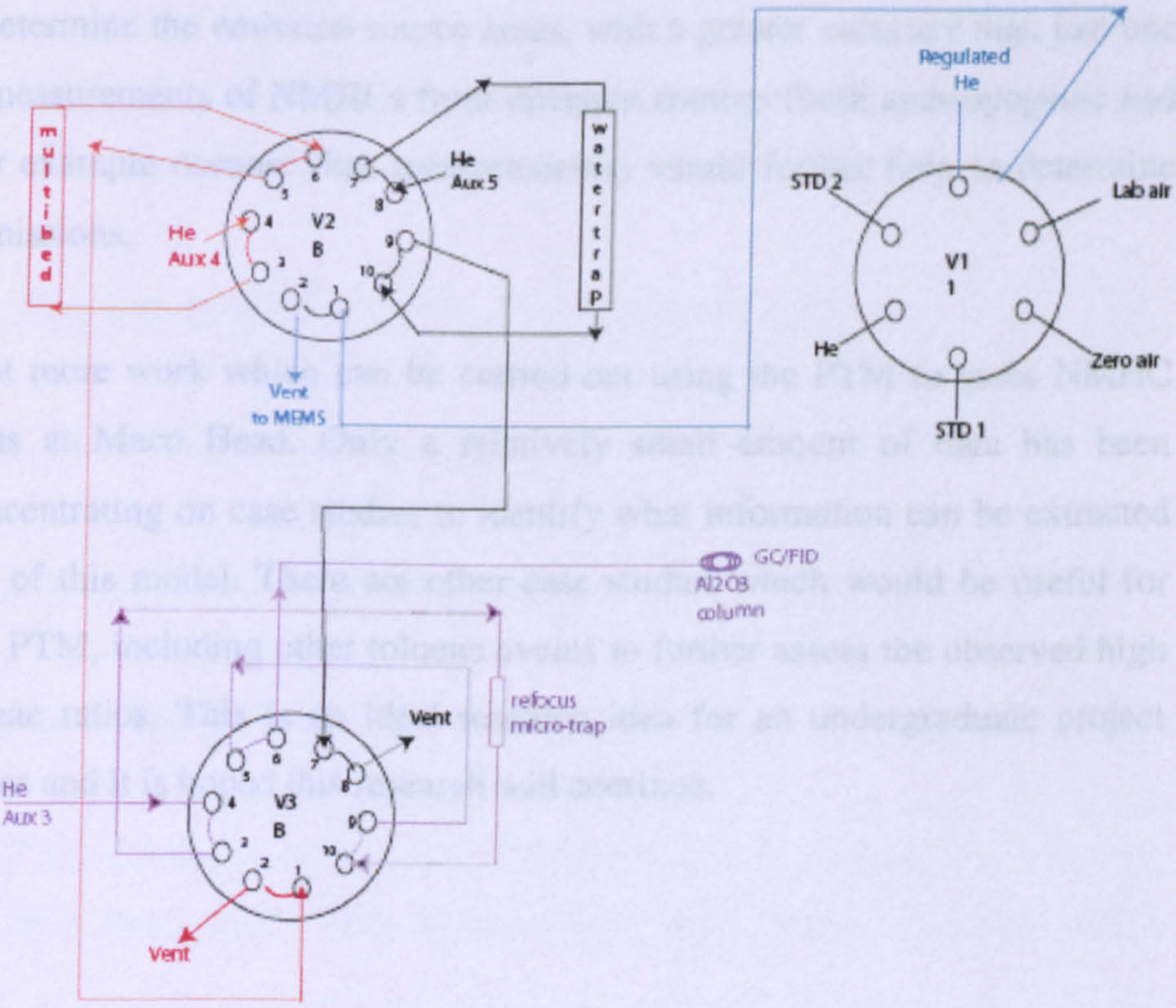

Figure 7.1 Suggested valve configuration.

Once these instrumental changes have been made, the instrument will need to be operated in Bristol before being deployed to Mace Head. Instrument testing includes; running Bristol air samples, calibration with the Apel-Reimer standard to give accurate concentrations and testing the general operational procedures required. There is probably 6-12 months worth of work to prepare the instrument for deployment in Mace Head and it is hoped another PhD student (funding pending) will continue this work.

The in-situ long-term measurements of NMHCs at Mace Head have provided a lot of useful information in terms of assessing the seasonal NMHC cycles to determine any

deviations in sources, assessments of the photochemical processing of air masses during transport to Mace Head and identifying biogenic emissions. This study as speculated how change in sources can explain changes in NMHC ratios and suggested evidence for Cl and NO_3 chemistry. To further examine these conclusions extra information is needed, in terms of measurements of NO_3, Cl related species and measurements of NMHCs in other European sites. NMHC measurements in other European sites could be analysed by the NAME model and by back-attribution techniques determine the emission source areas, with a greater accuracy than just one site. Direct measurements of NMHCs from different sources (both anthropogenic and biogenic; for example oceanic flux measurements) would further help to determine the source emissions.

There is a lot more work which can be carried out using the PTM to asses NMHC concentrations at Mace Head. Only a relatively small amount of data has been assessed, concentrating on case studies to identify what information can be extracted from the use of this model. There are other case studies which would be useful for analysis with PTM, including other toluene events to further assess the observed high toluene/benzene ratios. This is an ideal research idea for an undergraduate project student to asses and it is hoped this research will continue.

References

AGAGE, (2007) www.agage.eas.gatech.edu

B. J. Allan, N. Carslaw, H. Coe, R. A. Burgess and J. M. C. Plane, **J. Atmos. Chem.,** 33 (1999) 129-154

C. Anastasi, L. Hopkinson and V. J. Simpson, **Atmos. Environ., 25A** (1991) 1403-1408

P. W. Atkins, **Physical chemistry**, Oxford university press, (1998)

R. Atkinson, **J. Phys. Chem. Ref. Data, 20** (1991) 459-507

R. Atkinson, **J. Phys. Chem. Ref. Data, 26** (1997) 215-290

R. Atkinson, **Atmos. Chem. Phys., 3** (2003) 2233-2307

R. Atkinson, D. L. Baulch, R. A. Cox, J. N. Crowley, R. F. Hampson, R. G. Hynes, M. E. Jenkin, M. J. Rossi and J. Troe, **Atmos. Chem. Phys. Discuss., 5** (2005) 6295-7168

R. Atkinson, D. L. Baulch, R. A. Cox, J. N. Crowley, R. F. Hampson, R. G. Hynes, M. E. Jenkin, M. J. Rossi and J. Troe, **Atmos. Chem. Phys., 6** (2006) 3625-4055

C. Badol, A. Borbon, N. Locoge, T. Léonardis and J. C. Galloo, **Anal. Bioanal. Chem., 378** (2004) 1815 - 1827

S. Bartenbach, J. Williams, C. Plass-Dulmer, H. Berresheim and J. Lelieveld, **Atmos. Chem. Phys, 7** (2007) 1-14

N. J. Blake, S. A. Penkett, K. C. Clemitshaw, P. Anwyl, P. Lightman, A. R. W. Marsh and G. Butcher, **J. Geophys. Res, 98** (1993) 2851-2864

J. W. Bottenheim and M. F. Shepherd, **Atmos. Environ, 29** (1995) 647-664

H. Boudries, G. Toupance and A. L. Dutot, **Atmos. Environ, 28** (1994) 1095-1112

A. Braithwaite and F. Smith, J, **Chromatographic Methods**, Chapmann and Hall, (1996)

W. J. Broadgate, P. S. Liss and S. A. Penkett, **Geophys. Res. Lett., 24** (1997) 2675-2678

R. G. Derwent, M. E. Jenkin and S. M. Saunders, **Atmos. Environ, 30** (1996) 181-199

R. G. Derwent, Davies, T. J., Delaney, M., Dollard, G. J., Field, R. A., Dumitrean, P., Nason, P. D., Jones, B. M. R., Pepler, S. A., **Atmos. Environ, 34** (2000) 297-312

R. G. Derwent, Jenkin, M. E., Saunders, S. M., Pilling, M. J., Simmonds, P. G., Passat, N. R., Dollard, G. J., Dumitrean, P., Kent, A., **Atmos. Environ, 37** (2003) 1983-1991

C. H. Dimmer, A. McCulloch, P. G. Simmonds, G. Nickless, M. R. Bassford and D. Smythe-Wright, **Atmos. Environ, 35** (2001) 1171-1182

G. Dollard, J., P. Dumitrean, S. Telling, J. Dixon and R. G. Derwent, **Atmos. Environ, 41** (2007) 2559-2569

C. J. Dore, J. D. Watterson, T. P. Murrells, N. R. Passant, M. M. Hobson, S. L. Baggott, G. Thistlethwaite, J. W. L. Goodwin, K. R. King, M. Adams, C. Walker, M. K. Downes, P. J. Coleman, R. A. Stewart, A. Wagner, J. Sturman, C. Conolly, H. Lawrence, Y. Li, J. Jackson, T. Bush, S. Grice and N. Brophy, UK Emissions of Air Pollutants 1970 to 2004, AEA Energy & Environment: (2006)

K. Dettmer and W. Engewald, **Anal. Bioanal. Chem,** 373 (2002) 490-500

P. V. Doskey, **J. High Res. Chromatogr,** 14 (1991) 724-728

EPA, (2007) www.epa.gov

D.Gray (2002) PhD thesis, School of Chemistry, University of Bristol, UK

B. R. Greally, A. J. Manning, S. Reimann, A. McCulloch, J. Huang, B. L. Dunse, P. G. Simmonds, R. G. Prinn, P. J. Fraser, D. M. Cunnold, S. O'Doherty, L. W. Porter, K. Stemmler, M. K. Vollmer, C. R. Lunder, N. Schmidbauer, O. Hermansen, J. Arduini, P. K. Salameh, P. B. Krummel, R. H. J. Wang, D. Folini, R. F. Weiss, M. Maione, G. Nickless, F. Stordal and R. G. Derwent, **J. Geophys. Res,** 112 (2007)

R. L. Grob and E. F. Barry, **Modern practise of gas chromatography,** John Wiley & Sons, Inc, (2004)

A. J. Haagen-Smit and M. M. Fox, **Ind. Eng. Chem,** 48 (1956) 1484

M. Harper, **J. Chrom. A.,** 885 (2000) 129-151

F. Heintz, U. Platt, H. Flentje and R. Dubois, **J. Geophys. Res,** 101 (1996) 22891-22910

D. Helmig, **J. Chromatogr. A,** 843 (1999) 129-146

C. N. Hewitt, **Reactive Hydrocarbons in the Atmosphere,** Academic Press, (1999)

J. R. Hopkins, I. D. Jones, A. C. Lewis, J. B. McQuaid and P. W. Seakins, **Atmos. Environ,** 36 (2002) 3217-3229

M. Z. Jacobson, **Fundamentals of atmopsheric modelling,** Cambridge university press, (2005)

M. E. Jenkin and K. C. Clemitshaw, **Atmos. Environ,** 34 (2000) 2499-2527

M. E. Jenkin, S. M. Saunders, R. G. Derwent and M. J. Pilling, **Atmos. Environ, 36** (2002) 4725-4734

S. Kent, Adsorbent Selection, Adsorption Research, Inc. (2005)

A. Kroupa, J. Dewulf, H. Van Langenhove and I. Viden, **J. Chromatogr. A, 1038** (2004) 215-223

A. Latella, G. Stani, L. Cobelli, M. Duane, H. Junninen, C. Astorga and B. R. Larsen, **J. Chromatogr. A, 1071** (2005) 29-39

B. H. Lee, W. J. Munger, S. C. Wofsy and A. H. Goldstein, **J. Geophys. Res, 111** (2006)

A. C. Lewis, K. D. Bartle, D. E. Heard, J. B. McQuaid, M. J. Pilling and P. W. Seakins, **J. Chem Soc., Faraday Trans. 1, 93** (1997) 2921-2927

A. C. Lewis, L. J. Carpenter and M. J. Pilling, **J. Geophys. Res, 106** (2001) 4987

Z. H. Ji, R. E. Majors and E. J. Guthrie, **J. Chromatogr. A, 842** (1999) 115-142

A. J. Manning, D. B. Ryall, R. G. Derwent, P. G. Simmonds and S. O'Doherty, **J. Geophys. Res, 108** (2003)

D. Martin, (2002) PhD thesis, School of Chemistry, University of Bristol, UK

S. A. McKeen and S. C. Liu, **Geophys. Res. Lett, 20** (1993) 2363-2366

R. McLaren, R. A. Salmon, J. Liggio, K. L. Hayden, K. G. Anlauf and W. R. Leaitch, **Atmos. Environ, 38** (2004) 5837-5848

A. Monod, B. C. Sive, P. Avino, T. Chen, D. R. Blake and F. S. Rowland, **Atmos. Environ, 35** (2001) 135-149

Nilu (2007) www.nilu.no

NIST (2007) www.webbook.nist.gov

NUI, (2007) www.macehead.nuigalway.ie

S. O'Doherty, D. M. Cunnold, A. J. Manning, B. R. Miller, R. H. J. Wang, P. B. Krummel, P. J. Fraser, P. G. Simmonds, A. McCulloch, R. F. Weiss, P. Salameh, L. W. Porter, R. G. Prinn, J. Huang, G. Sturrock, D. B. Ryall, R. Derwent, G. and S. A. Montzka, **J. Geophys. Res, 109** (2004)

D. D. Parrish, C. J. Hahn, E. J. Williams, R. B. Norton and F. C. Fehsenfeld, **J. Geophys. Res, 97** (1992) 15,883-15,901

S. A. Penkett, R. A. Burgess, H. Coe, I. Coll, O. Hov, A. Lindskog, N. Schmidbauer, S. Solberg, M. Roemer, T. Thijsse, J. Beck and C. E. Reeves, **Atmos. Environ, 41** (2007) 3465-3478

Permapure (2007) www.permapure.com

R. J. B. Peters and H. A. Bakkeren, **Analyst, 119** (1994) 71-74

C. Plass-Dulmer, R. Koppmann, M. Ratte and J. Rudolph, **Global Biogeochem. Cycles, 9** (1995) 79-100

PORG, Ozone in the United Kingdom, Forth Report of the Photochemical Oxidants Review Group., (1997)

R. G. Prinn, R. F. Weiss, P. J. Fraser, P. G. Simmonds, D. M. Cunnold, F. N. Alyea, S. O'Doherty, P. Salameh, B. R. Miller, J. Huang, R. H. J. Wang, D. E. Hartley, C. Harth, L. P. Steele, G. Sturrock, P. M. Midgley and A. McCulloch, **J. Geophys. Res, 105** (2000) 17751-17792

A. A. P. Pszenny, E. V. Fischer, R. S. Russo, B. C. Sive and R. K. Varner, **J. Geophys. Res, 112** (2007) doi:10.1029/2006JD007725

G. L. Reid, C. A. Monge, W. T. Wall and D. W. Amstrong, **J. Chromatogr. A, 633** (1993) 135-142

S. Reimann, Personal communication, (2006) EMPA

S. Reimann, P. Calanca and P. Hofer, **Atmos. Environ, 34** (2000) 109-115

D. D. Riemer, P. J. Milne, R. G. Zika and W. H. Pos, **MARINE CHEMISTRY, 71** (2000) 177-198

J. Rudolph, Ramacher, B., PlassDulmer, C., Muller, K. P., Koppmann, R., **Tellus B, 49** (1997) 592-601

D. B. Ryall, R. G. Derwent, A. J. Manning, P. G. Simmonds and S. O'Doherty, **Atmos. Environ, 35** (2001) 2507-2523

T. Saito, Y. Yokouchi and K. Kawamura, **Atmos. Environ, 34** (2000) 4373-4381

Scanview (8.0) Scanview Database of chromatography, spectroscopy and sample preparation applications

J. H. Seinfeld and S. N. Pandis, **Atmospheric chemistry and physics from air pollution to climate change**, John Wiley & sons, inc, (1998)
J. H. Seinfeld, **Reactive Hydrocarbons in the atmosphere**, Academic Press, (1999)

S. Silman, **Atmos. Environ, 33** (1999) 1821-1845

P. G. Simmonds, O'Doherty.S., G. Nickless, G. A. Sturrock., R. Swaby., P. Knight., J. Ricketts., G. Woffendin. and R. Smith., **Anal. Chem.,, 67** (1997) 717 - 723

P. G. Simmonds, A. J. Manning, D. M. Cunnold, A. McCulloch, S. O'Doherty, R. Derwent, G., P. B. Krummel, P. J. Fraser, B. L. Dunse, L. W. Porter, R. H. J. Wang, B. R. Greally, B. R. Miller, P. Salameh, R. F. Weiss and R. G. Prinn, **J. Geophys. Res, 111** (2006) D18304

H. B. Singh and J. F. Kasting, **J. Atmos. Chem, 7** (1988) 261-285

B. C. Sive, Y. Zhou, D. Troop, Y. Wang, W. C. Little, O. W. Wingenter, R. S. Russo, R. K. Varner and R. Talbot, **Anal. Chem.,, 77** (2005) 6989 -6998

J. Slemr, F. Slemr, H. D'Souza and R. Partridge, **J. Chromatogr. A, 1061** (2004) 75-84

SOGE, (2007) www.nilu.no/soge

A. L. Swanson, N. J. Blake, E. Atlas, F. Flocke, D. R. Blake and F. S. Rowland, **J. Geophys. Res, 108** (2003) 4065

D. Tholl, W. Boland, A. Hansel, F. Loreto, U. S. R. Ro¨se and J. P. Schnitzler, **Plant J, 45** (2006) 540-560

Varian (2007) www.varianinc.com

C. Warneke, S. A. McKeen, J. A. de Gouw, P. D. Goldan, W. C. Kuster, J. S. Holloway, E. J. Williams, B. M. Lerner, D. D. Parrish, M. Trainer, F. C. Fehsenfeld, S. Kato, E. L. Atlas, A. Baker and D. R. Blake, **J. Geophys. Res, 112** (2007) doi:10.1029/2006JD007930

J. L. Wang, G. Z. Din and C. C. Chan, **J. Chrom. A., 1027** (2004) 11-18

R. P. Wayne, I. Barnes, P. Biggs, J. P. Burrows, C. E. Canosa-Mas, J. Hjorth, G. Le Bras, G. K. Moortgat, D. Perner and G. Poulet, **Atmos. Environ, 25** (1991) 1-203

O. W. Wingenter, M. K. Kubo, N. J. Blake, T. W. Smith, D. R. Blake and F. S. Rowland, **J. Geophys. Res, 101** (1996) 4331-4340